UNIVERSITY OF THE BASQUE COUNTRY

DOCTORAL THESIS

Non-equilibrium glass dynamics of amorphous polymers and other materials

---

Author:
Vasiliki Maria STAVROPOULOU

Supervisor:
Daniele CANGIALOSI

2026

Declaration of Authorship

I, Vasiliki Maria STAVROPOULOU, declare that this thesis titled, "Non-equilibrium glass dynamics of amorphous polymers and other materials" and the work presented in it are my own. I confirm that:

- This work was done wholly or mainly while in candidature for a research degree at this University.
- Where any part of this thesis has previously been submitted for a degree or any other qualification at this University or any other institution, this has been clearly stated.
- Where I have consulted the published work of others, this is always clearly attributed.
- Where I have quoted from the work of others, the source is always given. With the exception of such quotations, this thesis is entirely my own work.
- I have acknowledged all main sources of help.
- Where the thesis is based on work done by myself jointly with others, I have made clear exactly what was done by others and what I have contributed myself.

"Νίκησα; Νικήθηκα; Τούτο μόνο ξέρω: Είμαι γεμάτος πληγές και στέκομαι όρθιος."

Νίκος Καζαντζάκης

Resumen

Los vidrios constituyen sistemas prototípicos fuera del equilibrio cuyas propiedades termodinámicas y dinámicas siguen estando solo parcialmente comprendidas a pesar de décadas de investigación teórica y experimental. En particular, los mecanismos microscópicos que gobiernan la transición vítrea y la posterior relajación estructural hacia el equilibrio, conocida como envejecimiento físico, continúan siendo objeto de intensa investigación. Una comprensión más profunda de estos procesos es esencial no solo para la física fundamental de la materia condensada, sino también para el diseño racional y la optimización de materiales ampliamente utilizados en aplicaciones tecnológicas. El objetivo principal de esta tesis es investigar la dinámica del estado vítreo en un amplio espectro de materiales que forman vidrios, incluyendo vidrios moleculares de Van der Waals, vidrios poliméricos y redes poliméricas reticuladas. Para alcanzar este objetivo, se emplearon técnicas calorimétricas avanzadas— principalmente la Calorimetría de Barrido Rápido (Fast Scanning Calorimetry, FSC)— con el fin de estudiar la cinética de la relajación estructural en intervalos de tiempo y temperatura que resultan inaccesibles mediante métodos calorimétricos convencionales.

La primera parte de este trabajo se centra en la cinética del envejecimiento físico en pequeñas moléculas que interactúan a través de fuerzas de Van der Waals y que han sido profundamente templados dentro del estado vítreo. Aprovechando las elevadas velocidades de calentamiento y enfriamiento alcanzadas mediante FSC, se caracterizó el envejecimiento de cinco vidrios moleculares representativos a lo largo de seis órdenes de magnitud en el tiempo de envejecimiento. El comportamiento experimental de la relajación fue analizado mediante dos enfoques complementarios: un método basado en los tiempos de equilibrio y un modelo modificado de Envejecimiento de Parámetro Único (Single Parameter Aging, SPA) que incorpora escalado de densidad para tener en cuenta la no linealidad de la cinética de envejecimiento. Mientras que las etapas finales de la equilibración fueron razonablemente descritas por el modelo SPA y resultaron consistentes con el papel dominante de la relajación α, se observaron desviaciones significativas a bajas temperaturas de envejecimiento correspondientes a grandes saltos de temperatura. Bajo estas condiciones, los resultados experimentales de relajación mostraron un "stretch" considerablemente mayor que el predicho por modelos basados exclusivamente en la dinámica de la relajación α, lo que indica la presencia de mecanismos adicionales de equilibración rápida activos en las etapas iniciales del envejecimiento.

Para esclarecer estos mecanismos con mayor detalle, se aplicó un análisis cinético

isoconversional tanto a vidrios moleculares como poliméricos con el fin de determinar la evolución de las barreras efectivas de activación durante la relajación estructural. Los resultados revelan un aumento sistemático de la energía de activación a medida que progresa el envejecimiento, desde valores relativamente bajos en pequeños grados de relajación hasta valores comparables a los de la relajación α en las etapas finales. Estos hallazgos apoyan un escenario de equilibración vítrea en múltiples etapas en el que procesos de baja barrera— posiblemente relacionados con relajaciones secundarias o con el denominado Proceso Arrhenius Lento (Slow Arrhenius Process, SAP) asociado a movimientos colectivos localizados— gobiernan las primeras etapas del envejecimiento, mientras que la relajación α domina la aproximación final al equilibrio.

Además, se realizaron experimentos complementarios de espectroscopía dieléctrica de banda ancha (Broadband Dielectric Spectroscopy, BDS) en un formador de vidrio molecular arquetípico, monitorizando simultáneamente la pérdida dieléctrica en el flanco de alta frecuencia de la relajación α y la capacitancia a alta frecuencia. Estos resultados demostraron la validez del escalado de densidad en condiciones fuera del equilibrio, sugiriendo que la incapacidad de la relajación α por sí sola para describir completamente la fenomenología del envejecimiento físico se debe a la contribución de relajaciones secundarias adicionales.

La segunda parte de esta tesis aborda el comportamiento de redes poliméricas vitriméricas reticuladas mediante enlaces reversibles de enamina. En estos sistemas, un parámetro clave es la temperatura de congelación topológica, por encima de la cual la red experimenta una transición de sólido viscoelástico a líquido viscoelástico a través de reacciones dinámicas de intercambio de enlaces. La Calorimetría de Barrido Rápido fue empleada por primera vez para desarrollar protocolos experimentales capaces de separar la temperatura de transición vítrea de la temperatura de congelación topológica, que a menudo resultan difíciles de distinguir mediante técnicas calorimétricas convencionales debido a su proximidad. El análisis reveló que la transformación vitrimérica implica dos etapas diferenciadas: un proceso inicial fuertemente acoplado a la dinámica segmentaria del polímero asociada con la transición vítrea, seguido de un régimen a temperaturas más elevadas dominado por el intercambio reversible de enlaces covalentes. El análisis cinético basado en el método de Kissinger permitió determinar las energías de activación asociadas a estos procesos, revelando energías de activación significativamente menores para la reacción de intercambio de enlaces en comparación con aquellas asociadas con la transición vítrea.

En conjunto, los resultados presentados en esta tesis ponen de manifiesto la potencia y versatilidad de la Calorimetría de Barrido Rápido para investigar la dinámica de sistemas formadores de vidrio complejos. Los hallazgos proporcionan nuevos conocimientos sobre los mecanismos que gobiernan el envejecimiento físico en vidrios moleculares y poliméricos, y establecen metodologías experimentales para estudiar el comportamiento térmico y cinético de redes vitriméricas. Estos avances contribuyen a una comprensión más profunda de la dinámica vítrea fuera del equilibrio y abren nuevas perspectivas para la exploración de estados vítreos de baja energía y el diseño racional de materiales poliméricos.

La tesis se estructura de la siguiente manera. El Capítulo 1 presenta una introducción al contexto científico y a los desafíos asociados al estudio del estado vítreo, además de describir los principales conceptos teóricos relacionados con este trabajo y los objetivos de la tesis. El Capítulo 2 presenta los materiales estudiados, así como las técnicas experimentales empleadas en el análisis térmico, concretamente la Calorimetría Diferencial de Barrido (DSC), la Calorimetría de Barrido Rápido (FSC) y la Espectroscopía Dieléctrica. Se pone especial énfasis en los protocolos térmicos específicos utilizados para desentrañar distintos aspectos de la vitrificación y del envejecimiento físico. El Capítulo 3 ofrece una visión general de los principales resultados, organizados en secciones correspondientes a cada una de las publicaciones incluidas en la presente tesis. El Capítulo 4 presenta las conclusiones principales y discute las implicaciones derivadas de este trabajo. Finalmente, en el Capítulo 5 se incluyen los tres artículos publicados que forman parte de la tesis, mientras que en el Apéndice A se incorpora un cuarto artículo también presentado en esta tesis, actualmente en estado de prepublicación.

Abstract

Glasses constitute prototypical non-equilibrium systems whose thermodynamic and dynamic properties remain only partially understood despite decades of theoretical and experimental investigation. In particular, the microscopic mechanisms governing the glass transition and the subsequent structural relaxation toward equilibrium, known as physical aging, continue to be the subject of intense research. A deeper understanding of these processes is essential not only for fundamental condensed matter physics but also for the rational design and optimization of materials widely used in technological applications. The primary objective of this thesis is to investigate the dynamics of the glassy state across a broad spectrum of glass-forming materials, including Van der Waals molecular glasses, polymeric glasses, and cross-linked polymer networks. To achieve this goal, advanced calorimetric techniques— primarily Fast Scanning Calorimetry (FSC)— were employed to probe structural relaxation kinetics over extended time and temperature ranges that are inaccessible to conventional calorimetric methods.

The first part of this work focuses on the kinetics of physical aging in small-molecule glass formers interacting through Van der Waals forces that are deeply quenched into the glassy state. By exploiting the high heating and cooling rates achievable with FSC, the aging behavior of five representative molecular glasses was characterized across approximately six decades of aging time. The experimental relaxation behavior was analyzed using two complementary approaches: a model-independent method based on equilibration times and a modified Single Parameter Aging (SPA) model incorporating density scaling to account for the nonlinearity of aging kinetics. While equilibration close to T_g and the final stages of equilibration at temperatures farther from T_g were reasonably captured by the SPA model and were consistent with the dominant role of the α-relaxation, significant deviations were observed at low aging temperatures corresponding to large temperature jumps. Under these conditions, the experimental relaxation functions exhibited a substantially stronger stretching than predicted by models relying solely on α-relaxation dynamics, indicating the presence of additional fast equilibration mechanisms active in the early stages of aging.

To further elucidate these mechanisms, isoconversional kinetic analysis was applied to both molecular and polymeric glasses in order to determine the evolution of effective activation barriers during structural relaxation. The results reveal a systematic increase in activation energy as aging progresses, from relatively low values at small extents of relaxation to values comparable to those of the α- relaxation in the

last stages. These findings support a multi-step scenario of glass equilibration in which low-barrier processes— possibly related to secondary relaxations or the Slow Arrhenius Process (SAP) associated with localized collective motions— govern the initial stages of aging, whereas α- relaxation dominates the final approach to equilibrium.

Moreover, complementary broadband dielectric spectroscopy experiments were performed on an archetypal molecular glass former, by monitoring the dielectric loss on the high-frequency flank of the α- relaxation together with the high-frequency capacitance. These demonstrated the validity of density scaling under out-of-equilibrium conditions, thereby suggesting that the inability of the α- relaxation alone to capture the overall phenomenology of physical aging is due to the contribution of additional secondary relaxations.

The second part of this thesis addresses the behavior of vitrimeric polymer networks cross-linked through reversible enamine bonds. In these systems, a key parameter is the topology freezing transition temperature, above which the network undergoes a transition from a viscoelastic solid to a viscoelastic liquid via dynamic bond exchange reactions. Fast Scanning Calorimetry was employed for the first time to develop experimental protocols enabling the separation of the glass transition temperature and the topology freezing transition temperature, which are often difficult to distinguish using conventional calorimetric techniques due to their proximity. The analysis revealed that the vitrimeric transformation involves two distinct stages; an initial process strongly coupled to polymer segmental dynamics associated with the glass transition, followed by a higher-temperature regime dominated by reversible covalent bond exchange. Kinetic analysis based on Kissinger methods allowed the determination of activation energies associated with these processes, revealing significantly lower activation energies for the bond exchange reaction compared with those associated with the glass transition.

Overall, the results presented in this thesis highlight the power and versatility of Fast Scanning Calorimetry for investigating the dynamics of complex glass-forming systems. The findings provide new insights into the mechanisms governing physical aging in molecular and polymeric glasses and establish experimental methodologies for probing the thermal and kinetic behavior of vitrimeric networks. These advances contribute to a deeper understanding of out-of-equilibrium glassy dynamics and open new perspectives for the exploration of low-energy glass states and the rational design of polymer and small molecules materials.

The thesis has the following structure. Chapter 1 makes an introduction to the scientific context and the challenges encountered in the field of the glassy state. It also describes the principal theoretical concepts related to our study and the main goals of the thesis. Chapter 2 presents the materials under study, as well as the experimental techniques associated to the thermal analysis employed in this work, namely the Standard Differential Calorimetry (DSC), the Fast Scanning Calorimetry (FSC) and the Dielectric Spectroscopy. Special emphasis is placed on the specific thermal protocols applied here for unraveling different aspects of vitrification and physical aging. Then, Chapter 3 offers a general view of the main results, organized in sections corresponding to each one of the publications included in the present thesis. Chapter 4 presents the major conclusions and discusses the implications that stem from this work. Last, in Chapter 5 the three published articles that form part of the thesis are attached and in Appendix A we include the fourth article also presented here, currently found in pre-print state.

Acknowledgements

To begin with, I would like to express my deepest gratitude to my supervisor, Dr. Daniele Cangialosi, for trusting me to carry out this project and for his constant support throughout the years. I am grateful for his guidance and the fruitful discussions which have been a fundamental part of my training as a young researcher and they provided me with invaluable experience for my future professional life. I would like to extend my gratitude to my university tutor, Prof. Ángel Alegría, for his help with the administrative work and the clarifications concerning the complex bureaucratic processes.

I would also like to acknowledge the financial support provided by the Materials Physics Center (CSIC-EHU) through my pre-doctoral contract and its short extension that allowed me to complete this thesis. Likewise, I would like to extend my acknowledgements to the University of the Basque Country (EHU) for financing my participation in international conferences.

I am mostly grateful to Dr. Valerio Di Lisio, my calorimetry tutor, who taught me everything about Flash DSC and provided me with all the necessary tools and guidelines for the experimental procedures. Thank you for all the insightful conversations and suggestions in moments of doubt. Also, I would like to thank Dr. Lorenzo Augusto Rocchi, for sharing the lab with me, for the scientific conversations and above all, the coffee breaks that have always fueled the long working days.

Moreover, I would like to extend my gratitude to all the members of the Polymers and Soft Matter Group in Materials Physics Center, including senior researchers, technical staff, post-doctoral researchers, PhD and Master students for the nice working environment and the collaboration that has been developed all these years.

Part of this thesis is based on experiments performed in the facilities of the Université Libre de Bruxelles (ULB), in Brussels, Belgium. Firstly, I want to thank Prof. Simone Napolitano for hosting me in his Polymer and Soft Matter Dynamics group, for the good collaboration and for his invaluable indications. I am also grateful to Dr. Federico Caporaletti for the time he spent to introduce me to the experimental protocols and guide me throughout my stay. A special mention also goes to Pascal Pirotte who was always willing to solve any technical issue, as well as to Prof. Patricia Losada-Pérez and Dr. Martín Eduardo Villanueva for their advice and the friendly atmosphere.

This journey would not have been the same without the people I am lucky to call friends. I shall start from my old colleagues, Claudia, Francesco and Phuong, I was glad to share the office with you and enjoy your friendship. To Sofia, thank you for our discussions and your advice, they have been truly important to me. A special mention to Ebtisam and Trini, thank you for all the girl plans we made together and for listening to me when it mattered the most. I would also like to express my gratitude to Caro, Fonsi, Renata and Alaa for all the nice moments we have shared together and the conversations. And of course, to the friends I made later on, Amaia and Irene, eskerrik asko for your company and the nice memories. I could not disregard my two housemates, Πασχάλης and Tom, your friendship, support and the funny moments will be unforgettable to me. And to my friends in Greece, Βίκυ και Αθανασία, σας ευχαριστώ για την υποστήριξη και τις καλοκαιρινές αναμνήσεις, ελπίζω να βλεπόμαστε πιο συχνά από εδώ και στο εξής!

No podría faltar en esta sección de los agradecimientos la persona más fascinante del mundo y, me atrevo a decir, mi mayor descubrimiento de los últimos tres años. Αγάπη μου, Pelayo, no hay suficientes palabras para expresar cuánto te agradezco todo el cariño y el apoyo que me has dado durante este tiempo. Ha sido una verdadera suerte haber compartido este viaje contigo, en las buenas y en las malas, y ¡brindo por todos los que aún nos quedan!

Asimismo me gustaría extender mis agradecimientos a Teresa y José. Gracias por acogerme desde el primer momento y por todos vuestros consejos; para mí sois una segunda familia en España.

Last but not least, I would like to express my deepest gratitude to my parents and my sister. Στους γονείς μου, σας ευχαριστώ πολύ για την ανιδιοτελή αγάπη και την εμπιστοσύνη που μου έχετε δείξει καθόλη τη διάρκεια της σταδιοδρομίας μου. Λυπάμαι που οι συνθήκες δε μου επέτρεψαν να σας επισκέπτομαι πιο συχνά κατά τη διάρκεια του διδακτορικού. Ευχαριστώ που ήσασταν πάντα εκεί για εμένα, όπως επίσης και για όλη την ηθική, συναισθηματική και οικονομική στήριξη που μου έχετε προσφέρει. Έχετε συμβάλει τα μέγιστα σε αυτήν την προσπάθεια, ελπίζω να είστε υπερήφανοι! Ηλιάνα, νομίζω ότι ήδη ξέρεις ότι εκτός απο δικηγόρος μου, είσαι και η ψυχολόγος μου. Δεν έχω λόγια για τις ατελείωτες ώρες που παρέμεινες στο ακουστικό να ακούσεις το ρεσιτάλ απόγνωσής μου και για τις πολύτιμες συμβουλές σου. Οι επισκέψεις σου επί ισπανικού και βελγικού εδάφους ήταν ενέσεις σεροτονίνης για εμένα. Σε ευχαριστώ για όλα!

Contents

List of Figures

List of Abbreviations

AIE	**A**ggregation **I**nduced **E**mission
BDS	**B**roadband **D**ielectric **S**pectroscopy
BMMPC	1, 1 - **b**is(4 - **m**ethoxyphenyl) **c**yclohexane
BMPC	**b**isphenol -C- di**m**ethylether
CAN	**C**ovalent **A**daptable **N**etwork
CM	**C**lausius-**M**ossotti
CSD	**C**ollective **S**mall **D**isplacements
DAP	1,3-**di**amino**p**ropane
DCB	**D**ynamic **C**ovalent **B**ond
DFFT	**D**iscrete **F**ast **F**ourier **T**ransform
DFT	**D**issipation **F**luctuation **T**heorem
DMA	**D**ynamic Mechanical **A**nalysis
DRS	**D**ielectric **R**elaxation **s**pectroscopy
DSC	**D**ifferential **S**canning **C**alorimetry
EDO	2, 2′-(**e**thylene**di**o**o**xy) bis(ethylamine)
FSC	**F**ast **S**canning **C**alorimetry
FTIR	**F**ourier **T**ransform **I**nf**r**ared Spectroscopy
KAHR	**K**ovacs- **A**klonis- **H**utchinson- **R**amos
KDE	o-**C**resolphthalein **D**imethyl **E**ther
KWW	**K**ohlrausch-**W**illiams-**W**atts
OTP	**o**-**t**er**p**henyl
P4BrS	**p**oly(**4**-**br**omo **s**tyrene)
P4ClS	**p**oly(**4**-**cl**oro **s**tyrene)
PDE	**p**henolphthalein **d**imethyl **e**ther
PG	**p**oly**g**lycerol
PS	**p**oly**s**tyrene
SAP	**S**low **A**rrhenius **P**rocess
SPA	**S**ingle **P**arameter **A**ging
TBAA	**t**ert-**b**utyl **a**ceto**a**cetate
TGA	**T**hermo**g**ravimetric **A**nalysis
TNM	**T**ool-**N**arayanaswamy-**M**oynihan

VFT	**V**ogel-**F**ulcher-**T**ammann
WLF	**W**illiams-**L**andel-**F**erry

To my family

Chapter 1

Introduction

"Who, when he saw the first sand or ashes, by a casual intenseness of heat, melted into a 'metalline' form, rugged with excrescences, and clouded with impurities, would have imagined, that in this shapeless lump lay concealed so many conveniences of life, as would in time constitute a great part of the happiness of the world?

~Samuel Johnson, *No. 9. The fondness of every man for his profession* in the Rambler

1.1 Equilibrium phases and relevant transitions

The matter that surrounds us exists in different forms called phases. A phase is a macroscopic amount of substance which possesses uniform chemical composition and physical properties and is confined by a boundary phase [1]. Single-component substances can exist in four major states of matter: gas, liquid, crystal and glass. The first three of them are known as equilibrium phases.

The transformation from one state to another is called a phase transition. At constant pressure, phase transitions occur due to changes in the temperature. Such new phase must be energetically favorable, which entails that it must be characterized by lower free energy Gibbs (G). This is shown schematically in Fig. 1.1, where all possible phase transitions are displayed. It is clearly seen that a phase transition takes place at the temperature at which the two phases have the same Gibbs energy, i.e. $\Delta G = 0$. This means that at this temperature the two phases can co-exist in equilibrium.

Starting from the crystalline state, the system upon heating will first melt at the melting temperature, T_m. During this transition, the crystalline lattice is rearranged into a loosely packed, disordered structure. Further heating up to the boiling temperature, T_b, leads to vaporization of the liquid. At this temperature, the liquid

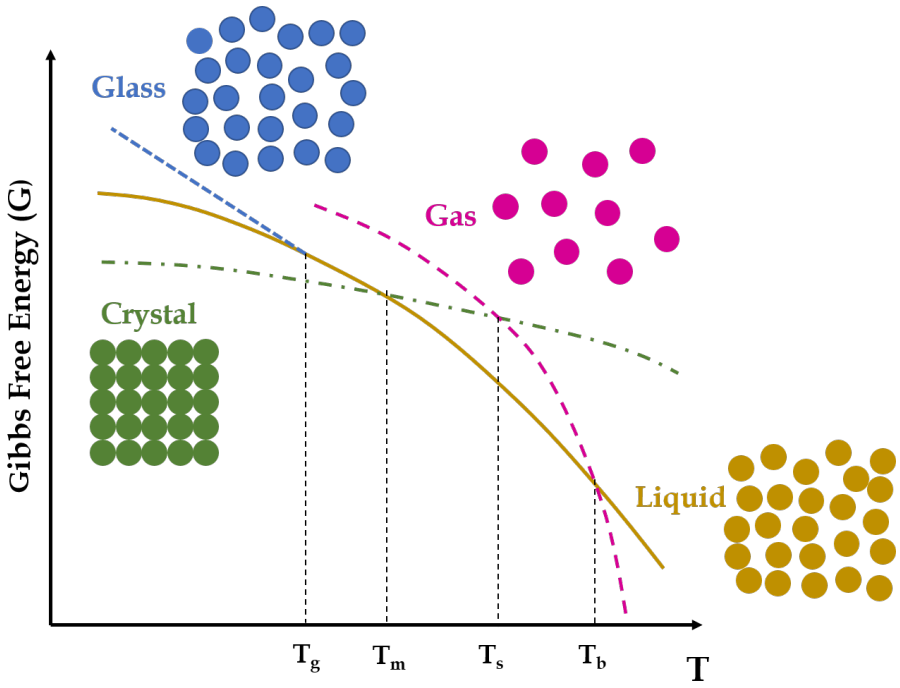

FIGURE 1.1: Temperature dependence of the Gibbs free energy for crystal, glass, liquid and gas phases at constant pressure (T_g: glass transition temperature, T_m: melting temperature, T_s: sublimation temperature, T_b: boiling temperature).

structure unpacks to practically unbound molecules in the gaseous phase. The direct transition from the crystalline to the gaseous phase, without passing from melting, is also possible, as long as the liquid state exhibits free energy larger than those of the other phases at a given pressure. This transition is called sublimation and it occurs at temperature equal to T_s.

An important thermodynamic feature of these equilibrium phase transitions, which is already visible in Fig. 1.1, is the abrupt change of the slope in the graph of G vs T at the transition temperature. This change is translated into a discontinuity in the first partial derivatives of the free energy with respect to T and is attributed to the latent heat absorbed or released during a so-called first-order transition, which will be discussed later.

1.2 Non-equilibrium systems and glass transition

Physical systems exhibiting permanently stable and reversible behavior are rare in nature. In contrast, non-equilibrium systems are ubiquitous and have always played a fundamental role in the formation and time evolution of our universe.

Such systems spontaneously evolve toward the most stable thermodynamic state, which is the one with the lowest free energy [2]. Elucidating the kinetics governing this evolution, has long been a central challenge in the study of unstable natural phenomena and related processes.

Among the numerous examples of non-equilibrium systems, glasses constitute a mostly important class owing to their widespread presence in nature and their extensive use since the dawn of the human civilization [3]. Glass has always captivated human interest due to its special nature. The production of glass is estimated to be 5000 years old and at the beginning it was used for aesthetic reasons. It probably first appeared in the Middle East, between Phoenicia (Lebanon), Syria and Egypt, and the most ancient glass objects discovered in excavations, such as beads, date back to 3000-2000 BC [4].

The glass phase is formed when supercooled liquids are cooled fast enough to avoid reaching the ordered crystalline state, which is the most stable and favorable one, from a thermodynamic point of view [5–7]. Liquids that exhibit slow crystallization are classified as good glass-formers. On the other hand, liquids that have a strong tendency to crystallize can form glasses if sufficiently fast cooling rates are employed and/or crystallization nuclei are eliminated. Among the liquids that can be supercooled easily below their melting temperature, polymers are notable representatives due to their versatility and significant technological relevance. Nevertheless, there is a much wider range of glass-forming materials, including silicates, oxides, chalcogenides, metals, organic compounds, van-der-Waals small molecules and colloidal glasses.

The fundamental reason for the glass formation lies in the limited rate of the molecular/atomic mobility that slows down progressively as the liquid is cooled. At a certain point, the mobility becomes insufficient to maintain the equilibrium liquid structure and the supercooled liquid transforms into a glass [8–10]. This transformation is known as *glass-transition* or *vitrification* and during the last decades there has been considerable effort to unveil the thermodynamic and dynamic aspects of this process.

1.2.1 About the thermodynamics of glass transition

The transformation of a supercooled liquid into a glass can be studied from different viewpoints, but here we will focus on the second-order thermodynamic properties.

This approach is commonly adopted when calorimetry is employed, since it delivers the step in specific heat, which is the signature of glass transition. Fig. 1.2 describes schematically the temperature dependence of any first-order thermodynamic property, such as enthalpy (H), specific volume (V), or entropy (S) during vitrification. It can be seen clearly that for this kind of properties, a kink is observed as the supercooled liquid is cooled down and transforms into a glass, at a temperature which is commonly referred to as glass transition temperature (T_g) [11]. On the right part of Fig. 1.2 the stability plots of the free energy of the configurational space are shown. These plots demonstrate that below the T_g the glassy state is unstable with respect to both the supercooled liquid and the crystalline solid. As a consequence, the glass is bound to relax continuously toward the metastable supercooled liquid state. Unlike the equilibrium phases, glasses cannot co-exist in equilibrium with other phases and as a result, the T_g cannot be defined with the same certainty as the transition temperatures for equilibrium phases. Fig. 1.2 also shows the so-called fictive temperature, T_f, which is defined as the temperature at which a glass would be at equilibrium in a given thermodynamic state [11]. The concept of the fictive temperature was introduced by Tool [11] and it has been a common way to define the thermodynamic state of a glass eversince.

The glass transition is accompanied by qualitative changes of the response of the system to variations of external control parameters like temperature and pressure. These changes of the reponse of the system are reflected in jumps in thermodynamic coefficients like specific heat, thermal expansion coefficient or compressibility. The Prigogine-Defay ratio, Π [6, 12], provides a general correlation between the jumps of compressibility, $\Delta\kappa$, thermal expansion coefficient, $\Delta\alpha$ and the isobaric heat capacity, ΔC_p near the glass transition temperature, T_g, and is defined as:

$$\Pi = \frac{1}{VT}\frac{\Delta C_p \Delta\kappa}{(\Delta\alpha)^2}\bigg|_{T=T_g} \tag{1.1}$$

Here, V is the volume of the system under consideration and T the absolute temperature. Considering the concept of the glass transition developed by Simon [13, 14], when glass-forming liquids are cooled from the melt, a transformation of the metastable equilibrium state into a frozen-in, thermodynamically unstable state takes place at a certain, well-defined temperature, T_g. One of the consequences of the vitrification is that the thermodynamic coefficients exhibit a step-like dependence on temperature in the glass transition region. This step in the coefficients is a reminiscent of a second-order thermodynamic transition according to the Ehrenfest classification (1933) [15].

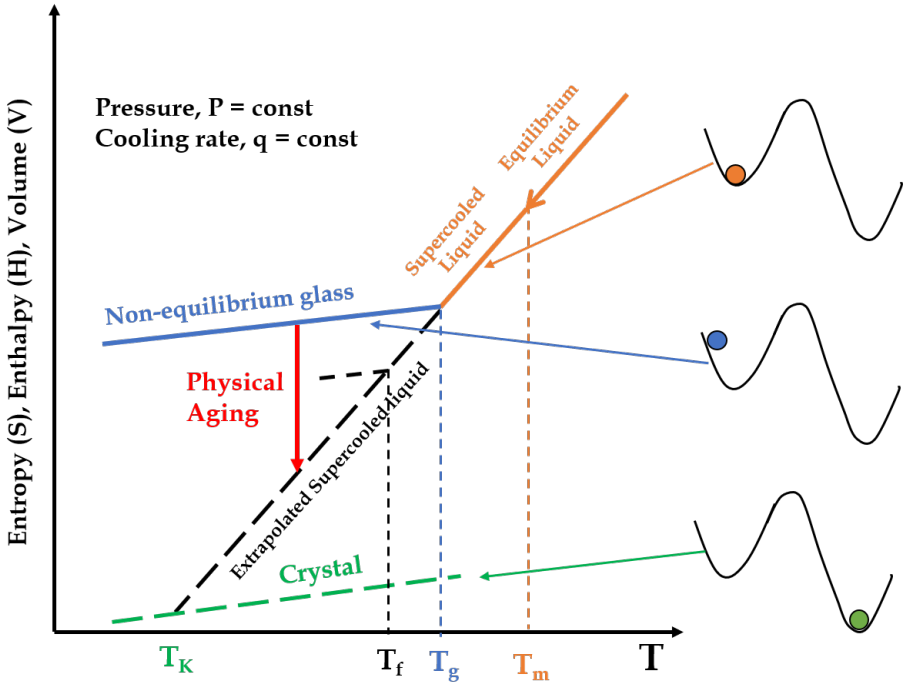

FIGURE 1.2: Schematic representation of the temperature dependence of the first-order thermodynamic properties in glass-forming systems under constant pressure and cooling rate (T_m: melting temperature, T_K: the Kauzmann temperature, where the entropy of the supercooled liquid equals that of the corresponding crystal). The right part depicts the stability plots of the free energy.

Ehrenfest considered surfaces of constant Gibbs free energy, $G = U - TS + PV$ (where U the energy, S the entropy and P the pressure), which possess continuous derivatives away from the transition points. He then called the transformations that showed a discontinuity in any of the first partial derivatives of the free energy *first-order phase-transitions*. Such transitions are characterized by a jump in entropy (S), volume (V) or enthalpy (H), which are expressed as:

$$S = -\left(\frac{\partial G}{\partial T}\right)_P \qquad V = \left(\frac{\partial G}{\partial P}\right)_T \qquad H = -\left[\frac{\partial(\frac{G}{T})}{\partial(\frac{1}{T})}\right]_P \tag{1.2}$$

Similarly, he called *second-order phase-transitions* those where neither the free energy, G, nor its first derivatives are discontinuous, but there is a jump in a second derivative. In second-order transitions, there is no discontinuity in V, H, S at the transition point, but there is in the heat capacity (C_p), thermal expansion (α) or compressibility (κ), defined by [16, 17]:

$$C_p = -\left(\frac{\partial H}{\partial T}\right)_P \qquad \alpha = \frac{1}{V}\left(\frac{\partial V}{\partial T}\right)_P \qquad \kappa = -\frac{1}{V}\left(\frac{\partial V}{\partial P}\right)_T \tag{1.3}$$

During both vitrification and the Ehrenfest second-order phase transitions, the response of the system, in other words its susceptibility, is changed qualitatively, while the state of the system (structure and thermodynamic functions) remains the same at the transition point [18]. However, a striking difference between these two cases is that in Ehrenfest´s theoretical approach the system passes from one equilibrium state to another, while in glass transition it is transferred from a metastable state into a glassy, non-equilibrium one. This qualitative difference is also reflected in the Prigogine-Defay and Ehrenfest ratios, which are formally identical relations. The Ehrenfest ratio, which applies to second-order transitions, has been shown theoretically and experimentally to be equal to $\Pi_E = 1$ [19, 20]. In contrast, the values of the Prigogine-Defay ratio for the glass transition are typically $\Pi > 1$ [21]. This discrepancy in the values of Π is an additional verification of the fact that vitrification should not be treated as a second-order transition, but rather as a kinetic phenomenon.

Another experimental observation that reinforces the kinetic nature of the glass transition, is the dependence of the T_g on the applied cooling rate, which defines the time scale of the experiment. More precisely, for lower cooling rates, the lower will also be the T_g. This can be understood better considering the molecular motions responsible for vitrification, whose time scale becomes increasingly larger by lowering the temperature. As a consequence, at lower temperatures the supercooled liquid requires larger times to maintain equilibrium [22].

1.2.2 Dynamics of glass transition and molecular mobility

According to experimental observations, glass transition occurs when the system is unable to perform -in the observation time scale imposed by the cooling rate- the molecular rearrangement that would allow the supercooled liquid to remain in a relative equilibrium [5]. In the supercooled regime, its viscosity increases dramatically with the decrease of temperature and as a result, the slowing down of the relaxation time, τ, of spontaneous fluctuations is recorded [23]. The process related to such slowing down of τ is commonly called *α- relaxation*. The dynamics of the glass transition in the different glass-formers is conventionally characterized by the attributes strong or fragile, a classification that was first introduced by Angell (1985) [24].

By plotting the logarithm of the viscosity or the relaxation time as a function of the reciprocal temperature, we obtain curves with different degrees of non-Arrhenius behavior. The Arrhenius law for the relaxation time (or the viscosity) is expressed mathematicallly as :

$$\tau = \tau_0 exp\left(\frac{E_a}{k_B T}\right) \tag{1.4}$$

where τ_0 is a pre-exponential factor, E_a the activation energy of any thermally activated process and k_B the Boltzmann constant. A plot of the logarithm of τ as the one described above, would give a straight line for Eq. 1.4 and the glass formers that can be well-described by a simple Arrhenius law are characterized as *strong*. Eq.1.4 implies that strong glass formers are characterized by a constant activation energy, which is independent of the temperature. On the other hand, the glasses that highly deviate from the Arrhenius law are called *fragile* and their activation energy increases with decreasing temperature. An appropriate description of τ in this case is provided by the Vogel-Fulcher-Tammann (VFT) equation [25–27]:

$$\tau = \tau_0 exp\left(\frac{B}{T - T_0}\right) \tag{1.5}$$

where τ_0 the pre-exponential factor, B the Vogel activation energy and T_0 the so-called Vogel temperature, which is usually located 30-70 degrees below T_g [28].

The rapidity of the increase of the relaxation time with decreasing temperature is called dynamic fragility of the glass former [29] and the most common measuring parameter is the steepness index which is expressed as [30]:

$$m = \left(\frac{\partial log\tau}{\partial(T_g/T)}\right)_{T=T_g} \tag{1.6}$$

Typically, the strong liquids are inorganic glass-formers, while the fragile ones include mostly polymers. In Fig. 1.3 a plot of the temperature dependence of the logarithm of the viscosity is shown, published by Angell [24], where there is a clear distinction in the behavior of strong and fragile glass formers. Specifically, the more fragile the glass-former is, the more it deviates from the Arrhenius-like behavior, introducing a very rapid slowing down of the molecular mobility below the T_g.

A variety of experimental techniques provide measurements of the molecular

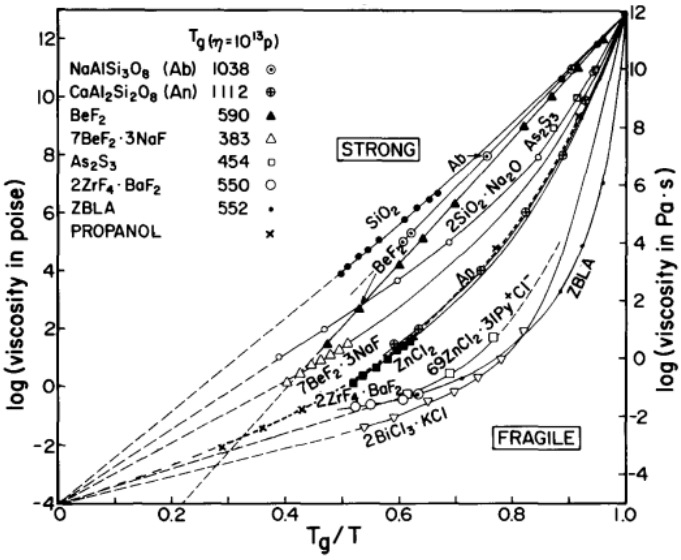

FIGURE 1.3: Data of the temperature dependence of the viscosity, η, of various glass-forming liquids, as published by Angell [24].

mobility by applying a linear perturbation to the system, such as dynamical mechanic analysis, broadband dielectric spectroscopy, specific heat dynamic measurements, neutron scattering, light scattering etc. Here, it is crucial to distinguish between the *equilibrium glass dynamics* and the *non-equilibrium dynamics* and emphasize their conceptual difference. For the study of the former, which is also known as "dynamic glass transition", the experimental protocol should fulfill the fluctuation dissipation theorem (DFT) of statistical physics [31, 32]. According to this, the amplitudes of the external perturbations should be smaller than the spontaneous fluctuations. This delivers the so-called "linear" or equilibrium response of the system, which allows the study of the time scale of the linear relaxation of the property being probed. On the other hand, if the applied perturbation is larger than the spontaneous fluctuations, the liquid is taken to a thermodynamic state different from the one corresponding to equilibrium, giving rise to the so-called "thermal glass transition". This can be achieved experimentally by applying a temperature ramp in calorimetry measurements and monitoring the way the perturbed property recovers equilibrium.

1.3 Physical aging

Due to the kinetic nature of vitrification, as it has been mentioned above, from a thermodynamic point of view, a glass is a non-equilibrium system with respect both to the crystalline state and the supercooled liquid (see Fig. 1.2). This entails that in the

glassy state, there is an excess in the thermodynamic properties (H, S, V) compared to the supercooled liquid and thus, the system will spontaneously evolve toward the closest equilibrium, that is, the supercooled equilibrium state. This phenomenon is addressed as *structural recovery* [33, 34] or *physical aging* [35, 36]. Thermodynamically, this is an exotherm process and is characterized by a decrease in enthalpy, entropy and volume. In this way, the glass becomes more structurally ordered and its volume shrinks.

The main consequence of physical aging is that it is accompanied by a change in the mechanical, dielectric, magnetic and optical properties of a glass. The natural consequence of this slow yet irreversible process, is the alteration of the functional properties of a wide range of materials that are industrially manufactured and used in various applications. Among those, polymer-based materials, which during the last decades have been increasingly employed in many aspects of everyday life, are reported to be particularly susceptible to the effects of physical aging. For instance, for Poly(Lactic acid) (PLA)- a well-known biopolymer and a good candidate for packaging and engineering applications- it was found that aging leads to a pronounced increase in stiffness and the development of internal stresses, eventually resulting in brittle failure[37]. Similarly, aging in chalogenide glasses, which are useful in electronics and as biosensors owing to their exceptional optical properties, have been reported to show a decrease in microhardness due to aging [38]. Taking all this into account, it is clear that the study and thorough understanding of the kinetics of physical aging is of utmost importance for the development of materials with the tailored properties and long-term stability, ensuring they meet their performance standards throughout their predicted lifetime.

1.3.1 Study of the kinetics of physical aging via monitoring thermodynamic properties

The kinetics of physical aging generally depend on the time scale of the instantaneous fluctuations and on the distance of the instantaneous thermodynamic state of the glass from equilibrium. The thermodynamic state of the glass is usually defined by using the concept of the fictive temperature, T_f, which, as mentioned above, was first introduced by Tool [11] and then implemented by Moynihan [39], who came up with a methodology to estimate its value. This method is based on the definition of the fictive temperature as the intersection of the glassy line drawn from a given thermodynamic state of the glass, with the extrapolated supercooled liquid line, as seen in Fig. 1.4.

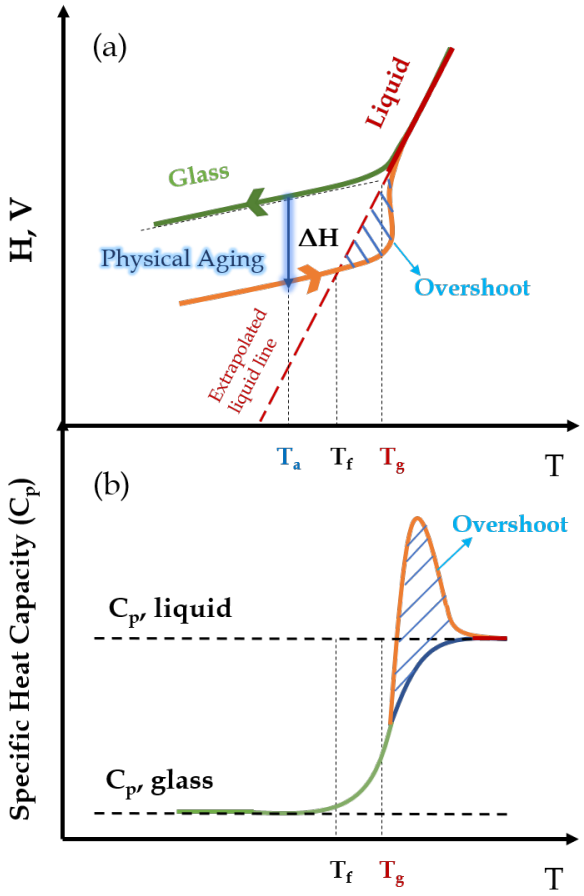

FIGURE 1.4: Schematic illustration of the (a) enthalpy and (b) specific heat capacity recovery of a glass-forming system during physical aging (T_a: aging temperature, T_f: fictive temperature, T_g: glass transition temperature).

The study of the kinetics of equilibrium recovery of the glass in the aging regime provides valuable information about the dynamics of the system below T_g. This can be achieved by monitoring the time evolution of a thermodynamic property, the enthalpy for instance, by means of calorimetry. As can be observed in Fig. 1.4 the enthalpy of a glass that has previously undergone aging, recovers equilibrium on heating. When a glass ages, it acquires a denser and more ordered structure, that results in the loss of molecular mobility and an increase in the relaxation time. Thus, the longer the glass ages, the larger is the overshoot that appears in the enthalpy recovery or the heat capacity, as can be seen in Fig. 1.5 (a). This overshoot is proportional to the enthalpy loss on aging and it delivers information on the energy released.

If we consider a normalized recovery function $\Phi(t) = (P(t) - P_0)/(P_\infty - P_0)$ of

any property P sensitive to physical aging (for instance, the volume (V) or enthalpy (H), as in Fig. 1.4 (a)) and study its time evolution, we will observe that it exhibits a sigmoidal form, as shown schematically in Fig. 1.5 (b) and it is usually described by the Kohlrausch-Williams-Watts (KWW) equation:

$$\Phi(t) = exp\left[-\left(\frac{t}{\tau_{ag}}\right)^{\beta_{KWW}}\right] \tag{1.7}$$

where $\beta_{KWW} < 1$ is the stretching exponent and τ_{ag} a characteristic time of the physical aging. In general, aging performed slightly below the T_g is uniquely associated to the α- relaxation. Given these premises, the τ_{ag} can be related to the typical time scale of the α- relaxation and this gives rise to one of the basic characteristics of the physical aging, which is its non-exponentiality.

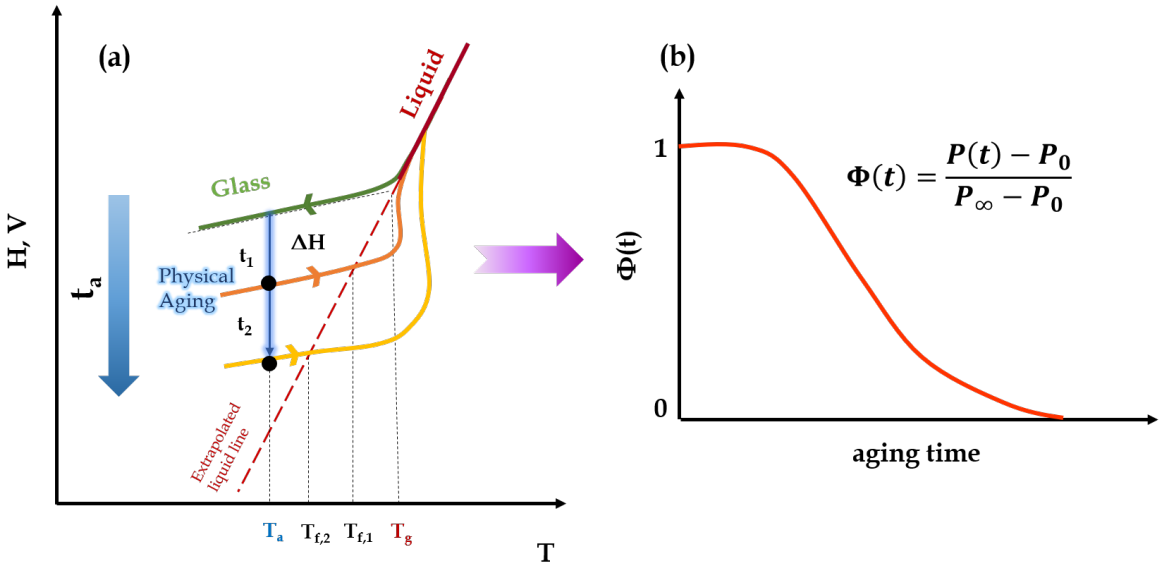

FIGURE 1.5: (a) The increase of the overshoot in the enthalpy recovery for longer aging times ($t_1 < t_2$) (T_a: aging temperature, $T_{f,1}$: fictive temperature for aging time t_1, $T_{f,2}$: fictive temperature for aging time t_2, T_g: glass transition temperature). (b) The normalized recovery function of any property $P(t)$ sensitive to physical aging.

The approach to equilibrium entails an increase in the density of the glass, which is the cause of the second basic feature of physical aging, its non-linearity. Particularly, the density increase will provoke an increase in the τ_{ag} of Eq. 1.7 as well. As a result, this non-linear nature induces an additional stretching apart from the one induced by the KWW equation, in such a way that the kinetics of aging encompass many decades of aging time. The non-exponentiality and non-linearity

of physical aging are incorporated in different models, like the Kovacs-Huchinson-Aklonis-Ramos (KAHR) [40] and the Tool-Narayanaswamy-Moynihan (TNM) [41].

It is commonly accepted that the mechanism that mediates the kinetics of both vitrification and physical aging, is the main α- relaxation with the super-Arrhenius temperature dependence. Concerning vitrification, studies have been focused on the cooling rate-dependent glass transition temperature, T_g and the temperature-dependent α- relaxation time, τ_α. Experiments conducted both for low-molecular-weight glasses [42, 43] and for polymers [44–46] revealed that the cooling rate-dependent glass transition follows the same super-Arrhenius behavior as the τ_α. As for physical aging, studies that involve thermal [47–50] or dielectric [51] non-linear perturbations in the proximity of T_g, demonstrate that the typical time scale has the same behavior as τ_α.

In recent years, nonetheless, the universal description of these phenomena by the α- relaxation has been disputed, since there is numerous evidence suggesting its inadequacy in certain conditions. Such cases include experiments on vitrification kinetics of metallic glasses in a wide range of cooling rates, where it was shown that vitrification was taking place at lower temperatures than predicted by the α- relaxation [52]. The same behavior has been observed for metallic [53] and polymeric [54] glass formers under geometrical confinement as well.

Concerning physical aging, there is also a plethora of experimental results that suggest that the simple case of the α- relaxation being the only mechanism driving the system to the closest equilibrium state needs to be reconsidered. According to studies carried out in polymeric [55–57], metallic [58, 59], chalcogenide [60] and simple molecule glass formers [61, 62], the kinetics of physical aging towards equilibrium exhibit at least two steps when it takes place far below T_g. In polymers, for instance, aging experiments performed in a broad range of aging temperatures and times, revealed the existence of a slow and a fast step [55]. The former was associated with the α- relaxation, the latter, however, exhibited a temperature-independent activation energy, as shown in Fig. 1.6, which reinforces the scenario of the existence of at least one different molecular mechanism at short aging times.

Despite all the above, a systematic study of the multiple equilibration mechanisms that seem to govern physical aging, has been until recently elusive, especially in small-molecule glass-formers. Among them, van-der-Waals liquids are an excellent choice for the study of vitrification, owing to their special nature. More

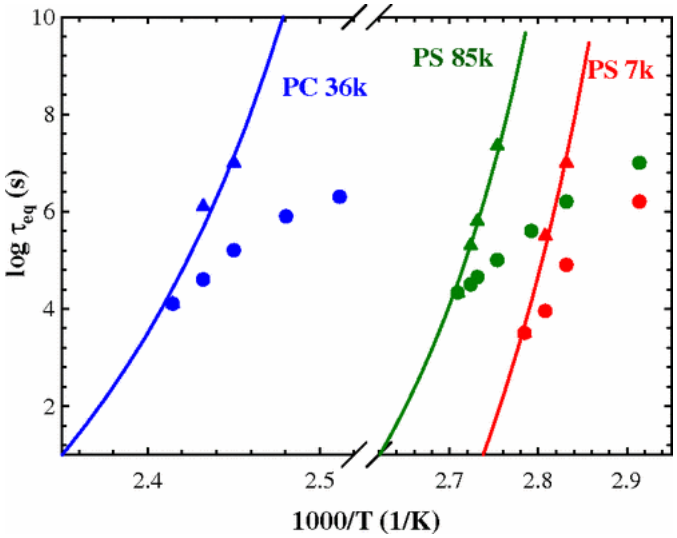

FIGURE 1.6: Logarithm of equilibration times corresponding to the two steps of equilibration as a function of the inverse temperature for PC 36k, (polycarbonate, $M_n = 36$ kg/mol), PS 85k, (polystyrene, $M_n = 85$ kg/mol) and PS 7k, (polystyrene, $M_n = 7$ kg/mol). A splitting (merging) scenario is evident resulting from the presence of a single equilibration mechanism at relatively high temperatures and a double decay recovery at lower temperatures. The equilibration mechanism with the higher activation energy can be fitted by VFT equation (lines). Reprinted from [55].

precisely, van-der-Waals liquids are characterized by the dominant role of the short-range repulsive intermolecular forces in determining the structural arrangement of the molecules in the liquid, while neglecting the influence of longer-range attractive interactions. This practically means that average relative arrangements and motions in such liquids are determined by local packing and steric effects, while attractive forces, dipole-dipole interactions and other slowly-varying interactions play a minor role [63]. In this framework, the effect of the attractive forces can be seen as a mean field that exerts no intermolecular force and thus, has no effect on the structure or dynamics, providing only the cohesive energy required to ensure the stability of the system at a particular density and pressure.

1.4 Methodological Tools for the Study of Physical Aging

In this section we will discuss the principal methodological tools that were employed in this work for the study and modelling of physical aging.

1.4.1 Density scaling approach

A physical description of vitrification that focuses on the energy landscape, takes into account that the cooling of a liquid causes the gradual decrease of its thermal energy and the entrapment in potential wells. The slowing down of the dynamics then results from the progressive decrease of the available configurations. For isobaric measurements, two convoluted factors determine the number of the accessible configurations: (i) the changes in the thermal energy which determine the accessible region of the energy landscape and (ii) the changes of the energy landscape itself, due to the changes in the intermolecular distances and the subsequent variation of density with temperature [64, 65].

The relative importance of these two factors, i.e. the temperature (T) and the volume (V), cannot be resolved experimentally by a simple variation of the former, since both of them would be affected. Experiments during which the pressure was used as a variable and volume could be changed while maintaining temperature constant, showed that for the majority of glass formers, neither temperature nor volume is the dominant variable for the determination of the temperature-dependent relaxation times. Therefore, these results rather suggest that a suitable function of these two quantities is required for a unique representation of the relaxation times and/or viscosities.

Studies of inelastic neutron scattering under high pressure for *o*-terpehnyl (OTP) [66], which is a fragile glass former, demonstrated that its behavior can be modeled as soft spheres ineteracting with an r^{-12} repulsive potential. This yields a combined scaling variable proportional to $T^{-1}V^{-4}$, which was also found to adequately describe light-scattering data for the same material, thereby providing an effective rescaling onto a master curve [67]. Nevertheless, when an extension of this scaling to other materials was attempted, such as in 1,1'-di(4-methoxy-5-methylphenyl) cyclohexane (BMMPC) [68] and D-sorbitol [69] it was found that superposition could not be achieved. This led to the consideration of the potential r^{-12} as a special case of a more general $r^{-3\gamma}$ interaction energy. In such a case, the scaling employed for OTP can be seen as a specific application of a general relation $log\tau \propto T^{-1}V^{-\gamma}$, where γ a material constant applied to various glass formers.

This hypothesis proved to be effective for a wide range of materials, including representatives of different kinds of prototypical glass formers, such as strong van der Waals liquids, moderately fragile van der Waals liquids, H-bonded liquids, polymers. In Fig. 1.7 dielectric relaxation times measured at different temperature and

pressure conditions are plotted versus $T^{-1}V^{-\gamma}$, with γ being adjusted adequately to achieve superposition of the curves. It is clearly seen that for a certain material-specific constant, γ, a master curve is obtained, that encloses many decades of frequency under very different temperature and volume conditions.

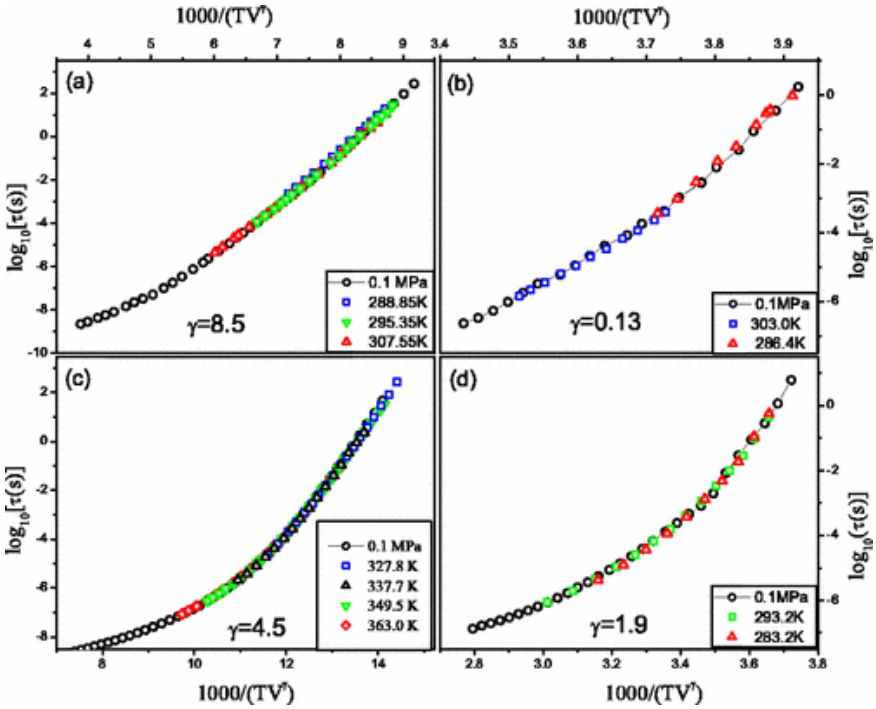

FIGURE 1.7: Dielectric relaxation times vs the scaling variable $T^{-1}V^{-\gamma}$ for (a) BMMPC, (b) PDE, (c) d-Sorbitol and (d) 1,2-PB. Data were obtained for varying temperature at atmospheric pressure $P = 0.1MPa$ and varying pressure at constant temperature. Reprinted from [64].

The exponent γ accounts for the volume contribution to the dynamics of the system. For systems where the thermal energy has a strictly dominant role, $\gamma = 0$, while for the hard sphere limit, $\gamma \to \infty$ [70, 71]. In this framework, we can consider a simple dependence of the relaxation time, τ, on V and T, which can be expressed as:

$$\tau(T, V) = \tau_0 exp\left(\frac{C}{TV^{\gamma}}\right) \tag{1.8}$$

where τ_0 the pre-exponential factor and C a material-specific constant.

All the above demonstrate that a large class of glass formers obeys density scaling in equilibrium. However, the application of this methodology in out-of-equilibrium conditions has been long debated. More specifically, the validity of the density scaling in such systems has been challenged by simulations in isochoric conditions,

which indicate that the relaxation time or any other related observable changes even when both temperature and volume remain constant [72–75].

Another theoretical approach for the description of the relaxation time (or equivalently the relaxation rate, which is the inverse of the relaxation time) of an out-of-equilibrium system suggested by Niss [76, 77], employs the concepts of the fictive temperature and the isomorph theory. The latter was introduced by Dyre and co-workers [78, 79] and holds for strongly correlated liquids where the repulsive short-range interactions dominate over intermolecular forces (as in van der Waals liquids). According to this theory, for two macroscopic points (ρ_1, T_1) and (ρ_2, T_2) on an isomorph, if the positions of the particles are described by a vector $\overrightarrow{R}$, then for any two microstates for which it holds that $\overrightarrow{R}_1\rho_1^{1/3} = \overrightarrow{R}_2\rho_2^{1/3}$, they have proportional Boltzmann factors, $e^{-U(\overrightarrow{R}_1)/k_BT_1} = C_{12}e^{-U(\overrightarrow{R}_2)/k_BT_2}$ -where U the potential energy- and thus, they will have the same probability. Therefore, it follows from this approach that for equilibrium systems, the relaxation time and the scaling variable, referred to as Γ in their work, remain constant along the isomorph.

Concerning the application of the isomorph theory in physical aging, an isobaric quench to the glassy state was considered, during which the structure only marginally changes, but the density and the enthalpy do. This is in agreement with the concept of the fictive temperature and it is attributed to the glassy expansion coefficient and the glassy heat capacity that allow for an isostructural contraction of the sample. In other words, the relative positions of all particles remain the same and in terms of position vectors, this gives $\overrightarrow{R}_{liq}\rho_{liq}^{1/3} = \overrightarrow{R}_{glass}\rho_{glass}^{1/3}$. Since in equilibrium the scaling variable remains constant along the isomorph, the idea was to define a fictive scaling variable, Γ_{fic}, which would remain constant when the structure does not change. In this framework, for systems that obey the density scaling in equilibrium, in the glassy state the relaxation times could be expressed in terms of this fictive scaling variable. The only two requirements in this description is that $\Gamma_{fic} = \Gamma$ in the equilibrium limit and the equilibrium behavior of the relaxation time be recovered. The relaxation time in this approach is written as a function of both the fictive scaling parameter, Γ_{fic} and the equilibrium value, Γ, leading to:

$$\tau(\Gamma, \Gamma_{fic}) = \tau_0 exp(\Gamma F(\Gamma_{fic})) \tag{1.9}$$

where F a system-dependent function describing the scaled activation energy. Thus, according to this analysis, the description of the non-equilibrium phase diagram of density, temperature and at least one non-equiliibrium parameter collapses to the two dimensions defined by Γ and Γ_{fic} [77].

1.4.2 Single Parameter Aging (SPA) model

Another method to define an expression for the relaxation time during physical aging is the implementation of the Single Parameter Aging model (SPA), which accounts for the concept of the material time. This idea, which was introduced in the 1970s [40, 41], supports that aging becomes linear when it is described in terms of the material time, $\xi(t)$, instead of the laboratory time, t. The material time corresponds to the time measured by a clock with a rate that reflects the state of the system, which results in the non-linearity of physical aging [40, 41, 80, 81]. It can be perceived as an analogous to the time recorded on a clock following the observer in the theory of relativity. This concept has been shown to provide a good description of the physical aging involving small temperature variations [82].

To achieve a connection between the laboratory and material time, the time-dependent aging rate, $\gamma(t)$ was introduced and it was defined by:

$$\gamma(t) = \frac{d\xi}{dt} \tag{1.10}$$

In equilibrium, the aging rate is equal to the relaxation rate, γ_{eq}, which is the inverse of the equlibrium relaxation time, τ_{eq}. If we express $\gamma(t)$ as the inverse of the relaxation time during aging, eq. 1.10 can be rewritten as:

$$d\xi = \tau^{-1}dt \tag{1.11}$$

According to the Single Parameter Aging ansatz, the aging rate or equivalently the relaxation time during aging, τ, is controlled by the measured quantity that describes the thermodynamic state of the glass. In the present thesis, the property monitored during physical aging is the fictive temperature, T_f. Thus, in the simplest scenario where the time dependence of τ is assumed to be linear with the thermodynamic state of the glass, SPA can be expressed as:

$$log\tau = log\tau_{eq} + \Lambda(T_f(t) - T_{f,eq}) \tag{1.12}$$

where, τ_{eq} and $T_{f,eq}$ the values at equilibrium for the relaxation time and the fictive temperature, respectively. If, additionally, we take into account that when equilibrium is achieved T_f is equal to the aging temperature, T_a, eq. 1.12 can be rewritten as:

$$log\tau = log\tau_{eq} + \Lambda(T_f(t) - T_a) \tag{1.13}$$

In the equation above, Λ is a single-fitting parameter that depends only on the substance and the monitored property. It should be pointed out that eq. 1.13 is derived from first-order Taylor expansions and therefore, it is expected to be applicable only for small temperature variations.

1.4.3 Study of the kinetics of physical aging via Isoconversional methodology

Isoconversional kinetics analysis is a model-free approach, capable of unraveling the activation energies associated with the different stages of the glass equilibration, providing this way information about the molecular mechanisms that mediate physical aging. This methodology has been already extensively employed in the study of a wide range of chemical reactions, such as polymerization, cross-linking, thermal and thermo-oxidative degradation and crystallization/melting processes [83]. The application of Isoconversional analysis in the study of physical aging was first introduced by Vyazovkin [10, 84, 85].

In this type of analysis, individual Arrhenius equations are applied to evaluate the effective activation energy at different extents of the conversion. On this basis, complex temperature dependences which may involve a change in the principal relaxation process or the emergence of additional ones, can be revealed via the systematic variation of the activation energy with conversion.

One of the major advantages of isoconversional analysis is the fact that it is not restricted only to processes that follow simple Arrhenius kinetics, but actually it is an excellent tool for the study of non-Arrhenius processes as well, such as those typically involved in glass trnasition and physical aging.

Isoconversional kinetics provide a system of methods that facilitate the calculation of the kinetic triplet, i.e. the activation energy (E_a), the pre-exponential factor and the transformation model, allowing at the same time making kinetic predictions and obtaining mechanistic insights. These methods are particularly useful when the transformation mechanism is unknown or when complex reactions involving several steps take place. The main advantage of this methodology resides in the assessment of the activation energy at any level of conversion during the transformation. The latter can be measured with thermoanalytical techniques, the most common of which are thermogravimetric analysis (TGA), differential scanning calorimetry (DSC) and dielectric relaxation spectroscopy (DRS) [83].

As a general rule, the isoconversional method requires performing a series of experiments, where the transformation under investigation is followed at different temperatures and times. Subsequently, these kinetic data are analyzed to obtain the values of the activation energy as a function of coversion, X, which, for aging data is usually expressed as the extent of relaxation, $R = 1 - X$. The activation energy at a given conversion, E_R, can be obtained considering the variation with temperature of the time to reach such an extent of relaxation, t_R, in isothermal kinetics data:

$$E_R = k_B \left[\frac{\partial \ln t_R}{\partial T^{-1}} \right]_R \tag{1.14}$$

where k_B the Boltzmann constant.

In the present thesis, isoconversional analysis is performed by studying the enthalpy evolution toward equilibrium via calorimetry. The extent of enthalpy change is quantified via the fictive temperature, T_f, and thus the extent of relaxation can be written as:

$$R(t) = \frac{T_f(t) - T_a}{T_f(0) - T_a} \tag{1.15}$$

where $T_f(t)$ and $T_f(0)$ the time-dependent fictive temperature and the one at the beginning of the process, respectively, and T_a the aging temperature.

1.5 Viscoelastic behavior of polymer networks

This section provides a brief introduction to the concept of the dynamic covalent bonds and the thermal events that take place in polymer networks. Particular emphasis is placed on vitrimeric materials, which constitute a special class of polymer networks and the characteristic thermal processes observed in these systems, which have been the focus of the final part of the present thesis.

1.5.1 Covalent adaptable networks (CANs)

In recent years, the incorporation of dynamic (or reversible) chemical bonds into cross-linked polymer networks has emerged as an effective strategy for the development of materials with enhanced functionalities, such as plasticity, reprocessability, self-healing, and recyclability [86–90]. A bond is considered dynamic if it can undergo reversible dissociation and reassociation under appropriate conditions. Such

bonds can be broadly classified into two categories: non-covalent bonds and dynamic covalent bonds (DCBs). The former include ionic interactions, hydrogen bonds, van der Waals forces, and $\pi - \pi$ interactions, whereas the latter involve covalent bonding, in which electron pairs are shared between atoms. Dynamic covalent bonds remain stable within the required range of operating conditions, but they can reversibly dissociate and rearrange in response to external stimuli, such as changes in temperature, solvent environment, pH, or exposure to UV radiation [86, 87]. Polymer networks incorporating DCBs are commonly referred to as dynamic covalent polymer networks or Covalent Adaptable Networks (CANs) [91–93].

Depending on their exchange mechanism, CANs can be classified into two groups; the first group includes those CANs that make use of a *dissociative* cross-link exchange mechanism, which entails that chemical bonds are first broken and then formed again at another position, as can be seen n Fig. 1.8 (a). The second group is characterized by associative bond exchanges between the polymer chains, during which the cross-link breaks only when a new covalent bond has already been formed in another position [94, 95]. In this second case, which will be the one under study here, the polymer networks are characterized by a fixed cross-link density, making them both permanent and dynamic (Fig. 1.8 (b)).

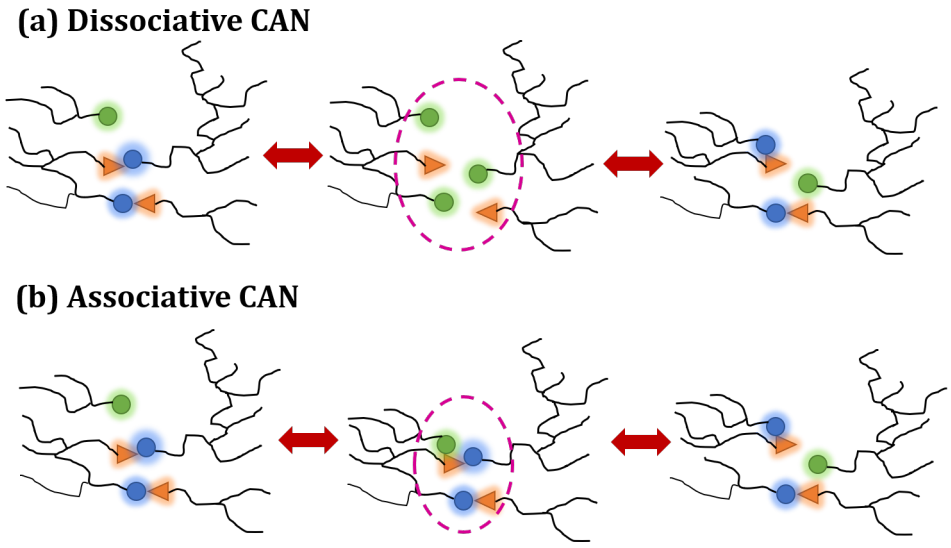

FIGURE 1.8: Schematic illustration of (a) a dissociative CAN, where the network integrity is lost in the intermedium stage and (b) an associative CAN, where the cross-link density remains fixed at all stages.

1.5.2 Vitrimers

In 2011, Leibler and co-workers developed a new kind of associative CANs by adding a suitable transesterification catalyst to polyester-based networks [96]. This resulted in permanent polyester/polyol networks that show a gradual viscosity decrease upon heating, which is typical behavior of vitreous silica [8] and had never been observed before in organic polymers. These materials were named *vitrimers* [97] and after extensive studies [98, 99], a few criteria were proposed for their identification. According to them, vitrimers are made of covalently bound chains forming organic networks, which are able to change their topology *via* exchange reactions that are associative in nature and thermally triggered. At higher temperatures, the viscosity of vitrimers is mainly controlled by the exchange reactions, which give rise to a decrease in viscocity with an Arrhenius-like temperature dependence. This is a distinctive feature of the associative CANs with respect to the dissociative ones, since for the latter, the transition from solid to liquid is much more abrupt, following the Williams-Landel-Ferry (WLF) model for thermoplastics.

The viscoelastic behavior of the vitrimers is described by two distinct transition temperatures. The first one is the glass transition temperature,T_g, which marks the transition from the glassy to the rubbery state of the polymer networks and it is associated with the onset of the long-range molecular mobility. The second transiton temperature is related with the dynamic bond exchange reactions within the network and the consequent rearrangements of its topology. These processes become relevant when the characteristic timescale of the bond exchange becomes shorter than that correspondng to the deformation of the material. As a result, the material undergoes a transition from the viscoelastic solid to the viscoelastic liquid at a temperature commonly referred to as topology freezing transition or vitrimer transition temperature, T_v, a concept introduced by Leibler and co-workers. This transition is coventionally determined at the temperature where a viscosity of 10^{12} $Pa \cdot s$ is reached [96, 100].

For a better understanding of the relevance between the T_g and T_v, two cases of vitrimeric systems will be presented below. In the first case, which is shown in Fig. 1.9 (a), we consider a system for which it holds $T_g < T_v$. Upon heating from a starting temperature $T < T_g$ to a temperature between T_g and T_v, the material will undergo a transition from the glassy to the rubbery state and it will behave as an elastomer. In this temperature range, the exchange reactions are still slow, so the network structure is practically fixed. On further heating, the exchange reactions

speed up and become relevant at temperatures $T > T_v$, where the elastomer transforms into a viscoelastic liquid. In this state, the flow is principally controlled by the exchange reactions, reulting into a typical Arrhenius-like decrease of viscosity.

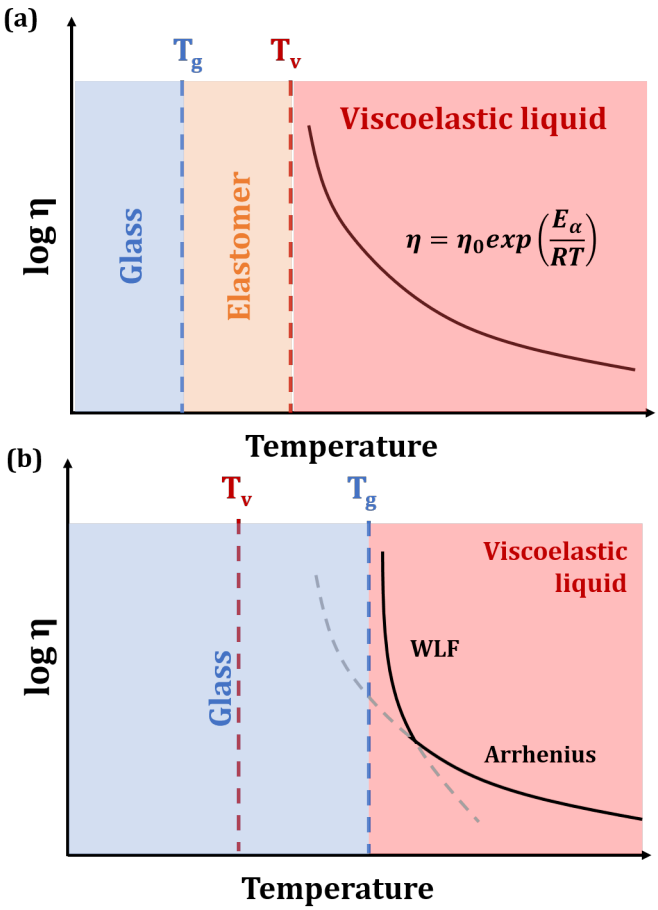

FIGURE 1.9: Schematic illustration of the viscoelastic behavior of a vitrimer with (a) $T_g < T_v$ and (b) $T_g > T_v$.

In the second case we consider a vitrimeric system where $T_g > T_v$, i.e. fast exchange reactions are embedded in a rigid polymer matrix. Under these conditions, the vitrimeric transition is only hypothetical, since the network is not frozen by the exchange reactions, but by the the lack of segmental mobility associated with the T_g. In this case, the calculation of the T_v can be performed *via* extrapolation of stress-relaxation or creep experiments. More precisely, at $T < T_g$, no segmental motion takes place, and thus, no exchange reaction can occur either, so the network remains frozen. Upon heating above T_g, the segmental motions are initiated, whereas the exchange reactions are already fast. In this initial stage, the network rearrangement kinetics are controlled by diffusion and the network topology rearrangement is dominated by segmental motions, which results in WLF viscosity behavior. On further heating, the exchange kinetics switch from a diffusion-controlled regime to

an exchange reaction controlled regime, following the Arrhenius law. This behavior is displayed in Fig. 1.9 (b).

The transition temperatures, T_g and T_v, can be controlled through parameters such as the cross-link density, the nature of the covalent bonds, the density of exchangeable bonds and groups, the rigidity of the monomers and the catalyst loading [86, 101].

One of the major challenges in the field of vitrimeric materials has been the accurate determination of the topology freezing transition temperature, T_v. As mentioned above, the original method for estimating T_v relies on the extrapolation of the viscosity up to a value of 10^{12} $Pa \cdot s$. However, this approach can introduce significant errors when the extrapolation is performed over a wide temperature range. From a thermodynamic viewpoint, the vitrimeric transition activates translational and rotational degrees of freedom in a way analogous to the glass transition. Therefore, it is expected to observe a step-like increase in thermodynamic coefficients (thermal expansion coefficient, specific heat capacity, for instance) at this temperature when methods that provide first-order thermodynamic properties, such as dilatometry or calorimetry are employed. Nevertheless, the simultaneous estimation of both T_g and T_v has in most cases been unattainable -apart from some exceptions [98, 102]. The possible factors thought to be responsible for that are: (i) the proximity between T_g and T_v that does not allow their separation *via* conventional methods, such as standard dilatomoetry or differential calorimetry (DSC) that operate in rates of the order of K min^{-1} and (ii) the wide temperature range over which the step-like variation of the thermodynamic coefficients may be distributed during the vitrimeric transformation, which complicates the accurate determination of T_v. These experimental limitations may be overcome by extending the heating/cooling rates of the experiments and/or tailoring the thermal protocols so as to enhance the contribution of the thermal event under investigation, which has been explored in the final part of this thesis.

1.6 Goals of This Thesis

As stated previously, the nature of glasses has remained ambiguous to this day and has been at the center of theoretical and experimental investigation during many decades. Hence, the general goal of this thesis is to achieve a deep understanding of the dynamics of the glassy state across a broad range of materials with varying degree of complexity, including small molecules, polymers, and cross-linked polymer networks. To this end, we have employed calorimetric techniques to study the kinetics of glass transition, which is associated with the transformation of a supercooled liquid into a glass and the subsequent reduction of the free energy of the glass to the closest equilibrium state, known as physical aging.

Specifically, this work has focused on two fundamental topics. The first one, is related to small molecule glass formers interacting *via* Van der Waals forces deeply quenched in the glassy state. Numerous studies in polymeric, metallic, chalgogenide and other glasses have recorded multiple steps, apart from the α- relaxation, in the kinetics of physical aging, especially when the latter takes place far from T_g. Considering this and the scarce relevant information available for Van der Waals glass formers, our objective was to challenge the sufficiency of the α- relaxation for the description of the kinetics of the recovery of equilibrium in these materials.

The first step to this direction, entailed the study of the kinetics of physical aging over a wide temperature range in five representative Van der Waals molecules, monitoring the time evolution of their glassy enthalpic state. This was achieved by means of Fast Scanning Calorimetry, which gives access to a wide range of aging times and two approaches were used; a model-independent one, based on the time to reach equilibrium, and a modified version of the Single Parameter Aging (SPA) model, that incorporates the density scaling, accounting for the non-linearity of physical aging. This is described in detail in the first publication that makes part of this thesis.

The next step was to gain insights into the aging time-dependent thermal barriers in glasses evolving towards equilibrium. To this aim, we have applied isoconversional analysis not only on the small molecules previously studied, but also on a few polymeric glasses. This kinetic approach is known for its ability to unravel the activation energies associated with different stages of glass equilibration, thereby providing information on the molecular mechanisms that mediate physical aging as a function of the thermodynamic state of the glass. Isoconversional analysis has

been applied extensively in the study of the kinetics of chemical reactions, including polymerization, cross-linking etc. and it is not restricted to the processes that obey simple Arrhenius kinetics. Thus, it bears great potential to disentangle the multiple mechanisms that are expected to be involved in physical aging. The results of this analysis are included in the second publication annexed to this thesis.

As a complementary test, we investigated the validity of density scaling in out-of-equilibrium glasses by analyzing the physical aging of an archetypal molecular glass former through broadband dielectric spectroscopy. Specifically, during isothermal aging below the glass transition temperature, T_g, we simultaneously tracked the dielectric loss on the high-frequency flank of the α- relaxation and the high-frequency value of the capacitance, reflecting glass densification and we studied the evolution of the two observables. The methodology and the outcome of this work is analyzed in the pre-print publication, included in the Appendix A.

The second thematical section of this work addresses systems of greater chemical complexity and more precisely, branched polymer networks cross-linked through reversible enamine bonds forming vitrimers. A relevant parameter of these systems is the topology freezing or vitrimer transition temperature, T_v, above which the vitrimers undergo a topological transition from viscoelastic solid to viscoelastic liquid and its reliable determination still remains an open question, particularly by means of calorimetry. So far, the simultaneous determination of T_g and T_v *via* standard calorimetry has remained elusive, mainly due to the proximity of the two values, which makes their separation challenging at such low heating/cooling rates. Thus, here we employed Fast Scanning Calorimetry for the first time in such systems, aiming to reduce the experimetntal time scale and we developed experimental protocols that facilitate the separation of the glass and vitrimeric transitions. Finally, a further step was taken to define the activation energy of the vitrimeric transformation. These findings are described in the third publication included in the thesis.

Chapter 2

Materials and Experimental Techniques

2.1 Materials

2.1.1 Van der Waals glass formers and polymers

Fig. 2.1 presents the Van der Waals glass formers that were used for the application of the density scaling approach and the SPA model. These very same materials were also studied by means of the Isoconversional method, along with some polymer glasses that are shown in Fig. 2.2.

Van der Waals liquids					
Short name	**KDE**	**PDE**	**OTP**	**BMMPC**	**BMPC**
Full Name	**o-cresolphthalein dimethyl ether**	**phenolphthalein dimethyl ether**	***o*-terphenyl**	**1,1-bis (4-methoxyphenyl) cyclohexane**	**1,1-di(*p*-methoxyphenyl) cyclohexane**
Chemical Structure	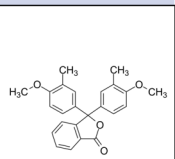	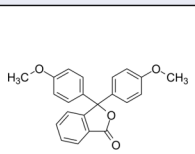	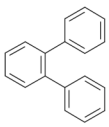	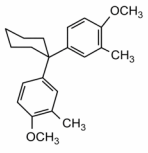	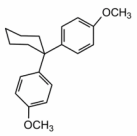

FIGURE 2.1: Name and chemical structure of the Van der Waals glass formers studied in the framework of the present thesis.

2.1.2 Vitrimeric materials

For the development of the vitrimeric materials that were studied in the third part of this thesis, enamine Dynamic Covalent Bonds (DCBs) were used. More precisely, branched polyglycerol (PG), which has multiple hydroxyl groups and a branched

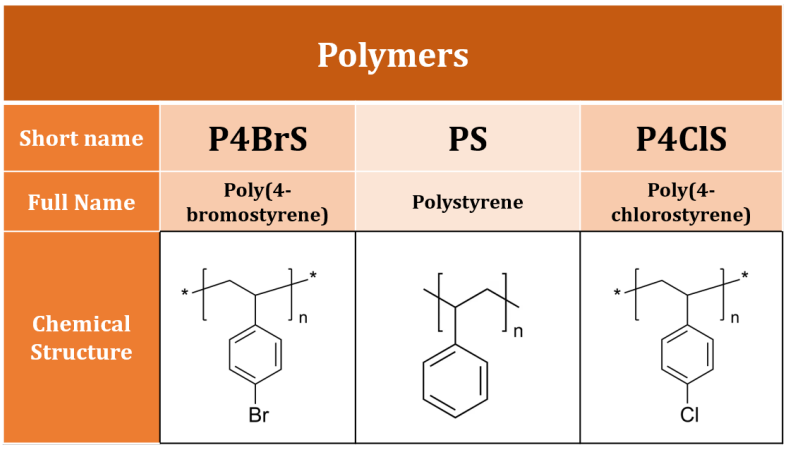

FIGURE 2.2: Name and chemical structure of the polymer glasses studied in the framework of the present thesis.

structure, was functionalized with β-ketoester groups via a transesterification reaction with *tert*-butyl acetoacetate (TBAA). In this way, polymer networks cross-linked through enamine DCBs based on β-ketoester-functionalized branched polyglycerol (PG-βkest) and three different diamines, i.e. DAP (1,3-diaminopropane), EDO (2, 2′-(ethylenedioxy) bis(ethylamine)) and Jeff (Jeffamine D230), were synthesized. The synthesis is shown schematically in Fig. 2.3. Analytical details about the conditions and the specific procedure of the synthesis are displayed in the experimental section of the relevant publication included in Chapter 3.

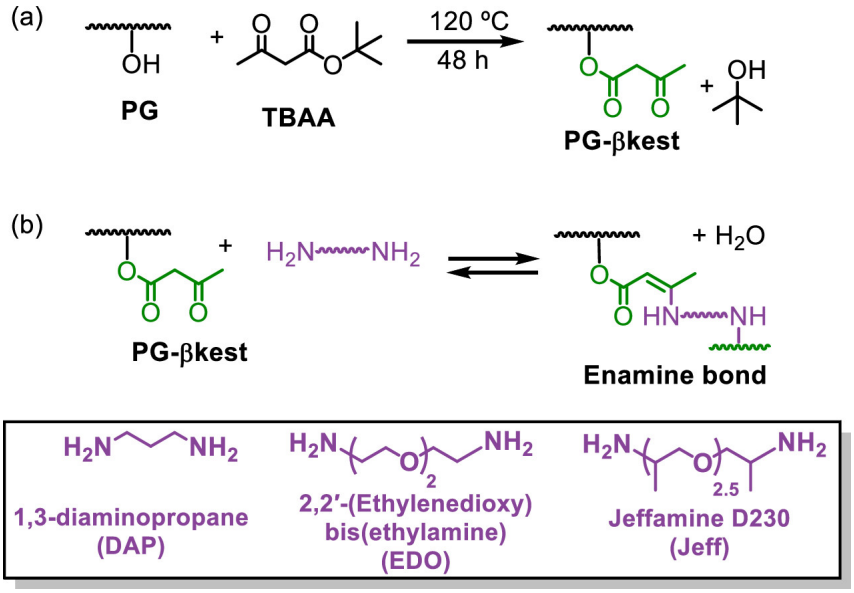

FIGURE 2.3: (a) Functionalization of PG with TBAA. (b) Formation of Enamine bonds by reaction of PG-βkest with a diamine. In the box at the bottom: Diamines used in present study.

2.2 Introduction to Thermal Analysis

Thermal analysis includes all kinds of experimental techniques that measure a material´s response to a thermal protocol, during which the material under study can undergo heating, cooling or isothermal aging [103]. The objective is to study how temperature is connected to specific physical properties, which here are mostly connected to the glass transition and the physical aging of various systems. Among the most suitable techniques for the observation of such phenomena, calorimetry and dielectric spectroscopy stand out. By calorimetry, it is possible to measure the heat flow, which is the flow of energy into or out of the sample as a function of temperature or time [104]. More precisely, the heat flow rate difference between a substance and a reference is measured as a function of temperature, while the sample is being subjected to a specific temperature program. On the other hand, dielectric spectroscopy allows the measurement of the change in the physical properties of polar materials, such as polarization, permittivity and conductivity with temperature or frequency. The basis of these methods is the reorientation of the material´s dipoles and the movement of charged particles when alternating current (AC) is applied and the complex permittivity (ϵ^*) is measured in the frequency or time domain at a constant or changing temperature [28]. In the present thesis, the combination of these two experimental methods enabled the study of the aging of the materials under study in temperatures slighlty lower than the T_g.

2.3 Basic principles of Calorimetry

Calorimetry is a well-known technique that facilitates the direct mesurement of the heat associated with physical transitions and chemical reactions. When speaking of calorimetric measurements, Differential Scanning Calorimetry (DSC) is the most popular method, used in a broad range of fields, including polymers science, plastics, pharmaceuticals, glasses, ceramics, proteins, etc. [104–106]. The operation of DSC involves the subjection of the sample to a heat signal and measure its response in terms of the energy and temperature of the thermal events that take place in the temperature range or time interval of the experiment [105]. More precisely, the energy changes which the sample and the reference undergo during a specific thermal protocol, are measured with a DSC calorimeter, along with the temperatures at which they occur. These changes enable the detection of characteristic temperatures at which physical transitions take place and the performance of a quantitative study of processes such as melting, crystallization, glass transition and other complex events [104, 107].

DSC data are usually illustrated in terms of power as a function of temperature. A typical DSC thermogram represents the heat flow (power) required to raise the temperature of the sample as much as needed in order to keep up with the heating program. Thus, it is easily understood that heat flow has to be a function of the heat capacity of the sample, C_p, since this parameter indicates the energy required to raise the temperature of the sample by 1K.

Mathematically, the DSC signal can be expressed as:

$$\frac{dQ}{dt} = C_p \cdot \frac{dT}{dt} \tag{2.1}$$

where dQ/dt is the heat flow rate and and dT/dt is the heating (or cooling) rate. Equation 2.1 can also be written as:

$$\frac{dQ}{dt} = m \cdot c_p \cdot \frac{dT}{dt} \tag{2.2}$$

where m is the mass of the sample and c_p its specific heat capacity.

2.3.1 Standard DSC

Standard DSC experiments can be performed with two types of instruments: the *heat flux* and *power compensation*.

The heat flux DSC (Fig. 2.4) is made up of a cell that contains the reference and sample holders, in the form of two elevated platforms connected by a bridge that allows heat transfer. On top of these holders, the reference and sample pans are placed, respectively. Below each platform, a temperature sensor is located and the cell is connected to a furnace that supplies heat. An inert gas, also known as purge gas, flows through the cell. The cell is designed in such a way, so that the heat paths from the furnace to the sample and the reference are identical and stable in both cases. The equation for the heat flow rate from the furnace to each pan is given by:

$$\frac{dQ}{dt} = \frac{\Delta T}{R} \tag{2.3}$$

where ΔT is the temperature difference between the furnace and each pan and R the thermal resistance of the heat path between the furnace and the pan.

From equation 2.3 it is clear that the temperature difference between the sample and the reference, is a measure of the difference in the heat flow rate, which results from the presence or not of the sample in the pans. When a heating program is initiated at a linear rate, the sample and reference pans are also heated linearly.

As the heat capacity of the sample is higher as a consequence of the bigger mass, its temperature will lag behind in a greater extent compared to the empty reference pan. If the pan masses are identical, the temperature differences between the furnace and the each pan can provide information about the heat capacity of the sample. If additionally a thermal event takes place in the sample (i.e. melting, crystallization, glass transition) its temperature will not change or it will change in a non-linear way, while the reference will keep being heated linearly. Once the thermal event is completed, the temperature of the sample starts increasing linearly again. In this case, the temperature differences supply insghts into the latent heat of the thermal event [105, 107, 108].

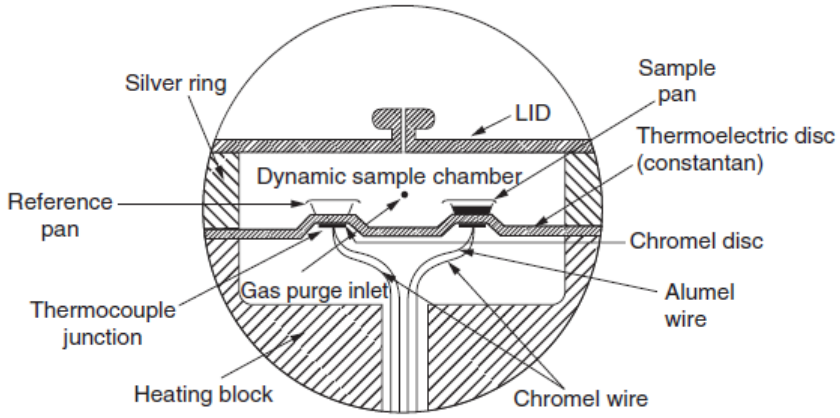

FIGURE 2.4: Intersection of a heat-flux type DSC cell [107].

On the other hand, a *power compensation* DSC (Fig. 2.5) has one furnace for the sample and a second for the reference, separated from each other. Both furnaces follow the same temperature program and the difference of the supplied electric power is measured. Since the only difference between them is the presence of the sample, the differential signal provides information about the thermal properties of the substance under study. When one of the pans has higher heat capacity, (which normally is the sample pan due to the bigger mass), its heating will be slower and it will lag behind the reference. The signal of this difference in temperature is sent to a differential amplifier, which supplies extra power to the lagging pan so as to re-establish the balance and equalize the temperatures between the two recipients [107].

In the present thesis, the standard DSC experiments were performed by means of the heat-flux-type calorimeter, Q2000 by TA Instruments, which is equipped with an intracooler and operates in a temperature range between 193 K and 873 K. The temperature control is achieved by purging dry nitrogen into the oven at a flow rate

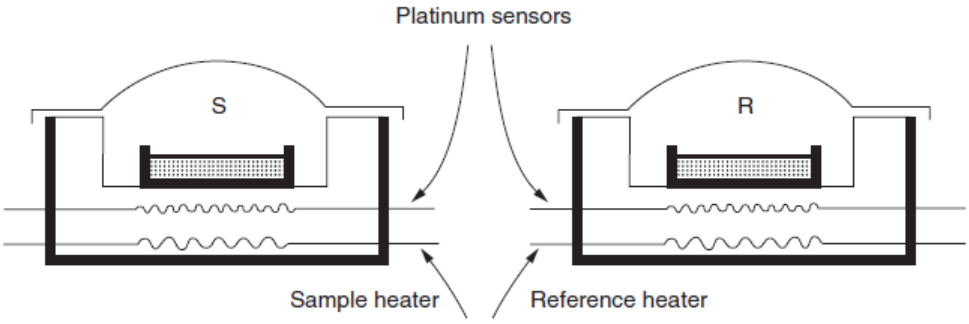

FIGURE 2.5: Typical power compensation DSC sample holders with twin furnaces and sensors [107].

of 50 ml/min. The measured samples had a mass of approximaetely 10 mg and they were placed in 40 μl aluminum pans without a lid.

2.3.2 Fast Scanning Calorimetry

Since DSC techniques were introduced in the 1960s, the most commonly used scanning rate has been 10 K/min, which generally allows the observation of the most important thermal transitions, while slower rates have also been applied for better resolution. However, it has been challenging to perform experiments at rates faster than 20 K/min with such setups, due to two principal reasons, (i) the thermal lag developed at such rates can affect the accuracy of the temperature measurements and (ii) the thermal gradients across the sample mass would make the data unreliable.

In the decades that followed, the need for high scan rates, which would have a complementary role beside the existing low ones and give insights into new aspects of the material, kept growing. More specifically, the awareness (or speculation) of the existence of a rather large number of processes that occur much faster than the conventional rates of 10 K/min and the kinetics of which are extremely difficult to be explored with Standard DSC, urged the development of methods for the application of faster scans [104, 109]. An important step to this direction was the development of High Performance DSC, which was commercially distributed by PerkinElmer under the the name 'HyperDSC' and it could achieve scan rates up to 750 $^oC/min$ [110]. Later, TA Instruments created also the rapid scanning DSC from the project RHC, reaching rates up to 2000 $^oC/min$ [111]. Nevertheless, the most remarkable breakthrough was the development of chip-based calorimeters operating at extremely fast rates, as has been reported by Allen et al. [112] or Schick et al. [113]. Performing

experiments with this type of Fast Scanning Calorimeters (FSC) in such high rates, demands a drastic reduction in the sample mass, from the mg that are used in standard DSC to micrograms or nanograms, in order to minimize thermal lags.

In this framework, Mettler-Toledo came up with the Flash DSC 1 calorimeter (Fig. 2.6), which was designed and commercialized for the needs of investigation both on academic and industrial level. This instrument, where the FSC experiments for the present were performed, uses MEMS (Micro-Electro-Mechanical Systems) sensor technology which broadens the scan rate operating window to more than 8 orders of magnitude, partly overlapping with the standard DSC. It is operating in a temperature range between 173 K and 723 K and the scanning rates vary between 0.1 to 4000 K/s on cooling and 0.5 to 40000 K/s on heating [109].

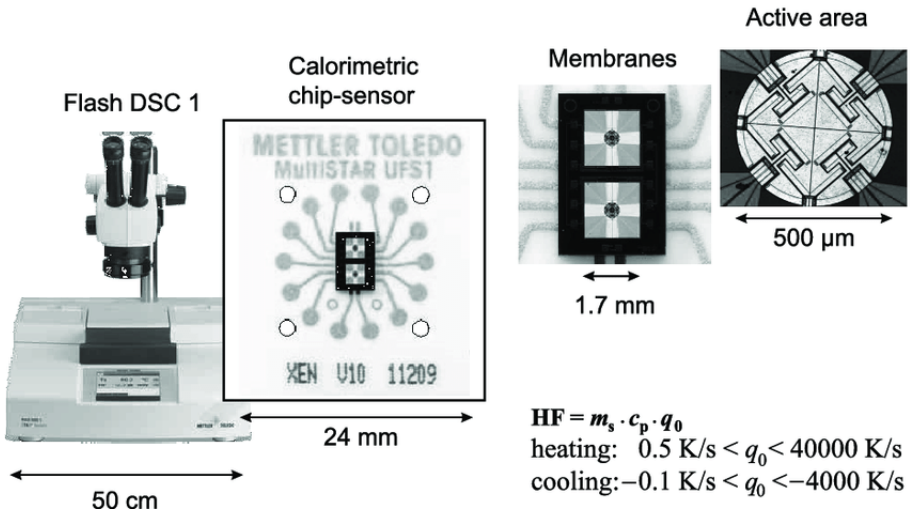

FIGURE 2.6: The Flash DSC 1 by Mettler-Toledo and the chip-sensor MultiSTAR UFS1 in different magnifications [114].

For the fulfillment of the differential character of the technique, the microchip UFS 1 with a twin sensor was developed and can be seen in Fig. 2.6. This chip is made up of two identical quadratic membranes of silicon nitride with a length of 1.6 mm each and a total thickness of approximately 2 μm and it is placed on a ceramic support. On the opposite side of the membrane, there is a dielectric layer of silicon oxide. The sample area is located in the middle of the membrane, with a diameter of 0.5 mm, and it is coated with an aluminum layer that ensures the homogeneous distribution of temperature [109, 115]. Eight thermocouples measure the temperature of each membrane. The sample chamber is purged with liquid nitrogen, although other gases can be used as well, so as to avoid the condensation of water in atmosphere. In addition, the calorimeter is equipped with a Huber TC100 intracooler

for the temperature control, a Leica M60 optical microscope for the deposition of the sample and the revision of the chip quality and a Leica IC80 HD camera that allows the instantaneous observation of the deposition and the acquirement of micrographs.

The two furnaces of the UFS1 chip are independent and the calorimeter operates in a power-compensated mode. This entails that the temperature difference for both furnaces equals zero and the the electrical power required to maintain this state is measured. When a new chip is used, it is necessary to calibrate it. The first step is to perform the *conditioning*, the goal of which is to heat the sensor to the maximum temperature in order to delete possible memory effects and test the behavior of the sensor [115]. The thermal protocol includes the heating of an empty sensor at 100 K/s from room temperature (318 K) up to 723 K, an isotherm of 4 s at this high temperature, then cooling at the same rate down to 318 K and finally an isotherm of 4 s. This process is repeated until the heat fow rate curves of two consecutive experiments coincide, which usually takes up to 4-5 repetitions. The conditionings can be performed at standby temperature, which means with an open lid. After that, the *correction* is to be performed. This procedure has to be performed at closed FSC lid and the temperature must be equilibrated at the ready temperature, which in this case is 173 K. Even small deviations from the ready temperature can affect the accuracy of the temperature measurements later. The correction begins with an isotherm of 0.1 s at 173 K and goes on with a heating at 550 K/s up to 723 K and a last isotherm for 1 s. In this way, the thermocouple signal (T_s) is corrected with respect to the actual cold-junction temperature (T_{ss}) (see Fig. 2.7) [114].

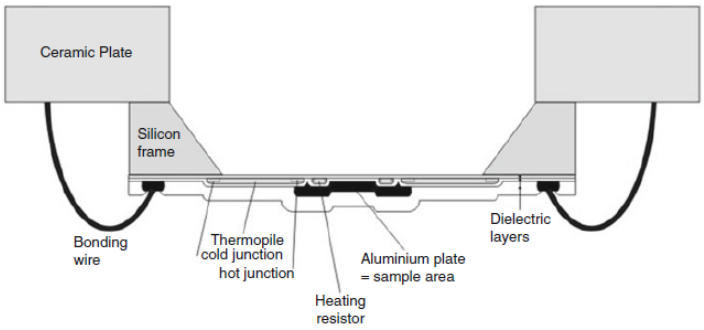

FIGURE 2.7: Schematic cross-section of the chip-sensor MultiSTAR UFS1 [114].

Concerning the thermal lag, in Fast Scanning Calorimetry it depends almost exclusively on the sample and its contact to the sensor and more precisely, the main factors that affect it are the sample mass, its geometry, its thermal conductivity and

the scanning rate [115, 116]. As it was mentioned above, running experiments at rates of the order of 1000 K/s requires small sample masses, from a few nanograms to no more than a few hundreds of nanograms. Also, from a technical point of view, only the part of the sample that is directly in contact with the sensor exhibits the temperature of the thermocouple. For this reason, ideally the samples should be in the form of films. If this is not possible, a method that can improve the thermal contact is the introduction of a medium between the sample and the chip. This was partly applied in the present thesis, when vitrimeric polymer networks were studied and polydimethylsiloxane (PDMS) was used to improve the thermal contact.

The determination of sample masses of the order of some hundreds of nanograms cannot be achieved even with the most accurate balances. Thus, the mass can only be estimated by considering thermal properties, like the melting enthalpy, the glass transition step or the heat capacity in a given thermodynamic state [114].

In this work, the mass was calculated -when needed- from the heat flow rate step in the temperature range of the glass transtiiton, $\Delta HF(T_g)$. From equation 2.2, $\Delta HF(T_g)$ can be written as:

$$\Delta HF(T_g) = m \cdot \Delta c_p(T_g) \cdot \frac{dT}{dt} \tag{2.4}$$

$\Delta c_p(T_g)$ can be found from experiments with the Standard DSC, as long as it is possible to prepare an amorphous sample (by quenching from melt, for instance). Then the sample mass, m, can be easily estimated from equation 2.4.

2.3.3 Thermal protocols and data analysis

The fictive temperature (T_f) is a fundamental concept for the study of physical aging and consequently, it is important to be able to determine it accurately. As it was described in Chapter 1, fictive temperature was initially introduced by Tool in 1946 [117] and it is defined as the intersection of the extrapolated glass line with the extrapolated liquid line. It is calculated by the Moynihan or so-called matching-area method [39], according to which, the T_f has to obey the following property: the area included between the liquid and glass specific heat, should match the area included between the experimental and liquid specific heat (Fig. 2.8). This can be expressed mathematically as:

$$\int_{T_f}^{T>>T_g} (c_{pm} - c_{pg})\, dT = \int_{T<<T_g}^{T>>T_g} (c_p - c_{pg})\, dT \tag{2.5}$$

where c_{pm} and c_{pg} are the melt and glass specific heat capacities respectively and c_p the experimental specific heat capacity.

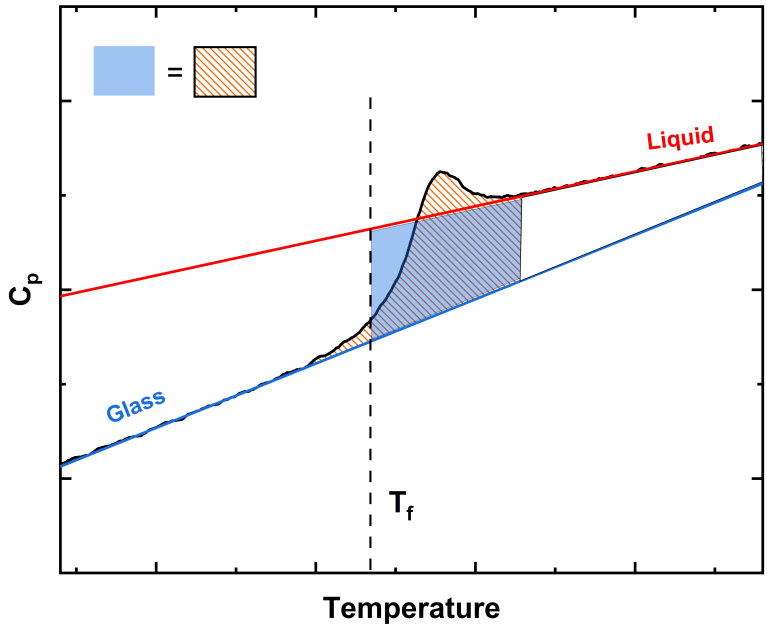

FIGURE 2.8: Schematic representation of the Moynihan method.

For single measurements, the application of the Moynihan method is quite straightforward and it only depends on the correct selection of the glass and liquid lines (Fig. 2.8). Nonetheless, for thermal protocols that include varying cooling rates or isothermal aging at different aging times (see Fig. 2.9), the calculation of the T_f might be more complex, because of the baseline mismatch among different scans. The procedure to overcome this challenge consists in the realignment of the calorimetric scans, that is (a) the change of the slope and/or (b) the vertical shift of a given c_p scan to the reference, c_p^{Ref}, which corresponds to the heating scan for zero aging time, obtained at heating a glass immediately after supercooling.

Another factor that urges the superposition of all glass and liquid lines to the ones of the reference, is the calculation of the recovered enthaply, ΔH, which is given by:

$$\Delta H = \int_{T_{min}}^{T_{max}} (c_p(T) - c_p^{Ref}(T))\, dT \tag{2.6}$$

where T_{min} and T_{max} are the temperatures that include the range of the enthalpic recovery.

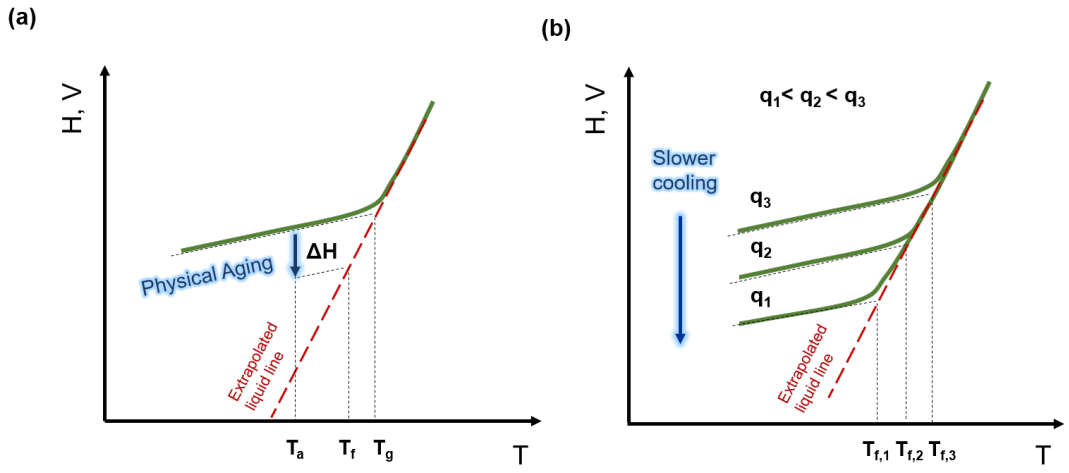

FIGURE 2.9: Schematic illustration for the thermal protocols of (a) physical aging and (b) cooling-rate-dependent vitrification.

Performing the superposition of the curves manually demands tedious calculations and it can be time-consuming, for this reason the VITRIFAST method, which was developed by Abate et al [118], was employed for this thesis. This method defines in the first place the model function that describes the corrected curve of the specific heat, $c_p^{New}(T)$, with respect to the measured aged one, $c_p^{Aged}(T)$, as follows:

$$c_p^{New}(a,b,T) = S(a,T) \cdot c_p^{Aged}(T) + b \tag{2.7}$$

The function $S(a,T)$ accounts for the change of the slope, while the parameter b is responsible for the vertical shift. Thus, the correction of the aged curve basically involves the adjustment of the two parameters, a and b. I t should be noted here that although the formalism of the specific heat is used, this methodology is applied also for heat flow rate data, as the fictive temperature computations require no knowledge of the sample mass. The optimization of the parameters is carried out by the least-squares fitting, performed with the Python programming language. The goal is to minimize the function $F(a,b,T)$ which is defined as:

$$F(a,b,T) = \sum_{i=0}^{N} \rho(f_i(a,b,T))^2 \tag{2.8}$$

where ρ is a loss function filtering the data in the temperature range the glass transition occurs and $f_i(a,b,T)$ is the $i-th$ component of the vector of residuals which correspond to the difference of the new, corrected specific heat, $c_p^{New}(T)$ and the reference one, $c_p^{Ref}(T)$ for all experimental points, N [118]. The latter can be mathematically expressed as:

$$f_i(a,b,T) = c_p^{New}(a,b,T) - c_p^{Ref}(T) \tag{2.9}$$

The physical meaning of this procedure is to minimize the difference between $c_p^{New}(T)$ and $c_p^{Ref}(T)$, so that they overlap for temperatures much below and above the T_g, where no thermal events take place.

After performing the correction, the next step is to calculate the enthalpy recovery from Equation 2.6, where the $c_p(T)$ corresponds to the specific heat capacity of the aged sample. This can be seen schematically in Fig. 2.10 (a) , where the recovered enthalpy is equal to the shaded area included between the reference and the aged curve. Equivalently, the enthalpy recovery can be calculated from the area between the excess of heat capacity of the aged asample and the baseline, as illustrated in Fig. 2.10 (b).

Another important tool for the calorimetric measurements, is the *step response analysis*, which is employed for the study of the dynamic heat capacity, c_p^*. This protocol was first introduced by Schick et al. [119, 120] and uses a single step in program temperature followed by an isothermal segment to obtain the spectrum of heat capacity. The c_p^* spectrum provides valuable information about the dynamic glass transition and the kinetics of reversible and irreversible processes. A periodic heating rate $q(t)$ that contains a delta function is applied to generate a uniform heat flow rate spectrum, which is equal to $A_q(\omega_k)$ for different frequencies $\omega_k = k\omega_0$ (where $\omega_0 = 2\pi/t_p$, t_p the basic period of $q(t)$ and k integer).

The temperature-time profile should consist in infinitely sharp single or multiple steps. The step-scan protocol that was applied in this work, includes a loop of down-jumps of $\Delta T = -2K$ at a nominal cooling/heating rate, β, followed by an isotherm of duration equal to t_{iso}. According to this, the base angular frequency is defined as:

$$\omega_0 = \frac{2\pi}{t_p} = \frac{2\pi}{t_{iso} + \Delta T/\beta} \tag{2.10}$$

Fig. 2.11 shows the applied thermal protocol and the obtained heat flow rate. Fig. 2.12 provides an example of the heat low rate response (upper panel) and a magnification of this response close to the baseline.

As shown in Equation 2.10, the total period of the stimulation, t_p, is computed as the sum of the isotherm and the time needed for the down-jump. The experiments were performed by means of both FSC and standard DSC, thus, the parameters vary in such a way so that $c_p^*(\omega, T)$ is studied in the widest frequency range available

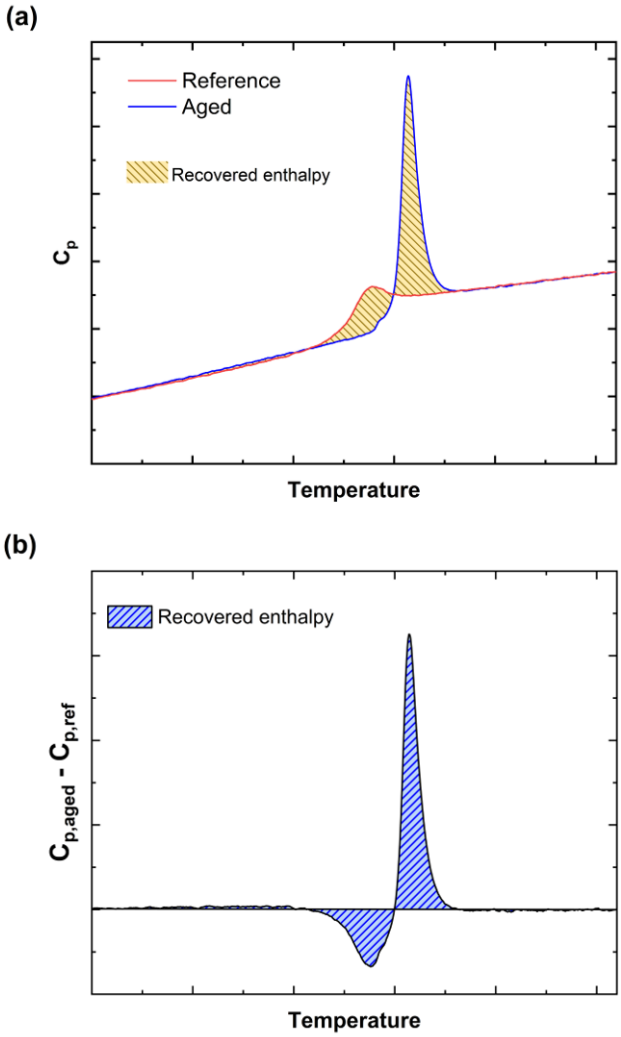

FIGURE 2.10: (a) Calorimetric scans of the specific heat capacity for the unaged (red) and aged (blue) sample (b) Excess of heat capacity of the aged sample corresponding to the measurement of (a). Data for PDE aged at 255 K for 20000 s.

and at the same time, good accuracy and low signal-to-noise ratio is maintained. The next step is to calculate the real (c_p') and imaginary part (c_p'') of the complex heat capacity, as well as the reversible specific heat, c_p^{rev}, which is the modulus of the complex heat capacity, for ω_0 and higher harmonics, $\omega = k\omega_0$. To achieve this, a Discrete Fast Fourier Transform (DFFT) is used, which has the form:

$$c_p^*(\omega) = c_p'(\omega) - ic_p''(\omega) = \frac{\sum_{t=0}^{t_p} HF(t)\exp(-i\omega t)\Delta t}{\sum_{t=0}^{t_p} q(t)\exp(-i\omega t)\Delta t} \tag{2.11}$$

where, $HF(T)$ and $q(t)$ are the instantaneous heat flow and cooling/heating rate, respectively.

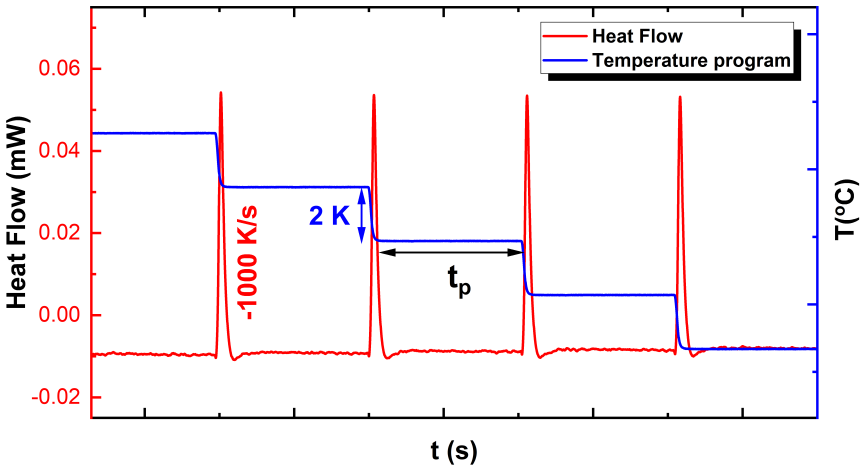

FIGURE 2.11: The step response thermal protocol (blue line) and the obtained heat flow rate (red line). The cooling rate was equal to -1000 K/s and t_p is the modulation period.

By running the DFFT for all the measured loops, it is possible to obtain the temperature dependence of the complex $c_p^*(\omega, T)$. Then, in order to find the temperature-dependent relaxation time, $\tau(T) = (2\pi\omega)^{-1}(T)$, the inflection point of the $c_p^{rev}(\omega, T)$, which is found easily from the position of the peak of its first derivative. The $c_p^{rev}(\omega, T)$ is almost equal to $c_p'(\omega, T)$, since the imaginary part, $c_p''(\omega, T)$ is at least one order of magnitude smaller.

It should be outlined here that step-scan response measurements yield simultaneously information about two aspects of the glass transition, the *thermal glass transition* or *vitrification* and the *dynamic glass transition*, which is a relaxation process. Athough they often tend to be considered identical, these are actually the responses to two independent perturbations: the thermal glass transition ($T_g(q)$) is the non-linear response to the underlying cooling rate while the dynamic glass transition ($T_g(\omega)$) is the linear response to the temperature modulation (see Fig. 2.13) [121]. The thermal glass transition can be evaluated by the total heat capacity, $C_{p,total}$, which is equal to:

$$C_{p,total} = \frac{\langle HF \rangle}{q_0} \tag{2.12}$$

where $\langle HF \rangle$ is the average heat flow over one modulation period and q_0 is the underlying heating/cooling rate.

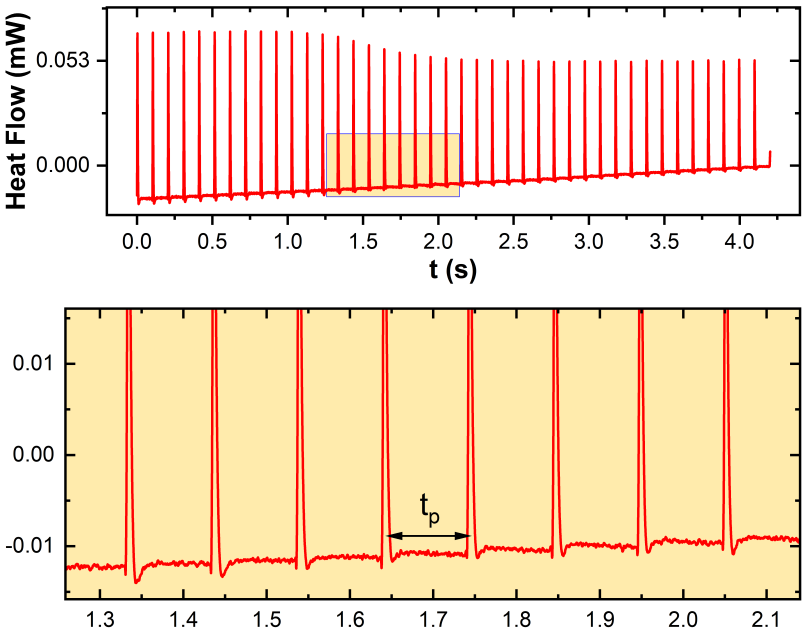

FIGURE 2.12: Upper panel: The heat flow rate response for BMMPC at cooling rate -1000 K/s and $t_p = 0.1024$ s. Lower panel: Magnification of the heat flow rate response.

Step-scan response experiments are focused on the complex $c_p^*(\omega)$, which, as can be seen in Fig. 2.13, is made up of two components, the real part, c_p' which is step-wise and the imaginary part, c_p'', that forms a peak. Sometimes, the contribution of the total heat capacity may overlap with that of the c_p' and make the study of the dynamic glass transition in equilibrium challenging. For this reason, it is important that the heating/cooling rate and the temperature jumps are small enough for the vitrification to be well-separated from the dynamic process and for the linearity conditions to be respected [121].

2.4 Dielectric spectroscopy

Dielectric Spectroscopy is utilized for the study of the properties of polar materials. Broadband Dielectric Spectroscopy (BDS) in particular, is a powerful technique that allows the study of the relaxation mechanisms that take place in a wide frequency range, approximately between 10^{-3} Hz and 10^{9} Hz. An oscillating electric field is applied and the reorientation of the dipoles of the material or the diffusion of charged particles, allow the evaluation of the complex permittivity, ϵ^*. This can be analyzed into its real and imaginary components, ϵ' and ϵ'', respectively, and thus be written as:

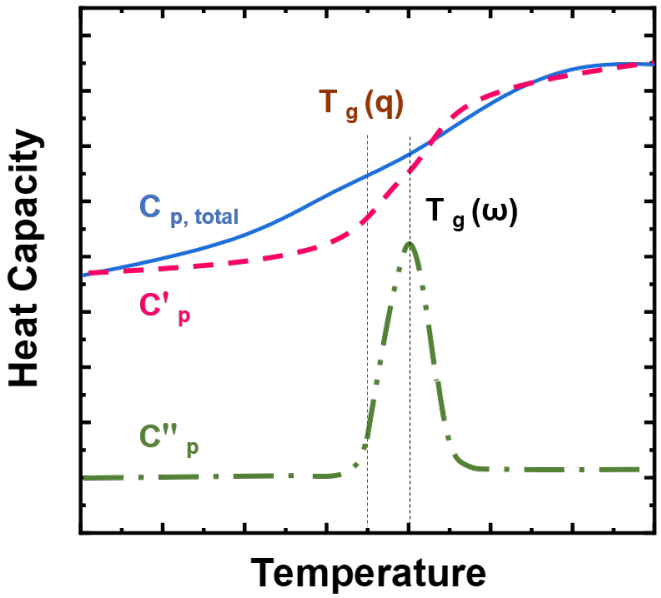

FIGURE 2.13: Calorimetric heat scan for PDE in Flash DSC 1 measured by the step response method at a period of t_p =1024 s (blue line). The deconvolution of the complex heat capacity, $C_{p,total}$ into the real part C'_p (pink dashed line) and the imaginary part, C''_p (green dashed-dotted line) is illustrated. $T_g(\omega)$ is the dynamic glass transition temperature determined by C'_p and C''_p, while $T_g(q)$ is the calorimetric glass transition temperature, determined by $C_{p,total}$.

$$\epsilon^*(\omega) = \epsilon'(\omega) - i\epsilon''(\omega) \tag{2.13}$$

where $i^2 = -1$. The real component is related to the ability of the material to store energy and it includes the contributions both of the vacuum and the real part of the susceptibility of the medium, whilst, the imaginary component expresses the energy losses that are exclusively connected to the medium. These parameters vary with the frequency of the applied voltage, which is known as *dispersion*.

For the measurement, the sample is located in the middle of a parallel-plate capacitor and an alternating voltage of angular frequency ω is applied. In this way, the complex impedance of the material, $Z^*(\omega)$, is measured and the complex capacitance $C^*(\omega)$ can be found as:

$$C^*(\omega) = \frac{-i}{\omega} Z^*(\omega) \tag{2.14}$$

The knowledge of the geometrical characteristics of the capacitor allows the calculation of the real part of the capacitance, C, which is expressed as:

$$C'(\omega) = \epsilon_0 \epsilon'(\omega) \frac{S}{d} \tag{2.15}$$

where S is the area of the cross-section, d the thickness of the capacitor and ϵ_0 the permittivity of the vacuum. Then, via eq. 2.15 the real component of the permittivity $\epsilon'(\omega)$ is obtained. For experiments conducted at very low frequencies, the system is completely relaxed as molecular motions take place at higher frequencies, consequently the storage part of the permittivity takes the value ϵ_s, which is known as static permittivity. If no other polarization phenomena are present, ϵ_s is the maximum value of ϵ', correponding to the orientation of all dipoles to the direction of the applied field.

If, on the other hand, the frequency of the electric field is higher than the ones of the different dipolar reorientation mechanisms, only the atomic and electronic polarizations contribute to the dielectric response and they result in the unrelaxed value of the real part of the permittivity, ϵ_∞. The knowledge of this value is important since it is connected to the density, ρ, of the system, via the Clausius-Mossotti equation:

$$\frac{\epsilon_\infty - \epsilon_0}{\epsilon_\infty + 2\epsilon_0} = \frac{4\pi N_A \alpha}{3} \frac{\rho}{M} \tag{2.16}$$

where ϵ_0 the vacuum permittivity, N_A the Avogadro number, α the polarization and M the molar mass. Relaxation processes that occur in intermediate frequencies, are characterized by a step-like decrease in the ϵ' and a peak in the ϵ''. Conduction phenomena are observed in the low frequency flank of the spectra and they show an increase of the imaginary part of the dielectric permittivity with decreasing frequency [28, 122].

2.4.1 Dielectric Spectroscopy and Aging

The typical behavior of the ϵ' and ϵ'' spectra for a system that undergoes physical aging is schematically portrayed in Fig. 2.14. If no other seconadary relaxation processes are present, only the α- relaxation process contributes to the dielectric response. Since such a system is an out-of-equilibrium glass, the dielectric spectra will only include the high-frequency flank of the α- relaxation, which is considered the principal mechasnism that mediates physical aging. The thermodynamic evolution of the glass to the closest equilibrium state gives rise to several modifications in the image of the spectra. First, as the molecular mobility decreases during aging, the α-

relaxation slows down and a shift to lower frequencies is observed [123, 124]. This shift also results in the decrease of the value of ϵ'' in intermediate frequencies, in accordance with previous reports from literature [124]. Concerning the real part of the permittivity, an increase in the value of ϵ_∞ is observed due to the densification of the aging system [125].

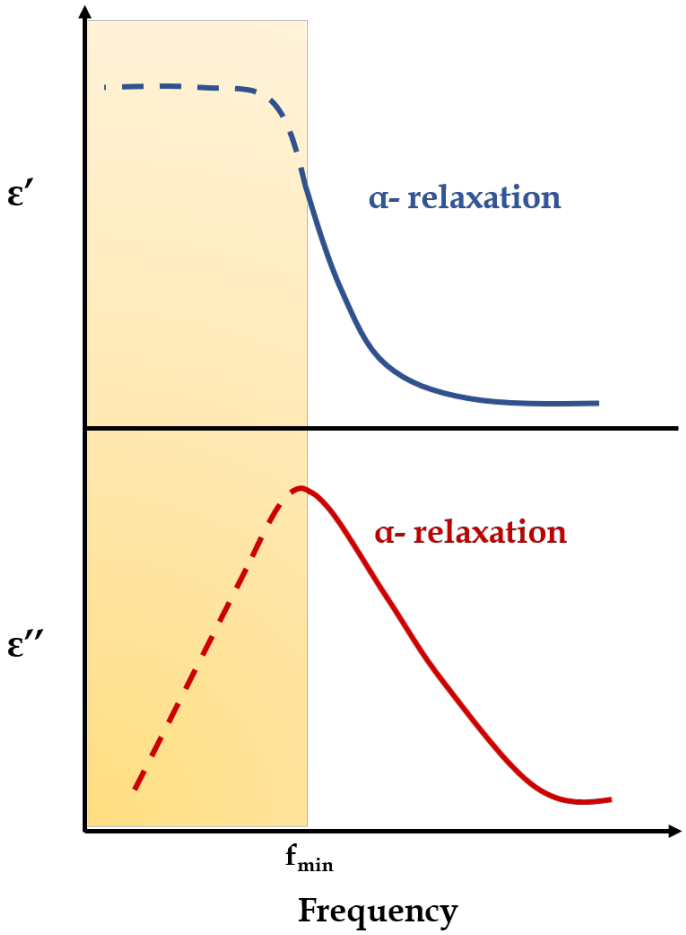

FIGURE 2.14: Schematic illustration of a typical dielectric spectrum for an aging system in terms of ϵ' (upper panel) and ϵ'' (lower panel). The dashed part represents the frequency range that cannot be accessed for the experimental timescale.

2.4.2 Sample preparation and experimental setup

For the measurements, nanocapacitors were used, where the dielectric medium was a thin film of the material under study sandwiched between aluminum electrodes. For the preparation of these capacitors, a thin layer of aluminum (Sigma-Aldrich, purity $\geq$ 99%) was placed on a circular glass substrate via physical vapor deposition. A small quantity of the material ($\sim$ 50 mg) was then dissolved in chloroform,

leading to the formation of solutions with a concentration of $\sim 3-5\%$ w/w, which were later spin-coated at a steady spinning rate and room temperature directly onto the lower electrode, creating this way the dielectric film. Before deposition, the solution was passed through a 0.4-μm polytetrafluoroethylene filter. Where necessary, after spin-coating, the sample was annealed at a temperature equal to $T_g + 15K$, for 20 min, to ensure the complete evaporation of residual chloroform. Afterwards, the upper electrode was added by depositing another layer of aluminum the same way the lower electrode was deposited. The final form of the sample can be seen schematically in Fig. 2.15. In the end, six independent capacitors are created for each substrate.

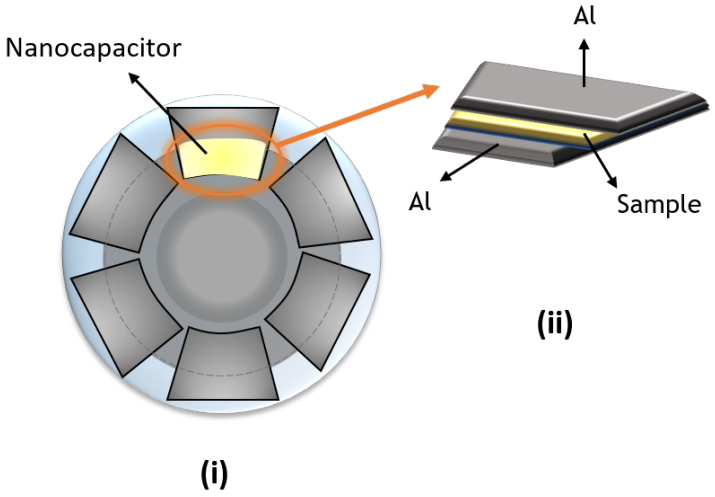

FIGURE 2.15: (i) Schematic illustration of the six nanocapacitors formed on the same glass substrate used for the BDS and aging experiments. (ii) Magnification of the sample sandwiched between the aluminum electrodes in one of the nanocapacitors.

The thickness of the films can be calculated by measuring the capacitance at room temperature considering a parallel plate approximation, from the equation $C_\infty = \epsilon_\infty \epsilon_0 (S/d)$, where C_∞ and ϵ_∞ are the capacitance and dielectric permittivity, respectively, of the sample at high frequencies and temperatures much below T_g, where no polarization takes place, $\epsilon_0 = 8.85 \cdot 10^{-12}\ Fm^{-1}$ is the vacuum permittivity, S the area of the electrode surface and d the thickness of the dielectric medium. The area was easily measured by means of optical microscopy. Typical values for the area are $\sim 5 \cdot 10^{-6}\ m^2$ and thickness was approximately 0.15 μm for KDE and 0.35 μm for P4CS. The advantage of using such small sample thicknesses for the dielectric experiments, is the suppression of the contributions of electrode polarization, which often conceal relaxation processes that are observed in the low-frequency and high-temperature region [122, 126, 127]. After the sample preparation, each one of

the nanocapacitors was tested and only those that were not affected by an electrical shortcut were eligible for the experiments.

BDS experiments were then performed under isothermal conditions, in a frequency range between 0.1 Hz and 1 MHz, using an impedance analyzer (ModuLab XM MTS, Solartron Analytical) and the complex capacitance, C^*, was delivered as $C^* = \frac{1}{j2\pi f Z^*}$.

The experimental setup used for the aging experiments consisted of a furnace with four sample slots, which could be heated independently at temperatures higher than ambient temperature. Once placed in the furnace, the sample started to shift positions automatically, according to the program written by the user, to achieve a progressive increase in its temperature. In this way, the sample was eventually heated up to some $T > T_g + 20K$ and left there to anneal long enough to reach equilibrium. Then, a down-jump at $\sim 5\,\mathrm{K\,s^{-1}}$ took place until a temperature T_{ag} was reached, where $T_g - 10K \leq T_{ag} \leq T_g$. The sample underwent physical aging at T_{ag}, until it approached equilibrium. An Alpha impedance analyzer was used for the analysis of the dielectric signal and the delivery of the real and imaginary part of the capacitance. Up to about 1000 s, only three frequencies (25 Hz, 5 kHz and 10 kHz) were recorded and after that the full spectrum was measured, from 0.1 Hz to 10^5 Hz. The combination of these data provided the time evolutions of the real part of the capacitance, C' at high frequencies and of the imaginary part of the capacitance, C'' at low frequencies, which convey invaluable information about the volume recovery and polarization mechanisms, respectively.

Chapter 3

Overview of the results

This chapter summarizes the main findings of the published works that are part of this thesis.

3.1 The study of physical aging in small molecular glasses via the Single Parameter Aging (SPA) model

3.1.1 Introduction

This article explores the kinetics of the physical aging of five small molecular glass-formers interacting via Van der Waals forces by means of Fast Scanning Calorimetry. The aim of this study was to challenge the exclusive role of the α- relaxation in the evolution of an aging system towards equilibrium by performing experiments in a wide range of aging times and temperatures.

In recent years, there has been numerous evidence suggesting the inadequacy of the α- relaxation in certain conditions, including experiments on vitrification kinetics of metallic glasses in a wide range of cooling rates, where it was shown that vitrification was taking place at lower temperatures than predicted by the α- relaxation [52]. The same behavior has also been observed for metallic [53] and polymeric [54] glass formers under geometrical confinement.

Concerning physical aging, there is also a plethora of experimental results that suggest that the simple case of the α- relaxation being the only mechanism driving the system to the closest equilibrium state needs to be reconsidered. According to studies carried out in polymeric [55–57], metallic [58, 59], chalcogenide [60] and simple molecule glass formers [61, 62], the kinetics of physical aging towards equilibrium exhibit at least two steps when it takes place far below T_g.

Taking this into account, the aim of this article was to provide a comprehensive

characterization of physical aging in five small-molecule glass-formers interacting *via* van-der-Waals forces, whose systematic investigation had so far remained elusive. This was achieved by monitoring the evolution of the enthalpic relaxation under isothermal conditions and analyzing their kinetics. The glass-formers under study were o-Cresolphthalein dimethyl ether (KDE), phenolphthalein dimethyl ether (PDE), o-terphenyl (OTP), $1,1-bis(4-methoxyphenyl)$ cyclohexane (BMMPC) and BMPC (also referred to as bisphenol -C- dimethylether).

To this end, we employed on one side a model-independent approach, based on the determination of the aging temperature-dependent time to reach equilibrium, and on the other side, a modified version of the so-called Single Parameter Aging (SPA) model, which has been shown to capture the entire phenomenology of physical aging after temperature jumps of some Kelvin [81, 128, 129]. To account for the thermodynamic state dependence of the relaxation time of the α- process, τ, the density scaling approach [130] was employed, which includes the contributions of both temperature and volume to τ.

3.1.2 Results and Discussion

A systematic characterization of physical aging in small-molecular glasses was performed, accessing a wide range of time scales and temperatures. Two approaches were utilized to challenge the current understanding of physical aging: a model-independent one based exclusively on the time scale to reach equilibrium and a second one, based on the SPA model. Both approaches reveal that the aging behavior at high aging temperatures is well-described by considering only the α- relaxation. This is implied by the aging temperature dependence of the time to reach equilibrium, τ_{eq}, which exhibits the same super-Arrhenius behavior as the α- relaxation, and the ability of the model to capture completely the time evolution of the thermodynamic state at such high temperatures. The latter is in agreement with previous reports on the application of SPA model on aging data after small temperature jumps [81, 128, 129].

In the model-independent appoach, the aging temperature dependence of τ_{eq} seems to mimic that of the α- relaxation in the cases of KDE, OTP, BMMPC and BMPC, while for PDE minor deviations appear, as shown in Fig. 3.1. In line with this, the prediction of the model, which is presented in Fig. 3.2, fits well the experimental data that correspond to the last stages of the evolution of the thermodynamic state. The fit works well over the entire aging time range for small jumps below T_g, which

is in agreement with previous reports [81, 128, 129]. As far as the anomalous behavior of PDE is concerned, it is ascribed to the poor extrapolation of the equilibrium time, τ, to the lowest temperatures at which physical aging was investigated [131].

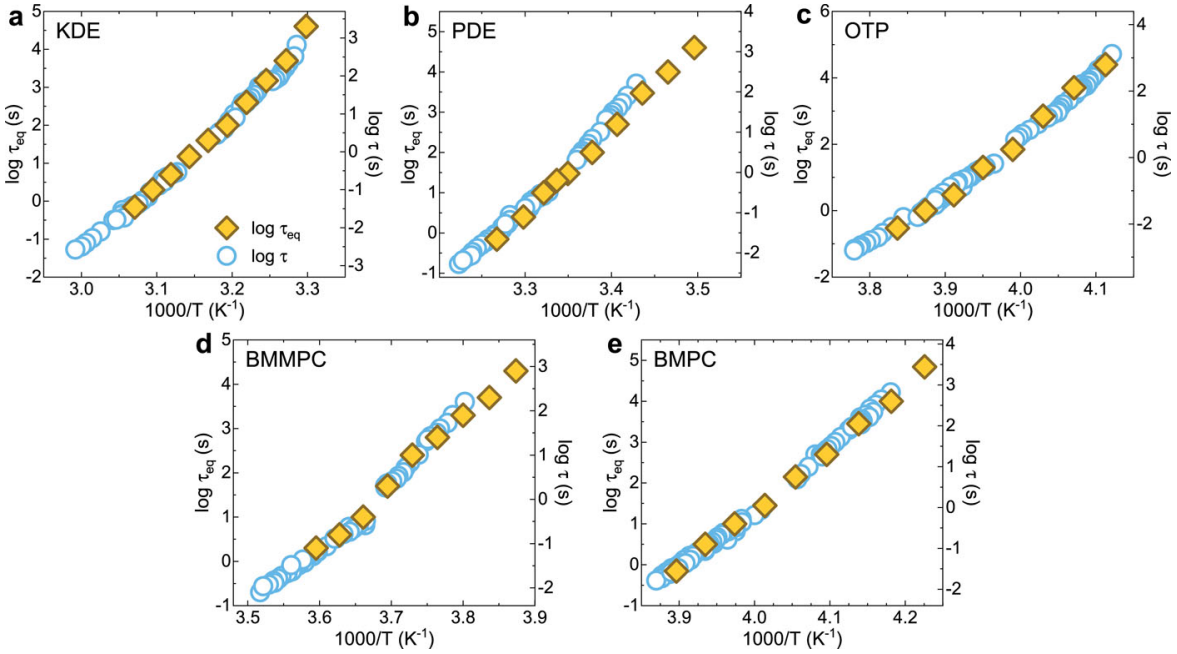

FIGURE 3.1: Time scale to reach equilibrium (left axis) and relaxation time of the α- relaxation (right axis) as a function of the inverse temperature for all investigated glasses.

Nevertheless, when it comes to physical aging far below T_g, corresponding to large jumps in the fictive temperature, the kinetics of equilibrium recovery become significantly more complex. More precisely, the prediction of the model based solely on the α- relaxation, fails to describe the normalized relaxation function, $R(t)$ in the low temperature regime, where the experimental data are far more stretched than the predicted behavior. In line with this, during the early stages of aging, the experimental $R(t)$ exhibits a faster evolution than the one expected when only accounting for the α- process.

The failure of the α- relaxation as the only associated mechanism to describe satisfactorily glass equilibration after large jumps, has been reported by several other studies [132–136]. In these studies, different variants of the Tool-Narayanaswamy-Moynihan (TNM) [137] and Kovacs- Aklonis- Hutchinson- Ramos (KAHR) [40] models were applied. The inadequacy of these models, was explained on the basis of the need to modify the explicit analytical expression for the non-linearity of the physical aging. However, here it is shown that even when the non-linearity is introduced without making an explicit assumption on its mathematical form, we still observe large deviations between the theoretical predictions and the experimental

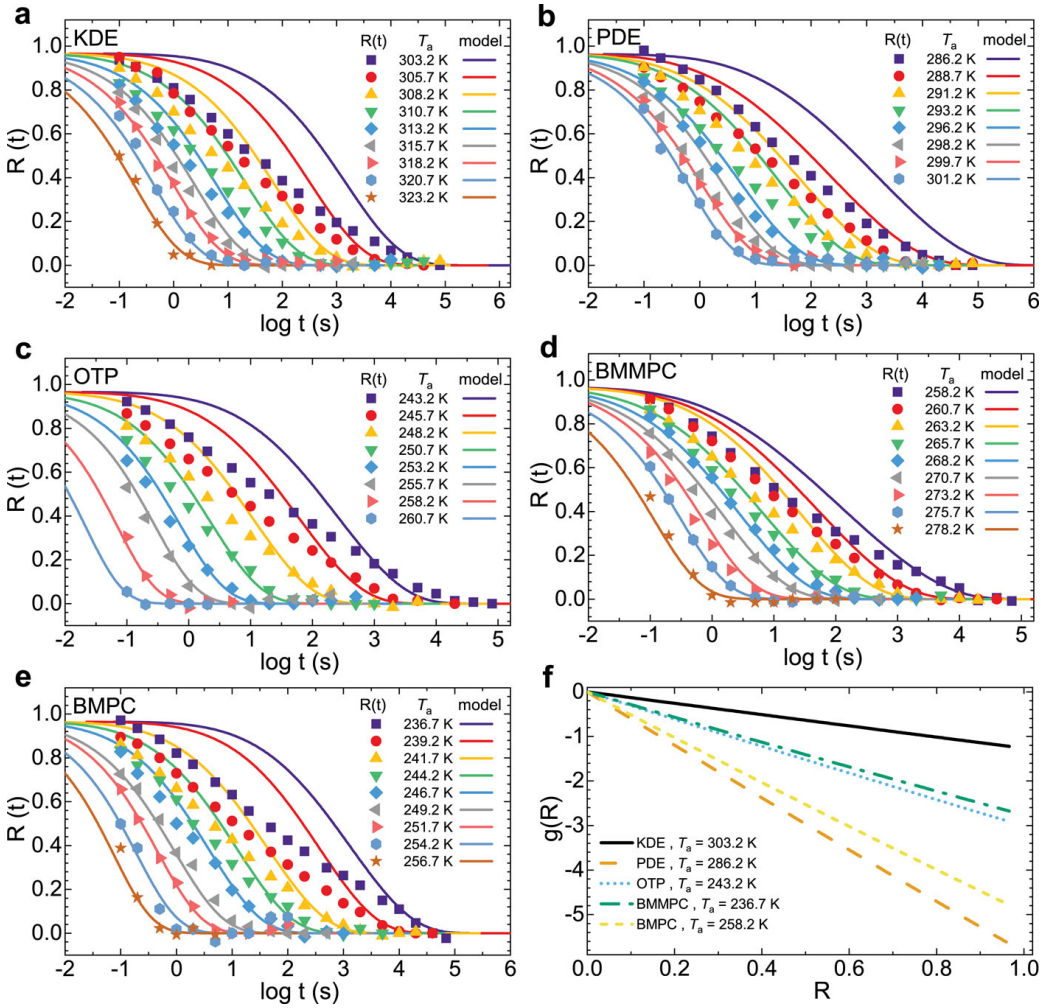

FIGURE 3.2: **Panels (a)–(e):** Experimental (points) and predicted (lines) normalized relaxation function vs aging time for all investigated temperatures and glasses. **Panel (f) :** g(R(t)), the deviation of τ from its equilibrium value, as a function of R(t) at the lowest investigated aging temperatures.

data. Thus, our findings rather suggest that the problem lies in the fact that such models contain only one time scale, that of the α- relaxation.

The cause for the discrepancy between the predicted behavior and the experimental results must be sought in the role of the fast, non-α molecular mechanisms initiating physical aging. In fact, there are already extensive references in literature about their role in polymers, metal alloys, chalcogenides and glycerol (see 3.1.1), where multiple decays were detected and separated. Here, although multiple steps cannot be discerned clearly, the stretched normalized relaxation function indicates the presence of multiple decays, not yet well-separated in the approach to equilibrium. A closer inspection of our data in the lowest aging temperature provides hints for a splitting

of the last stages of aging into two steps. More precisely, for all the glass-formers we studied, a slowdown of the relaxation takes place at about 10^3 s, followed by a late evolution to the final equilibrium. This is an important observation, since it rules out the possibility that the deviations of the model from the experimental data ar due to the inaccurate description of the α- relaxation by the density scaling.

The decoupling between the aging behavior and the α- relaxation can be understood better by considering the conceptual difference between the linear and non-linear responses [138, 139]. This interpretation suggests that for small temperature jumps the α- relaxation contains all the information to describe weakly non-linear aging, a statement that agrees with various experimental findings [81, 128, 129], including ours. Concerning the undelying non- α relaxation mechanism that triggers aging under certain conditions but remains unresolved during linear measurements, here we provide a reasonable explanation. In this work, the characterization of the glass linear response was carried out by monitoring the thermal susceptibility, which is the complex specific heat, a second-order thermodynamic property. However, the use of the time-dependent fictive temperature in the aging regime implies monitoring the evolution of a first-order thermodynamic property, which is the enthalpy in this case. If one of the molecular relaxation mechanisms involved in physical aging has a number of temperature-independent degrees of freedom, its associated entropy, $S(t)$, will be temperature-independent as well and thus, it shall deliver a null contribution to the specific heat $C_p(T) = T\frac{\partial S(T)}{\partial T}\big|_p$ [140]. From this point of view, it is justified why linear response is unable to describe equilibrium recovery of an aging glass, where a first-order thermodynamic property is monitored.

Although these fluctuations that are not related to the α- process remain undetected during the thermal susceptibility measurements, they might be visible when other fields are applied, like for instance dielectric or mechanical linear perturbations. The most immediate candidates to explain the fast evolution of the glass thermodynamic state, are secondary β- relaxations, which are normally detected by dielectric and mechanical spectroscopies below T_g [141]. These are well-known and characterized for the materials under study. In particular, it has been found that PDE [142], OTP [143] and BMPC [144] exhibit a secondary relaxation, while KDE [142] and BMMPC [144] do not. This comes to contradict our findings, where deviations from the behavior predicted by considering exclusively the α relaxation were observed for all materials. Furthermore, the time scales of the β relaxation for OTP become of the order of seconds at much lower temperatures than the ones at which we observe a strong effect of non-α processes during aging equilibration. All these arguments

lead to the assumption that β relaxation may not have a leading role as the mechanism driving fast aging.

To explain the fast non-α- relaxation, a suitable candidate, which bears large potential to equilibrate and has time scales comparable to this evolution, could be the recently identified slow Arrhenius process (SAP). This mechanism has been shown to play a role of utmost significance in the kinetics of equilibration of phenomena including physical aging, polymer adsorption and dewetting [126]. A way to verify its presence would be to perform experiments at lower temperatures and longer aging times, which would allow the analysis of the activation energy of the fast equilibration mechanism and the splitting from the α- relaxation.

One of the consequences of our findings is that the material time has to be tuned by the time scale of both the α relaxation and of the additional mechanism. In this case, it should be rewritten as $d\xi = (\alpha\tau_{\alpha}^{-1} + (1-\alpha)\tau_{non-\alpha}^{-1})d\tau$, where α is a parameter that contains information about the potential of equilibration born by each mechanism. Last but not least, our results grant access to the pronounced effects of physical aging far below T_g [35], which can only be rationalized in the framework of non-α relaxations, whose potential of equilibration survives where the α- relaxation is completely frozen.

3.2 Identifying the Thermal Barriers of Glass Aging via Isoconversional Analysis

3.2.1 Introduction

Building upon the results of Section 3.1, this article aimed to provide insight into the aging time-dependent thermal barriers in glasses evolving towards equilibrium. In this case, a further step was taken by extending the study to include polymeric materials, in addition to the small molecules mentioned above.

According to the results of our previous work and other studies, there is strong evidence that the α- relaxation is inadequate to fully account for the recovery to equilibrium following deep quenches into the glassy state. This suggests that more than one mechanisms contribute to this process, although their number and nature remain elusive.

Given these premises, isoconversional kinetics analysis was employed, which is capable of unraveling the activation energies associated with different stages of glass equilibration, allowing us to extract information on the molecular mechanisms that mediate physical aging as a function of the thermodynamic state of the glass as well as of aging time and temperature. The extension of isoconversional methods to the study of glass transition phenomena, and in particular to physical aging [85, 145], was pioneered by Vyazovkin et al. [146–148]

As mentioned previously, instead of assuming a single constant activation barrier, the isoconversional approach maps out how the effective activation energy evolves with conversion, providing a sensitive probe of the underlying molecular mechanisms. Also, an important advantage of this methodology is that it is particularly suited to deal with non-Arrhenius processes, such as those typically involved in the glass transition and physical aging, where the apparent activation energy is known to evolve with temperature and observation time.

In the present work, isoconversional kinetics analysis was applied to a set of physical aging data on different glasses, including the small molecules of Section 3.1 and three glassy polymers, polystyrene (PS), poly(4-chloro styrene) (P4ClS), and poly(4-bromo styrene) (P4BrS). In the case of small molecules, we used the data discussed in Section 3.1, while for PS and P4ClS, we refer to previously reported physical aging kinetics [149, 150], where the enthalpy evolution toward equilibrium was determined by fast scanning calorimetry (FSC) after rapid quenches (1000 K s^{-1}) from the supercooled liquid to various aging temperatures. As for P4BrS, new data was acquired applying an analogous protocol.

3.2.2 Results and Discussion

Figures 3.3, 3.4 and 3.5, panel (a), show the aging time-dependent evolution of the R(t) function at different aging temperatures for three of the materials under study, o-terphenyl (OTP) [53], P4BrS, and PS. It is reminded here that R(t) is calculated from eq. 3.1 as:

$$R(t) = \frac{T_f(t) - T_a}{T_f(0) - T_a} \tag{3.1}$$

where $T_f(t)$ and $T_f(0)$ the time-dependent fictive temperature and the one at the beginning of the process, respectively, and T_a the aging temperature.

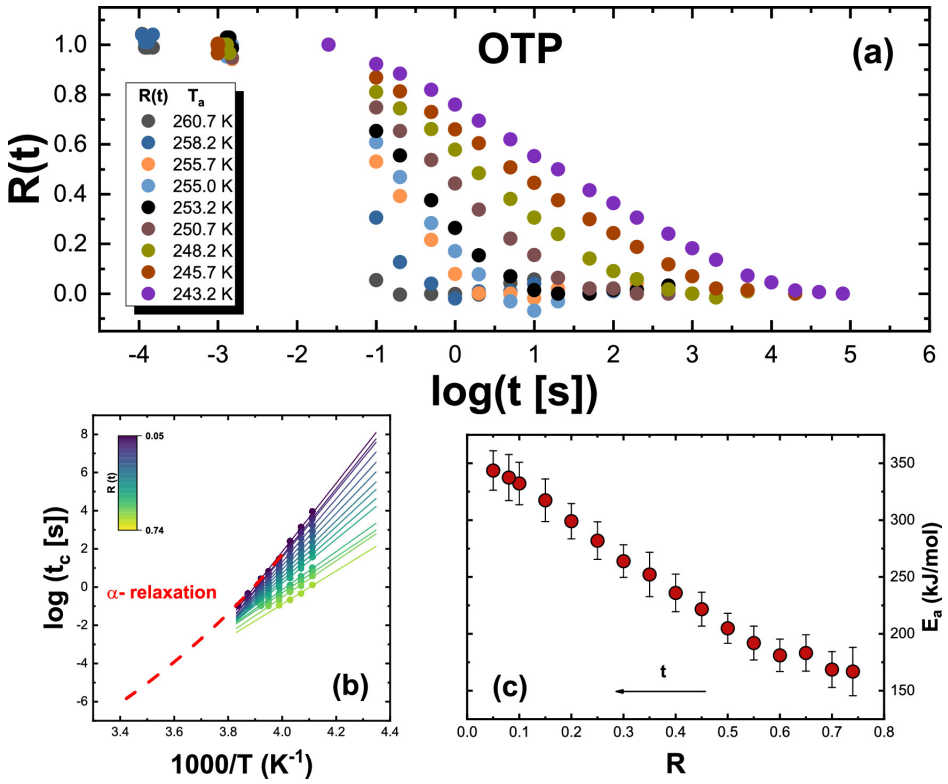

FIGURE 3.3: (a) Experimental data of the normalized relaxation function R(t) for all investigated aging temperatures for OTP (T_g = 263 K at 1000 K s^{-1}). (b) Logarithm of t_c, the time to reach the degree of relaxation R(t), indicated in the color map as a function of the inverse temperature. The dashed line is the temperature dependence of the α-relaxation time taken from broadband dielectric spectroscopy (BDS) data, (45) and it has been shifted by $logt = +2$ to match the experimental data. (c) Dependence of the activation energy obtained from the isoconversional method on the extent of aging.

As can be observed, the aging time evolution of R(t) exhibits the common patterns typical of glass aging, which are the shifts of R(t) to longer aging times with decreasing temperature and the typical sigmoidal shape. Nevertheless, the aging time evolution of R(t) appears to be more or less stretched, depending on the material. Specifically, PS appears to exhibit a more stretched aging evolution with respect to its bromo-substituted homologue, P4BrS, hinting at the influence of chemical structure on aging behavior.

For experiments conducted under isothermal conditions, the activation energy, E_R, at a given extent of relaxation R,is given by eq. 3.2:

$$E_R = k_B \left[\frac{\partial \ln t_R}{\partial T^{-1}} \right]_R \tag{3.2}$$

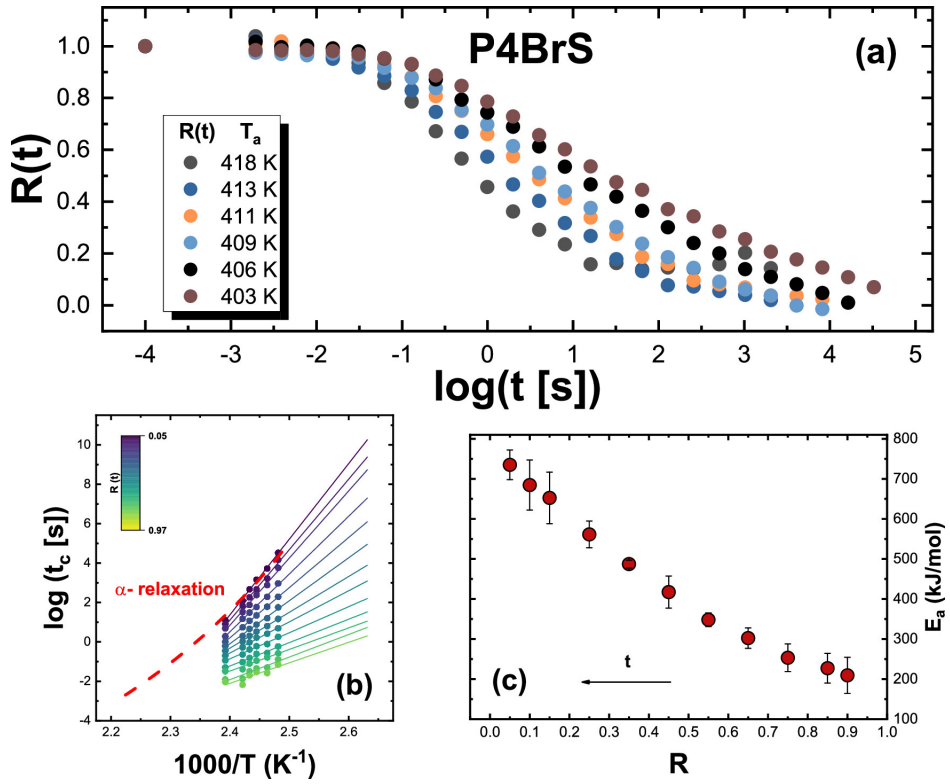

FIGURE 3.4: (a) Experimental data of the normalized relaxation function R(t) for all investigated aging temperatures for P4BrS (T_g = 435 K at 1000 K s^{-1}). (b) Logarithm of t_c, the time to reach the degree of relaxation R(t), indicated in the color map as a function of the inverse temperature. The dashed line is the temperature dependence of the α-relaxation time taken from broadband dielectric spectroscopy (BDS) data, (45) and it has been shifted by $logt = +0.65$ to match the experimental data. (c) Dependence of the activation energy obtained from the isoconversional method on the extent of aging.

Panels (b) of Figures 3.3, 3.4 and 3.5 show the outcome of the analysis of relaxation data reported in panels (a) of the same figures for a discrete set of R(t) at different temperatures and times for OTP, P4BrS, and PS. More precisely, several isoconversional plots with $logt$ vs $1000/T$ for different extents of R(t) are shown. As can be observed, as R(t) decreases, the slope of the linear fittings increases and, as a consequence, so does the effective activation energy during the aging process. This can be seen in panels (c) of the same Figures for OTP, P4BrS, and PS, where the dependence of the activation energy on the extent of relaxation is presented.

A common feature of the dependence of the activation energy on the extent of relaxation, in line with previous reports [84, 85], is that it varies from a lower bound in the order of $\sim 100\,\mathrm{kJ\,mol^{-1}}$ to values as large as several hundreds $\mathrm{kJ\,mol^{-1}}$ at the

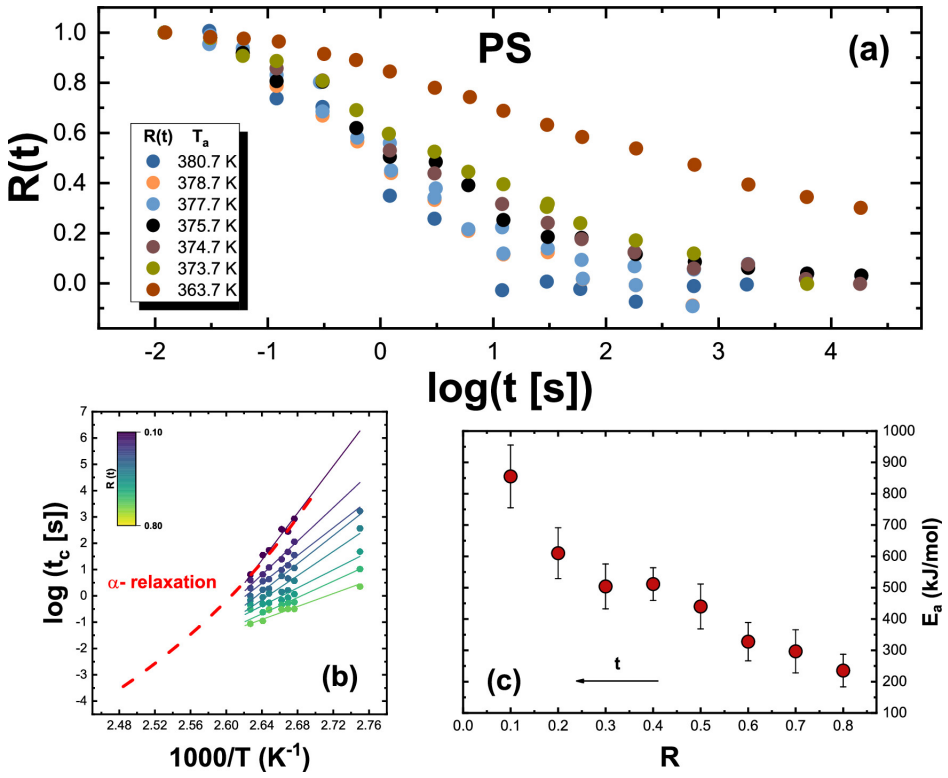

FIGURE 3.5: (a) Experimental data of the normalized relaxation function R(t) for all investigated aging temperatures for PS (T_g = 390 K at 1000 K s^{-1}). (b) Logarithm of t_c, the time to reach the degree of relaxation R(t), indicated in the color map as a function of the inverse temperature. The dashed line is the temperature dependence of the α-relaxation time taken from broadband dielectric spectroscopy (BDS) data, (45) and it has been shifted by $logt = -0.22$ to match the experimental data. (c) Dependence of the activation energy obtained from the isoconversional method on the extent of aging.

end of the aging process. The latter can be compared to that of the main α- relaxation, whose temperature dependence of the typical relaxation time, conveniently shifted to match aging times, is presented in panels (b) of Figures 3.3, 3.4 and 3.5. As can be observed, in all cases, the activation energy at the end of the aging process matches with that of the α-relaxation, indicating that the latter is the leading mechanism mediating the final stages of approach to equilibrium.

The relatively low activation energy at small and intermediate extents of relaxation could also be attributed to the role of the α-relaxation in non-equilibrium conditions. A wealth of experiments carried out in the non-equilibrium glass actually show that the measured relaxation time exhibits moderate activation energy [151–157], in line with the outcome of our analysis. However, this interpretation would entail a discontinuity of the temperature dependence of the α-relaxation time as the

system transforms from the supercooled liquid to the non-equilibrium glass. This scenario is at odds with the description of aging kinetics as a single activated event [158]. Specifically, within the thermally activated description of the dynamics of glass forming systems, the freezing of configurational degrees of freedom leading to vitrification results in a temperature independent activation energy equal to that of the equilibrium systems just before vitrification. Seen from the viewpoint of the Adam-Gibbs theory [159], the aforementioned freezing implies that the configurational entropy remains constant below T_g and equal to that of the supercooled liquid before vitrification takes over.

Given these premises, the discontinuity in the glass activation energy with respect to that of the equilibrium supercooled liquid warrants an interpretation based on the role of other molecular mechanisms mediating physical aging at weak and moderate extents of relaxation. The most immediate candidate would be the β-relaxation detected by standard spectroscopic techniques [160]. This was actually the interpretation in studies where isoconversional analysis conveyed a relaxation-dependent evolution of the activation energy analogous to that of our work [84, 85]. Furthermore, this is in line with recent analysis on a metallic glasses where the kinetics of devitrification a previously aged glass was shown to be sequentually mediated by γ, β, and ultimately α relaxation [161]. However, among the investigated glass formers, KDE and BMMPC do not exhibit any trace of a β-relaxation by dielectric relaxation spectroscopy [142, 144]. Nevertheless, their behavior in terms of relaxation-dependent activation energy, as detected by isoconversional analysis, is completely analogous to that of their homologous glass formers, PDE and BMPC, where a secondary relaxation is clearly visible in dielectric relaxation spectroscopy experiments [142, 144]. The absence of β-relaxation in KDE and BMMPC may reflect limitations of the technique rather than a genuine lack of secondary dynamics and therefore, β-processes cannot be entirely ruled out.

At the same time, the systematic observation of low-E_a values across different glass formers suggests the involvement of a more universal mechanism. A strong candidate is the slow Arrhenius process (SAP) [126], a relaxation mode consistently identified in both polymers [162, 163] and small molecule glasses [127, 164], and commonly ascribed to collective small displacements (CSD) involving localized, constrained rearrangements of molecular groups [165]. Unlike the β-relaxation, which is often material-specific and sensitive to detection methods, SAP is characterized by a nearly temperature-invariant activation barrier, with values ranging from roughly

30-200 kJ mol^{-1} depending on the system. Importantly, the SAP has also been associated with other equilibration mechanisms in molecular glasses [126, 166, 167], further strengthening its relevance as a generic contributor to structural recovery both above and below T_g.

Within this framework, the low thermal barriers detected as $R \rightarrow 1$ could be attributed to SAP-mediated rearrangements, which remain active even deep below T_g, where the α-process is essentially frozen. Previous studies have already correlated the first regime of physical aging kinetics with the SAP [126], associating the early stages of equilibration with these localized displacements, before the system gradually crosses over to the higher barriers characteristic of α-controlled recovery and our results reinforce this view. This supports a two-step equilibration scenario in which the SAP governs the onset of aging and the α-process dominates the final approach to equilibrium.

3.3 Testing the Validity of Density Scaling in Glass Physical Aging

3.3.1 Introduction

An additional method to reinforce the findings of the previous publications, was to test directly the validity of the density scaling approach in out-of-equilibrium systems. We addressed this issue by combining time-dependent broadband dielectric spectroscopy measurements with a detailed analysis of aging kinetics in the model van der Waals molecular glass former, o-cresolphthalein dimethyl ether (KDE). During isothermal aging below the glass transition temperature, T_g, we simultaneously tracked the dielectric loss on the high-frequency flank of the α- relaxation and the high-frequency value of the capacitance, reflecting glass densification.

The density scaling approach has emerged as a unifying framework to rationalize the dynamics of equilibrium glass-formers [64, 130]. According to this approach, the typical time τ of the main α- relaxation of a wide variety of liquids and polymers can be expressed as a function of the temperature, T, and the density, ρ, plus a material specific variable, γ, reflecting the relative importance of density and temperature. The analytical form of this expression has been extensively tested in the following equation:

$$\tau = \tau_0 \exp \frac{C}{T\rho^{-\gamma}} \tag{3.3}$$

As its application over a wide temperature range generally requires refinement, implementation of density scaling has been proposed by Avramov [168, 169].

$$\tau = \tau_0 \exp\left(\frac{C_{\text{Avr}}}{T\rho^{-\gamma_{\text{Avr}}}}\right)^{n_{\text{Avr}}} \tag{3.4}$$

Where the subscript *Avr* is intended to distinguish the scaling parameters within this approach and the standard scaling.

Both the standard empirical and Avramov scaling -the former over relatively narrow temperature/pressure intervals and the latter over a much broader temperature/pressure range- have been remarkably successful in superposing relaxation times measured under diverse thermodynamic conditions, leading to master curves covering several decades in τ. Density scaling has been validated for van der Waals liquids [170–173], hydrogen-bonded systems [170, 171], ionic liquids [174], and polymers [175, 176] of varying fragility, as well as simulated glass formers, underscoring its broad applicability. However, whether the principles of density scaling extend to out-of-equilibrium systems and aging glasses in particular, remains an open question of both fundamental and practical relevance. A positive answer would suggest that the same scaling variable governs relaxation not only at equilibrium but also during the progressive equilibration of glasses.

The applicability of this approach to out-of-equilibrium conditions has been challenged by the outcome of aging performed by simulations in isochoric conditions [72–75], which indicate that the relaxation time or any observable related to it changes even when both temperature and volume are kept constant. For the varying-pressure conditions under which those simulations were carried out, this implies that density scaling can only remain valid if eq. 3.3 is extended to include a pressure contribution, or, as recently proposed [81], an explicit nonequilibrium term written in terms of the glass fictive temperature, T_f.

In this work, we test the validity of density scaling during physical aging by analyzing broadband dielectric spectroscopy (BDS) measurements on the archetypal small-molecule glass-former, KDE. As our experiments are conducted at constant atmospheric pressure, the aforementioned scenarios, where either a pressure or a nonequilibrium term must be included in the original scaling relation, can be discriminated. By monitoring both the dielectric loss associated with the α-relaxation and the high-frequency capacitance reflecting densification, we investigated whether τ and ρ remain coupled in a way consistent with density scaling predictions.

3.3.2 Results and Discussion

The observables chosen for this analysis providing complementary information were the low frequency C'', that reflects the main α relaxation dynamics [48, 123], and C' at high frequencies, which is directly sensitive to changes in density. Specifically, if C' is measured at frequencies larger than those at which all relaxation processes in the glass take place, the high frequency capacitance, $C_\infty = \epsilon_\infty \epsilon_0 S/h$ is obtained; where ϵ_r, ϵ_0, S and h are the high frequency dielectric permittivity, the vacuum permittivity, and the area and thickness of the capacitor, respectively. ϵ_∞ provides direct information on the glass density via the Clausius-Mossotti (CM) equation [124, 125, 177]:

$$\frac{\epsilon_\infty - 1}{\epsilon_\infty + 2} = \frac{4\pi N\alpha}{3\varepsilon_0 M}\rho \tag{3.5}$$

Where N, α and M are the number of dipoles per unit volume, the polarizability and the molecular weight, respectively.

By combining 3.3 and 3.5 (see Apppendix A for details) and analyzing them accordingly, we finally obtain the relation:

$$\Delta \log \tau(t) = \frac{C\gamma}{\ln 10 T_a C_\infty \Lambda}\Delta C_\infty(t) \tag{3.6}$$

Where T_a the aging temperature and Λ a macroscopic pre-factor. From the differential form of the Clausius-Mossotti equation, considering a value of $\varepsilon_\infty = n^2 \sim 2.25$ (with n the refractive index for a typical transparent glass) and ρ = 1.1 g cm^{-3} for KDE [65], we obtain a value of: $\Lambda \sim 1.61$. Thus, a quantitative test of the density scaling relation via eq. 3.6 implies that the proportionality between the variation of τ and that of C_∞ must be fulfilled; and that the proportionality coefficient, that is, the slope of the line $\Delta \log \tau$ vs ΔC_∞ must have a specified value, derived from the density scaling parameters obtained at equilibrium.

In way analogous to the classical scaling, by combining 3.4 and 3.5, we obtain the relation between the variation of the relaxation time and that of the high frequency capacitance within the Avramov variant of the scaling:

$$\Delta \log \tau(t) = \frac{C_{\mathrm{Avr}} n_{\mathrm{Avr}} \gamma_{\mathrm{Avr}} \rho(0)^{\gamma_{\mathrm{Avr}} n_{\mathrm{Avr}} - 1}}{\ln 10 T_a^{n_{Avr}} C_\infty \Lambda}\Delta C_\infty(t) \tag{3.7}$$

Considering that C_∞ undergoes small variations during aging, a quantitative test of the density scaling relations via eqs. 3.6 and 3.7 implies that the proportionality

between the variation of τ and that of C_∞ must be fulfilled; and that the proportionality coefficient, that is, the slope of the line $\Delta \log \tau$ vs ΔC_∞ must have a specified value, derived from the density scaling parameters obtained at equilibrium.

The dielectric response of KDE in terms of the loss part of the permittivity, C'' (3.6), shows the α- relaxation as a peak shifting to lower frequencies with decreasing temperature. The downward shift of the peak frequency with decreasing temperature, can be tracked by a concomitant decrease in C'' in the high frequency flank of the relaxation. The inset of Fig. 1.2 shows the time evolution of C'' when the KDE sample was cooled below T_g and held isothermally at 298.2 K. The reduction of C'' reflects the progressive slowing-down of the α- relaxation as the glass evolves toward equilibrium.

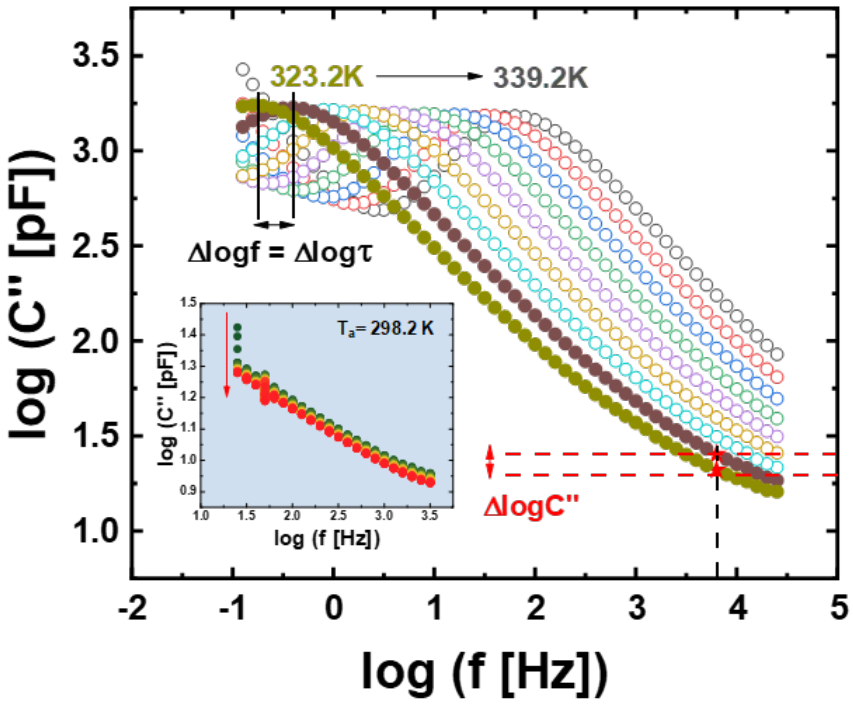

FIGURE 3.6: Loss part of the capacitance at different frequencies and temperatures for KDE. The way a reduction in C'' reflects in shift to lower frequency of the peak in C'' is indicated. (Inset) Time dependent evolution of C'' during physical aging. The arrow marks increasing aging times at 298.2 K.

The frequency/temperature evolution of C' above T_g, exhibits the typical step from high to low values when increasing the frequency, whereas in the aging regime, only the high frequency flank of the α- relaxation is visible, and at higher frequencies the C' approaches a plateau (for details see the correponding pre-print publication in the Appendix A).

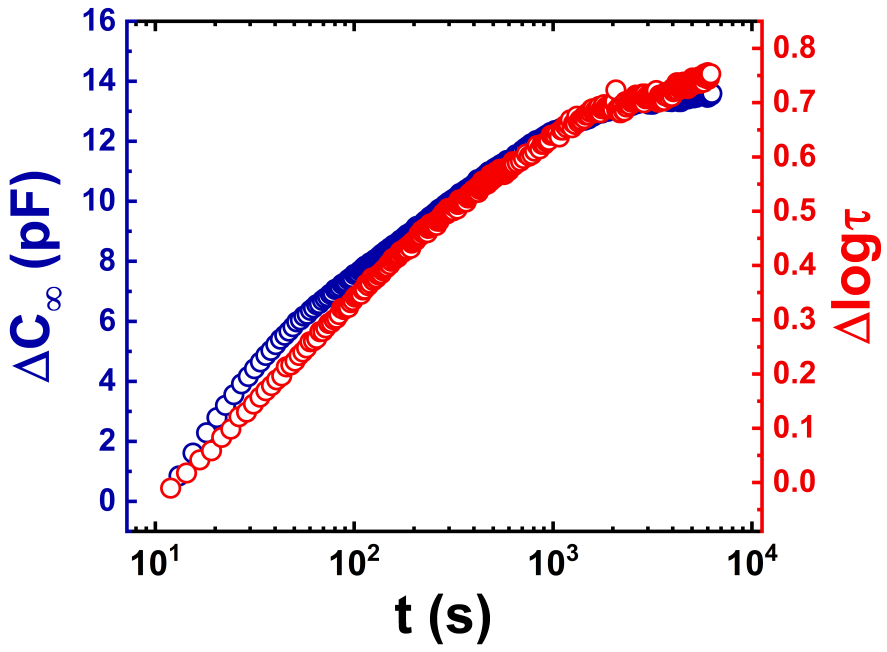

FIGURE 3.7: Aging time evolution of the high frequency capacitance (left axis) and the relaxation time (right part) at 298.2 K.

Fig. 3.7 shows the aging time evolution of both the variation of the relaxation time, $\Delta \log \tau(t)$, and that of the high frequency capacitance $\Delta C_\infty(t)$ for KDE at 298.2 K. We observe a general trend toward a reduction of the time to reach equilibrium and the amount of recovery of both observables with increasing aging temperature, in line with the general phenomenology of physical aging [36]. Importantly, the evolution of the two observables exhibits analogous aging time dependence, both reaching a stable equilibrium value after sufficiently long times at all investigated temperatures. These parallel trends already qualitatively suggest a strong coupling between structural relaxation and volume recovery.

A step forward in the analysis of aging data is reported in Fig. 3.8 where the time evolution of $\Delta \log \tau(t)$ is reported as a function of $\Delta C_\infty(t)$ at 298.2 K. In all cases, a linear dependence between the two observables is observed, which fulfills the predictions of density scaling (eq. 3.6). A more stringent test of density scaling can be done predicting the slope of $\Delta \log \tau(t)$ *vs* $\Delta C_\infty(t)$ according to eqs. 3.6 and 3.7 for both classical and Avramov scaling employing parameters for KDE at equilibrium. These are generally obtained by BDS experiments over a wide range of temperature and pressure [130, 178]. Figure 3.8 shows the range of prediction based on density scaling considering both mentioned variants of density scaling. Considering that all

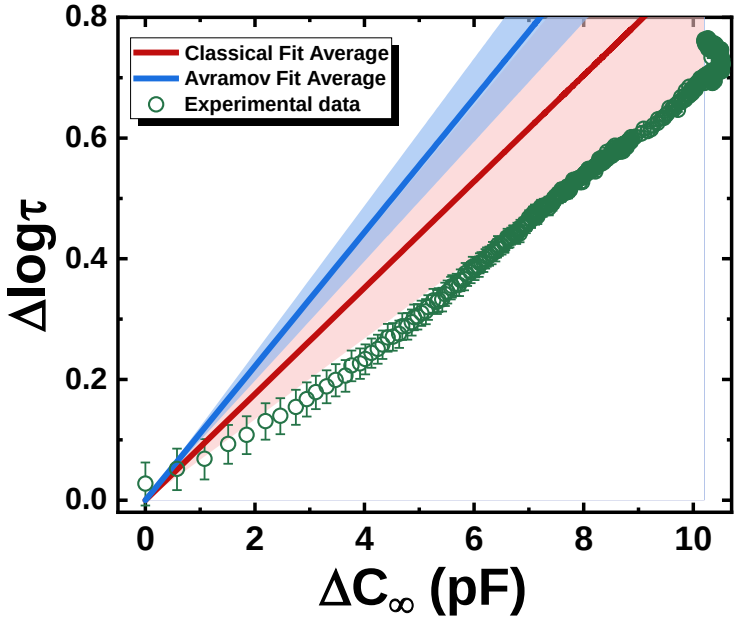

FIGURE 3.8: Time dependent variation of the relaxation time as a function of the corresponding variation of the high frequency capacitance at 298.2 K.

parameters are taken from relaxation data at equilibrium and, therefore, no fitting parameters are required, the agreement of density scaling with experimental results is remarkable, although the slope predicted by the classical scaling appears to be closer to the experimental one than that predicted within the Avramov variant.

3.4 Vitrimeric Behavior Revealed by Fast Scanning Calorimetry in Branched Polyglycerol Networks Cross-Linked by Reversible Enamine Bonds

3.4.1 Introduction

This article aimed to study the thermal properties of vitrimeric materials developed *via* enamine covalent dynamic bonds (see Section 2.1.2 and corresponding publication for details) and the separation of the thermal events taking place within the network, thereby elucidating their vitrimeric character.

As has been previously mentioned, the covalent adaptable networks (CANs) that possess associative dynamic covalent bonds (DCBs) and show an Arrhenius temperature dependence of the viscosity approaching the glass transition temperature (T_g) are called vitrimers [97]. A relevant parameter of these systems is the topology freezing or vitrimer transition temperature (T_v), which Leibler and co-workers defined as the temperature at which the network freezes due to the inability of DCBs to undergo exchange reactions [96]. Increasing the temperature just above T_v causes vitrimers to undergo a topological transition from viscoelastic solid to viscoelastic liquid behavior.

Reliably determining T_v remains an unsolved problem in this emerging field. An extrapolation of the vitrimer viscosity to a value of 10^{12} Pa s is taken as the original criterion to estimate the so-called "apparent" T_v, even if large extrapolations prone to large errors are often involved [179, 180]. Other attempts to obtain T_v have relied on the use of stress-relaxation measurements combined with non-isothermal and isothermal creep experiments [181], dilatometry [98], thermomechanical analysis [182], aggregation-induced-emission (AIE) luminogen fluorescence [183] and X-ray scattering experiments supported by DSC measurements [184].

The simultaneous determination of T_g and T_v by means of methods that provide first-order thermodynamic properties, such as dilatometry for specific volume and DSC for enthalpy, has hitherto remained vastly elusive, with only a few exceptions [98, 102]. This is likely because at the rates of K min^{-1} explored by standard dilatometry and DSC, T_g and T_v are often too close and, therefore, their separation may be challenging. Furthermore, the step-like variation in thermodynamic coefficients underlying the vitrimeric transformation can span a broad temperature range, which complicates its detection. These experimental flaws can be overcome by expanding

the range of the heating/cooling rate in the experiment and by applying thermal protocols that aim to magnify the thermal events under investigation. As with T_g, it is expected that T_v depends on several experimental parameters in addition to the specific chemistry of the material [101]. Moreover, T_v can be above, below or near T_g. In fact, there is no general agreement on a protocol or experimental setup to assess T_v.

Concerning the separation between glass and vitrimeric transitions, the latter generally exhibits a lower apparent activation energy than the segmental relaxation associated with the glass transition, as shown in Fig. Therefore, reducing the experimental time scale can be an effective way of identifying the thermal events involved in vitrimers. FSC enables heating and cooling scans as large as several thousand $K\,s^{-1}$, [185] which greatly reduces the time scale of probed molecular motion compared to conventional DSC.

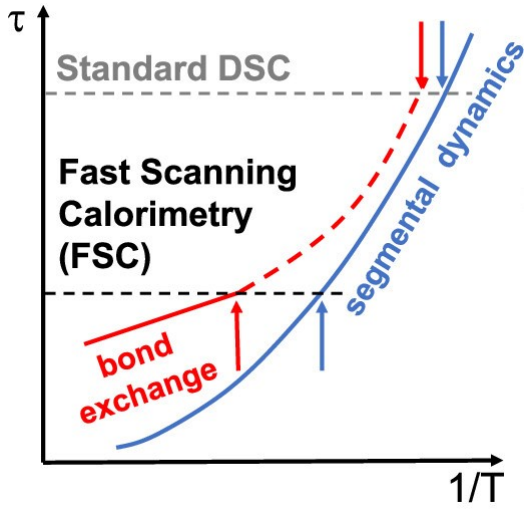

FIGURE 3.9: Scheme showing the mild Arrhenius temperature dependence of dynamic bond exchange typical time scale as opposed to the strong super-Arrhenius dependence of segmental relaxation time scale.

In this work, networks cross-linked through enamine DCBs- which have become one of the canonical reversible bonds used in the development of vitrimers made from synthetic [186, 187] and biobased materials [188, 189]- based on β-ketoester-decorated branched polyglycerol [190] (PG-βkest) and different diamines, i.e. DAP, EDO and Jeff were synthesized. Furthermore, an experimental protocol was developed to assess T_v using FSC of the synthesized cross-linked networks with Jeff and Kissinger analysis [191, 192] was employed, to obtain information about the apparent activation energies of the two thermal events.

3.4.2 Results and Discussion

The vitrimeric materials that occured after the cross-linking of βkest with the different types of diamines through enamine bonds are presented in Fig. 3.10 (a). Excess of diamine was removed by either evaporation or Soxhlet extraction. As a result, films with a thickness of approximately 100 μm were obtained, displaying distinct textural characteristics contingent solely on the nature of the amine employed in the synthesis.

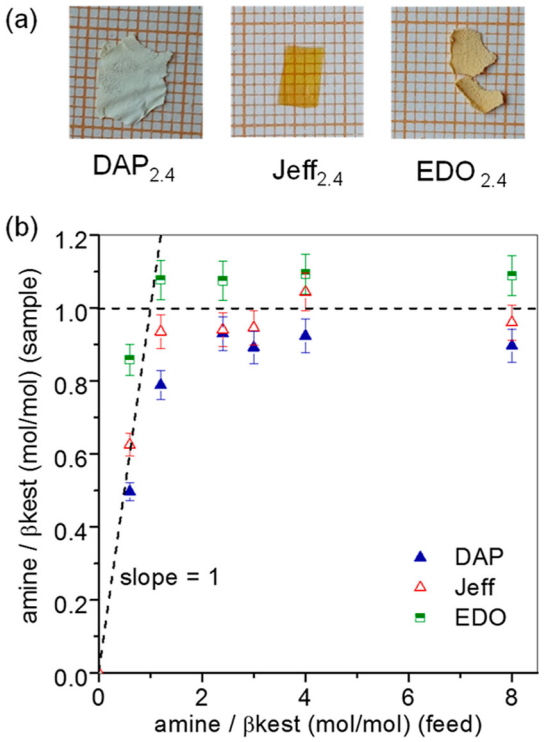

FIGURE 3.10: (a) Photographs of films over millimeter graph paper (samples obtained with an amine/βkest (feed) molar ratio of 2.4). (b) Composition of polymer networks cross-linked with DAP, EDO and Jeff.

Fig. 3.10 (b) shows the moles of amine per mol of βkest obtained in the sample as a function of the moles of amine per mol of βkest used to prepare the networks (feed). Sample values below feed values of 1 exhibit a growing trend with a slope near 1 indicating that all the diamine used in the feed is retained in the polymer network through covalent bonds. However, at feed values above 1, the amount of amine in the sample does not follow this trend and remains in the range of 0.9-1.1 indicating that the excess of diamine has been removed during purification. Thermogravimetric Analysis (TGA) and Fourier Transform Infrared Spectroscopy (FTIR) measurements also confirm the formation of the enamine bonds (for details see corresponding publication).

The characterization of the T_g of the cross-linked networks obtained with different amounts of diamine is shown in Figure 3.11 (a). For a given amount of amine in the feed, a significant increase in T_g can be observed when moving from Jeff to EDO to DAP. It is noteworthy that, while the glass transition range for Jeff and EDO is relatively narrow, it is remarkably broader for DAP, which indicates that the latter system exhibits an anomalous, heterogeneous glass-to-rubber transformation, likely due to the formation of non-cross-linked aminal structures.

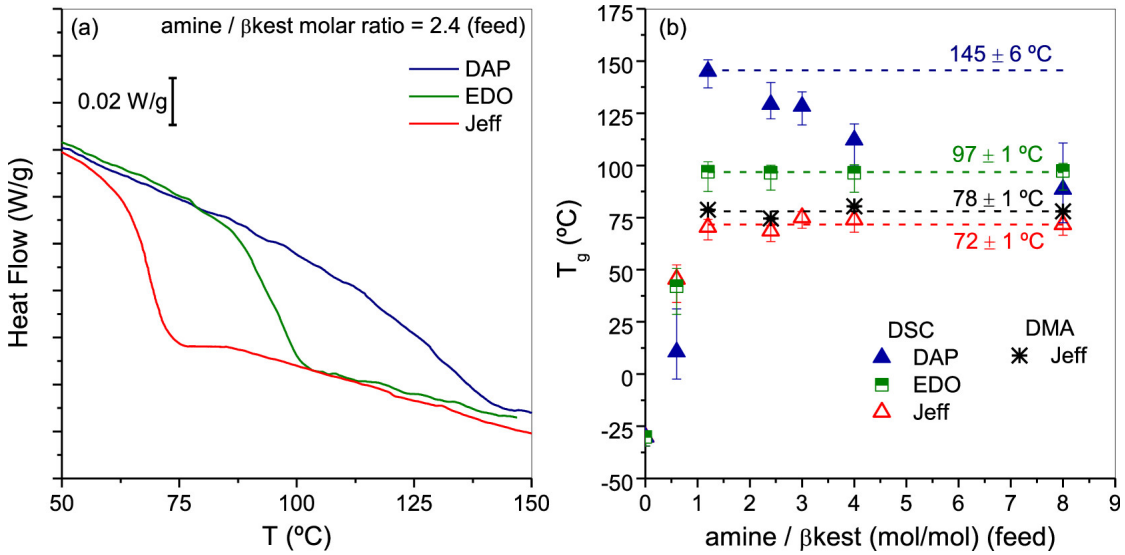

FIGURE 3.11: (a) DSC traces obtained in three cross-linked networks obtained using different amines but maintaining a constant ratio amine/βkest (feed) = 2 (b) T_g of cross-linked networks as a function of amine/βkest (feed) molar ratios determined by DSC and DMA. Asterisks correspond to values obtained for the Jeff networks by DMA at 1 Hz.

Fig. 3.11 (b) summarizes the dependence of T_g on the amount of amine in the feed for networks cross-linked with Jeff, EDO and DAP. Those cross-linked with Jeff and EDO showed the expected increase in T_g with increasing amount of amine in the feed to reach a plateau where a further increase in amine content does not result in further cross-links. However, the networks cross-linked with DAP showed an initial rapid increase in T_g with increasing amounts of amine up to values as high as 145 ^{o}C, followed by a decrease in T_g, which is thought to be due to the favored intramolecular reaction at amine/βkest (feed) molar ratios $\geq$ 2.4, which causes a decrease in the number of cross-links by the formation of 2-methyl hexahydropyrimidine moieties. Fig. 3.11 (b) also shows that Dynamic Mechanical Analysis (DMA) measurements at 1 Hz provide values of the T_g for the networks cross-linked with Jeff consistent with the ones obtained by DSC.

So far, it has not been provided any evidence of the manifestation of the vitrimeric character of the materials under study, most probably due to the similar time scales of bond exchange and segmental motions. For this reason, Fast Scanning Calorimetry was employed, which allows identifying thermal events at experimental time scales much shorter than in standard DSC. The detection of multiple thermal events was provided by thermal protocols in which the cooling rate is varied over the wide range, which are typically adopted to emphasize the presence of kinetic thermal events such as the glass transition [52, 193, 194], even when these are barely visible in simple heating/cooling scans at the same rate [195].

Here, we subjected a number of studied networks to cooling rates ranging from 0.05 to 1000 Ks^{-1} and assessed how the variation in cooling rates was reflected in the heating scan at 500 Ks^{-1} performed immediately after. The results (Fig. 3.12) show that heating after slow cooling results in the development of an endothermic overshoot, indicating the attainment of glassy states with low enthalpy. Importantly, on heating after cooling at the lowest rates, a bimodal overshoot is observed, or at least a very broad endotherm encompassing almost 100 K is evident.

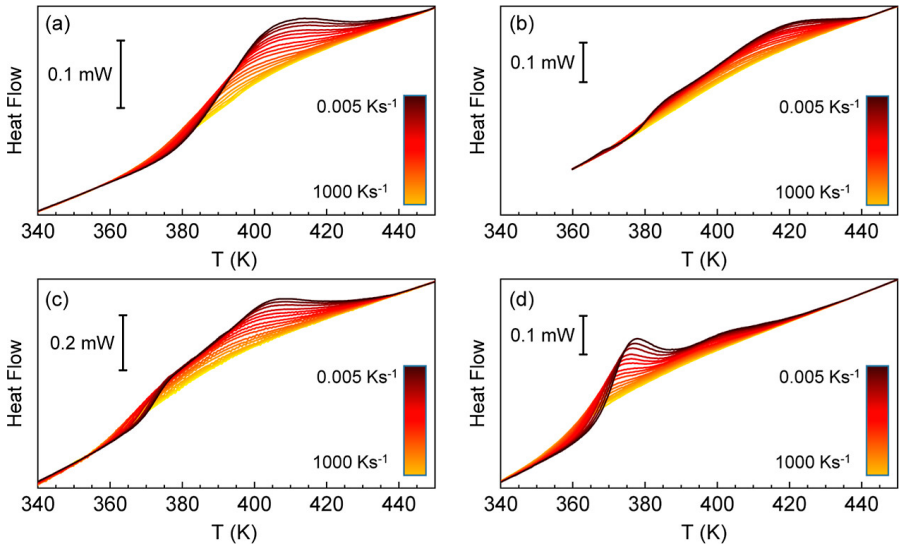

FIGURE 3.12: Heat flow rate temperature scans upon heating at 500 Ks^{-1} after cooling at the indicated rates for samples obtained with Jeff at an amine/βkest (feed) molar ratio of (a) 1.2, (b) 2.4, (c) 4 and (d) 8.

To unambiguously disentangle the two thermal events and gain insight into their relation with the glass and topological transition temperatures, T_g and T_V, respectively, we have enriched our calorimetric analysis by subjecting two judiciously selected networks to increasingly complex thermal protocols. The selected samples

were those obtained with Jeff at an amine/βkest (feed) molar ratio of 2.4 and 8 (hereafter named $Jeff_{2.4}$ and $Jeff_8$, respectively), which clearly exhibit two distinguishable thermal events (Figure 3.12). Specifically, our thermal protocol consisted of varying the heating rate after cooling at different rates.

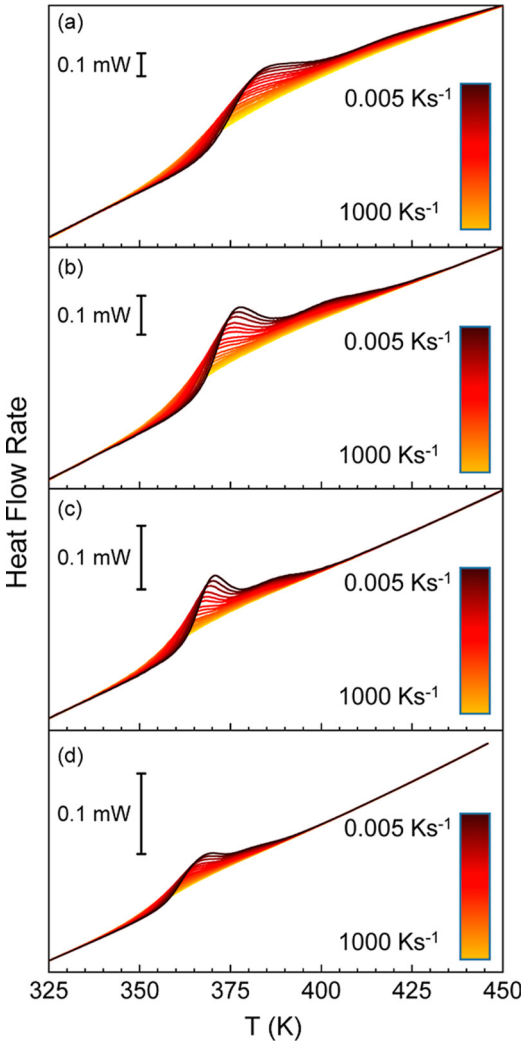

FIGURE 3.13: Heat flow rate scans obtained upon heating at (a) 1000 Ks^{-1}, (b) 500 Ks^{-1}, (c) 200 Ks^{-1} and (d) 100 Ks^{-1} after cooling in a range between 0.005 and 1000 Ks^{-1} for $Jeff_8$.

The results for $Jeff_8$ are shown in Fig. 3.13, where two thermal events can be detected for all investigated heating rates. Interestingly, the separation of both thermal events appears to be more pronounced at higher heating rates. This latter observation qualitatively indicates that the high temperature event presents a lower apparent activation energy than the low temperature event. An analogous behavior was also observed for $Jeff_{2.4}$, although in that case the low temperature thermal event exhibits a smaller endothermic effect with respect to the high temperature one (see corresponding publication).

Next, Kissinger analysis was implemented, which is widely used to gain insights into the kinetic mechanisms underlying non-isothermal chemical reactions [191] and crystallization [196]. Within this framework, we aimed to convey information about the apparent activation energies (E_a) of the two thermal events underlying the non-isothermal kinetic transformations, in this case from the frozen-in glass to the high temperature viscous flow regime [197]. To do so, we considered the temperature T_p, which corresponds to the maximum rate of enthalpy change and in our case it was identified where the rate of change of the heat flow is maximum for each one of the two thermal events. Considering also the criterion of maximum enthalpy transformation, at T_p, the first derivative of the rate of change of the kinetic transformation must be zero, which results in:

$$ln\frac{\beta}{T_p^2} = -\frac{E_a}{RT_p} + c \tag{3.8}$$

where β the heating rate dT/dt and c a temperature independent parameter, whose invariance is strictly valid only if the E_a of the thermal event under investigation is also temperature independent, which can be considered valid for the segmental relaxation for the small temperature range explored in our study.

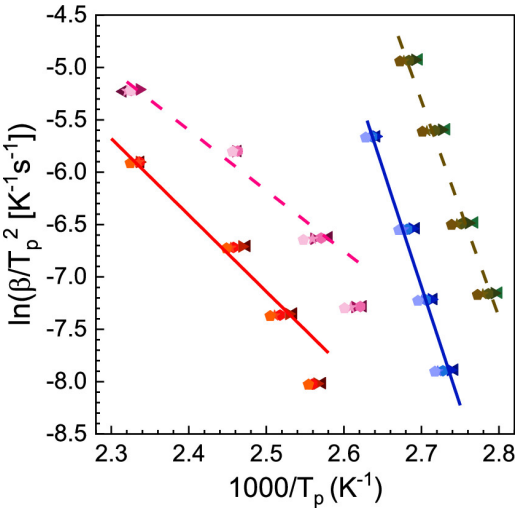

FIGURE 3.14: Kissinger plot of the thermal transformation events observed in $Jeff_{2.4}$ (solid, red and blue) and $Jeff_8$ (dash, pink and khaki) after cooling at the following rates: 0.1 (left triangles), 0.05 (right triangles), 0.02 (hexagons), 0.01 (stars) and 0.005 (pentagons) Ks^{-1}. The straight lines are the fits to eq. 3.8, which yields the following apparent activation energies for the higher and lower temperature events, respectively: $E_a = 60 \pm 5 kJmol^{-1}$ and $E_a = 190 \pm 5 kJmol^{-1}$ for $Jeff_{2.4}$ and $E_a = 50 \pm 5 kJmol^{-1}$ and $E_a = 170 \pm 5 kJmol^{-1}$ for $Jeff_8$.

The correlation established by eq. 3.8 is presented in Fig. 3.14. According to eq. 3.8, the slope of $ln(\beta/T_p^2)$ as a function of $1/T_p$ allows obtaining E_a of the molecular mechanism mediating the kinetic transformation process. As can be observed for both systems, the high temperature thermal event has a lower E_a compared to the low temperature one.

In continuation, measurements in the linear regime [198] employing step response analysis [120, 199] were performed in order to understand the values of E_a of the two transformation kinetics observed in the vitrimeric materials. The temperature and frequency dependent normalized reversing specific heat, $C^N_{p,rev}$, shows a single relatively narrow step, which can be unambiguously attributed to spontaneous fluctuations of the polymer segments associated with the glass transition, as commonly observed in all types of glass-forming systems [200, 201]. The relaxation time of these fluctuations exhibits a super-Arrhenius temperature dependence, described by the Vogel-Fulcher-Tammann (VFT) empirical equation [25–27]: $\tau(T) = \tau_0 exp(B/(T - T_0))$. The apparent activation energy obtained from the VFT equation is temperature-dependent and is given by $E_{VFT} = T^2B/(T - T_0)^2$. To verify how the two kinetic processes identified by FSC are related to the polymer segmental dynamics, we analyzed the temperature dependence of $T/E_a^{1/2}$ vs T, which for the VFT case would result in a linear plot: $T/E_{VFT}^{1/2} = (T - T_0)/B^{1/2}$.

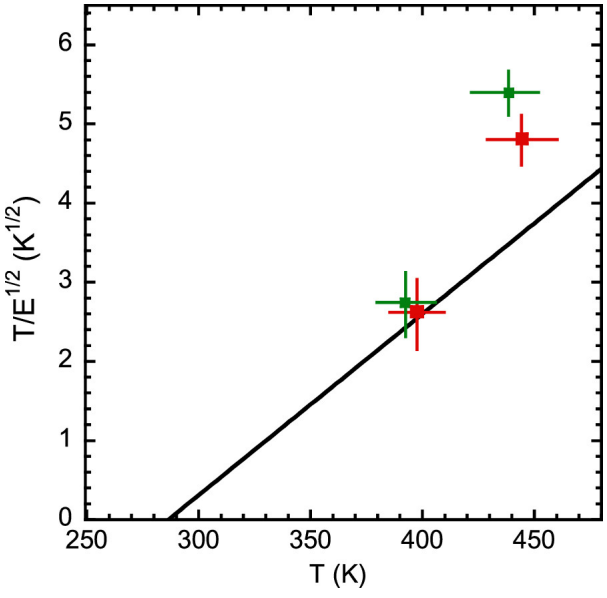

FIGURE 3.15: Comparison of the apparent activation energies obtained from FSC for the two kinetic processes for $Jeff_{2.4}$ (green) and $Jeff_8$ (red) with that corresponding to the VFT equation describing the relaxation times determined in the linear regime. The size of the crosses corresponds to the estimated uncertainties.

Fig. 3.15 shows such a comparison, from which it is clear that the low-temperature thermal event agrees well with the expectation from the VFT equation, while, in contrast, the data for the high-temperature kinetic process are far above the VFT line, indicating a significantly lower apparent activation energy, as expected for a vitrimeric-related phenomenon.

Overall, our results on the kinetic transformation from frozen-in glass to fully relaxed network indicate that it occurs via a low and a high temperature event, the former being completely coupled to the polymer segmental relaxation responsible for the glass transition. The high temperature event has a lower apparent activation energy, which is consistent with a reversible covalent bond exchange reaction [86]. The latter process is generally described as occurring in two steps: (i) approach of two active sites by segmental diffusion and (ii) bond exchange once these active sites are brought into close contact [202]. In the high temperature regime, the low activation energy is representative of the bond exchange process alone, that is, the slow step of the overall bond exchange reaction. At lower temperatures, segmental diffusion rapidly becomes slower, thereby making the overall covalent bond exchange reaction to be controlled by both steps, which is fully compatible with our results. Last, in the low-temperature regime, the overall process of the reversible covalent bond exchange reaction is expected to be completely controlled by the ultraslow segmental relaxation and becomes indistinguishable from segmental relaxation [102, 202].

Chapter 4

Conclusions and Outlook

In this thesis, we have presented a systematic investigation of the thermal events that govern the glass transition across a broad range of glass-forming materials. The non-equilibrium evolution in the glassy state has long remained elusive and numerous theories have sought to establish a connection between glass transition and molecular motions. Within the same framework, the physical aging or structural relaxation– which describes the reduction of the free energy of a glass towards the closest equilibrium state– remains an active field of research, with different approaches attempting to shed light on the uderlying mechanisms. A profound understanding of these phenomena would not only enrich our current knowledge and perception of the glassy state, but it would also provide valuable insights into the properties of materials used in a wide range of applications, thereby enabling the appropriate tailoring of their functional characteristics.

This work focused on two fundamental topics. The first one concerned the study and modeling of the kinetics of physical aging in typical Van der Waals glass-formers deeply quenched into the glassy state. The second addressed materials of greater chemical complexity, namely polymer networks forming vitrimers, with the aim of elucidating their vitrimeric character and its connection to segmental dynamics.

To begin with, we were able to perform an extensive characterization of the kinetics of physical aging in five small molecule glasses interacting via van der Waals forces, exploiting the ability of FSC to access a wide range of time scales. In this way, we covered a wide spectrum of aging time, covering about six decades. With the aim of challenging the role of the α- relaxation, we adopted two different approaches to obtain insights into the underlying molecular mechanisms mediating physical aging: (i) a model-independent approach based on the time to reach equilibrium and (ii) the SPA model, where the non-exponentiality and non-linearity of physical aging are considered employing the density scaling approach to connect the aging time-dependent α- relaxation time with the glass thermodynamic state.

The model-independent approach based on the equilibration time generally shows that the final equilibrium is attained in ways compatible with the exclusive role of the α- relaxation. In the same way, the final stages of physical aging are reasonably captured by the modified SPA model. Furthermore, the whole experimental relaxation function at the highest investigated aging temperatures is accurately described by the model. However, the central finding of the present study is that, at low aging temperatures, corresponding to large jumps in the fictive temperature, the model based on the exclusive role of the α- relaxation largely fails to describe the whole relaxation function. In particular, the experimental relaxation function is vastly more stretched than that predicted by the model, implying that, at the beginning of the equilibration process, aging proceeds faster than predicted by the model.

The main consequence of these results and their analysis is that physical aging in glasses aged significantly below T_g cannot be described as exclusively triggered by the α- relaxation and, therefore, other fast mechanisms of equilibration must be considered. As a consequence, physical aging can survive with rates amenable to the experimental practice even way below T_g, where the α- relaxation is frozen, a result that, under certain conditions, may convey glasses to low energies.

To obtain a comprehensive picture of the relaxation mechanisms that mediate physical aging in the early stages, we employed isoconversional analysis, that provides insights into the aging time-dependent thermal barriers in glasses evolving toward equilibrium. This analysis was applied not only on the small molecules studied previously, but it was also extended to a few polymer glasses. This approach allowed us to map the evolution of the effective activation barrier as a function of the extent of relaxation and our results reveal a systematic increase of the activation energy from relatively small extent of relaxation to values comparable with the α- relaxation at large ones. The low barriers detected at the onset of relaxation indicate that, in addition to the α-process, additional molecular mechanisms must contribute to equilibration. These early stages could involve secondary relaxations, such as the β-process, but the systematic character of the low activation energies across different systems points to the relevance of the slow Arrhenius process (SAP), associated with localized collective displacements and nearly temperature-invariant barriers. Taking all this into account, our findings support a multiple-step scenario of glass equilibration in which low-barrier processes mediate the initial stages of aging, while the α-relaxation dominates the final approach to equilibrium. This outcome also reinforces the results of our first publication, where the presence of fast equilibration mechanisms in the early stages of aging is suggested.

The last work related to the first thematical section of the thesis was the investigation of the validity of density scaling in out-of-equilibrium glasses by analyzing the physical aging of an archetypal molecular glass former (KDE) through broadband dielectric spectroscopy. That was done by monitoring the dielectric loss on the high-frequency flank of the α-relaxation together with the high-frequency capacitance. The main hypothesis was that if density scaling is valid in non-equilibrium conditions, the connection between the variation of the α- relaxation time and that of the high frequency capacitance must fulfill two main conditions: (i) the two magnitudes must be proportional; and (ii) the proportionality factor between them must be a specific value derived from intrinsic properties of the glass, including the fitting parameters used to describe relaxation data at equilibrium. Our results demonstrate that both conditions are generally fulfilled, thereby providing the first evidence of the validity of density scaling in out-of-equilibrium conditions.

The ability of describing aging data with the γ value obtained from equilibrium relaxation data has two important implications. First, it confirms that γ is indeed a material constant that does not depend on the thermodynamic path used to probe the relationship between τ, T, and ρ. Second, it suggests that the molecular interactions governing the relative importance of thermal energy and packing are unchanged as the system falls out of equilibrium. Moreover, our results imply that applying density scaling in the aging regime does not require the introduction of any additional term accounting for the nonequilibrium nature of glasses. The main consequence of this outcome is that the description via density scaling of aging results obtained in simulations must account for the change of pressure taking place in these conditions rather than requiring a non-equilibrium additional term. In addition, the most important implication of these results is that density scaling approach can be applied to predict the evolution of a given observable with aging time, as was done in combination with the single parameter aging (SPA) approach in the first work presented in this thesis. Given the outcome of the present work, the failure of density scaling combined with the SPA approach, rather than being due to inaccuracy of density scaling, must be attributed to the inability of the α- relaxation alone to catch the overall phenomenology of physical aging. Hence, the role of secondary mechanisms in the kinetics of physical aging must be considered.

Concerning the outlook and future work associated with the first part of this thesis, an important implication of our findings is that they open the door to accessing glasses with low energy. Within the scenario of physical aging exclusively driven

by the α- relaxation, the tremendous growth of the associated time scale with decreasing temperature would imply that aging would disappear not too far from T_g, thereby preventing the exploration of low energy states. Nevertheless, physical aging is known to exhibit pronounced effects even way below T_g [35, 203–209], which can be rationalized considering non-α relaxations, whose potential to equilibrate glasses survives where the α- relaxation is completely frozen. Reducing the sample size may significantly shorten the time scale of glass relaxation via fast non-α mechanisms and thus, make feasible the exploration of topics of utmost importance, such as the existence of the ideal glass transition [210] at the Kauzmann temperature [211, 212].

Regarding the isoconversional methods, although they are very powerful owing to their model-free character, their applicability is intrinsically limited to regions of the kinetics, where the extent of relaxation evolves measurably with time. As a consequence, they do not allow one to reliably access the limiting activation barriers in the asymptotic regimes $R \to 0$ and $R \to 1$, nor in the presence of intermediate plateaus associated with nearly invariant relaxation rates [55]. In such flat regions of the kinetics, the characteristic time associated with a given relaxation becomes poorly defined, and even small experimental noise in the relaxation can translate into large uncertainties in the extracted times and, consequently, in the apparent activation energies. A promising strategy to overcome this obstacle would be the combination of isoconversional and inflectional analyses. In such cases, the latter strategy, based on determining via model-free approaches the time scales associated with changes in the logarithmic slopes of the relaxation function, as originally proposed by Kovacs [213], provides a viable pathway. Extending this approach to systems in which the activation barriers of the SAP and the β- process are known and sufficiently distinct would enable quantitative separation of their respective contributions. Additionally, systematic aging studies should be performed far below T_g so as to capture the non-monotonic evolution of the activation energy and to unravel the interplay of relaxation mechanisms governing long-term equilibration in glassy materials, where different processes are expected to become increasingly separated, potentially allowing distinct γ, β/SAP and α activation barriers to emerge also in organic glasses.

Moving on to the conclusions of the second part of this thesis, Fast Scanning Calorimetry was employed for the first time to evaluate the tempeature of the topology freezing transition (T_v) of cross-linked networks. Our results on the kinetic transformation from the glassy state to fully relaxed network suggest that it occurs via a low

and a high temperature event, the former being completely coupled to the polymer segmental relaxation responsible for the glass transition. Concerning the high temperature event, it appears to have a lower apparent activation energy, which is consistent with a reversible covalent bond exchange reaction. Two stages of the bond exchange process have been established, (i) approach of two active sites by segmental diffusion and; (ii) bond exchange once these active sites are brought into close contact.

In the high temperature regime, we found that it is the bond exchange alone that drives the overall reaction, due to the extremely short time scales of the segemental diffusion in that region. In an intermediate temperature range, segmental diffusion rapidly becomes slower, thereby making the overall covalent bond exchange reaction to be controlled by both steps, in agreement with our results which show an increasing apparent activation energy at low temperatures. In the low temperature regime, the two stages of the bond exchange process, that is, diffusion and chemical bond exchange, become coupled, leading to an apparent increase in activation energy. The latter observations may explain why only a relatively narrow specific heat step is observed by standard DSC, considering that the latter technique, due to the long accessible observation times, i.e. much lower heating/cooling rates compared to FSC, actually explores the low temperature regime. This is found only for very large separation between segmental relaxation and bond exchange reaction time, which is rarely observed unless nanophase separation takes place [214, 215]. Standard DSC has previously been shown to provide convincing evidence of the two thermal events only in some rare cases [102].

It is also worth-mentioning that the amount of amine used in the preparation of the cross-linked networks affects the range over which T_g is distributed and its degree of separation from the T_v. These considerations are also relevant to the relative intensity of the glass transition and vitrimeric kinetics obtained from FSC. It was found that for the sample that the dynamic bond exchange occurs intradendrimerically ($Jeff_8$), the glass transition is more intense than the vitrimeric transformation compared to the sample that it occurs more interdendrimerically ($Jeff_{2.4}$).

All these findings treated with the Kissinger analysis, eventually allowed us to determine the activation energy of the bond exchange, using a protocol of different heating and cooling rates in the FSC that separates this process from the T_g. As expected, the activation energy obtained from the bond exchange was much lower, in

the range of $50 - 60$ kJ/mol, than the apparent activation energy of the glass transition, in the range of $170 - 190$ kJ/mol. Our FSC protocol, here developed, can be extended to the detection of T_v and the study of the bond exchange kinetics of a number of vitrimeric networks, highlighting the versatility of this approach in characterizing dynamic covalent materials. By enabling rapid and precise thermal analysis, the method provides critical insight into the temperature-dependent kinetic processes and the influence of network composition, and cross-link density on the vitrimeric behavior.

Last but not least, the most fundamental component– and undoubtedly the principal unifying factor– of this thesis, is the versatility and the wide range of possibilities of Fast Scanning Calorimetry. This technique allows us to access very short time scales, by applying extremely high heating/cooling rates of the order of 1000 K/s, thereby providing insights into the dynamics of out-of-equilibrium systems, not accessible by conventional methods. The study of structural relaxation kinetics, the calculation of fictive temperatures, the construction of relaxation maps and the separation of thermal events are only the most significant aspects of the potential of FSC. Moreover, as shown here, it can be applied to materials of completely different nature, providing invaluable information on their molecular dynamics.

We anticipate that the insights gained from this thesis will pave the way for further research in the field of low-energy glasses and exploration of the potential of calorimetric techniques. We also expect that the findings on vitrimeric polymer networks will provide a solid basis for their further development and the tailoring of their properties.

Chapter 5

Full List of Publications

The following works have been published as part of this thesis (in chronological order):

- **Physical aging in molecular glasses beyond the α relaxation.** Di Lisio, V.; Stavropoulou, V.-M.; Cangialosi, D. , *J. Chem. Phys.* 2023, 159, 064505. Impact Factor: 3.1 (Q1).
- **Vitrimeric Behavior Revealed by Fast Scanning Calorimetry in Branched Polyglycerol Networks Cross-Linked by Reversible Enamine Bonds.** Stavropoulou, V. M.; Aldecoa-Ortueta, M.; Verde-Sesto, E.; Di Lisio, V.; Lam, A.; Pomposo, J. A.; Alegría, A.; Cangialosi, D.; Barroso-Bujans, F., *Macromolecules* 2025, 58 (18), 9993- 10006. Impact Factor: 5.2 (Q1).
- **Identifying the Thermal Barriers of Glass Aging via Isoconversional Analysis.** Stavropoulou, V. M.; Caporaletti, F.; Pabst, F.; Di Lisio, V.; Napolitano, S.; Cangialosi, D., *J. Phys. Chem. B* 2026, 130 (5), 1716–1723. Impact Factor: 2.9 (Q1).

There is an additional work currently in pre-print format which is included in the Appendix A:

- **Testing the Validity of Density Scaling in Out-of-Equilibrium Systems** Stavropoulou, V. M.; Caporaletti, F.; Napolitano, S.; Cangialosi, D.

RESEARCH ARTICLE | AUGUST 08 2023

Physical aging in molecular glasses beyond the *α* relaxation

Valerio Di Lisio ; Vasiliki-Maria Stavropoulou ; Daniele Cangialosi

J. Chem. Phys. 159, 064505 (2023)
https://doi.org/10.1063/5.0157994

The Journal of Chemical Physics ARTICLE pubs.aip.org/aip/jcp

Physical aging in molecular glasses beyond the α relaxation

Cite as: J. Chem. Phys. 159, 064505 (2023); doi: 10.1063/5.0157994
Submitted: 13 May 2023 • Accepted: 17 July 2023 •
Published Online: 8 August 2023

Valerio Di Lisio,[1] Vasiliki-Maria Stavropoulou,[2] and Daniele Cangialosi[1,2,a)]

AFFILIATIONS

[1] Donostia International Physics Center, Paseo Manuel de Lardizabal 4, 20018 San Sebastián, Spain
[2] Centro de Física de Materiales (CSIC–UPV/EHU), Paseo Manuel de Lardizabal 5, 20018 San Sebastián, Spain

[a)] Author to whom correspondence should be addressed: daniele.cangialosi@ehu.eus

ABSTRACT

The description of kinetics of physical aging, namely the slow evolution of a glass thermodynamic state toward equilibrium, generally relies on the exclusive role of the main α relaxation. Here, we study the kinetics of physical aging over a wide temperature range in five small molecules interacting via van der Waals forces monitoring the time evolution of the glass enthalpic state. To this aim, we employ fast scanning calorimetry, which permits exploring a wide range of aging times. To challenge the role of the α relaxation in the description of physical aging, we employ a model-independent approach, based on the time to reach equilibrium, and a modified version of the single parameter aging model. The latter accounts for the non-linearity of aging making use of the so-called density scaling approach to describe the dependence of the α relaxation time on the glass thermodynamic state. We show that the α relaxation is generally adequate to describe aging at temperatures close to the glass transition and, for lower temperatures, the latest stages of equilibration. In contrast, at low aging temperatures, it fails to catch a wide portion of the time-dependent evolution of the glass thermodynamic state, which is found to be much faster than predicted considering only the α relaxation. Hence, our results and analysis provide compelling arguments that the description of glass equilibration under a wide range of aging conditions is conveyed by different molecular mechanisms, beyond the mere role of the α relaxation.

I. INTRODUCTION

Liquids can be supercooled below their melting temperature, provided that crystallization is avoided. On further cooling and depending on the applied rate of temperature decrease, the supercooled liquid transforms into a non-equilibrium glass, a phenomenon addressed as vitrification or glass transition.[1] The non-equilibrium glass exhibits a solid-like behavior and excess free energy with respect to the metastable supercooled liquid. The time-dependent reduction in the glass free energy toward equilibrium defined by the metastable supercooled liquid is known as physical aging[2,3] or structural recovery.[4,5]

The kinetic nature of vitrification and, once in the glassy state, of physical aging implies that both phenomena must be mediated by at least one molecular mechanism. Within the commonly accepted picture, in both vitrification and physical aging, the main α relaxation with super-Arrhenius temperature dependence has been regarded as the only relevant mechanism. Concerning vitrification kinetics, this has been shown studying the cooling rate dependent glass transition temperature, T_g, and the temperature-dependent α relaxation time, τ_α. It was shown that, in both polymeric[6–8] and low molecular weight glass formers,[9,10] the cooling rate dependent glass transition exhibits the same super-Arrhenius temperature dependence as τ_α. Furthermore, several studies where physical aging after non-linear thermal[11–14] and dielectric[15] perturbations is monitored in a limited range in the proximity of T_g showed that the typical time scale of aging follows the same behavior as τ_α.

The paradigmatic picture addressing the role of the α relaxation has recently been challenged. Experiments where the vitrification kinetics was explored in a wide range of cooling rates for a metallic glass former showed that this takes place at lower temperatures than expected only accounting for the α relaxation.[16] This behavior is exacerbated in polymeric[17] and metallic glass formers[18] subjected to geometrical confinement. Regarding physical aging, there exists increasing evidence that the simple scenario where the approach to equilibrium exclusively depends on the α relaxation must be deeply

revisited. When aged significantly below T_g, polymeric,[19–21] chalcogenide,[22] metallic,[23,24] and simple molecule[25,26] glasses exhibit at least two steps in the kinetics of equilibrium recovery. In polymeric glass formers, for which aging experiments at various aging temperatures and times were carried out,[19] while the slow step can be associated with the α relaxation, the fast one exhibits mild temperature independent activation energy, underlying the existence of molecular mechanisms different from the α relaxation triggering physical aging at short aging times.

While the mentioned activity evidences the presence of multiple mechanisms of equilibration, a systematic study, above all in small molecule glasses, has so far remained elusive. The present study aims to provide a comprehensive characterization of physical aging, monitored following isothermal enthalpy relaxation, of five small molecule glasses, interacting via van der Waals forces, and challenges the role of the α relaxation in the kinetics of physical aging. To this aim, on the one hand, we consider a model-independent metric, based on the determination of the aging temperature-dependent time to reach equilibrium. On the other hand, we employ a modified version of the so-called single parameter aging (SPA) model, which has been shown to catch the entire phenomenology of physical aging after temperature jumps of a few Kelvin.[27–29] To account for the thermodynamic state dependence of the α relaxation time, τ, our approach employs the density scaling relation,[30] where both temperature and volume contributions to τ are included. Based on these two complementary approaches, we show that the α relaxation is able to provide a complete description only in a limited temperature range in the proximity of the glass T_g. In contrast, when the aging temperature largely departs from T_g, accounting exclusively for the α relaxation generally fails to describe the kinetics of glass equilibration. The natural consequence of this finding is that mechanisms beyond the α relaxation contribute to glass equilibration significantly below T_g and must be accounted for in both theoretical modeling of aging and lifetime prediction of products made of glass,[31] where modifications of properties may be detrimental to practical applications.

II. EXPERIMENTAL

o-Cresolphthalein dimethyl ether (KDE ≥98% purity), phenolphthalein dimethyl ether (PDE ≥98% purity), and 1,1-bis (4-methoxyphenyl)cyclohexane (BMMPC ≥98% purity) were provided by Polymer Source, while o-terphenyl (OTP, ≥99% purity) was provided by Sigma-Aldrich. BMPC (also referred to as bisphenol-C-dimethylether) was obtained from the Max Planck Institute for Polymer Research, Mainz, Germany. All materials were used as received.

Fast Scanning Calorimetry (FSC) was performed using a Mettler-Toledo Flash Differential Scanning Calorimeter (DSC) 1 equipped with an intracooler and operating in a temperature range between 173 and 723 K. A Leica M60 optical microscope is integrated in the FSC system, and it is operating at a 400× magnification, allowing the evaluation of the quality of the chip and the observation of the deposition of the sample on it. Furthermore, a Leica IC80 HD camera is connected, offering the possibility of acquiring micrographs of the chip. The sample chamber was purged with dry nitrogen at a flow rate of 20 ml/min. The specimens were prepared by the direct deposition of the material (sample mass ≈100 ng) onto a Mettler-Toledo UFS 1 chip. The samples deposited on the chip exhibited an equivalent diameter of ≈200 μm, which, given the sample mass of ≈100 ng and densities of our materials between 1 and 1.3 g/cm^3, resulted in samples' thickness of the order of 10 μm.

Standard Differential Scanning Calorimetry (DSC) was performed by means of a TA Instruments DSC Q2000, equipped with an intracooler and operating in a temperature range between 193 and 873 K. The oven was purged with dry nitrogen at a flow rate of 50 ml/min. Specimens have been prepared by weighing about 10 mg of sample in a 40 μl aluminum pan without lid.

Isothermal aging experiments at different times were performed for all samples, aiming to characterize the vitrification kinetics. The temperature program comprises heating and cooling scans at a rate of 1000 K/s in a temperature range between 173 K and T_m + 10 K, depending on the melting temperature of the compound. After cooling from the melt, the samples were kept at T_a for different aging times (t_a), ranging from 0.1 to 80 000 s. After each isotherm, the samples were immediately cooled down to 173 K and a heating scan was recorded. Prior to the evaluation of the time- and temperature-dependent fictive temperature $T_f(T_a, t_a)$ (see Sec. III), the glass and liquid heat flow rates of a given set of experiments were superposed on the unaged reference via the VITRIFAST method, recently introduced by Abate *et al.*,[32] an optimization procedure based on the minimization of the mean squared error between aged and unaged scans in the glass and liquid.

For each specimen, the time scale of spontaneous fluctuations associated with the α relaxation was characterized in terms of frequency-dependent complex thermal susceptibility (i.e., the complex specific heat, c_p^*) by means of FSC and DSC step-response analyses.[33–35] The step-response protocol, spanning the whole range of the glass transition, consists of a loop of down-jumps of $\Delta T = -2$ K at a nominal cooling rate (β), followed by an isotherm of duration t_{iso}. The base angular frequency ω_0 can be determined as

$$\omega_0 = 2\pi/t_p = 2\pi/(t_{iso} + \Delta T/\beta), \tag{1}$$

where the period of stimulation t_p is the cumulative time of the down-jump and the isotherm. The real (c_p') and imaginary (c_p'') contributions to the complex susceptibility c_p^*, as well as the reversing specific heat (c_p^{rev}), i.e., the modulus of the complex susceptibility, were calculated for ω_0 and higher-order harmonics $\omega = k\omega_0$ ($k = 2, 3, 4, \ldots$) by using a Discrete Fast Fourier Transform (DFFT) relationship of the form

$$c_p^*(\omega) = c_p'(\omega) - ic_p''(\omega) = \frac{\sum_{t=0}^{t_p} HF(t)\, e^{-i\omega t}\, \Delta t}{\sum_{t=0}^{t_p} q_c(t)\, e^{-i\omega t}\, \Delta t}, \tag{2}$$

where $HF(t)$ and $q_c(t)$ are the instantaneous heat flow and the instantaneous cooling rate, respectively. The temperature dependence of $c_p^*(\omega, T)$ has been assessed by running the DFFT algorithm for each loop composing the step-response protocol. Finally, the temperature-dependent relaxation time, $\tau(T) = (2\pi\omega)^{-1}(T)$, has been determined at the inflection point of $c_p^{rev}(\omega, T)$, that is, the modulus of the complex specific heat, which approximately equals the real part of the complex specific heat, $c_p'(\omega, T)$, due to the fact

TABLE I. Experimental parameters of the step-response protocol.

Technique	β	Isotherm (s)	t_p (s)	ω_0 (rad s^{-1})
FSC	2000 K s^{-1}	0.1014	0.1024	61.3
FSC	500	1.6344	1.6384	3.83
FSC	100	16.364	16.384	0.38
DSC	15 K min^{-1}	120	128	0.049
DSC	1.875	960	1024	0.006 1
DSC	0.5	7956	8196	0.000 77

that c_p'' is at least one order of magnitude smaller than c_p'. The determination of the time scale of spontaneous fluctuations in a frequency range of about six orders of magnitude is achieved by performing six different step-response experiments for each specimen and combining the measurements of FSC and DSC. Table I reports the experimental parameters of the step-response protocols that have been adequately chosen to probe $c_p^*(\omega, T)$ in the largest frequency range available, while maintaining a good accuracy and low signal-to-noise ratio (Table I).

III. RESULTS

We begin presenting the calorimetric response underlying physical aging at one aging temperature for each investigated system as showcases. Similar results were obtained at the other aging temperatures. Figure 1 shows the heat flow rate scans, proportional to the specific heat, c_p, collected at 1000 K/s on samples cooled down at the same rate to the indicated temperature and aged isothermally in a wide range of times. The typical signature of glass equilibration resulting from physical aging—that is, the development of an endothermic overshoot with magnitude increasing with aging time[5,36]—can be observed. The temperature interval where the overshoot is located depends on the aging time. Shortly after the beginning of aging, it grows on top of the specific heat step underlying the glass transition. At longer aging times, the endothermic overshoot shifts to higher temperatures, indicating that accessing low energy states delays devitrification when heating the aged samples.

From the connection between specific heat and enthalpy: $c_p = \left(\frac{\partial H}{\partial T}\right)_p$, the area between the aged and unaged scans contains the amount of enthalpy relaxed during physical aging. The enthalpic state of the glass can be parameterized via the concept of fictive temperature, T_f, that is, the temperature at which the glass line drawn from the glass thermodynamic state crosses the supercooled liquid line.[36,37] Hence, low T_f(s) are characteristic of low enthalpy glasses. The fictive temperature is obtained via the Moynihan method,[38]

$$\int_{T_f}^{T_1}(c_{p,l}-c_{p,g})dT = \int_{T_2}^{T_1}(c_p-c_{p,g})dT, \tag{3}$$

where c_p is the specific heat of the sample, $c_{p,l}$ and $c_{p,g}$ are the liquid and glassy lines, respectively—fitted by linear equations (see the dashed lines in Fig. 1)—and T_1 and T_2 are the temperatures well above and below T_g, respectively.

The aging time and temperature evolution of T_f is presented in Fig. 2 for all investigated systems. The T_f of OTP at zero aging time and after cooling at 1000 K/s, T_f = 263 K, agrees with previous reports.[32,39] Data at such a high rate for the other glass formers are not available. However, as expected, the zero aging time T_f of these glass formers is systematically larger than T_g at rates of several K/min.[40] As a general rule, decreasing the aging temperature entails increasing times to reach equilibrium and lower T_f. In all cases, the values of T_f at the end of the aging process lie in close proximity to the aging temperature, apart from some minor deviations for aging temperatures significantly lower than T_g, likely resulting from the inaccurate extrapolation of $c_{p,l}$ below T_g.[41]

The aging time evolution of T_f allows obtaining insights into aging kinetics. A model-independent approach relies on the use of the time to reach equilibrium, τ_{eq}, indicated with open symbols in Fig. 2, which does not depend on the previous thermal history[42] and is representative of the glass close to equilibrium.[19] Here, τ_{eq} was determined considering that equilibrium was reached when T_f was less ±1 K different from its average plateau value. Figure 3 depicts the aging temperature dependence of τ_{eq} for all investigated systems. In the same figure, the temperature dependence of the α relaxation time, τ, obtained from the step-response analysis in the linear regime delivering the frequency and temperature dependence of complex specific heat,[34,35] is presented (see Sec. II for details). As a general feature, τ_{eq} follows the same temperature dependence of τ at large aging temperatures. In all cases, except for PDE, the same applies for lower aging temperatures. For PDE at low aging temperatures, τ_{eq} seemingly exhibits a slight deviation from τ toward a mildly activated temperature dependence.

A. Modeling the kinetics of physical aging

The time to reach equilibrium is representative of the kinetics of physical aging of the glass in the proximity of equilibrium and, therefore, only conveys information on molecular mechanisms active under these conditions. For a comprehensive description of the overall kinetics of physical aging, the entire aging time evolution of the glass thermodynamic state must be described. For this purpose, the unavoidable requirement stands on implementing a framework including the typical signature of physical aging, that is, its non-exponentiality and non-linearity.[4] The former regards the intrinsic nature of the α relaxation, resulting in a response more stretched than a simple exponential.[43] The non-linearity of physical aging is due to the fact that the relaxation time of molecular mechanisms assisting equilibration changes with the glass thermodynamic state. In particular, in aging protocols where a reduction in T_f takes place—as is the case of the present study—τ progressively increases during aging, whereas the opposite holds for experiments entailing a T_f increase.

The non-linearity of aging can be quantified employing the concept of material time, ξ, related to the clock rate, that is, the inverse of the relaxation time, by[27–29,44]

$$d\xi = \tau^{-1}dt. \tag{4}$$

Within the conventional description of physical aging, the relaxation time is identified with that of the α relaxation. In such

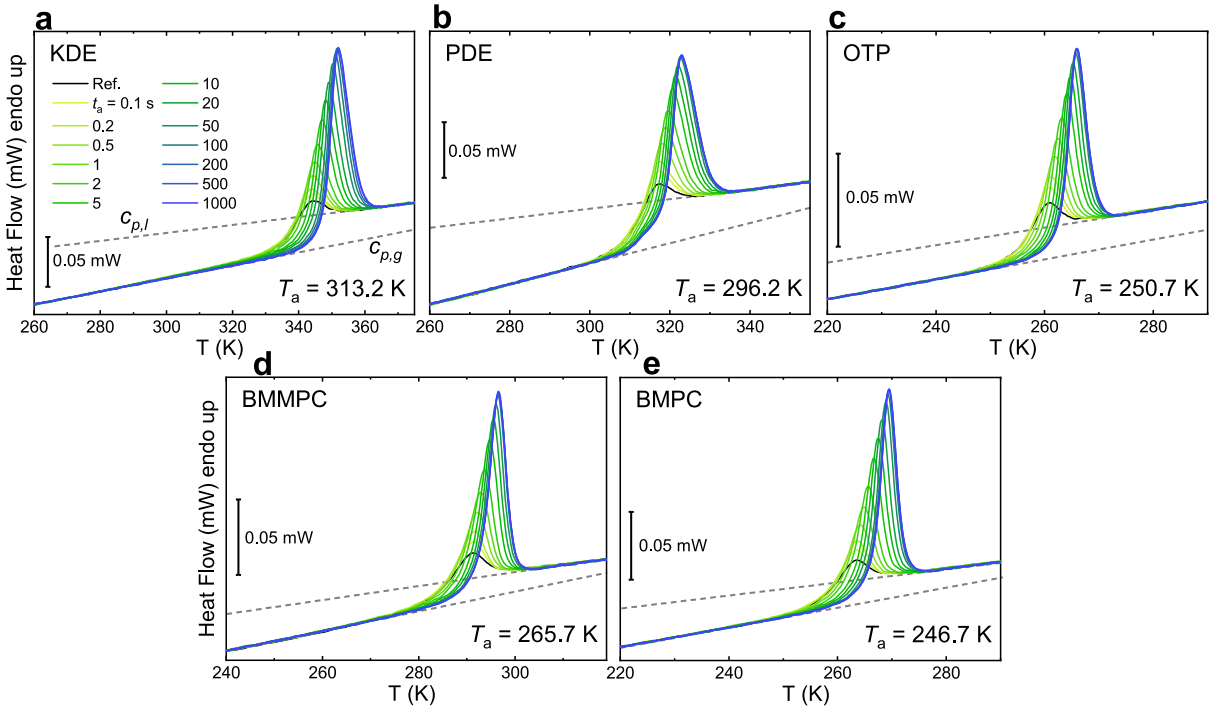

FIG. 1. Heat flow rate scans, proportional to the specific heat, for all glasses at the indicated aging temperatures and times.

a way, the non-linear response of physical aging can be reduced to the linear response at equilibrium by simply replacing the time, t, with the material time, ξ.[29] Popular phenomenological approaches, implementing the non-exponential and non-linear behavior of aging, are the Tool–Narayanaswamy–Moynihan (TNM)[38] and Kovacs–Aklonis–Hutchinson–Ramos (KAHR)[45] models, which share the common feature of requiring multi-parameter fitting. Furthermore, both models impose a temperature independent activation energy at equilibrium, which is at odds with the super-Arrhenius temperature dependence of the α relaxation time. Efforts to account for the increasing activation energy with decreasing temperature have recently been implemented.[46–49]

Here, differently from TNM and KAHR approaches, we describe α relaxation driven aging without making an explicit assumption on the mathematical form of non-linearity. This approach, known as single parameter aging (SPA), has recently been shown to accurately describe aging of several glasses[27,28] and, for the first time, to predict non-linear aging from linear response.[29] Given the relatively small temperature jumps explored in previous applications of SPA, the aging time dependence of $\ln\tau$ was assumed to be linear with the instantaneous thermodynamic state of the glass: $\ln\tau(t) = \ln\tau_\infty + \Lambda(T_f(t) - T_a)$, where Λ is the single fitting parameter and $\ln\tau_\infty$ is the equilibrium relaxation time, attained after aging completion, at the aging temperature, T_a. In this way, higher order terms of the Taylor expansion are neglected. While this assumption is certainly acceptable for temperature jumps of a few Kelvin, our study entails changes of T_f with the aging time as large as more than 20 K (see Fig. 2), for which the linear assumption may be inadequate.

While keeping the overall philosophy, we implement the SPA model describing the dependence of τ on the aging temperature, T_a, and specific volume, $V(T_a,t)$, of the glass, namely its thermodynamic state, via the so-called density scaling approach,[30] which has recently been rationalized on the basis of free volume models.[50] The underlying idea is in the same spirit as the density scaling approach to non-equilibrium glasses recently proposed by Niss,[51]

$$\tau(T_a,t) = \tau_0 \exp\frac{C}{T_a V(T_a,t)^\gamma}, \tag{5}$$

where C and γ are material specific constants.

In Eq. (5), the dependence of both $\tau(T_a,t)$ and $V(T_a,t)$ are shown in Fig. 4 for OTP at equilibrium, just after cooling to T_a and at a given aging time at T_a. In our study, the relaxation time at equilibrium, τ_∞, is obtained from calorimetric measurements in the linear regime (the same data as shown in Fig. 3). The specific volume at the beginning of aging, $V(0)$, and that at equilibrium, V_{eq}, can be calculated from the equilibrium volume, V_0, at the initial fictive

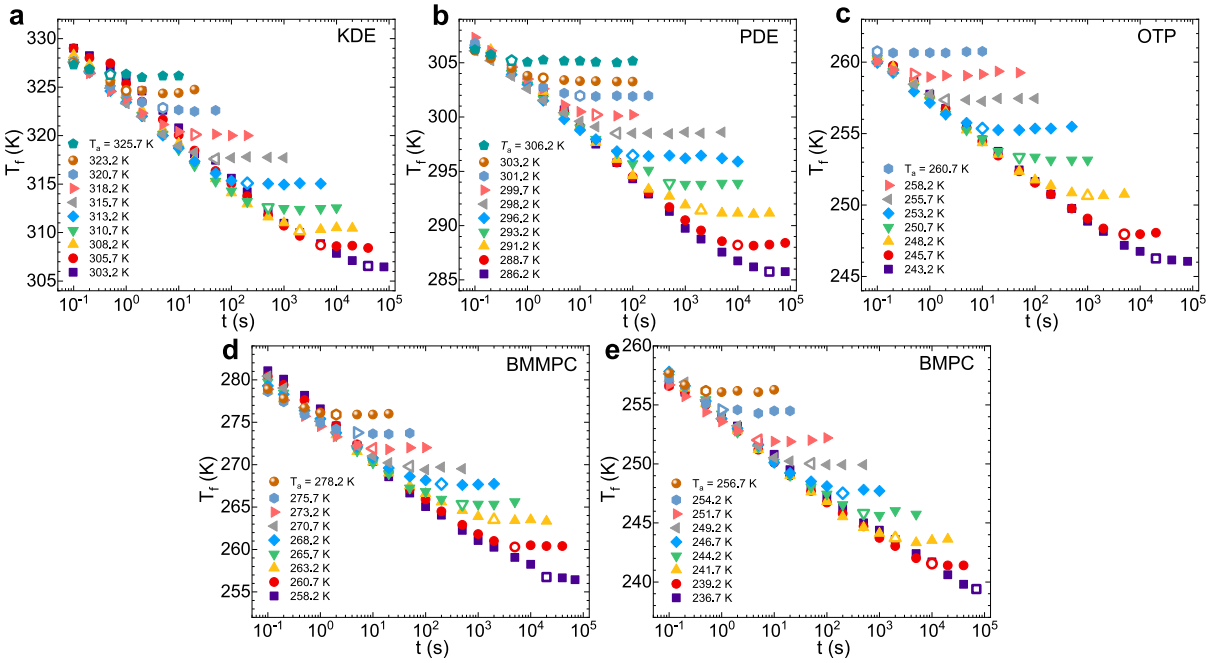

FIG. 2. Aging time evolution of the fictive temperature at different aging temperatures for all investigated glasses. The open symbols indicate the time to reach equilibrium τ_{eq}.

temperature, $T_f(0)$—in our case, the fictive temperature after cooling at 1000 K/s—by the following equations:

$$V(0) = V_0(1 - \alpha_g(T_f(0) - T_a)) \tag{6}$$

and

$$V_{eq} = V_0(1 - \alpha_l(T_f(0) - T_a)), \tag{7}$$

where α_g and α_l are the coefficients of thermal expansion in the glassy and liquid states, respectively. Here, we have implicitly assumed that T_f from enthalpy relaxation experiments coincides with that of volume relaxation, which was shown to be approximately correct.[11,42,52,53] In analogy to Eq. (6), as depicted in Fig. 4, the time-dependent volume is connected to the time-dependent fictive temperature by

$$V(t) = V_0(1 - \alpha_l(T_f(0) - T_f(t)) - \alpha_g(T_f(t) - T_a)). \tag{8}$$

Before expressing the instantaneous volume during aging, $V(t)$, as a function of $T_f(t)$, we define the normalized relaxation function, varying between the unity, at the beginning of aging, and zero, once aging is completed,

$$R(t) = \frac{T_f(t) - T_a}{T_f(0) - T_a}. \tag{9}$$

Hence, combining Eqs. (7)–(9), we obtain the following expression, where the aging time dependence is exclusively contained in $R(t)$,

$$V(t) = V_0(1 - \Delta T_f(\alpha_l - \Delta\alpha R(t))), \tag{10}$$

where $\Delta\alpha = \alpha_l - \alpha_g$ and $\Delta T_f = T_f(0) - T_a$.

From the explicit aging time dependence of $V(t)$, the relaxation time at a given aging temperature and time can be written combining Eqs. (5) and (10),

$$\tau(T_a, t) = \tau_0 \exp \frac{C}{T_a(V_0(1 - \Delta T_f(\alpha_l - \Delta\alpha R(t))))^y}, \tag{11}$$

and analogously, the equilibrium relaxation time is given by

$$\tau_\infty = \tau_0 \exp \frac{C}{T_a(V_0(1 - \alpha_l \Delta T_f))^y}. \tag{12}$$

Combining Eqs. (11) and (12), the aging time-dependent relaxation time can be rewritten as

$$\ln \tau(T_a, t) = \ln \tau_\infty(T_a) + \frac{C}{T_a V_0^y} \times \left(\frac{1}{(1 - \Delta T_f(\alpha_l - \Delta\alpha R(t)))^y} - \frac{1}{(1 - \alpha_l \Delta T_f)^y} \right). \tag{13}$$

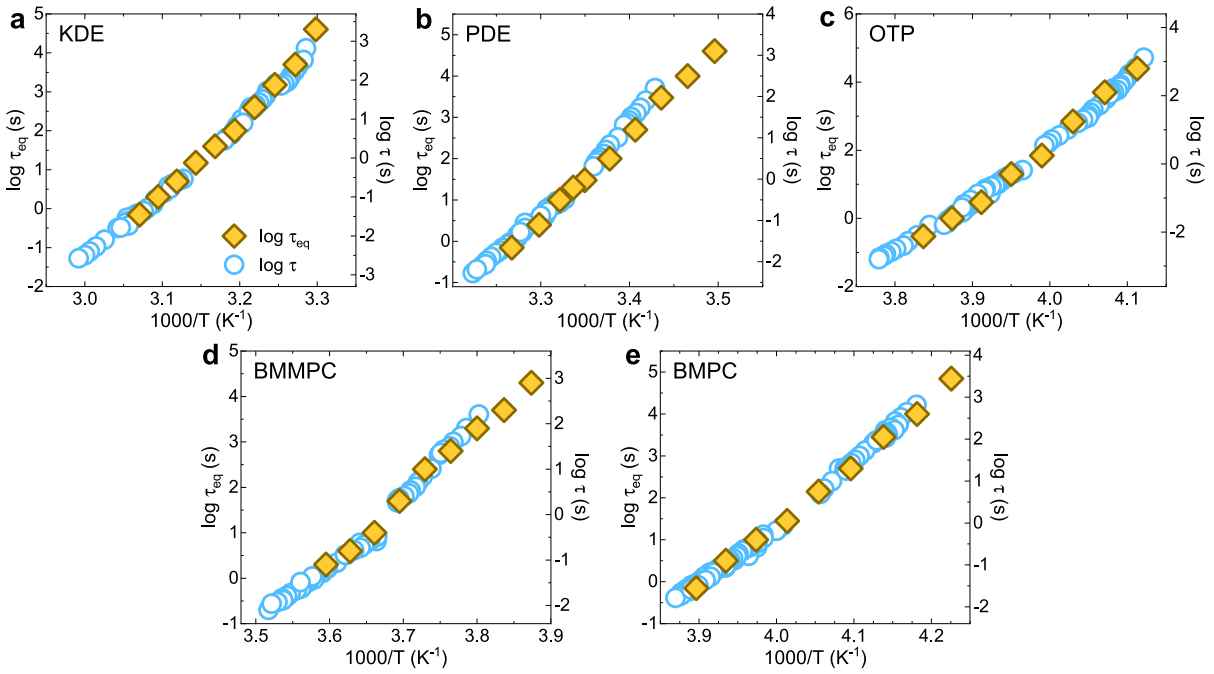

FIG. 3. Time scale to reach equilibrium (left axis) and relaxation time of the α relaxation (right axis) as a function of the inverse temperature for all investigated glasses.

We now define the following function of $R(t)$, corresponding to the second addend of the right-hand side of Eq. (13):

$$g(R(t)) = \frac{C}{T_a V_0^{\gamma}}\left(\frac{1}{(1-\Delta T_f(\alpha_l - \Delta\alpha R(t)))^{\gamma}} - \frac{1}{(1-\alpha_l \Delta T_f)^{\gamma}}\right). \tag{14}$$

In such a way, the aging time and temperature-dependent relaxation time are expressed by

$$\ln \tau(T_a, t) = \ln \tau_{\infty} + g(R(t)). \tag{15}$$

For temperature down-jumps, where the relaxation time during aging is always smaller than or equal to τ_{∞}, $g(R(t)) \le 0$.

To model physical aging results of a given glass, the knowledge of the normalized relaxation function at a reference aging temperature $R_1(t)$ is required. This can be obtained by interpolating or fitting with an appropriate function experimental aging data at that temperature. The reduction in the non-linear response after an arbitrarily chosen temperature jump to the linear response after a jump smaller than the amplitude of spontaneous thermal fluctuations[29] implies that the normalized relaxation function is a unique function of the material time: $R_1(\xi) = R_2(\xi)$. This implies that a generic normalized relaxation function after an arbitrary temperature jump can be derived from the relaxation function at a reference temperature.[29]

The equality of $R(\xi)$ after different jumps holds for the derivatives, too,

$$\frac{dR_1(\xi)}{d\xi} = \frac{dR_2(\xi)}{d\xi}, \tag{16}$$

which can be rewritten in terms of absolute time considering Eq. (4),

$$\frac{dR_1(t_1^*)}{dt_1^*}\tau_1(t_1^*) = \frac{dR_2(t_2^*)}{dt_2^*}\tau_2(t_2^*). \tag{17}$$

Here, $\tau_1(t_1^*) = \tau(T_1, t_1^*)$ and $\tau_2(t_2^*) = \tau(T_2, t_2)^*$. Hence, combining Eq. (17) with Eq. (15), we obtain

$$\frac{dR_1(t_1^*)}{dt_1^*}\tau_{1,\infty}\exp\left(g(R_1(t_1^*))\right) = \frac{dR_2(t_2^*)}{dt_2^*}\tau_{2,\infty}\exp\left(g(R_2(t_2^*))\right). \tag{18}$$

If we consider identical changes in the normalized relaxation function, $dR_1(t_1^*) = dR_2(t_2^*)$, we can deduce the time increment for aging at the target temperature rearranging Eq. (18),

$$dt_2^* = \frac{\tau_{2,\infty}}{\tau_{1,\infty}}\exp\left[g_2(R) - g_1(R)\right]dt_1^*, \tag{19}$$

where $g(R_1(t_1^*))$ and $g(R_2(t_2^*))$ are replaced by $g_1(R)$ and $g_2(R)$, respectively. Integrating Eq. (19), we obtain

$$t_2 = \int_0^{t_2} dt_2^* = \frac{\tau_{2,\infty}}{\tau_{1,\infty}}\int_0^{t_1}\exp\left[g_2(R) - g_1(R)\right]dt_1^*. \tag{20}$$

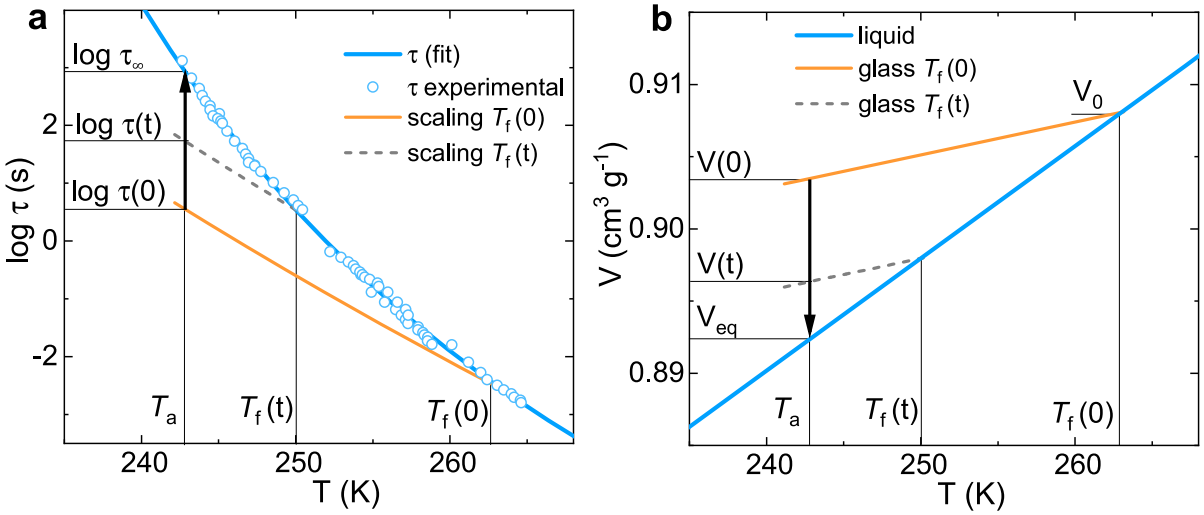

FIG. 4. Temperature dependence of the α relaxation time—described by the density scaling approach (lines) and experimental function (points)—[panel (a)] and the specific volume [panel (b)], and their relation with the fictive temperature, at equilibrium, after quenching at 1000 K/s to T_a, and after quenching under the same condition and aging for a given time for OTP.

TABLE II. Data required to obtain the α relaxation time within the density scaling approach for KDE,[54] PDE,[56] OTP,[54,55] BMMPC,[57] and BMPC.[57]

Glass formers	$T(0)$ (K)	V_0 (cm^3/g)	α_l (kK^{-1})	α_g (kK^{-1})	γ	C (K (g/cm^3)$^{\gamma}$)
KDE	330.5	0.87	0.505	0.25	4.5	7 100
PDE	306.5	0.735	0.765	0.25	4.5	8 100
OTP	263	0.905	0.87	0.25	4	12 000
BMMPC	277	0.91	0.635	0.25	8.5	6 100
BMPC	259	0.9	0.765	0.25	7	4 550

Hence, Eq. (20) allows converting a discrete set of experimental data points, the time vector $\mathbf{t_1} = (t_1^1, t_1^2, \ldots, t_1^n)$, corresponding to a set of normalized relaxation function vectors $\mathbf{R} = (R^1, R^2, \ldots, R^n)$, to a second set of data points corresponding to a different aging temperature, the time vector $\mathbf{t_2} = (t_2^1, t_2^2, \ldots, t_2^n)$. Plotting R vs t_2 delivers the model prediction at any aging temperature from the knowledge of the normalized relaxation function at a reference temperature. Importantly, this does not require any fitting parameter.

Before presenting the outcome of the model prediction, it is worth remarking that the description of $R(t)$ at the reference temperature contains the intrinsic non-exponential relaxation of the glass plus the non-linear behavior at that temperature. The magnitude of non-linearity, depending on the aging temperature, is tuned by the function $g(R)$ [see Eq. (15)]. Having summarized these general aspects of the model, the implementation within the density scaling description of the α relaxation time requires the knowledge of several inputs, which are reported in Table II. In the same table, we also report $T_f(0)$, that is, the fictive temperature after the quench at 1000 K/s and the specific volume at that temperature, V_0. The values reported in Table II are taken from the available literature data.[54–57] Due to data scarcity, the coefficient of thermal expansion in the glassy state was fixed at 2.5×10^{-4} K^{-1}, that is, the value reported for OTP.[55] This choice is highly reasonable as 2.5×10^{-4} K^{-1} lies in the tiny range of variation of small molecule glass formers.[58]

The outcome of the application of the model is shown in Fig. 5, where the experimental normalized relaxation functions (symbols) and those predicted by the model (lines) as a function of aging time and temperature are presented. Figure 6 shows the difference between the model prediction and $R(t)$ data from measured T_f, thus providing a representation of how much the models deviate from experiments. A common general observation that applies to all glasses is that the model is able to accurately catch the experimental data at high aging temperatures, specifically for temperatures larger than 313.2 K for KDE, 298.2 K for PDE, 250.7 K for OTP, 263.2 K for BMMPC, and 246.7 K for BMPC. At lower temperatures,

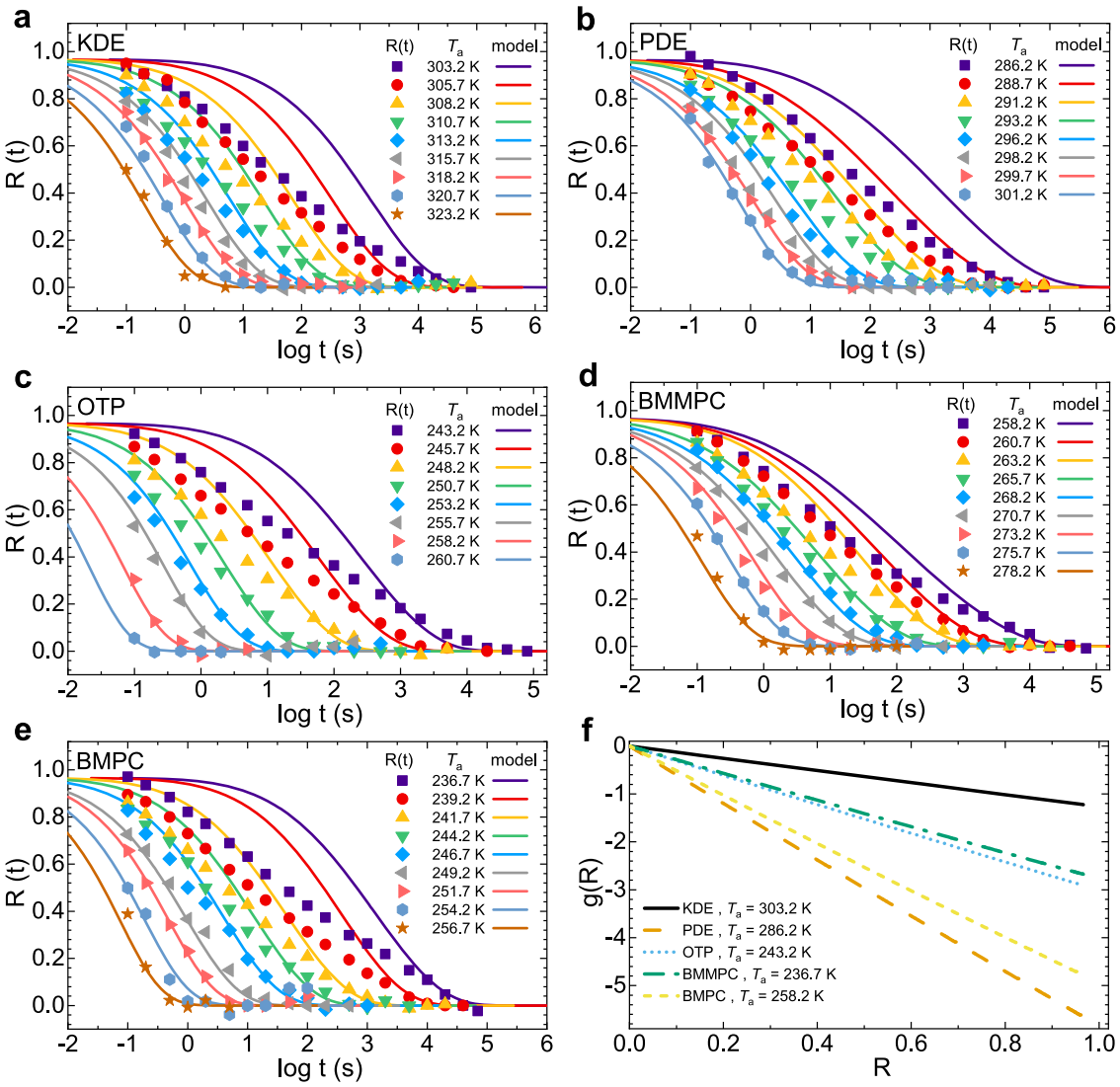

FIG. 5. [Panels (a)–(e)] Experimental (points) and predicted (lines) normalized relaxation function vs aging time for all investigated temperatures and glasses. [Panel (f)] $g(R(t))$, providing the deviation of τ from its equilibrium value [see Eq. (15)], as a function of $R(t)$ at the lowest investigated aging temperatures.

the model fails to capture the entire time evolution of $R(t)$ in both the shape and typical time scale of the relaxation. In all cases, the experimental $R(t)$ appears to be way more stretched than the model prediction. Altogether, the model predicts largely slower aging time evolution of the glass thermodynamic state than the experimental outcome. However, for all glasses except PDE, while failing to describe the whole aging behavior, the model is able to accurately catch the ultimate stages of approach to equilibrium. As an exception, the approach to equilibrium for PDE is found to be always faster than that predicted by the model, even at the final stages of the aging process.

A complementary way of visualizing how the model based on the α relaxation deviates from experimental aging data relies on depicting the normalized relaxation function vs the material time, ξ, which, as discussed, linearizes the aging response [see Eq. (4)]. This is shown in Fig. 7, where it can be observed that experimental data at high aging temperatures collapse on a single curve, which perfectly overlaps with that predicted by the

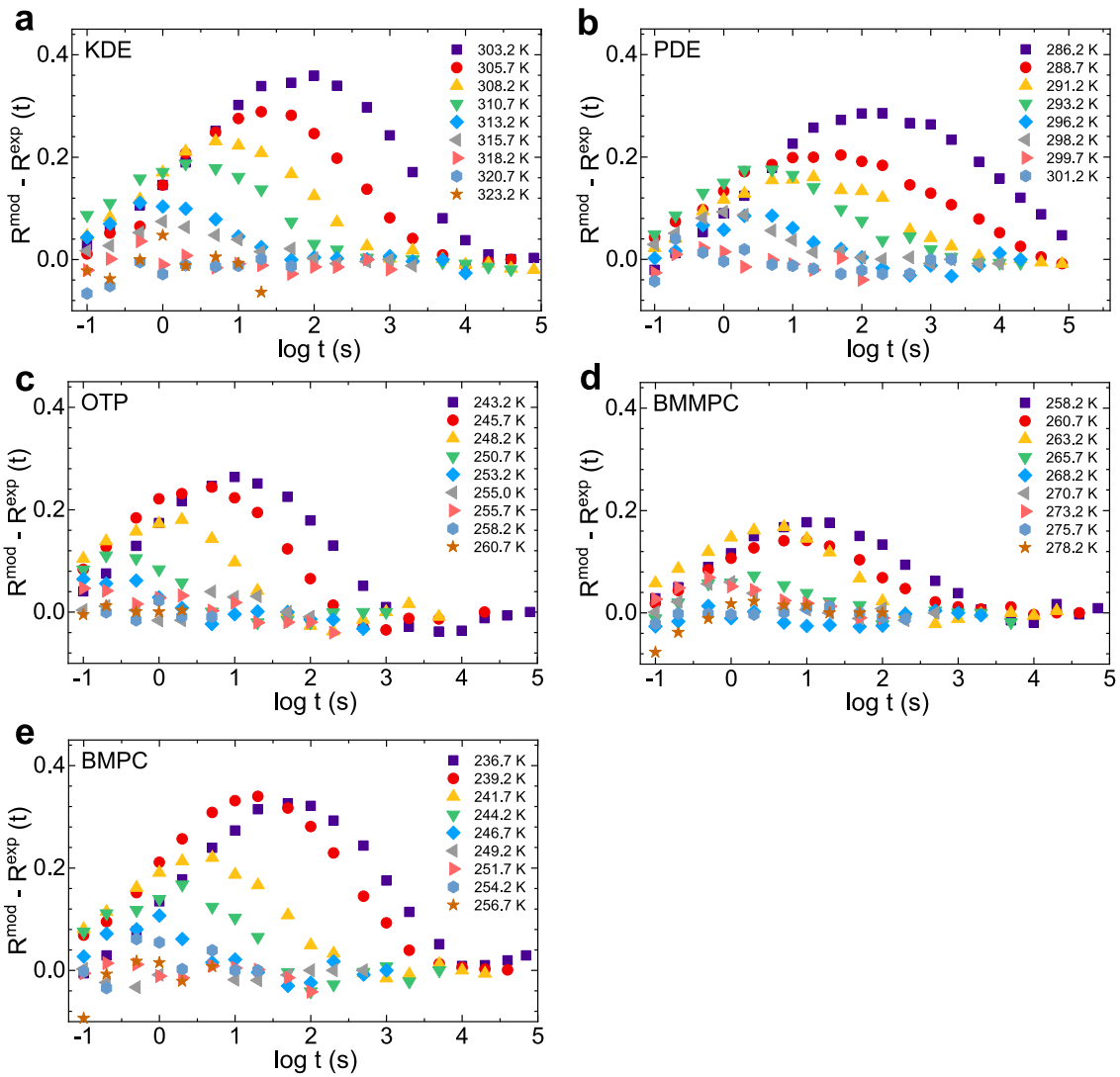

FIG. 6. Difference between the predicted and experimental relaxation function vs time for all investigated temperatures and glasses.

model. Experimental aging data gradually shift to lower ξ with decreasing aging temperatures. This way of showing data provides a plastic representation of how, in this low temperature regime, only the final part of aging is accurately caught by the α relaxation, whereas the overall aging response is more stretched and anticipated with respect to the prediction based on the α relaxation.

Before closing this section, it is worth pointing out that fitting of our data by the original SPA model[27–29] provides analogous deviations as those of our model based on density scaling. Furthermore, the $g(R)$ function, providing the deviation of $\ln \tau$ from its equilibrium value, varies linearly with $R(t)$ [see Fig. 4(f)], as in the original SPA model. However, apart from the absence of any fitting parameter, there are at least two reasons why it is worth including density scaling to describe our data: (i) the most important is that, within the original version of the model, it would have been unclear whether deviations from the model predictions were due to the inadequacy of the α relaxation alone to describe aging significantly below T_g or rather due to the inadequacy of the simple proportionality between $\log \tau$ and T_f; (ii) second, while for not too fragile systems and for

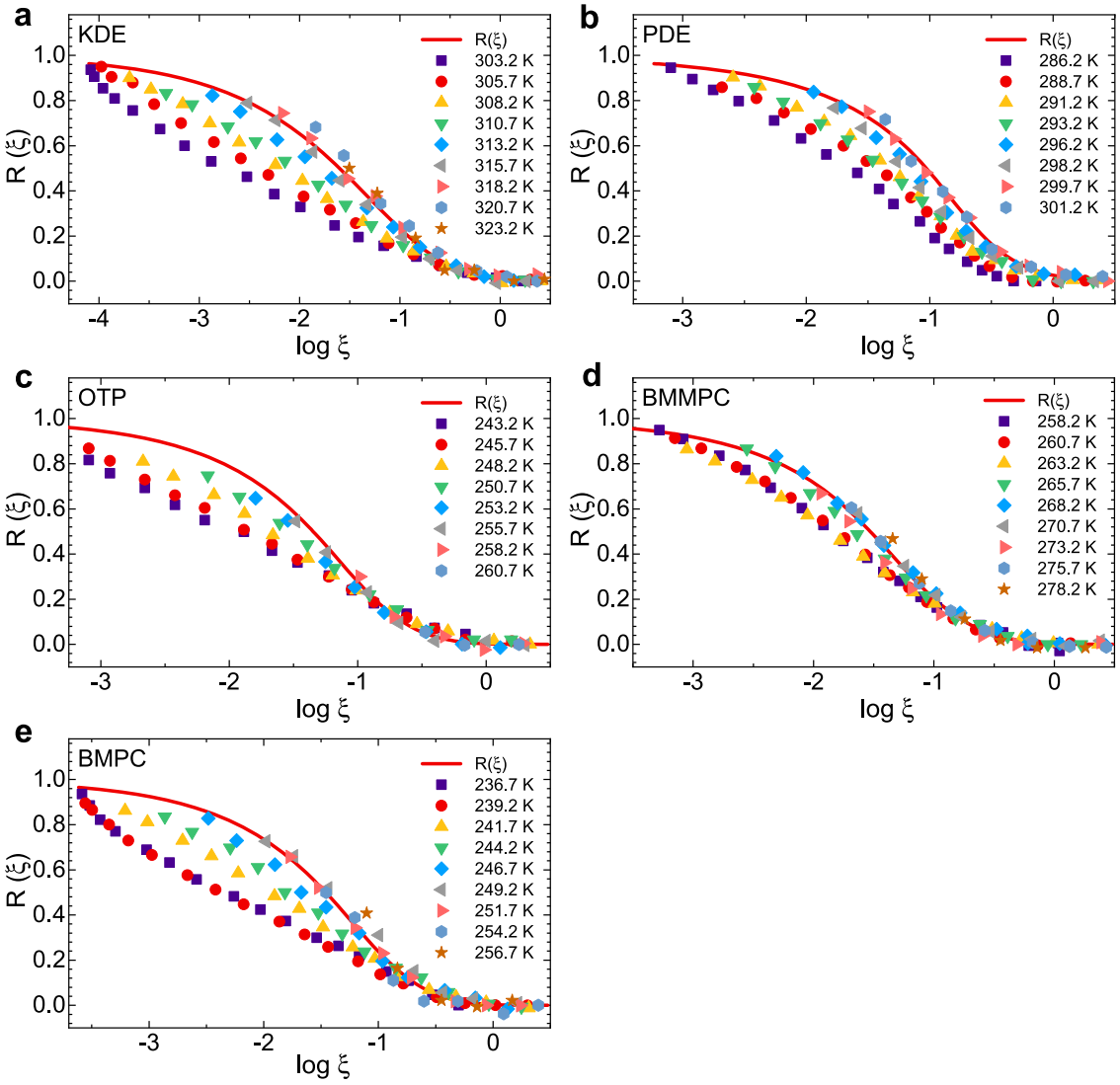

FIG. 7. Experimental (points) and predicted (red line) normalized relaxation function as a function of material time ξ for all investigated temperatures and glasses.

not too large temperature jumps, the proportionality between log τ and T_f may be acceptable [see Fig. 4(a)], this is not the case for highly fragile glass formers, such as polymers, and/or for very large temperature jumps.

IV. DISCUSSION

In Sec. III, we have presented a systematic characterization of physical aging in glasses made of small molecules via FSC, which permitted covering a wide range of time scales and temperatures. In such a way, the current understanding of physical aging has been challenged employing two different approaches: a model-independent one exclusively based on the time scale to reach equilibrium and an approach based on a model originally known as SPA.[27–29] Within both approaches, the aging behavior at the highest investigated temperatures is completely caught considering exclusively the α relaxation. This is evidenced by the aging temperature dependence of the time scale to reach equilibrium (see Fig. 3), which exhibits the same super-Arrhenius behavior as the α relaxation, and by the ability of the model to catch com-

pletely the time evolution of the glass thermodynamic state. The latter result is in line with previous reports in which SPA was fitted to aging data after small temperature steps.[27–29] Furthermore, the adequacy of the α relaxation to describe physical aging in the high temperature regime agrees with findings where aging is investigated in a limited temperature interval in the proximity of T_g.[12–15]

If we consider our model-independent approach at low aging temperatures, the temperature dependence of τ_{eq} generally mimics that of the α relaxation. This is certainly the case for KDE, OTP, BMMPC, and BMPC, whereas PDE appears to exhibit minor deviations from the super-Arrhenius temperature dependence of the α relaxation. Consistently with the analysis based on τ_{eq}, with the exception of PDE, the model prediction for these glasses close to equilibrium catches the experimental late stage evolution of the thermodynamic state. Regarding the anomalous behavior of PDE, we tentatively ascribe it to the poor extrapolation of equilibrium τ of the α relaxation to the lowest temperatures at which aging was investigated.[59] However, importantly, low aging temperatures, corresponding to large jumps in the fictive temperature, entail a considerable increase in the complexity of the overall kinetics of equilibrium recovery. Indeed, the common feature of the aging behavior of all glasses is that, when the description of the whole normalized relaxation function is realized in the low temperature regime, the prediction based exclusively on the role of the α relaxation largely fails for all investigated glasses. In particular, the experimental normalized relaxation function is way more stretched than the predicted behavior and, above all at the early stages of aging, exhibits a faster evolution than expected only accounting for the α relaxation.

The failure of the α relaxation as the only mechanism involved in glass equilibration after large temperature jumps has been shown in several studies where different variants of the TNM–KAHR models were applied.[60–64] The inadequacy of this class of models was explained as resulting from the need for refining/modifying the explicit analytical form expressing the non-linearity of physical aging. Here, we rather show that even introducing non-linearity without making an explicit assumption on its mathematical form brings about large discrepancies between model prediction and experimental data. Hence, our findings indicate that the inadequacy of the TNM–KAHR models to describe physical aging after large temperature jumps must be sought not so much in their analytical expressions *per se* but in the fact that they exclusively contain one time scale, namely that of the α relaxation.

The reason for the discrepancy between the predicted and experimental behaviors after large temperature jumps, especially at the beginning of aging, must be sought in the role of fast non-α molecular mechanisms triggering physical aging. Their role has been documented for a variety of glasses, including polymers,[19,20,65,66] metal alloys,[23,24] chalcogenides,[22] and glycerol,[25] where multiple decays toward equilibrium could be separated. Here, even if the splitting of multiple decays cannot be clearly discerned, the pronounced stretching of the normalized relaxation function indicates the presence of multiple steps not yet well separated in the approach to equilibrium. A close inspection of data at the lowest aging temperature actually hints toward a splitting of the approach to equilibrium in two steps. In particular, for all glasses at their lowest investigated aging temperature, a slowdown of relaxation takes place at about 10^3 s, followed by a late evolution to the final equilibrium (see Fig. 5). Importantly, this observation rules out the possibility that deviations of experimental data from the model could originate from the inaccurate description of the α relaxation time by the density scaling.

To understand the decoupling between aging behavior and α relaxation, the conceptual difference between the non-linear and linear responses can be invoked.[67,68] This interpretation agrees with the experimental findings,[27–29] including ours, showing that for limited temperature jumps, the α relaxation contains all the information to describe weakly non-linear aging. However, the evidence that there exists an underlying molecular non-α mechanism triggering aging under certain conditions requires a suitable explanation on why this is unresolved in linear measurements. Here, it is worth pointing out that our characterization of the glass linear response relies on the obtainment of the thermal susceptibility, that is, the complex specific heat, a second-order thermodynamic property. Instead, monitoring the time-dependent fictive temperature in the aging regime implies that the evolution of a first-order thermodynamic property, in this case, the enthalpy, is monitored. If one of the molecular motions triggering physical aging involves a temperature independent number of degrees of freedom, its associated entropy, $S(T)$, will be temperature independent, too.[69] As a result, the signature of this relaxation will deliver a null contribution to the specific heat as $C_p(T) = T\left.\frac{\partial S(T)}{\partial T}\right|_p$. This scenario is fully compatible with the inability of linear response—delivering a thermal susceptibility and containing information exclusively on the α relaxation—to describe equilibrium recovery in glass aging, where a first-order thermodynamic property as the enthalpy is monitored.

According to the previous considerations, fluctuations related to non-α relaxation processes may remain unidentified in thermal susceptibility measurements. However, those fluctuations may be visible if the susceptibility is obtained applying different fields, for instance, dielectric or mechanical linear perturbations.[70] The most immediate candidates to explain the fast evolution of the glass thermodynamic state are secondary β relaxations, generally detected by dielectric and mechanical spectroscopies below T_g.[71] These are well characterized in all glasses investigated by us.[40,72,73] PDE,[40] OTP,[72] and BMPC[73] exhibit a secondary relaxation, whereas KDE[40] and BMMPC[73] do not. In contrast, deviations of experimental aging behavior from the prediction expected considering exclusively the α relaxation are common to all glasses and, therefore, insensitive to the presence of secondary relaxations. Furthermore, the OTP β relaxation attains time scales of the order of seconds below 200 K,[72] that is, way below the temperatures at which we observe a strong influence of non-α mechanisms on OTP glass equilibration. All these arguments are at odds with the explanation of fast aging as triggered by the β relaxation.

The relaxation mechanism responsible for accelerated aging with respect to predictions based only on the α relaxation must bear large potential to equilibrate and exhibit time scales compatible to such a fast evolution. In this sense, a suitable candidate to explain the fast non-α relaxation can be a recently identified slow Arrhenius process (SAP), which has been shown to play a role of utmost

importance in the kinetics of equilibration of different phenomena, including physical aging, polymer adsorption, and dewetting.[74] A stringent test of the role of SAP would require an analysis on the activation energy of fast equilibration at aging temperatures lower than those of the present study and for longer times, where a complete splitting with the step of equilibration due to the α relaxation is attained.

The evidence of an additional mechanism of glass equilibration raises the question of how to apply the concept of material time under those conditions at which the α relaxation is insufficient to catch the overall aging behavior. The natural consequence of our findings is that the material time is tuned by the time scale of both α and non-α relaxation mechanisms. Hence, Eq. (4) should be rewritten as $d\xi = (a\tau_\alpha^{-1} + (1-a)\tau_{non-\alpha}^{-1})dt$. The implementation of the material time requires the knowledge on how much potential of equilibration is borne by each relaxation mechanism, contained in the parameter a, and the temperature dependence of $\tau_{non-\alpha}$.

A final important implication of our findings is that they open the door to accessing glasses with low energy. Within the scenario of physical aging exclusively driven by the α relaxation, the tremendous growth of the associated time scale with decreasing temperature would imply that aging would disappear not too far from T_g, thereby preventing the exploration of low energy states. In contrast, physical aging is known to exhibit pronounced effects even way below T_g,[2,75–81] which can be rationalized considering non-α relaxations, whose potential to equilibrate glasses survives where the α relaxation is completely frozen. Importantly, reducing the sample size may significantly shorten the time scale of glass relaxation via fast non-α mechanisms, as shown in glasses with largely diverse nature, such as polymers[17,68] and metallic glasses.[18] In such a way, topics of extraordinary importance, such as the existence of the ideal glass transition[82] at the Kauzmann temperature,[83,84] can be explored reducing the sample size and employing fast non-α mechanisms to reduce the glass energy over time scales amenable to the experimental practice.[85,86]

V. CONCLUSIONS

We have presented an extensive characterization of the kinetics of physical aging in five small molecule glasses interacting via van der Waals forces, exploiting the ability of FSC to access a wide range of time scales. In this way, we have covered a wide spectrum of aging time, covering about six decades. With the aim of challenging the role of the α relaxation, we have adopted two different approaches to obtain insights into the underlying molecular mechanisms mediating physical aging: (i) a model-independent approach based on the time to reach equilibrium and (ii) a model, previously addressed as SPA, where the non-exponentiality and non-linearity of physical aging are considered without providing an explicit mathematical form. Here, we have implemented the SPA model employing the density scaling approach to connect the aging time-dependent α relaxation time with the glass thermodynamic state.

The model-independent approach based on the equilibration time generally shows that the final equilibrium is attained in ways compatible with the exclusive role of the α relaxation. In the same way, the final stages of physical aging are reasonably captured by the modified SPA model. Furthermore, the whole experimental relaxation function at the highest investigated aging temperatures is accurately described by the model. However, the central finding of the present study is that, at low aging temperatures, corresponding to large jumps in the fictive temperature, the model based on the exclusive role of the α relaxation largely fails to describe the whole relaxation function. In particular, the experimental relaxation function is vastly more stretched than that predicted by the model, implying that, at the beginning of the equilibration process, aging proceeds faster than predicted by the model. The main consequence of our results and their analysis is that physical aging in glasses aged significantly below T_g cannot be described as exclusively triggered by the α relaxation and, therefore, other fast mechanisms of equilibration must be considered. As a consequence, physical aging can survive with rates amenable to the experimental practice even way below T_g, where the α relaxation is frozen, a result that, under certain conditions, may convey glasses to low energies.

ACKNOWLEDGMENTS

We thank Jeppe Dyre, Kristine Niss, Tina Hecksher, and Simone Napolitano for the inspiring discussions. We acknowledge Grant No. PID2021-123438NB-I00 funded by MCIN/AEI/10.13039/5011000 11033 and by "ERDF A way of making Europe"; the financial support of Eusko Jaurlaritza, code: IT1566-22; Grant No. PID2020-114506GB-I00 funded by the Spanish Ministry of Science and Innovation; and Grant No. TED2021-129457B-I00 funded by the Spanish Ministry of Science and Innovation.

AUTHOR DECLARATIONS

Conflict of Interest

The authors have no conflicts to disclose.

Author Contributions

Daniele Cangialosi: Conceptualization (lead); Data curation (equal); Formal analysis (equal); Funding acquisition (lead); Investigation (equal); Methodology (equal); Writing – original draft (lead); Writing – review and editing (equal). **Valerio Di Lisio:** Conceptualization (equal); Data curation (equal); Formal analysis (equal); Investigation (equal); Methodology (equal); Writing – original draft (equal); Writing – review and editing (lead). **Vasiliki-Maria Stavropoulou:** Data curation (equal); Formal analysis (equal); Investigation (equal); Methodology (equal); Writing – review and editing (supporting).

DATA AVAILABILITY

The data that support the findings of this study are available from the corresponding author upon reasonable request.

REFERENCES

[1] J. W. P. Schmelzer and I. S. Gutzow, *Glasses and the Glass Transition* (Wiley VCH, Weinheim, 2011).

[2]L. C. E. Struik, *Physical Aging in Amorphous Polymers and Other Materials* (Technische Hogeschool Delft, 1977).
[3]D. Cangialosi, V. M. Boucher, A. Alegria, and J. Colmenero, "Physical aging in polymers and polymer nanocomposites: Recent results and open questions," Soft Matter **9**, 8619–8630 (2013).
[4]A. J. Kovacs, *Glass Transition in Amorphous Polymers: A Phenomenological Study*, *Fortschr Hochpolym Forsch* (Springer, 1963), Vol. 3, pp. 394–508.
[5]I. M. Hodge, "Enthalpy relaxation and recovery in amorphous materials," J. Non-Cryst. Solids **169**, 211–266 (1994).
[6]E. Donth, J. Korus, E. Hempel, and M. Beiner, "Comparison of DSC heating rate and HCS frequency at the glass transition," Thermochim. Acta **304–305**, 239–249 (1997).
[7]J. E. K. Schawe, "Vitrification in a wide cooling rate range: The relations between cooling rate, relaxation time, transition width, and fragility," J. Chem. Phys. **141**, 184905 (2014).
[8]S. Lapuk, M. Ponomareva, M. Ziganshin, R. Larionov, T. Mukhametzyanov, C. Schick, I. Lounev, and A. Gerasimov, "Some aspects of the glass transition of polyvinylpyrrolidone depending on the molecular mass," Phys. Chem. Chem. Phys. **25**, 10706–10714 (2023).
[9]L.-M. Wang, V. Velikov, and C. A. Angell, "Direct determination of kinetic fragility indices of glassforming liquids by differential scanning calorimetry: Kinetic versus thermodynamic fragilities," J. Chem. Phys. **117**, 10184–10192 (2002).
[10]M. K. Saini, X. Jin, T. Wu, Y. Liu, and L.-M. Wang, "Interplay of intermolecular interactions and flexibility to mediate glass forming ability and fragility: A study of chemical analogs," J. Chem. Phys. **148**, 124504 (2018).
[11]J. Rault, "Ageing of glass: Role of the Vogel–Fulcher–Tamman law," J. Phys.: Condens. Matter **15**, S1193 (2003).
[12]P. Lunkenheimer, R. Wehn, U. Schneider, and A. Loidl, "Glassy aging dynamics," Phys. Rev. Lett. **95**, 055702 (2005).
[13]R. Richert, P. Lunkenheimer, S. Kastner, and A. Loidl, "On the derivation of equilibrium relaxation times from aging experiments," J. Phys. Chem. B **117**, 12689–12694 (2013).
[14]A. Mansuri, P. Münzner, T. Feuerbach, A. Vermeer, W. Hoheisel, R. Böhmer, M. Thommes, and C. Gainaru, "The relaxation behavior of supercooled and glassy imidacloprid," J. Chem. Phys. **155**, 174502 (2021).
[15]R. Richert, "One experiment makes a direct comparison of structural recovery with equilibrium relaxation," J. Chem. Phys. **157**, 224501 (2022).
[16]X. Monnier, D. Cangialosi, B. Ruta, R. Busch, and I. Gallino, "Vitrification decoupling from α-relaxation in a metallic glass," Sci. Adv. **6**, eaay1454 (2020).
[17]X. Monnier and D. Cangialosi, "Thermodynamic ultrastability of a polymer glass confined at the micrometer length scale," Phys. Rev. Lett. **121**, 137801 (2018).
[18]V. Di Lisio, I. Gallino, S. Riegler, M. Frey, N. Neuber, G. Kumar, J. Schroers, R. Busch, and D. Cangialosi, "Size dependent vitrification in metallic glasses," Nat. Commun. (in press).
[19]D. Cangialosi, V. M. Boucher, A. Alegría, and J. Colmenero, "Direct evidence of two equilibration mechanisms in glassy polymers," Phys. Rev. Lett. **111**, 095701 (2013).
[20]A. Morvan, N. Delpouve, A. Vella, and A. Saiter-Fourcin, "Physical aging of selenium glass: Assessing the double mechanism of equilibration and the crystallization process," J. Non-Cryst. Solids **570**, 121013 (2021).
[21]M. Pyda and A. Czerniecka-Kubicka, *Thermal Properties and Thermodynamics of Poly (L-Lactic Acid)*, *Advances in Polymer Science* (Springer, 2018), pp. 153–193.
[22]R. Golovchak, A. Kozdras, V. Balitska, and O. Shpotyuk, "Step-wise kinetics of natural physical ageing in arsenic selenide glasses," J. Phys.: Condens. Matter **24**, 505106 (2012).
[23]I. Gallino, D. Cangialosi, Z. Evenson, L. Schmitt, S. Hechler, M. Stolpe, and B. Ruta, "Hierarchical aging pathways and reversible fragile-to-strong transition upon annealing of a metallic glass former," Acta Mater. **144**, 400–410 (2018).
[24]L. Song, W. Xu, J. Huo, J.-Q. Wang, X. Wang, and R. Li, "Two-step relaxations in metallic glasses during isothermal annealing," Intermetallics **93**, 101–105 (2018).
[25]R. S. Miller and R. A. MacPhail, "Ultraslow nonequilibrium dynamics in supercooled glycerol by stimulated Brillouin gain spectroscopy," J. Chem. Phys. **106**, 3393–3401 (1997).
[26]Z. Wojnarowska and M. Paluch, "Two-step aging of highly polar glass," J. Phys. Chem. Lett. **12**, 11779–11783 (2021).
[27]T. Hecksher, N. B. Olsen, and J. C. Dyre, "Communication: Direct tests of single-parameter aging," J. Chem. Phys. **142**, 241103 (2015).
[28]L. A. Roed, T. Hecksher, J. C. Dyre, and K. Niss, "Generalized single-parameter aging tests and their application to glycerol," J. Chem. Phys. **150**, 044501 (2019).
[29]B. Riechers, L. A. Roed, S. Mehri, T. S. Ingebrigtsen, T. Hecksher, J. C. Dyre, and K. Niss, "Predicting nonlinear physical aging of glasses from equilibrium relaxation via the material time," Sci. Adv. **8**, eabl9809 (2022).
[30]C. Roland, S. Hensel-Bielowka, M. Paluch, and R. Casalini, "Supercooled dynamics of glass-forming liquids and polymers under hydrostatic pressure," Rep. Prog. Phys. **68**, 1405 (2005).
[31]I. Blanco, "Lifetime prediction of polymers: To bet, or not to bet—Is this the question?," Materials **11**, 1383 (2018).
[32]A. A. Abate, D. Cangialosi, and S. Napolitano, "High throughput optimization procedure to characterize vitrification kinetics," Thermochim. Acta **707**, 179084 (2022).
[33]M. Merzlyakov and C. Schick, "Step response analysis in DSC: A fast way to generate heat capacity spectra," Thermochim. Acta **380**, 5–12 (2001).
[34]E. Shoifet, G. Schulz, and C. Schick, "Temperature modulated differential scanning calorimetry: An extension to high and low frequencies," Thermochim. Acta **603**, 227–236 (2015).
[35]N. G. Perez-de Eulate, V. Di Lisio, and D. Cangialosi, "Glass transition and molecular dynamics in polystyrene nanospheres by fast scanning calorimetry," ACS Macro Lett. **6**, 859–863 (2017).
[36]D. Cangialosi, "Dynamics and thermodynamics of polymer glasses," J. Phys.: Condens. Matter **26**, 153101 (2014).
[37]A. Tool, "Relation between inelastic deformability and thermal expansion of glass in its annealing range," J. Am. Ceram. Soc. **29**, 240–253 (1946).
[38]C. T. Moynihan, P. B. Macedo, C. J. Montrose, C. J. Montrose, P. K. Gupta, M. A. DeBolt, J. F. Dill, B. E. Dom, P. W. Drake, A. J. Easteal, P. B. Elterman, R. P. Moeller, H. Sasabe, and J. A. Wilder, "Structural relaxation in vitreous materials," Ann. N. Y. Acad. Sci. **279**, 15–35 (1976).
[39]D. Sonaglioni, E. Tombari, and S. Capaccioli, "Fast differential scanning calorimetry: New solutions in data treatment and applications to molecular glass-formers," Thermochim. Acta **719**, 179385 (2023).
[40]S. Kahle, J. Gapinski, G. Hinze, A. Patkowski, and G. Meier, "A comparison of relaxation processes in structurally related van der Waals glass formers: The role of internal degrees of freedom," J. Chem. Phys. **122**, 074506 (2005).
[41]C. Angell, "Glass-formers and viscous liquid slowdown since David turnbull: Enduring puzzles and new twists," MRS Bull. **33**, 544–555 (2008).
[42]J. Hadac, P. Slobodian, P. Říha, P. Saha, R. Rychwalski, I. Emri, and J. Kubat, "Effect of cooling rate on enthalpy and volume relaxation of polystyrene," J. Non-Cryst. Solids **353**, 2681–2691 (2007).
[43]G. Williams and D. C. Watts, "Non-symmetrical dielectric relaxation behaviour arising from a simple empirical decay function," Trans. Faraday Soc. **66**, 80–85 (1970).
[44]O. Narayanaswamy, "A model of structural relaxation in glass," J. Am. Ceram. Soc. **54**, 491–498 (1971).
[45]A. J. Kovacs, J. J. Aklonis, J. M. Hutchinson, and A. R. Ramos, "Isobaric volume and enthalpy recovery of glasses. II. A transparent multiparameter theory," J. Polym. Sci., Polym. Phys. Ed. **17**, 1097–1162 (1979).
[46]L. Grassia and S. L. Simon, "Modeling volume relaxation of amorphous polymers: Modification of the equation for the relaxation time in the KAHR model," Polymer **53**, 3613–3620 (2012).
[47]T. V. Tropin, G. Schulz, J. W. Schmelzer, and C. Schick, "Heat capacity measurements and modeling of polystyrene glass transition in a wide range of cooling rates," J. Non-Cryst. Solids **409**, 63–75 (2015).
[48]L. Grassia, Y. P. Koh, M. Rosa, and S. L. Simon, "Complete set of enthalpy recovery data using flash DSC: Experiment and modeling," Macromolecules **51**, 1549–1558 (2018).
[49]J. Malek, "Structural relaxation rate and aging in amorphous solids," J. Phys. Chem. C **127**, 6080–6087 (2023).

[50]R. P. White and J. E. Lipson, "The cooperative free volume rate model for segmental dynamics: Application to glass-forming liquids and connections with the density scaling approach," Eur. Phys. J. E **42**, 100 (2019).
[51]K. Niss, "A density scaling conjecture for aging glasses," J. Chem. Phys. **157**, 054503 (2022).
[52]J. Málek, "Volume and enthalpy relaxation rate in glassy materials," Macromolecules **31**, 8312–8322 (1998).
[53]P. Badrinarayanan and S. L. Simon, "Origin of the divergence of the timescales for volume and enthalpy recovery," Polymer **48**, 1464–1470 (2007).
[54]C. Dreyfus, A. Le Grand, J. Gapinski, W. Steffen, and A. Patkowski, "Scaling the α-relaxation time of supercooled fragile organic liquids," Eur. Phys. J. B **42**, 309–319 (2004).
[55]S. Takahara, M. Ishikawa, O. Yamamuro, and T. Matsuo, "Structural relaxations of glassy polystyrene and *o*-terphenyl studied by simultaneous measurement of enthalpy and volume under high pressure," J. Phys. Chem. B **103**, 792–796 (1999).
[56]M. Paluch, R. Casalini, A. Best, and A. Patkowski, "Volume effects on the molecular mobility close to glass transition in supercooled phenylphthalein-dimethylether. II," J. Chem. Phys. **117**, 7624–7630 (2002).
[57]M. Paluch, C. Roland, R. Casalini, G. Meier, and A. Patkowski, "The relative contributions of temperature and volume to structural relaxation of van der Waals molecular liquids," J. Chem. Phys. **118**, 4578–4582 (2003).
[58]P. Lunkenheimer, A. Loidl, B. Riechers, A. Zaccone, and K. Samwer, "Thermal expansion and the glass transition," Nat. Phys. **19**, 694 (2023).
[59]T. Hecksher, A. I. Nielsen, N. B. Olsen, and J. C. Dyre, "Little evidence for dynamic divergences in ultraviscous molecular liquids," Nat. Phys. **4**, 737–741 (2008).
[60]I. M. Hodge, "Effects of annealing and prior history on enthalpy relaxation in glassy polymers. 4. Comparison of five polymers," Macromolecules **16**, 898–902 (1983).
[61]J. M. O'Reilly, "Review of structure and mobility in amorphous polymers," Crit. Rev. Solid State Mater. Sci. **13**, 259–277 (1987).
[62]G. McKenna and C. Angell, "The phenomenology and models of the kinetics of volume and enthalpy in the glass transition range," J. Non-Cryst. Solids **131-133**, 528–536 (1991).
[63]M. Righetti and G. Johari, "Enthalpy and entropy changes during physical ageing of 20% polystyrene–80% poly (α-methylstyrene) blend and the cooling rate effects," Thermochim. Acta **607**, 19–29 (2015).
[64]A. Toda, "Isothermal enthalpy relaxation of amorphous polystyrene studied using temperature-modulated fast scanning calorimetry," Thermochim. Acta **721**, 179433 (2023).
[65]X. Monnier, S. Marina, X. Lopez de Pariza, H. Sardón, J. Martin, and D. Cangialosi, "Physical aging behavior of a glassy polyether," Polymers **13**, 954 (2021).
[66]Y. Seo, B. Zuo, D. Cangialosi, and R. D. Priestley, "Physical aging of hydroxypropyl methylcellulose acetate succinate via enthalpy recovery," Soft Matter **18**, 8331–8341 (2022).
[67]E. J. Donth, *The Glass Transition* (Springer-Verlag, Berlin Heidelberg, 2001).
[68]D. Cangialosi, A. Alegria, and J. Colmenero, "Effect of nanostructure on the thermal glass transition and physical aging in polymer materials," Prog. Polym. Sci. **54–55**, 128–147 (2016).
[69]D. Cangialosi, A. Alegría, and J. Colmenero, "Comment on 'Vibrational and configurational parts of the specific heat at glass formation,'" Phys. Rev. B **78**, 176301 (2008).
[70]N. McCrum, B. Read, and G. Williams, *Anelastic and Dielectric Effects in Polymeric Solids* (John Wiley, 1967).
[71]K. Ngai, "The origin of the faster mechanism of partial enthalpy recovery deep in the glassy state of polymers," Phys. Chem. Chem. Phys. **23**, 13468–13472 (2021).
[72]G. P. Johari and M. Goldstein, "Viscous liquids and the glass transition. II. Secondary relaxations in glasses of rigid molecules," J. Chem. Phys. **53**, 2372–2388 (1970).
[73]G. Meier, B. Gerharz, D. Boese, and E. Fischer, "Dynamical processes in organic glassforming van der Waals liquids," J. Chem. Phys. **94**, 3050–3059 (1991).
[74]Z. Song, C. Rodríguez-Tinoco, A. Mathew, and S. Napolitano, "Fast equilibration mechanisms in disordered materials mediated by slow liquid dynamics," Sci. Adv. **8**, eabm7154 (2022).
[75]L. Boehm and C. Angell, "DC conductivity and secondary structural relaxations in high-conducting Li^+ glasses," J. Non-Cryst. Solids **40**, 83–92 (1980).
[76]R. Greiner and F. R. Schwarzl, "Thermal contraction and volume relaxation of amorphous polymers," Rheol. Acta **23**, 378–395 (1984).
[77]N. G. Perez-De Eulate and D. Cangialosi, "The very long-term physical aging of glassy polymers," Phys. Chem. Chem. Phys. **20**, 12356–12361 (2018).
[78]R. C. Welch, J. R. Smith, M. Potuzak, X. Guo, B. F. Bowden, T. Kiczenski, D. C. Allan, E. A. King, A. J. Ellison, and J. C. Mauro, "Dynamics of glass relaxation at room temperature," Phys. Rev. Lett. **110**, 265901 (2013).
[79]K. Grigoriadi, T. Putzeys, M. Wübbenhorst, L. C. A. Breemen, P. D. Anderson, and M. Hütter, "Effect of low-temperature physical aging on the dynamic transitions of atactic polystyrene in the glassy state," J. Polym. Sci., Part B: Polym. Phys. **57**, 1394–1401 (2019).
[80]H. Yin, P. Chapala, M. Bermeshev, A. Schönhals, and M. Böhning, "Molecular mobility and physical aging of a highly permeable glassy polynorbornene as revealed by dielectric spectroscopy," ACS Macro Lett. **6**, 813–818 (2017).
[81]G. G. Vogiatzis, L. C. van Breemen, M. Hütter, and D. N. Theodorou, "Network dynamics: A computational framework for the simulation of the glassy state," Mol. Syst. Des. Eng. (2023).
[82]J. H. Gibbs and E. A. DiMarzio, "Nature of the glass transition and the glassy state," J. Chem. Phys. **28**, 373–383 (1958).
[83]W. Kauzmann, "The nature of the glassy state and the behavior of liquids at low temperatures," Chem. Rev. **43**, 219–256 (1948).
[84]R. S. Welch, E. D. Zanotto, C. J. Wilkinson, D. R. Cassar, M. Montazerian, and J. C. Mauro, "Cracking the Kauzmann paradox," Acta Mater. **254**, 118994 (2023).
[85]V. M. Boucher, D. Cangialosi, A. Alegria, and J. Colmenero, "Reaching the ideal glass transition by aging polymer films," Phys. Chem. Chem. Phys. **19**, 961–965 (2017).
[86]X. Monnier, J. Colmenero, M. Wolf, and D. Cangialosi, "Reaching the ideal glass in polymer spheres: Thermodynamics and vibrational density of states," Phys. Rev. Lett. **126**, 118004 (2021).

Macromolecules

pubs.acs.org/Macromolecules
Article

Vitrimeric Behavior Revealed by Fast Scanning Calorimetry in Branched Polyglycerol Networks Cross-Linked by Reversible Enamine Bonds

Vasiliki Maria Stavropoulou,[#] Marta Aldecoa-Ortueta,[#] Ester Verde-Sesto, Valerio Di Lisio, Anabel Lam, José A. Pomposo, Angel Alegría, Daniele Cangialosi,* and Fabienne Barroso-Bujans*

Cite This: *Macromolecules* 2025, 58, 9993−10006

ABSTRACT: Dynamic covalent bonds formed by enamine have played a crucial role in the development of vitrimers by enabling their rearrangement and reprocessability. In this study, polymer networks obtained by cross-linking a β-ketoester-functionalized branched polyglycerol (PG-βkest) with three different diamines, i.e. diaminopropane (DAP), 2,2′-(ethylenedioxy)bis(ethylamine) (EDO) and Jeffamine D230 (Jeff) were generated through enamine bond formation enabling the formation of materials with tunable glass transition temperatures (T_g). A single, though broad, specific heat step was detected in all cases by conventional differential scanning calorimetry (DSC). However, by judiciously varying thermal protocols using fast scanning calorimetry (FSC), which permits heating/cooling rates as large as 1000 K s^{-1}, we were able to separate and identify two distinct thermal events in the network composed by Jeff, used as a vitrimeric network model. Using Kissinger analysis, we conveyed information about the apparent activation energies of the two thermal events. In such a way, we were able to provide compelling evidence that the high-temperature event is due to a vitrimeric transformation (T_v), while the low-temperature event exhibits all the features of a conventional glass transition.

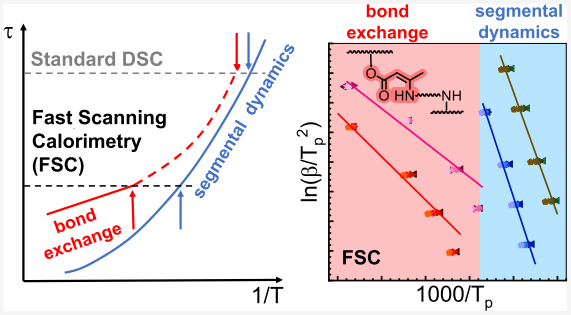

INTRODUCTION

Dynamic covalent polymer networks, also known as covalent adaptable networks (CANs), have emerged as an advanced form of classical polymer networks. They possess unique features such as reprocessability, self-healing, and reusability.[1] CANs are based on dynamic covalent bonds (DCBs) which allow the network topology to reorganize. Under appropriate conditions, CANs can flow, be remodeled and/or (self-)repair.[2] DCBs in CANs can be dissociative or associative, depending on whether they are disrupted before the exchange event or remain intact, respectively.[3,4] In particular, CANs possessing associative DCBs and showing an Arrhenius temperature dependence of viscosity approaching the glass transition temperature (T_g) are called vitrimers.[5] A relevant parameter of these systems is the topology freezing or vitrimer transition temperature (T_v), which Leibler and co-workers defined as the temperature at which the network freezes due to the inability of DCBs to undergo exchange reactions.[6] Increasing the temperature just above T_v causes vitrimers to undergo a topological transition from viscoelastic solid to viscoelastic liquid behavior.

Reliably determining T_v remains an unsolved problem in this emerging field. An extrapolation of the vitrimer viscosity to a value of 10^{12} Pa s is taken as the original criterion to estimate the so-called "apparent" T_v, even if large extrapolations prone to large errors are often involved.[7,8] Other attempts to obtain T_v have relied on the use of stress−relaxation measurements combined with nonisothermal and isothermal creep experiments,[9] dilatometry,[10] thermomechanical analysis,[11] aggregation-induced-emission (AIE) luminogen fluorescence[12] and X-ray scattering experiments supported by DSC measurements.[13]

Methods that provide first-order thermodynamic properties, such as dilatometry for specific volume and DSC for enthalpy, rely on the fact that the vitrimeric transition, in a manner analogous to the glass transition, activates translational and rotational degrees of freedom.[14] This is expected to result in a stepwise increase in the thermodynamic coefficients, that is, the coefficient of thermal expansion and the specific heat capacity. Despite this, the simultaneous determination of T_g and T_v has hitherto remained vastly elusive with only a few

Received: June 11, 2025
Revised: August 21, 2025
Accepted: August 21, 2025
Published: September 3, 2025

exceptions.[10,15] This is likely because at the rates of K min^{-1} explored by standard dilatometry and DSC, T_g and T_v are often too close and, therefore, their separation may be challenging. Furthermore, the step-like variation in thermodynamic coefficients underlying the vitrimeric transformation can span a broad temperature range, which complicates its detection. These experimental flaws can be overcome by expanding the range of the heating/cooling rate in the experiment and by applying thermal protocols that aim to magnify the thermal events under investigation. As with T_g, it is expected that T_v depends on several experimental parameters in addition to the specific chemistry of the material.[16] Moreover, T_v can be above, below or near T_g. In fact, there is no general agreement on a protocol or experimental setup to assess T_v.

With regards to the separation between glass and vitrimeric transitions specifically, the latter generally exhibits a lower apparent activation energy than the segmental relaxation associated with the glass transition (see Figure S1). Therefore, reducing the experimental time scale can be an effective way of identifying the thermal events involved in vitrimers. FSC enables heating and cooling scans as large as several thousand K s^{-1},[17] which greatly reduces the time scale of probed molecular motion compared to conventional DSC.

Enamine DCBs[18]—renamed as "vinylogous urethane" bonds by Du Prez and co-workers[19]—has become one of the canonical reversible bonds used in the development of vitrimers made from synthetic[20,21] and biobased materials.[22,23] Branched polyglycerol (PG),[24] which has multiple hydroxyl groups and a branched structure, can be easily decorated with β-ketoester functional groups through a transesterification reaction with *tert*-butyl acetoacetate (TBAA). In this work, we have synthesized networks cross-linked through enamine DCBs based on β-ketoester-decorated branched polyglycerol (PG-βkest) and different diamines, i.e. DAP, EDO and Jeff.

Furthermore, we have developed an experimental protocol to assess T_v using FSC of the synthesized cross-linked networks with Jeff. We have found that using DSC, these systems have T_v very close to T_g. However, the thermal protocols permitted by FSC allowed us to unambiguously resolve both thermal phenomena and to determine the activation energy of the vitrimeric transformation.

EXPERIMENTAL SECTION

Materials. (±)-Glycidol (Gly) (96%), *tert*-butyl acetoacetate (TBAA, 98%) and 1,3-diaminopropane (DAP, >99%), 2,2′-(ethylenedioxy)bis(ethylamine) (EDO), *N*,*N*-dimethylformamide (DMF) and CaH_2 were purchased from Sigma-Aldrich. $B(C_6F_5)_3$ (>98.0%) was obtained from TCI Europe and purified by sublimation under reduced pressure at 90 °C. Jeffamine D230 (Jeff) was purchased from Huntsman. Toluene, tetrahydrofuran (THF), ethanol (EtOH), diethyl ether (Et_2O) were purchased from Scharlab and methanol (MeOH) from Fischer Scientific. Deuterated chloroform ($CDCl_3$) and deuterated water (D_2O) were obtained from Euroisotop. Gly and toluene were distilled from CaH_2 under reduced pressure. They were stored under inert atmosphere and transferred either in glovebox or in a vacuum line. The rest of reagents and solvents were used as received.

Synthesis of PG. The synthesis of PG was performed in a three-necked flask equipped with a jacket and a magnetic stirrer under argon atmosphere. A flask with 6 mL of Gly (6.66 g, 90 mmol) and 20 mL of toluene was cooled to 0 °C, then 59 mg of $B(C_6F_5)_3$ (0.12 mmol) dissolved in 4 mL of toluene and 60 μL of water were added after stabilizing the temperature. The reaction was stirred for 22 h obtaining 99 mol % monomer conversion as determined by ^{1}H NMR. The polymer precipitated during the reaction as a viscous material generating two phases, the solvent and the precipitate, as expected from our previous study.[25] The polymer was separated from the solvent by decantation. Afterward, the resulting polymer was dissolved in MeOH (10 mL) and purified by precipitation in Et_2O (100 mL). Then, the polymer was again dissolved in MeOH (10 mL) and passed through basic alumina. The solvent was removed under vacuum in the rotary evaporator and finally, the isolated product was dried at 80 °C for 18 h in a vacuum oven. The product was obtained as a transparent viscous material (3.3 g, yield 60 wt %). M_n = 3 kg/mol ($Đ$ = 2.0) was determined by gel permeation chromatography (GPC) and a degree of branching of 0.39 by inverse-gated ^{13}C NMR in D_2O following our previous works.[25,26]

Synthesis of PG-βkest. PG (830 mg, 11 mmol of OH) and a large excess of TBAA (36 mL, 217 mmol) were added to a Schlenk flask of 250 mL. The reaction mixture was stirred at 120 °C for 22 h. Then, the reaction mixture was cooled down to room temperature and transferred to a round-bottom flask of 100 mL. The final product was purified by distillation at 130 °C and 50 mbar for 1 h. This process was used to remove the TBAA excess and the formed *tert*-butanol. The product was then washed with Et_2O. PG-βkest was obtained as a viscous yellow oil material (1.3 g, 74 wt % yield).

Synthesis of Cross-Linked Networks with Diamines. As an example of a network prepared with DAP/βkest (feed) molar ratio = 1.2, PG-βkest (83 mg) was first dissolved in 9.6 mL of THF in a vial to generate 0.05 mol(βkest)/L solution. Separately, in another vial, DAP (24 μL) was added to 288 μL of THF to generate a 1 mol/L of DAP solution. Then, the diamine solution was added to that of the polymer. The mixture was transferred into a Teflon Petri dish of 5 cm diameter, and the solvent was evaporated at room temperature overnight. The resulting film was cured at 85 °C for 1 h under vacuum conditions in a vacuum oven. See Table S1 for the amounts of reagents used for all samples prepared with DAP, and Tables S2 and S3 for samples prepared with Jeff and EDO. All the networks were prepared using the same batch of PG-βkest. The excess of Jeff was successfully removed using Soxhlet extraction with EtOH. The excess of DAP and EDO was removed by evaporation following a thorough evaluation of the thermal protocol to be used. The networks cross-linked with DAP and EDO were heated at 150 °C for 15 min to 1 h (depending on the sample) in a vacuum oven.

Characterization Techniques. ^{1}H and inverse gated ^{13}C NMR data were acquired on a Bruker Avance Neo 500 at 25 °C, employing D_2O for PG and $CDCl_3$ for PG-βkest. The degree of branching (DB) was calculated from $DB = \frac{2D}{2D + L_{1,3} + L_{1,4}}$, where, D, $L_{1,3}$ and $L_{1,4}$ are the relative abundance of dendritic and linear structures, respectively.[27]

GPC data were acquired on a Nexera instrument from Shimadzu using refractive index detector (RID-20A, Shimadzu) and MALS detector (λ = 663.89 nm, miniDawn, Wyatt) at a temperature of 40 °C. Separation was performed at 50 °C by using a CTO 40C column oven and Polargel-M Guard 50 × 7.5 mm and Polargel-M 300 × 7.5 mm, 8 μm, GPC columns. HPLC grade DMF containing 0.1% of LiBr with a flow of 1.0 mL/min was used as a mobile phase. The absolute molecular weight of PG was determined using a dn/dc value[28] of 0.054 mL/g and Astra 8.1 software from Wyatt Technology.

The determination of the amount of carbon, hydrogen and nitrogen of the networks was performed on a EuroEA 3000 elemental analyzer.

Fourier Transform Infrared Spectroscopy (FTIR) spectra were recorded at room temperature in the 600−4000 cm^{-1} spectral region on a JASCO 3600 FTIR spectrometer equipped with an ATR accessory. Each sample was analyzed with a resolution of 4 cm^{-1} and an average of 200 scans. The baseline of the spectra was not corrected and the spectrum was not smoothed.

Thermogravimetric analysis (TGA) data were recorded on a TA Instruments TGA Q500, under a nitrogen atmosphere (constant flow of 60 mL/min). Samples were heated from 25 to 600 °C with a heating ramp of 10 °C/min.

Standard DSC measurements were performed on ∼5 mg samples using a Q2000 TA Instrument. PG and PG-βkest were measured in aluminum pans without a lid, after it was confirmed that the type of

https://doi.org/10.1021/acs.macromol.5c01560
Macromolecules 2025, 58, 9993−10006

Scheme 1. (a) Functionalization of PG with TBAA. (b) Formation of Enamine Bonds by Reaction of PG-βkest with a Diamine. In the Box at the Bottom: Diamines Used in Present Study

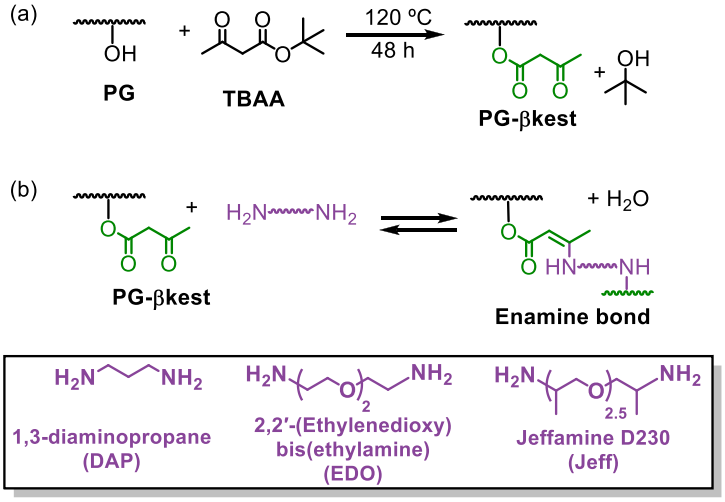

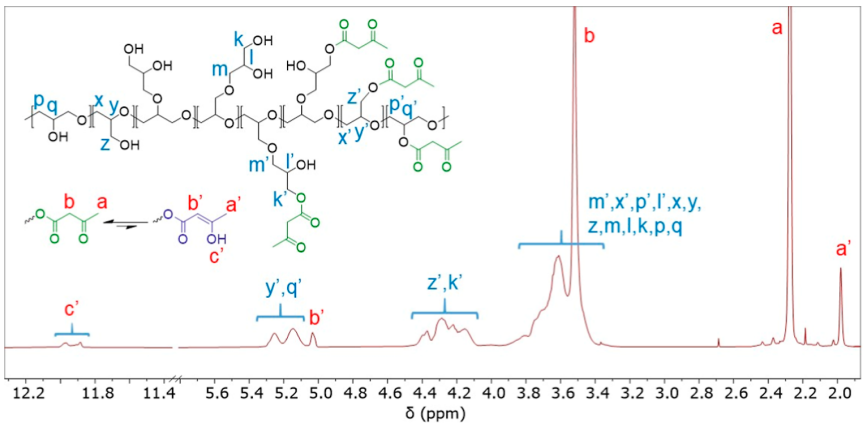

Figure 1. ^{1}H NMR ($CDCl_3$) spectrum of PG-βkest, showing the formation of tautomeric structures.

pan significantly affects the reproducibility of the PG data.[26] The cross-linked networks were measured in sealed aluminum pans for solid samples. The sample was first cooled from room temperature to −100 °C (or −50 °C for the networks) and then heated to 150 °C at 10 °C/min (first heating run). Then, samples were cooled back to −100 °C (or −50 °C for the networks) at 10 °C/min and heated to 150 °C at 10 °C/min (second heating run). A third cooling and heating cycle was then performed to verify reproducibility. A helium flow rate of 25 mL/min was used throughout. Glass transition temperatures (T_g) were determined from the maximum of the first derivative of the heat flow rate in the second heating run.

FSC measurements were carried out employing a Mettler Toledo Flash Differential Scanning Calorimeter (Flash DSC 1) complemented with an Uber TC100 intracooler, allowing to operate in a temperature range between 173 and 723 K. Dry nitrogen was pumped into the sample chamber at a flow rate of 20 mL/min. All samples were prepared by positioning a mass of ∼100 ng directly onto a Mettler Toledo UFS 1 chip. To minimize thermal gradients within the sample, special care was taken to keep the sample height below 10 μm. The absence of significant temperature gradient was verified depositing a little piece of indium on top of the sample. This served also for temperature calibration together with indium deposited on the reference area. All experiments began with a cooling scan from high temperature. The latter was judiciously chosen to guarantee that an equilibrium system is attained and to avoid polymer degradation. With the 2-fold aim of magnifying thermal events in the vitrimers and treating data via the Kissinger analysis (see Results and Discussion section), the cooling rate varied between 1000 and 10^{-3} K s^{-1} and heating rate between 50 and 1000 K s^{-1}. The absence of thermal degradation was verified by comparing reference scans at the beginning and at the end of each set of experiments. It is noteworthy that FSC generally enables success to avoid thermal degradation. The reason stands in the fact that the activation energy of the thermal degradation process is typically much smaller than that of both vitrimeric and glass transition. Details on the interplay between degradation and thermal events with large activation energies are reported in ref 29.

To gain insights into active calorimetric molecular relaxation processes, we applied the so-called step-response protocols.[30,31] This is based on measuring the heat flow after subjecting the sample to a small temperature down-jump followed by an isotherm. In our study the chosen temperature step was 2 K, a perturbation small enough to guarantee the linearity of the measurement.[32] Since our protocol was applied in both standard DSC and FSC, the cooling rate for the temperature step and the duration of the isotherm were optimized to minimize the signal-to-noise ratio and the thermal lag, and to explore

https://doi.org/10.1021/acs.macromol.5c01560
Macromolecules 2025, 58, 9993−10006

the widest possible frequency range. The ratio of Fourier transform of the instantaneous heat flow to the instantaneous cooling rate gives a quantity proportional to the frequency (f) dependent complex specific heat (eq 1), where ω is the angular frequency ($\omega = 2\pi f$).

$$C_p^*(\omega) = C_p'(\omega) + iC_p''(\omega) \quad (1)$$

The combination of standard DSC and FSC allowed us to access a frequency range between 10^{-3} and 50 Hz.

Dynamic mechanical (DMA) experiments were performed using an ARES-LS2 torsional rheometer (TA Instruments) with a parallel plate geometry (8 mm diameter). Experiments were performed by using samples of about 0.1 mm thickness with a 0.1% strain at 1 rad/s frequency and recording the complex shear modulus during temperature ramps at a rate of 1 K/min.

RESULTS AND DISCUSSION

Functionalization of Branched Polyglycidol. PG was functionalized with beta-ketoester groups (PG-βkest) by a transesterification reaction with *tert*-butyl acetoacetate (TBAA) (Scheme 1a). ^{1}H, ^{13}C, COSY, HSQC and DEPT 135° NMR and FTIR analysis confirmed the formation of targeted structures (Figures 1 and S2−S4). ^{1}H NMR data exhibited the formation of the enol form of the βkest (signals identified as a′, b′ and c′ in Figure 1) indicating the occurrence of keto−enol tautomerism in solution ($CDCl_3$), as previously observed in other polymeric systems.[33] Comparison of the peak integrals of $-CH_3$ in the keto (δ = 2.28 ppm) and enol forms (δ = 1.98 ppm) indicated that 89% existed in the keto form, which is the functionality that will react with amines to form enamines. The degree of functionalization was determined by comparing the proton integrals of both keto and enol forms (a + a′) relative to the CH and CH_2 protons from the polymer backbone. The results indicated that 83% of the hydroxyl groups of the polymer chain were reacted.

Synthesis of Cross-Linked Networks with Diamines. Polymer networks were obtained by reaction of PG-βkest with 1,3-diaminopropane (DAP), 2,2′-(ethylenedioxy)bis-(ethylamine) (EDO), or Jeffamine D230 (Jeff) (Scheme 1b). After mixing the polymer with the diamines at room temperature (25 °C) in Teflon Petri dishes for 24 h, homogeneous films were observed. Different mole equivalents of diamine were used to cross-link 1 mol equivalent of βkest motifs through enamine bonds. Excess of diamine was removed by either evaporation or Soxhlet extraction. As a result, films with a thickness of approximately 100 μm were obtained, displaying distinct textural characteristics contingent solely on the nature of the amine employed in the synthesis (Figure 2a). The composition of the polymer networks was calculated by employing the amount of nitrogen in the sample as determined by elemental analysis (eqs S1−S7). Figure 2b shows the moles of amine per mol of βkest obtained in the sample as a function of the moles of amine per mol of βkest used to prepare the networks (feed). Sample values below feed values of 1 exhibit a growing trend with a slope near 1 indicating that all the diamine used in the feed is retained in the polymer network through covalent bonds. However, at feed values above 1, the amount of amine in the sample does not follow this trend and remains in the range of 0.9−1.1 indicating that the excess of diamine has been removed during purification.

TGA data of PG-βkest and cross-linked networks exhibited important changes in their thermal stability compared to nonfunctionalized PG precursor (Figures 3 and S5). PG is thermally stable up to 300 °C (onset temperature) whereas its

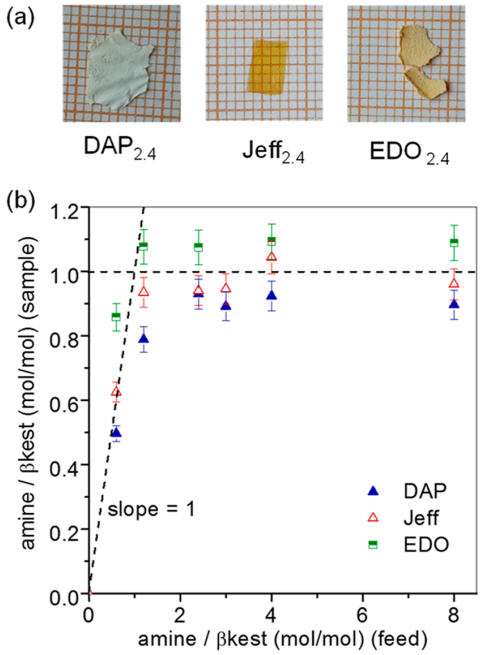

Figure 2. (a) Photographs of films over millimeter graph paper (samples obtained with an amine/βkest (feed) molar ratio of 2.4). (b) Composition of polymer networks cross-linked with DAP, EDO and Jeff.

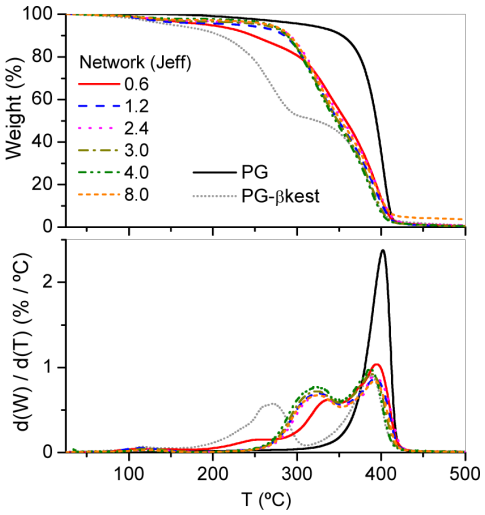

Figure 3. TGA data recorded at 10 °C/min under nitrogen atmosphere of PG, PG-βkest and cross-linked networks obtained by reaction of PG-βkest with Jeff using different amine/βkest molar ratios in the feed (from 0.6 to 8.0). (top) Weight loss. (bottom) First derivative of weight with respect to temperature.

βkest derivative starts to decompose at 170 °C due to the incorporation of thermally unstable carbonyl groups into the polymer structure. A weight loss of 51% is in agreement with the calculated weight loss of βkest group relative to the total mass of the polymer. TGA data of cross-linked networks showed that upon the formation of enamine groups, the

https://doi.org/10.1021/acs.macromol.5c01560
Macromolecules 2025, 58, 9993−10006

thermal stability slightly increased. The network obtained with an amount of amine below the stoichiometric one (amine/βkest (feed) molar ratio = 0.6) starts to decompose at a similar temperature than that of the PG-βkest precursor. However, the networks cross-linked with molar equivalents of amine per mole of βkest (feed) $\geq$ 1.2 exhibited higher thermal stability than the previous one and an identical decomposition profile, indicating a similar number of cross-linking points.

FTIR data of the cross-linked networks revealed the gradual disappearance of the β-ketoester peaks at 1739 ($\nu_{C=O\ ester}$) and 1714 cm^{-1} ($\nu_{C=O\ ketone}$) with the increasing amount of the diamine and the appearance of two bands centered at 1649 ($\nu_{C=O\ ester}$) and 1597 cm^{-1} ($\nu_{C=C}$) in all the systems investigated (Figures 4, 5 and S6), in agreement with the

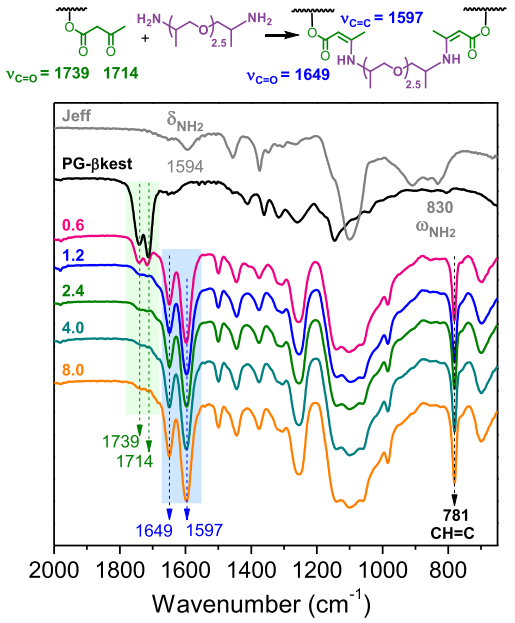

Figure 4. FTIR spectra of the cross-linked networks formed by PG-βkest and Jeff obtained with different amine/βkest molar ratios in the feed (from 0.6 to 8.0).

formation of enamine bonds.[34] Other features that characterize the cross-linked networks are the disappearance of the NH_2 wagging vibration of DAP (849 cm^{-1}) and Jeff (830 cm^{-1}) upon reaction, which is typical of primary amines, and the appearance of a CH out-of-plane deformation band of CH=C bonds at 781 cm^{-1}. The disappearance of the NH_2 internal deformation band detected at 1599, 1594, and 1598 cm^{-1} for DAP, Jeff and EDO, respectively, cannot be observed in the cross-linked networks due to the superposition of an absorption $\nu_{C=C}$ band at 1597 cm^{-1}. The NH deformation band of the formed secondary amine is too weak and cannot be detected readily.

In the case of the network obtained with DAP, the appearance of a band at 1739 cm^{-1} ($\nu_{C=O\ ester}$) and 1238 cm^{-1} (skeletal vibrations involving $\nu_{(NH)_2C-CH_3}$ and $\nu_{(NH)_2C-CH_2}$) was observed for a high excess of DAP in the feed, with amine/βkest molar ratios $\geq$2.4 (Figure 5). This result suggests that upon curing at 85 °C and further heating at 150 °C to remove excess DAP (see Figure S7), the formation

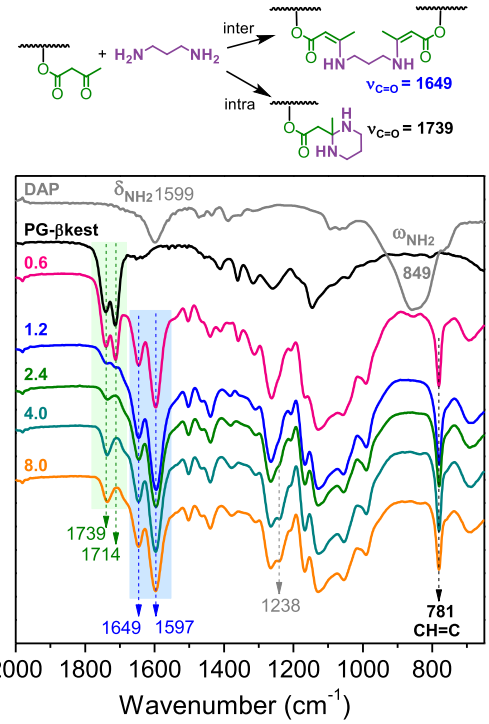

Figure 5. FTIR spectra of the cross-linked networks formed by PG-βkest and DAP obtained with different amine/βkest molar ratios in the feed (from 0.6 to 8.0).

of 2-methyl hexahydropyrimidine moieties is favored through an intramolecular cyclization reaction of the diamine. The results also indicate that this intramolecular reaction is more likely in an excess of DAP, where the diamine is expected to be largely anchored by only one amine group, enabling the second amine group to attack the quaternary carbon and to form an aminal group. The reaction of 1,3-diamines in poly(vinyl amine) with acetone to form aminal groups has been reported,[35] supporting the present findings. The aminal formation was not observed for the cross-linked networks formed by Jeff and EDO (Figures 4 and S6) due to the unlikely formation of less thermodynamically stable aminal groups compared to enamine groups. Discussion of thermodynamic aspects of these reactions using DFT calculations is given in the Supporting Information and Figure S13.

Glass Transition Temperature. The characterization of the T_g of the cross-linked networks obtained with different amounts of diamine is shown in Figure 6a. For a given amount of amine in the feed, a significant increase in T_g can be observed when moving from Jeff to EDO to DAP. This is expected considering the flexibility of these amines. It is also noteworthy that, while the glass transition range for Jeff and EDO is relatively narrow (similar to that of the precursor for Jeff and slightly broader for EDO), it is remarkably broader for DAP. This finding indicates that the latter system exhibits an anomalous, heterogeneous glass-to-rubber transformation, likely due to the formation of non-cross-linked aminal structures, as described above.

Figure 6b summarizes the dependence of T_g on the amount of amine in the feed for networks cross-linked with Jeff, EDO and DAP (see also Figure S8). Those cross-linked with Jeff and

https://doi.org/10.1021/acs.macromol.5c01560
Macromolecules 2025, 58, 9993−10006

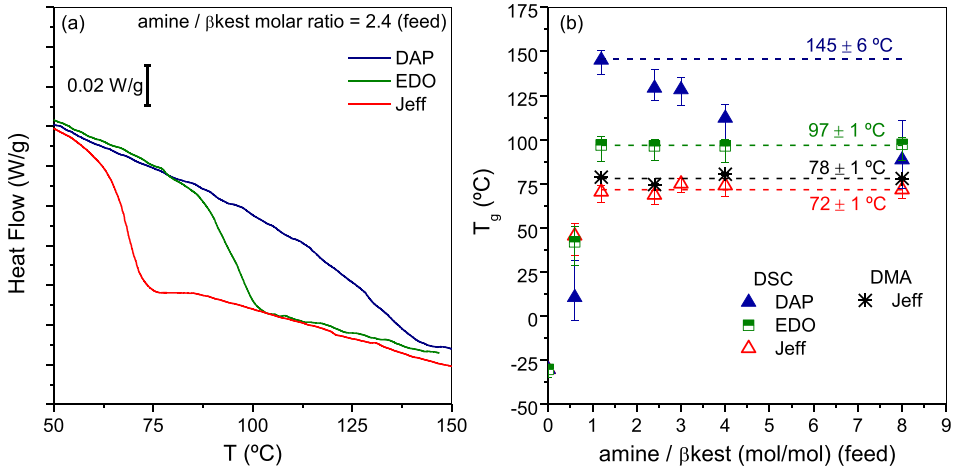

Figure 6. (a) DSC traces obtained in three cross-linked networks obtained using different amines but maintaining a constant ratio amine/βkest (feed) = 2 (b) T_g of cross-linked networks as a function of amine/βkest (feed) molar ratios determined by DSC and DMA. Error bars represent the T_g width. Dashed lines for Jeff and EDO are linear fittings at amine/βkest $\geq$ 1.2 (feed) with slopes fixed to zero. Dashed line for DAP shows the maximum T_g obtained. Asterisks correspond to values obtained for the Jeff networks by DMA at 1 Hz.

EDO showed the expected increase in T_g with increasing amount of amine in the feed to reach a plateau where a further increase in amine content does not result in further cross-links; the excess of amine being removed to reach final amine/βkest molar ratios near 1 (Figure 2b). In contrast, the networks cross-linked with DAP showed an initial rapid increase in T_g with increasing amounts of amine up to values as high as 145 °C, followed by a decrease in T_g. The favored intramolecular reaction at amine/βkest (feed) molar ratios $\geq$2.4, which causes a decrease in the number of cross-links by the formation of 2-methyl hexahydropyrimidine moieties, provides a possible explanation for this decrease in T_g. Unfortunately, the small sample size of the films precludes the ability to make a reliable determination of swelling, which is associated with the number of cross-linking units. Further evidence of this phenomenon is provided by FSC, as discussed below.

Considering that the network cross-linked with DAP at an amine/βkest (feed) = 1.2 does not show any sign of the formation of aminal structures, we describe the maximum T_g for this network as 145 °C. The differences in T_g for this network with respect to the other networks cross-linked with EDO and Jeff are as high as 48 and 73 °C, respectively. As already mentioned, this result can be attributed to the more rigid structure of DAP, which contains only one propylene unit. In contrast, the ethylene oxide and propylene oxide moieties introduce greater flexibility into the cross-linked units allowing for less constrained segmental movements throughout the network. In the case of Jeff, the methyl groups of the propylene units introduce additional bulkiness causing a further reduction in T_g.

Characterizing the Vitrimeric Character of the Cross-Linked Networks with Jeff. To gain more insights into the properties of this family of materials, we have performed dynamic mechanical analysis (DMA) of the networks cross-linked with Jeff, since in this series of samples we can explore a wider temperature range, avoiding thermal degradation. A representative curve is shown in Figure S9. In all the samples we found a similar behavior; a marked drop in storage modulus in the glass transition region and a very extended plateau region at higher temperatures, with no evidence of terminal relaxation indicative of flow. Unfortunately, due to the small sample size, we were unable to determine a reliable value for the plateau modulus of these samples. Associated with this drop in modulus is a pronounced peak in the loss tangent, which can also be used to determine T_g. The trend of these T_g data (shown in Figure 6b) is consistent with those obtained by DSC, although with values almost 6 °C higher. This is not surprising given the relatively high value of the frequency used in DMA (1 Hz). Moreover, the correspondence between the T_g obtained by linear measurements, as in DMA, and that obtained by measurements where the kinetic of vitrification is probed, as in DSC, is not obvious at all,[36,37] although the former is generally greater than the latter,[38] as in our case.

In the results presented so far, there is no clear manifestation of the vitrimeric character of these materials, which would be expected due to the dynamic nature of the covalent bonds involved in the cross-linking process. If dynamic bond exchange occurs at temperatures above T_g, the DSC curves do not provide clear evidence, suggesting that the typical time scale of bond exchange would be similar to that of the segmental motions responsible for T_g, i.e. the two phenomena would be strongly coupled on the time scale relevant to these measurements, that is, of the order of seconds. On the other hand, it is generally known that the segmental dynamics rate exhibits a strong non-Arrhenius temperature dependence and consequently a very high apparent activation energy, while the dynamic bond exchange rate generally follows Arrhenius behavior with a moderate activation energy.[6,14] This situation is schematically summarized in Figure S1. From this plot, it is clear that if the coupling between the two phenomena occurs around T_g, as detected by conventional DSC, a clear distinction could be detected by exploring faster rates. Based on these ideas, we studied the behavior of the samples cross-linked with Jeff using FSC, which allows identifying thermal events at experimental time scales much shorter than in standard DSC. Thanks to FSC's ability to access heating/cooling rates as large as thousands of K s^{-1}, we explored a wide

https://doi.org/10.1021/acs.macromol.5c01560
Macromolecules 2025, 58, 9993−10006

range of thermal protocols, far beyond those accessible by standard DSC.[17]

A preliminary look at the calorimetric response of FSC is provided in Figure 7 for several selected systems, including the precursor polymer prior to cross-linking. Specifically, we report heating scans at 500 K s^{-1} after cooling at 1000 K s^{-1} for the cross-linked networks formed by Jeff. The heat flow rate, HF, which is proportional to the specific heat, is shown in its normalized version (eq 2)

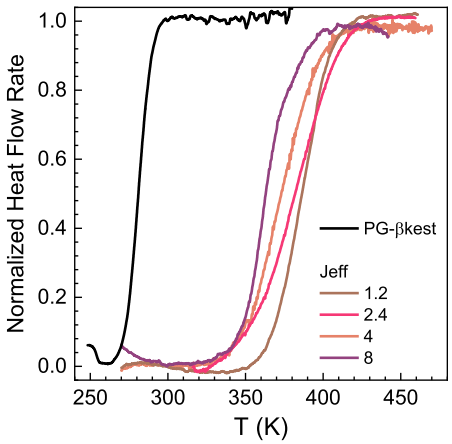

Figure 7. Normalized heat flow rate at 500 K s^{-1} after cooling at 1000 K s^{-1} for the networks obtained with Jeff at the indicated amine/βkest (feed) molar ratios.

$$HF_{norm}(T) = \frac{HF(T) - HF_{gl}(T)}{HF_{liq}(T) - HF_{gl}(T)} \quad (2)$$

where HF_{gl} and HF_{liq} are the glass and liquid heat flow rates, respectively. Although generally detected at higher temperatures with FSC than with standard DSC, we still observed a single step in the specific heat, albeit over a wider temperature interval. This was in some cases larger than 50 K, which is inconsistent with the detection of a single standard glass transition. In contrast, as shown in Figure 7, the FSC response under the same conditions for the PG-βkest precursor exhibited the typical glass transition behavior consisting of a relatively narrow heat flow rate step encompassing less than 30 K at the used high rates.

A step forward in the detection of multiple thermal events is provided by thermal protocols in which the cooling rate is varied over the wide range allowed by FSC. This type of protocol is typically adopted to emphasize the presence of kinetic thermal events such as the glass transition,[39−41] even when these are barely visible in simple heating/cooling scans at the same rate.[42] Here, we subjected a number of studied networks to cooling rates ranging from 0.05 to 1000 K s^{-1} and assessed how the variation in cooling rates was reflected in the heating scan at 500 K s^{-1} performed immediately after. The results (Figure 8) show that heating after slow cooling results in the development of an endothermic overshoot, indicating the attainment of glassy states with low enthalpy. Importantly, on heating after cooling at the lowest rates, a bimodal overshoot is observed, or at least a very broad endotherm encompassing almost 100 K is evident.

Unraveling the Vitrimeric Character of the Cross-Linked Networks by Fast Scanning Calorimetry. The observation of a single broad endotherm, though indicating the presence of different thermal events, does not allow to unambiguously disentangle them. Instead, this can be done in those cases where the bimodal character is more evident. To gain insight into the mechanisms underlying the presence of these two events—specifically their relation with the glass and topological transition temperatures, T_g and T_V, respectively, both expected to occur in vitrimers—we have enriched our calorimetric analysis by subjecting two judiciously selected networks to increasingly complex thermal protocols. The selected samples were those obtained with Jeff at an amine/βkest (feed) molar ratio of 2.4 and 8 (hereafter named $Jeff_{2.4}$ and $Jeff_8$, respectively), which clearly exhibit two distinguishable thermal events (Figure 8). Specifically, our thermal protocol consisted of varying the heating rate after cooling at different rates. The resulting set of heating scans is presented in Figures 9 and 10, which shows that two thermal events can be detected for all investigated heating rates. Here, it is worth pointing out that the maximum heating rate for $Jeff_{2.4}$ is 500 K

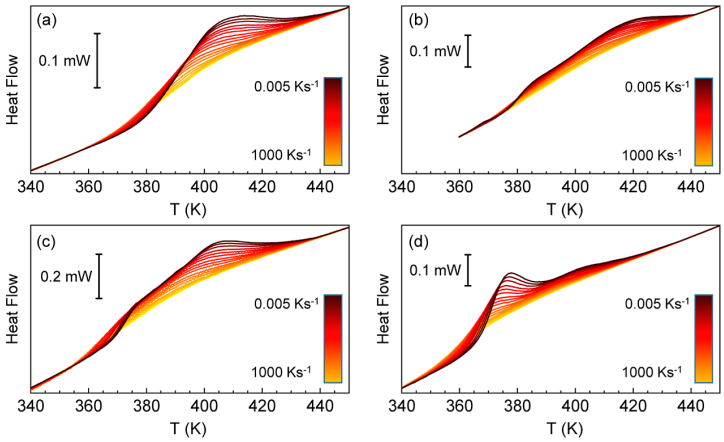

Figure 8. Heat flow rate temperature scans upon heating at 500 K s^{-1} after cooling at the indicated rates for samples obtained with Jeff at an amine/βkest (feed) molar ratio of (a) 1.2, (b) 2.4, (c) 4 and (d) 8.

https://doi.org/10.1021/acs.macromol.5c01560
Macromolecules 2025, 58, 9993−10006

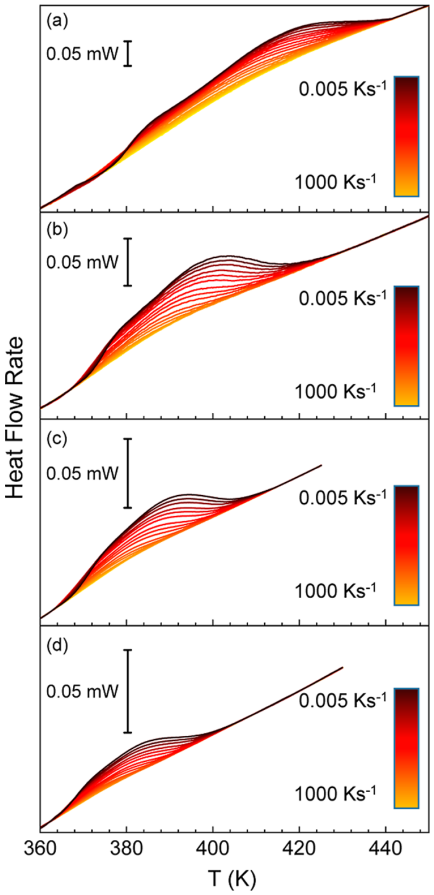

Figure 9. Heat flow rate scans obtained upon heating at (a) 500 K s^{-1}, (b) 200 K s^{-1}, (c) 100 K s^{-1} and (d) 50 K s^{-1} after cooling in a range between 0.005 and 1000 K s^{-1} for $Jeff_{2.4}$.

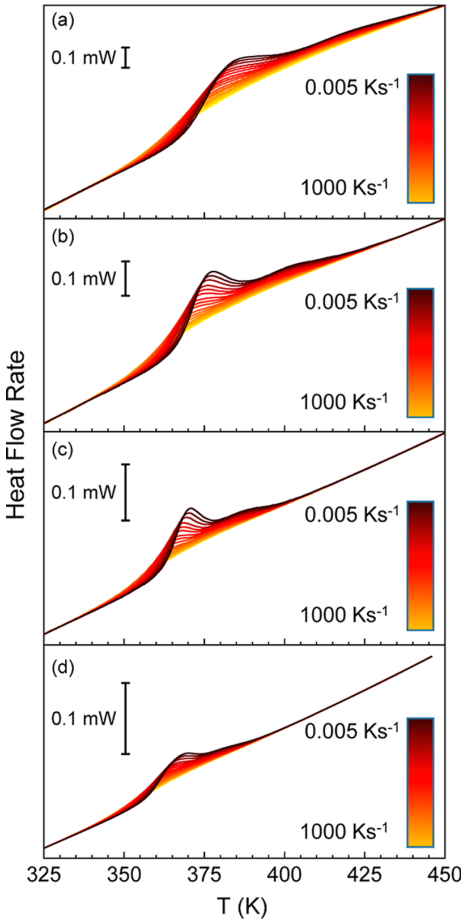

Figure 10. Heat flow rate scans obtained upon heating at (a) 1000 K s^{-1}, (b) 500 K s^{-1}, (c) 200 K s^{-1} and (d) 100 K s^{-1} after cooling in a range between 0.005 and 1000 K s^{-1} for $Jeff_8$.

s^{-1}, which is lower than that of Jeff 8 (1000 K s^{-1}). The reason is that the former sample has larger mass and, therefore, it exhibits significant thermal lag at 1000 K s^{-1} (Figure S10). Interestingly, the separation of both thermal events appears to be more pronounced at higher heating rates. This latter observation qualitatively indicates that the high temperature event presents a lower apparent activation energy than the low temperature event. Another interesting observation is that the comparison between both samples, obtained with different amounts of Jeff, suggests that the thermal response of the two events is unevenly distributed. Specifically, while the low temperature thermal event exhibits a large endothermic effect with respect to the high temperature one for $Jeff_8$, the opposite applies for $Jeff_{2.4}$.

The endothermic excess observed when samples previously cooled at low rates are heated underlines the kinetic transformations from the glass to states where configurational degrees of freedom are progressively activated. Insights into these transformations can be obtained by identifying the temperature, T_p, at which the rate of enthalpy change is maximum. While strictly speaking this corresponds to the peaks of the heat flow rate scans, inspection of Figures 9 and 10 reveals that in most cases these cannot be unambiguously separated. Consequently, to perform a simple data analysis, we assumed that the distribution of relaxation times of the two thermal events detected by FSC is temperature invariant. This implies that time−temperature superposition holds separately for each of the two events, which has been approximately verified over moderately wide temperature ranges in polymeric systems.[43,44] Starting from these premises, information about the transformation kinetics of the observed thermal events can be obtained considering representative temperatures at which these events do not overlap. Therefore, as a proxy for T_p—which for simplicity we will also refer to as T_p—we have resorted to the temperatures at which the rate of change of the heat flow rate is maximum. In both cases, a criterion of nonoverlap of the two events was chosen. Specifically, for the low temperature event the rate of maximum increase in heat flow rate was chosen, while for the high temperature one the criterion was based on the rate of maximum decrease in heat flow rate before the kinetic transformation ends. In this way we minimize the superposition effect of the two thermal events on characterizing each individual contribution by selecting the standard inflection point temperature for the lower-temperature event and the endset temperature for the higher-temperature event. Thus, these temperatures are unambiguously identified where the second derivatives of the heat flow

https://doi.org/10.1021/acs.macromol.5c01560
Macromolecules 2025, 58, 9993−10006

rate scans shown in Figures 9 and 10 become zero. An overview of the second derivatives of the heat flow rate scans is shown in Figure S11 for representative heating (200 K s^{-1}) and cooling rates (0.005−0.1 K s^{-1}).

The chosen proxy for the rates of maximum transformation at different heating rates underlined by the two T_p can be used to implement the so-called Kissinger analysis.[45,46] The latter is widely used in thermal analysis to gain insights into the kinetic mechanisms underlying nonisothermal chemical reactions[45] and crystallization.[47] Within this framework, we aim to convey information about the apparent activation energies (E_a) of the two thermal events underlying the nonisothermal kinetic transformations, in this case from the frozen-in glass to the high temperature viscous flow regime.[48] The rate of kinetic transformation, k, can be written as (eq 3)

$$k = k_0 \exp \frac{-E_a}{RT} \tag{3}$$

where k_0 is a pre-exponential factor, R is the gas constant, and E_a *is* apparent activation energy of the molecular mechanism supporting the kinetic transformation under study.

In the kinetic transformation from an initial state to a final state, e.g. from glass, with degree of transformation $X = 1$, to liquid, with $X = 0$, in the most general case the transformation rate is related to k as (eq 4)

$$\frac{dX}{dt} = k(1 - X)^n \tag{4}$$

where n is the order of the kinetic transformation.

Considering the criterion of maximum enthalpy transformation, at T_p the first derivative of the rate of change of the kinetic transformation must be zero (eq 5)

$$\frac{\frac{dX}{dt}}{dt} = k_0 \exp\left(\frac{-E_a}{RT_p}\right)\frac{-E_a}{RT_p^2}(1 - X)^n \frac{dT_p}{dt} - n(1 - X)^{n-1} \exp\left(\frac{-E_a}{RT_p}\right)\frac{dX}{dt} = 0 \tag{5}$$

In most cases the exponent n is close to unity[45] and, therefore, $n(1 - X)^{n-1} = 1$. Rearranging eq 5 and writing the heating rate $dT/dt = \beta$, we obtain (eq 6)

$$\ln \frac{\beta}{T_p^2} = -\frac{E_a}{RT_p} + c \tag{6}$$

where c is a temperature independent parameter, although its invariance is strictly valid only if E_a of the thermal event under consideration is also temperature independent. In the case of our study, this is not strictly true in the case of the glass transition,[48,49] generally associated with the polymer segmental motion, whose E_a is temperature dependent. However, given the relatively small temperature range explored in our study, eq 6 can still be considered valid.

According to eq 6, the slope of $\ln(\beta/T_p^2)$ as a function of $1/T_p$ allows obtaining E_a of the molecular mechanism mediating the kinetic transformation process. The correlation established by eq 6 is presented in Figure 11 for both $Jeff_{2.4}$ and $Jeff_8$, showing the T_p data of the two observed thermal events after cooling and heating at different heating rates. It should be noted that the fit via eq 6 for the high temperature event data was restricted to the three highest heating rates, since the lowest rate exhibits a clear deviation toward a higher E_a, a fact that will be discussed later. As can be observed for both systems, the high temperature thermal event has a lower E_a compared to the low temperature event. Furthermore, a comparison of the Kissinger plots of the two systems shows that $Jeff_8$ generally has lower transformation temperatures than $Jeff_{2.4}$. Although in the same range, the E_a of the two events for $Jeff_{2.4}$ appear to be slightly larger than those for $Jeff_8$.

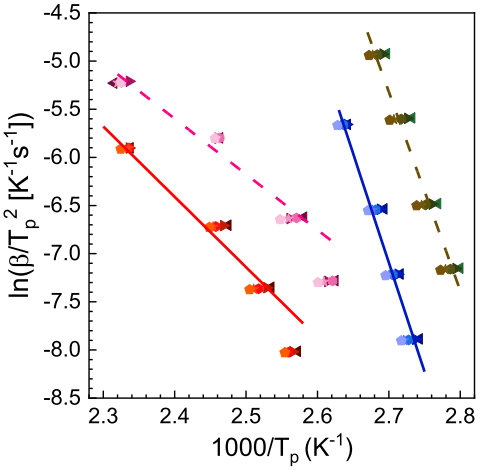

Figure 11. Kissinger plot of the thermal transformation events observed in $Jeff_{2.4}$ (solid, red and blue) and $Jeff_8$ (dash, pink and khaki) after cooling at the following rates: 0.1 (left triangles), 0.05 (right triangles), 0.02 (hexagons), 0.01 (stars) and 0.005 (pentagons) K s^{-1}. The straight lines are the fits to eq 6, which yields the following apparent activation energies for the higher and lower temperature events, respectively: $E_a = 60 \pm 5$ kJ mol^{-1} and $E_a = 190 \pm 5$ kJ mol^{-1} for $Jeff_{2.4}$ and $E_a = 50 \pm 5$ kJ mol^{-1} and $E_a = 170 \pm 5$ kJ mol^{-1} for $Jeff_8$.

The values of E_a of the two transformation kinetics observed in both $Jeff_{2.4}$ and $Jeff_8$ can be understood complementing this information with that obtained from experiments conducted in the linear regime.[37] This is done employing step response analysis.[30,31] Figure 12a,b show the temperature and frequency dependent normalized reversing specific heat, $C^N_{p,rev}$, which is approximately equal to the normalized real part of the complex specific heat.[41] A single relatively narrow step in $C^N_{p,rev}$ is observed. This can be unambiguously attributed to spontaneous fluctuations of the polymer segments associated with the glass transition, as commonly observed in all types of glass-forming systems.[50,51] The temperature dependence of the typical time scale of these fluctuations: $\tau = 1/(2\pi f)$, taken from the temperature of maximum inflection of $C^N_{p,rev}$, is shown in Figure 12c. As expected, this relaxation time exhibits a marked temperature dependence with super-Arrhenius temperature behavior, which can be described by the Vogel−Fulcher−Tammann (VFT) empirical equation[52−54] (gray line): $\tau(T) = \tau_0 \exp(B/(T - T_0))$. As noted above, the apparent activation energy obtained from the VFT equation is temperature dependent and is given by $E_{VFT} = T^2B/(T - T_0)^2$. To verify how the two kinetic processes identified by FSC are related to the polymer segmental dynamics, we have analyzed the temperature dependence of $T/E_a^{1/2}$ vs T, which for the VFT case would result in a linear plot: $T/E_{VFT}^{1/2} = (T - T_0)/B^{1/2}$. Figure 13 shows such a comparison, from which it is clear that

https://doi.org/10.1021/acs.macromol.5c01560
Macromolecules 2025, 58, 9993−10006

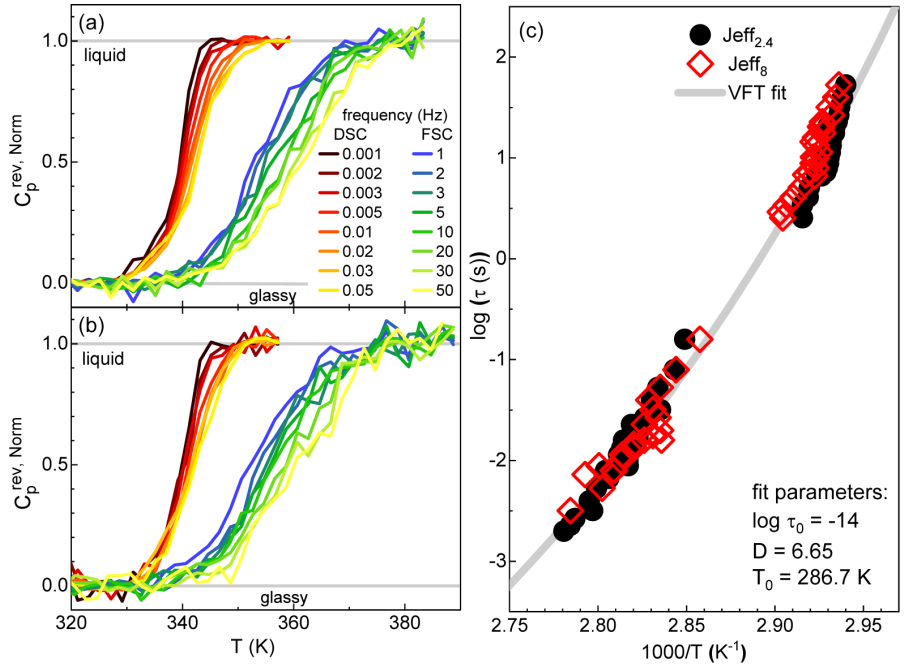

Figure 12. Normalized reversing specific heat as a function of temperature at different frequencies obtained from standard DSC and FSC for (a) $Jeff_{2.4}$ and (b) $Jeff_8$. (c) Temperature dependence of the relaxation time obtained from panels (a,b) at the temperature of maximum inflection of the normalized reversing specific heat. The line in panel (c) is the VFT fit with parameters given in the legend.

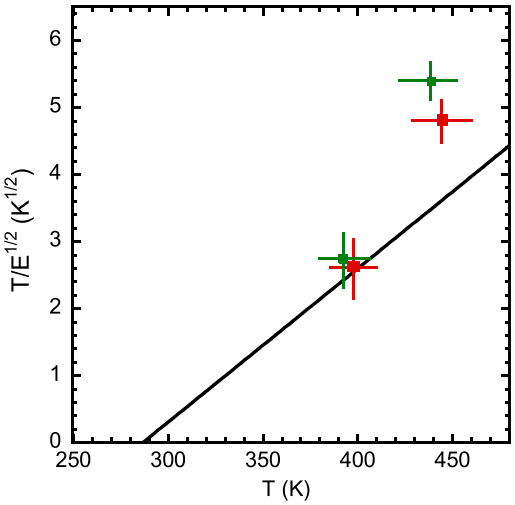

Figure 13. Comparison of the apparent activation energies obtained from FSC for the two kinetic processes for $Jeff_{2.4}$ (green) and $Jeff_8$ (red) with that corresponding to the VFT equation describing the relaxation times determined in the linear regime. The size of the crosses corresponds to the estimated uncertainties.

the low-temperature thermal event agrees well with the expectation from the VFT equation, while, in contrast, the data for the high-temperature kinetic process are far above the VFT line, indicating a significantly lower apparent activation energy as expected for a vitrimeric-related phenomenon. It should be noted that the underlying molecular mechanism for the high-temperature kinetic transformation remains invisible in the calorimetric characterization in the linear regime. This can be attributed to the two following reasons: (i) weakly activated thermal events are hardly visible due to the fact that they cover a wide temperature range;[44] (ii) the degrees of freedom activated by the high temperature event are limited, making the associated specific heat step small.

As a final complementary test of the vitrimeric character of the present networks, we performed experiments using parallel plate viscometry,[55] which records changes in sample thickness as a function of time while a constant small vertical force is applied. In this way, we found clear evidence of slow flow at temperatures above 370 K. Figure 14 shows that the high viscosity values obtained, around 10^{11} Pa s, follow an Arrhenius temperature dependence with an activation energy of about 100 kJ/mol, a value intermediate between those found for the two kinetic phenomena detected by FSC.

Overall, our results on the kinetic transformation from frozen-in glass to fully relaxed network indicate that it occurs via a low and a high temperature event, the former being completely coupled to the polymer segmental relaxation responsible for the glass transition. The high temperature event has a lower apparent activation energy, which is consistent with a reversible covalent bond exchange reaction.[14] The latter process is generally described as occurring in two steps: (i) approach of two active sites by segmental diffusion and; (ii) bond exchange once these active sites are brought into close contact.[56]

In the high temperature regime, in the case of $Jeff_{2.4}$ and $Jeff_8$ above ~390 and 400 K, respectively (see Figure 12), the segmental diffusion would exhibit a time scale much shorter than that responsible for bond exchange. As a result, the low activation energy in this regime is representative of the bond exchange process alone, that is, the slow step of the overall

https://doi.org/10.1021/acs.macromol.5c01560
Macromolecules 2025, 58, 9993−10006

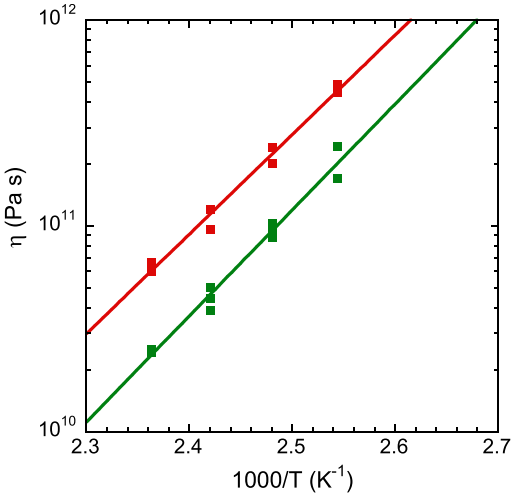

Figure 14. Arrhenius plot of the viscosity as determined by parallel plate viscometry for $Jeff_{2.4}$ (green) and $Jeff_8$ (red). Several experimental data points at each temperature are shown to illustrate typical uncertainties. The solid lines correspond to the corresponding Arrhenius fits.

bond exchange reaction. At lower temperatures, segmental diffusion rapidly becomes slower, thereby making the overall covalent bond exchange reaction to be controlled by both steps. This picture is fully compatible with our results on how the kinetic transformation of the high temperature event takes place, which shows an increasing apparent activation energy at low temperatures (see the data points deviating from the Kissinger fit in Figure 11). At lower temperatures, the overall process of the reversible covalent bond exchange reaction is expected to be completely controlled by the ultraslow segmental relaxation under these conditions. As a result, this process will be indistinguishable from segmental relaxation.[15,56] In other words, the two stages of the bond exchange process, that is, diffusion and chemical bond exchange, become coupled in the low-temperature regime, leading to an apparent increase in activation energy. The latter observations may explain why only a relatively narrow specific heat step is observed by standard DSC, considering that the latter technique, due to the long accessible observation times, i.e. much lower heating/cooling rates compared to FSC, actually explores the low temperature regime. This is found only for very large separation between segmental relaxation and bond exchange reaction time, which is rarely observed unless nanophase separation takes place.[57,58] Standard DSC has previously been shown to provide convincing evidence of the two thermal events only in some rare cases.[15]

The activation energy of temperature dependent viscosity can be compared with that found by FSC. As can be seen, the activation energy of viscosity obtained from Figure 14 has a value somewhat larger that of the high temperature bond exchange kinetics: 100 kJ mol^{-1} vs 50 and 60 kJ mol^{-1} for $Jeff_{2.4}$ and $Jeff_8$, respectively. These results indicate that the viscosity of the investigated vitrimers is only partly controlled by the bond exchange kinetics. A review of previous results in the literature indicates that this is the case for some vitrimeric systems, while for others bond exchange fully control the viscosity.[15]

An important point worth of discussion regards the difference in transformation kinetics and viscosity between $Jeff_{2.4}$ and $Jeff_8$. Although these samples exhibit an amine/beta-ketoester ratio of approximately 1, both were prepared with very different excess amounts of amine (2.4 for $Jeff_{2.4}$ and 8 for $Jeff_8$). At these amine concentrations, the formation of "dangling chains" is highly favored. Once the curing is performed at 85 °C, followed by the removal of excess amine, the enamines are reformed through reaction with the free amines from the "dangling chains", which results in the formation of diamines connected on both sides. This results in a network that is totally cross-linked both intra- and intermolecularly, where each beta-ketoester group corresponds to one amine (amine/β-ketoester molar ratio ~1). However, it is probable that the $Jeff_8$ sample contains a higher amount of amines that have initially penetrated into the interior of the branched structure compared to the $Jeff_{2.4}$ sample. This will conduct to a distribution of cross-linked units that differs between $Jeff_{2.4}$ and $Jeff_8$, as suggested by the narrower T_g range and the more pronounced separation from the T_v in $Jeff_8$ compared to $Jeff_{2.4}$. Therefore, we conclude that the amount of amine used in the preparation of the cross-linked networks is a pivotal parameter for obtaining more homogeneous materials.

These considerations are also relevant to the relative intensity of the glass transition and vitrimeric kinetics obtained from FSC. Specifically, a comparison of panels (b) and (d) in Figure 8 indicates that the event related with the glass transition is more intense than the vitrimeric transformation in $Jeff_8$, whereas the opposite applies for $Jeff_{2.4}$. Tentatively, this can be rationalized by considering that the dynamic bond exchange in $Jeff_8$ predominantly occurs intradendrimerically whereas that in $Jeff_{2.4}$ occurs more interdendrimerically. This makes the macroscopic FSC enthalpic variation in $Jeff_8$ milder than in $Jeff_{2.4}$. This interpretation is consistent with the increased viscosity observed for $Jeff_8$ compared to $Jeff_{2.4}$ (see Figure 14).

In the DAP series the amount of amine was also a relevant parameter. An excess of DAP led to the formation of non-cross-linked aminal structures as shown by decreasing T_g values (Figure 6b) and the appearance of bands at 1739 and 1238 cm^{-1} in the FTIR data (Figure 5). Examining the FSC data of $DAP_{2.4}$ and DAP_8 (Figure S12) using similar heating and cooling protocols as the Jeff series revealed clear differences between the two sample preparations. $DAP_{2.4}$ exhibited two thermal events related to glass transition and bond exchange, while DAP_8 showed only one event related to glass transition. This confirms the loss of bond exchange events in DAP_8 due to the formation of aminal structures.

SUMMARY

Cross-linked vitrimeric networks formed by dynamic enamine bonds were obtained through the reaction of β-ketoester-functionalized branched polyglycerol and diamines. This reaction achieved the maximum possible number of cross-links. The physical properties of these materials were found to be highly dependent on the type and amount of amine added relative to the amount of β-ketoesters, even after excess amine was removed. First, changing the type of amine alters the T_g, resulting in lower T_g for networks containing oligomeric and flexible diamines (e.g., Jeff and EDO) than for networks with smaller diamine molecules (e.g., DAP). We hypothesize that a greater number of intradendrimeric bonds are formed when there is a greater excess of amine during preparation. However,

https://doi.org/10.1021/acs.macromol.5c01560
Macromolecules 2025, 58, 9993−10006

with a smaller excess, interdendrimeric bonds appear to be favored. Finally, DAP is not recommended for forming covalent adaptable networks because it forms aminal groups that impede cross-linking between chains.

For the first time, the FSC was used to evaluate the T_v of cross-linked networks. Furthermore, we were able to determine the activation energy of the bond exchange using a protocol of different heating and cooling rates in the FSC that separates this process from the T_g. As expected, the activation energy obtained from the bond exchange was much lower, in the range of 50−60 kJ/mol, than the apparent activation energy of the glass transition, in the range of 170−190 kJ/mol.

Our FSC protocol, here developed, can be extended to the detection of T_v and the study of the bond exchange kinetics of a number of vitrimeric networks, highlighting the versatility of this approach in characterizing dynamic covalent materials. By enabling rapid and precise thermal analysis, the method provides critical insight into the temperature-dependent kinetic processes and the influence of network composition, and cross-link density on the vitrimeric behavior.

■ ASSOCIATED CONTENT

Supporting Information

The Supporting Information is available free of charge at https://pubs.acs.org/doi/10.1021/acs.macromol.5c01560.

Tables of composition (composition in the feed and elemental analysis results), supporting equations, NMR and FTIR spectra, TGA and DMA data, second derivative of FSC heat flow and DFT calculation results (PDF)

■ AUTHOR INFORMATION

Corresponding Authors

Daniele Cangialosi − *Materials Physics Center (CFM-MPC), CSIC-UPV/EHU, 20018 Donostia−San Sebastián, Spain; Donostia International Physics Center (DIPC), 20018 Donostia−San Sebastián, Spain;* orcid.org/0000-0002-5782-7725; Email: daniele.cangialosi@ehu.eus

Fabienne Barroso-Bujans − *Materials Physics Center (CFM-MPC), CSIC-UPV/EHU, 20018 Donostia−San Sebastián, Spain; PMAS, Faculty of Chemistry, University of the Basque Country (UPV/EHU), 20018 Donostia−San Sebastián, Spain; IKERBASQUE—Basque Foundation for Science, 48009 Bilbao, Spain; Donostia International Physics Center (DIPC), 20018 Donostia−San Sebastián, Spain;* orcid.org/0000-0002-9591-5646; Email: f.barroso@ehu.eus

Authors

Vasiliki Maria Stavropoulou − *Materials Physics Center (CFM-MPC), CSIC-UPV/EHU, 20018 Donostia−San Sebastián, Spain; PMAS, Faculty of Chemistry, University of the Basque Country (UPV/EHU), 20018 Donostia−San Sebastián, Spain;* orcid.org/0009-0009-8223-1438

Marta Aldecoa-Ortueta − *Materials Physics Center (CFM-MPC), CSIC-UPV/EHU, 20018 Donostia−San Sebastián, Spain; PMAS, Faculty of Chemistry, University of the Basque Country (UPV/EHU), 20018 Donostia−San Sebastián, Spain;* orcid.org/0009-0001-3544-3501

Ester Verde-Sesto − *Materials Physics Center (CFM-MPC), CSIC-UPV/EHU, 20018 Donostia−San Sebastián, Spain; IKERBASQUE—Basque Foundation for Science, 48009 Bilbao, Spain;* orcid.org/0000-0001-8748-5140

Valerio Di Lisio − *Materials Physics Center (CFM-MPC), CSIC-UPV/EHU, 20018 Donostia−San Sebastián, Spain; Donostia International Physics Center (DIPC), 20018 Donostia−San Sebastián, Spain;* orcid.org/0000-0001-7729-8069

Anabel Lam − *Donostia International Physics Center (DIPC), 20018 Donostia−San Sebastián, Spain; Zeolites Engineering Laboratory, Institute of Materials Science and Technology (IMRE), University of Havana, 10400 La Habana, Cuba;* orcid.org/0000-0001-5171-5020

José A. Pomposo − *Materials Physics Center (CFM-MPC), CSIC-UPV/EHU, 20018 Donostia−San Sebastián, Spain; PMAS, Faculty of Chemistry, University of the Basque Country (UPV/EHU), 20018 Donostia−San Sebastián, Spain; IKERBASQUE—Basque Foundation for Science, 48009 Bilbao, Spain;* orcid.org/0000-0003-4620-807X

Angel Alegría − *Materials Physics Center (CFM-MPC), CSIC-UPV/EHU, 20018 Donostia−San Sebastián, Spain; PMAS, Faculty of Chemistry, University of the Basque Country (UPV/EHU), 20018 Donostia−San Sebastián, Spain;* orcid.org/0000-0001-6125-8214

Complete contact information is available at: https://pubs.acs.org/10.1021/acs.macromol.5c01560

Author Contributions

#V.M.S. and M.A. authors contributed equally. The manuscript was written through contributions of all authors. All authors have given approval to the final version of the manuscript.

Notes

The authors declare no competing financial interest.

■ ACKNOWLEDGMENTS

The authors gratefully acknowledge the Grant PID2024-157988NB-I00 funded by MICIU/AEI/10.13039/501100011033 and ERDF/EU, and Grant IT-1566-22 by Eusko Jaurlaritza (Basque Government). E.V.S. acknowledges financial support from the "Ramón y Cajal" Program Grant No. RYC2022-037590-I funded by MICIU/AEI/10.13039/501100011033 and ESF+. A.L. acknowledges support from DIPC visiting program. Open Access funding provided by University of Basque Country.

■ REFERENCES

(1) Maes, S.; Badi, N.; Winne, J. M.; Du Prez, F. E. Taking dynamic covalent chemistry out of the lab and into reprocessable industrial thermosets. *Nat. Rev. Chem.* **2025**, *9* (3), 144−158.

(2) Zhang, V.; Kang, B.; Accardo, J. V.; Kalow, J. A. Structure−Reactivity−Property Relationships in Covalent Adaptable Networks. *J. Am. Chem. Soc.* **2022**, *144* (49), 22358−22377.

(3) Lei, Z.; Chen, H.; Huang, S.; Wayment, L. J.; Xu, Q.; Zhang, W. New Advances in Covalent Network Polymers via Dynamic Covalent Chemistry. *Chem. Rev.* **2024**, *124* (12), 7829−7906.

(4) Elling, B. R.; Dichtel, W. R. Reprocessable Cross-Linked Polymer Networks: Are Associative Exchange Mechanisms Desirable? *ACS Cent. Sci.* **2020**, *6* (9), 1488−1496.

(5) Van Zee, N. J.; Nicolaÿ, R. Vitrimers: Permanently crosslinked polymers with dynamic network topology. *Prog. Polym. Sci.* **2020**, *104*, 101233.

(6) Montarnal, D.; Capelot, M.; Tournilhac, F.; Leibler, L. Silica-Like Malleable Materials from Permanent Organic Networks. *Science* **2011**, *334* (6058), 965−968.

(7) Guerre, M.; Taplan, C.; Winne, J. M.; Du Prez, F. E. Vitrimers: directing chemical reactivity to control material properties. *Chem. Sci.* **2020**, *11* (19), 4855−4870.
(8) Martins, M. L.; Zhao, X.; Demchuk, Z.; Luo, J.; Carden, G. P.; Toleutay, G.; Sokolov, A. P. Viscoelasticity of Polymers with Dynamic Covalent Bonds: Concepts and Misconceptions. *Macromolecules* **2023**, *56* (21), 8688−8696.
(9) Hubbard, A. M.; Ren, Y.; Konkolewicz, D.; Sarvestani, A.; Picu, C. R.; Kedziora, G. S.; Roy, A.; Varshney, V.; Nepal, D. Vitrimer Transition Temperature Identification: Coupling Various Thermomechanical Methodologies. *ACS Appl. Polym. Mater.* **2021**, *3* (4), 1756−1766.
(10) Capelot, M.; Unterlass, M. M.; Tournilhac, F.; Leibler, L. Catalytic Control of the Vitrimer Glass Transition. *ACS Macro Lett.* **2012**, *1* (7), 789−792.
(11) Liu, T.; Zhao, B.; Zhang, J. Recent development of repairable, malleable and recyclable thermosetting polymers through dynamic transesterification. *Polymer* **2020**, *194*, 122392.
(12) Yang, Y.; Zhang, S.; Zhang, X.; Gao, L.; Wei, Y.; Ji, Y. Detecting topology freezing transition temperature of vitrimers by AIE luminogens. *Nat. Commun.* **2019**, *10* (1), 3165.
(13) Arbe, A.; Alegría, A.; Colmenero, J.; Bhaumik, S.; Ntetsikas, K.; Hadjichristidis, N. Microscopic Evidence for the Topological Transition in Model Vitrimers. *ACS Macro Lett.* **2023**, *12* (11), 1595−1601.
(14) Denissen, W.; Winne, J. M.; Du Prez, F. E. Vitrimers: permanent organic networks with glass-like fluidity. *Chem. Sci.* **2016**, *7* (1), 30−38.
(15) Soman, B.; Schweizer, K. S.; Evans, C. M. Fragile Glass Formation and Non-Arrhenius Upturns in Ethylene Vitrimers Revealed by Dielectric Spectroscopy. *Macromolecules* **2023**, *56* (1), 166−176.
(16) Porath, L.; Soman, B.; Jing, B. B.; Evans, C. M. Vitrimers: Using Dynamic Associative Bonds to Control Viscoelasticity, Assembly, and Functionality in Polymer Networks. *ACS Macro Lett.* **2022**, *11* (4), 475−483.
(17) Schick, C.; Mathot, V. *Fast Scanning Calorimetry*; Springer: Cham, 2016; p XIV, 801.
(18) Sanchez-Sanchez, A.; Fulton, D. A.; Pomposo, J. A. pH-responsive single-chain polymer nanoparticles utilising dynamic covalent enamine bonds. *Chem. Commun.* **2014**, *50* (15), 1871−1874.
(19) Denissen, W.; Rivero, G.; Nicolaÿ, R.; Leibler, L.; Winne, J. M.; Du Prez, F. E. Vinylogous Urethane Vitrimers. *Adv. Funct. Mater.* **2015**, *25* (16), 2451−2457.
(20) Lessard, J. J.; Garcia, L. F.; Easterling, C. P.; Sims, M. B.; Bentz, K. C.; Arencibia, S.; Savin, D. A.; Sumerlin, B. S. Catalyst-Free Vitrimers from Vinyl Polymers. *Macromolecules* **2019**, *52* (5), 2105−2111.
(21) Tellers, J.; Pinalli, R.; Soliman, M.; Vachon, J.; Dalcanale, E. Reprocessable vinylogous urethane cross-linked polyethylene via reactive extrusion. *Polym. Chem.* **2019**, *10* (40), 5534−5542.
(22) Zhu, Y.; Gao, F.; Zhong, J.; Shen, L.; Lin, Y. Renewable castor oil and DL-limonene derived fully bio-based vinylogous urethane vitrimers. *Eur. Polym. J.* **2020**, *135*, 109865.
(23) Hajiali, F.; Tajbakhsh, S.; Marić, M. Thermally reprocessable bio-based polymethacrylate vitrimers and nanocomposites. *Polymer* **2021**, *212*, 123126.
(24) Pagnacco, C. A.; Kravicz, M. H.; Sica, F. S.; Fontanini, V.; González de San Román, E.; Lund, R.; Re, F.; Barroso-Bujans, F. In Vitro Biocompatibility and Endothelial Permeability of Branched Polyglycidols Generated by Ring-Opening Polymerization of Glycidol with B(C6F5)3 under Dry and Wet Conditions. *Biomacromolecules* **2024**, *25* (6), 3583−3595.
(25) Gómez Urreizti, E.; Gastearena, X.; Lam, A.; González de San Román, E.; Miranda, J. I.; Matxain, J. M.; Barroso-Bujans, F. Kinetics of heterogeneous polymerization of glycidol with B(C6F5)3 in toluene in the absence and presence of water. *Mater. Today Chem.* **2024**, *37*, 101993.
(26) Al Assiri, M. A.; Gómez Urreizti, E.; Pagnacco, C. A.; Gónzalez de San Román, E.; Barroso-Bujans, F. Reactivity of B(C6F5)3 towards glycidol: The formation of branched cyclic polyglycidol structures. *Eur. Polym. J.* **2022**, *171*, 111194.
(27) Sunder, A.; Hanselmann, R.; Frey, H.; Mülhaupt, R. Controlled Synthesis of Hyperbranched Polyglycerols by Ring-Opening Multibranching Polymerization. *Macromolecules* **1999**, *32* (13), 4240−4246.
(28) Utrata-Wesołek, A.; Oleszko, N.; Trzebicka, B.; Anioł, J.; Zagdańska, M.; Lesiak, M.; Sieroń, A.; Dworak, A. Modified polyglycidol based nanolayers of switchable philicity and their interactions with skin cells. *Eur. Polym. J.* **2013**, *49* (1), 106−117.
(29) Monnier, X.; Napolitano, S.; Cangialosi, D. Direct observation of desorption of a melt of long polymer chains. *Nat. Commun.* **2020**, *11* (1), 4354.
(30) Shoifet, E.; Schulz, G.; Schick, C. Temperature modulated differential scanning calorimetry − extension to high and low frequencies. *Thermochim. Acta* **2015**, *603*, 227−236.
(31) Perez-de-Eulate, N. G.; Di Lisio, V.; Cangialosi, D. Glass Transition and Molecular Dynamics in Polystyrene Nanospheres by Fast Scanning Calorimetry. *ACS Macro Lett.* **2017**, *6* (8), 859−863.
(32) Hempel, E.; Hempel, G.; Hensel, A.; Schick, C.; Donth, E. Characteristic Length of Dynamic Glass Transition near Tg for a Wide Assortment of Glass-Forming Substances. *J. Phys. Chem. B* **2000**, *104* (11), 2460−2466.
(33) Efstathiou, S.; Ma, C.; Coursari, D.; Patias, G.; Al-Shok, L.; Eissa, A. M.; Haddleton, D. M. Functional pH-responsive polymers containing dynamic enaminone linkages for the release of active organic amines. *Polym. Chem.* **2022**, *13* (16), 2362−2374.
(34) Ma, Y.; Jiang, X.; Shi, Z.; Berrocal, J. A.; Weder, C. Closed-Loop Recycling of Vinylogous Urethane Vitrimers. *Angew. Chem., Int. Ed.* **2023**, *62* (36), No. e202306188.
(35) Trommler, K.; Walther, T.; Seifert, S.; Seifert, A.; Hähnle, H.; Anders, S.; Kroll, L.; Spange, S. The Reaction of Poly(Vinyl Amine) with Acetone in Water. *Macromol. Chem. Phys.* **2019**, *220* (3), 1800444.
(36) Kant, R.; Kumar, S. K.; Colby, R. H. What Length Scales Control the Dynamics of Miscible Polymer Blends? *Macromolecules* **2003**, *36* (26), 10087−10094.
(37) Cangialosi, D. Physical aging and vitrification in polymers and other glasses: Complex behavior and size effects. *J. Polym. Sci.* **2024**, *62* (9), 1952−1974.
(38) Donth, E.; Korus, J.; Hempel, E.; Beiner, M. Comparison of DSC heating rate and HCS frequency at the glass transition. *Thermochim. Acta* **1997**, *304*−*305*, 239−249.
(39) Tropin, T. V.; Schulz, G.; Schmelzer, J. W. P.; Schick, C. Heat capacity measurements and modeling of polystyrene glass transition in a wide range of cooling rates. *J. Non-Cryst. Solids* **2015**, *409*, 63−75.
(40) Monnier, X.; Cangialosi, D.; Ruta, B.; Busch, R.; Gallino, I. Vitrification decoupling from α-relaxation in a metallic glass. *Sci. Adv.* **2020**, *6* (17), No. eaay1454.
(41) Melillo, J. H.; Cangialosi, D.; Di Lisio, V.; Steinrücken, E.; Vogel, M.; Cerveny, S. Complexity of confined water vitrification and its glass transition temperature. *Proc. Natl. Acad. Sci. U.S.A.* **2024**, *121* (41), No. e2407030121.
(42) Martín, J.; Stingelin, N.; Cangialosi, D. Direct Calorimetric Observation of the Rigid Amorphous Fraction in a Semiconducting Polymer. *J. Phys. Chem. Lett.* **2018**, *9* (5), 990−995.
(43) Ferry, J. D. *Viscoelastic Properties of Polymers*, 3rd ed.; John Wiley and Sons: New York, 1980.
(44) Cangialosi, D.; Alegría, A.; Colmenero, J. On the temperature dependence of the nonexponentiality in glass-forming liquids. *J. Chem. Phys.* **2009**, *130* (12), 124902.
(45) Kissinger, H. E. Reaction Kinetics in Differential Thermal Analysis. *Anal. Chem.* **1957**, *29* (11), 1702−1706.
(46) Blaine, R. L.; Kissinger, H. E. Homer Kissinger and the Kissinger equation. *Thermochim. Acta* **2012**, *540*, 1−6.
(47) Mittemeijer, E. J. Analysis of the kinetics of phase transformations. *J. Mater. Sci.* **1992**, *27* (15), 3977−3987.

https://doi.org/10.1021/acs.macromol.5c01560
Macromolecules 2025, 58, 9993−10006

(48) Vyazovkin, S. Kissinger Method in Kinetics of Materials: Things to Beware and Be Aware of. *Molecules* **2020**, *25* (12), 2813.
(49) Svoboda, R.; Čičmanec, P.; Málek, J. Kissinger equation versus glass transition phenomenology. *J. Therm. Anal. Calorim.* **2013**, *114* (1), 285−293.
(50) Boller, A.; Schick, C.; Wunderlich, B. Modulated differential scanning calorimetry in the glass transition region. *Thermochim. Acta* **1995**, *266*, 97−111.
(51) Mike Reading, D. J. H. *Modulated Temperature Differential Scanning Calorimetry: Theoretical and Practical Applications in Polymer Characterisation*; Springer: Dordrecht, 2006; p XIV, 330.
(52) Vogel, H. Das Temperaturabhängigkeitsgesetz der Viskosität von Flüssigkeiten. *Phys. Zeitschrift* **1921**, *22*, 645.
(53) Fulcher, G. S. Analysis of recent measurements of the viscosity of glasses. *J. Am. Ceram. Soc.* **1925**, *8* (6), 339−355.
(54) Tammann, G.; Hesse, W. Die Abhängigkeit der Viscosität von der Temperatur bie unterkühlten Flüssigkeiten. *Z. Anorg. Allg. Chem.* **1926**, *156* (1), 245−257.
(55) Gent, A. N. Theory of the parallel plate viscometer. *Br. J. Appl. Phys.* **1960**, *11* (2), 85.
(56) Lin, T.-W.; Mei, B.; Dutta, S.; Schweizer, K. S.; Sing, C. E. Molecular Dynamics Simulation and Theoretical Analysis of Structural Relaxation, Bond Exchange Dynamics, and Glass Transition in Vitrimers. *Macromolecules* **2025**, *58* (3), 1481−1497.
(57) Xing, K.; Tress, M.; Cao, P.; Cheng, S.; Saito, T.; Novikov, V. N.; Sokolov, A. P. Hydrogen-bond strength changes network dynamics in associating telechelic PDMS. *Soft Matter* **2018**, *14* (7), 1235−1246.
(58) Robles-Hernández, B.; González-Burgos, M.; Malo de Molina, P.; Asenjo-Sanz, I.; Radulescu, A.; Pomposo, J. A.; Arbe, A.; Colmenero, J. Structure of Single-Chain Nanoparticles under Crowding Conditions: A Random Phase Approximation Approach. *Macromolecules* **2023**, *56* (21), 8971−8979.

https://doi.org/10.1021/acs.macromol.5c01560
Macromolecules 2025, 58, 9993−10006

Supporting Information

Vitrimeric behavior revealed by fast scanning calorimetry in branched polyglycerol networks crosslinked by reversible enamine bonds

Vasiliki Maria Stavropoulou,‡[a,b] Marta Aldecoa-Ortueta,‡[a,b] Ester Verde-Sesto,[a,c] Valerio Di Lisio,[a,d] Anabel Lam,[d,e] José A. Pomposo,[a,b,c] Angel Alegría,[a,b] Daniele Cangialosi,*[a,d] Fabienne Barroso-Bujans*[a,b,c,d]

[a]Materials Physics Center (CFM-MPC), CSIC-UPV/EHU, Paseo Manuel Lardizábal 5, 20018 Donostia−San Sebastián, Spain

[b]PMAS, Faculty of Chemistry, University of the Basque Country (UPV/EHU), Paseo Manuel Lardizábal 3, 20018 Donostia−San Sebastián, Spain

[c]IKERBASQUE - Basque Foundation for Science, Plaza Euskadi 5, 48009, Bilbao, Spain

[d]Donostia International Physics Center (DIPC), Paseo Manuel Lardizábal 4, 20018 Donostia−San Sebastián, Spain

[e]Zeolites Engineering Laboratory, Institute of Materials Science and Technology (IMRE), University of Havana, 10400, La Habana, Cuba

Table of Contents

1. Vitrimeric and segmental dynamics

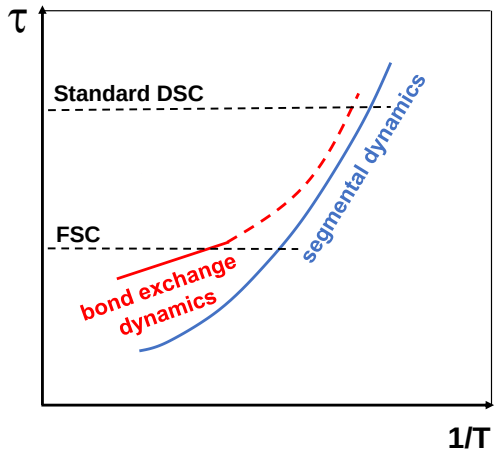

Figure S1. Scheme showing the mild Arrhenius temperature dependence of dynamic bond exchange typical time scale as opposed to the strong super-Arrhenius dependence of segmental relaxation time scale.

2. Synthesis of cross-linked networks with diamines

Table S1. Networks crosslinked with DAP.

		Vial 1		Vial 2	
Sample	**DAP / βkest (mol / mol)**	**$m_{PG\text{-}\beta kest}$ (mg)**	**V_{THF} (mL)**	**V_{DAP} (µL)**	**V_{THF} (µL)**
$DAP_{0.6}$	0.6	86	9.6	12	144
$DAP_{1.2}$	1.2	83	9.6	24	288
$DAP_{2.4}$	2.4	81	9.6	48	576
DAP_{3}	3.0	53	5.4	34	405
DAP_{4}	4	57	5.4	45	540
DAP_{8}	8	51	5.4	90	1080

Table S2. Networks crosslinked with Jeff.

		Vial 1		Vial 2	
Sample	**Jeff / βkest (mol / mol)**	**$m_{PG\text{-}\beta kest}$ (mg)**	**V_{THF} (mL)**	**V_{Jeff} (µL)**	**V_{THF} (µL)**
$Jeff_{0.6}$	0.6	78	9.6	35	144
$Jeff_{1.2}$	1.2	87	9.6	70	288
$Jeff_{2.4}$	2.4	84	9.6	140	576
$Jeff_{3}$	3.0	52	5.4	109	405
$Jeff_{4}$	4	53	5.4	147	601
$Jeff_{8}$	8	53	5.4	291	1200

Table S3. Networks crosslinked with EDO.

		Vial 1		Vial 2	
Sample	**EDO / βkest (mol / mol)**	**$m_{PG\text{-}\beta kest}$ (mg)**	**V_{THF} (mL)**	**V_{EDO} (μL)**	**V_{THF} (μL)**
$EDO_{0.6}$	0.6	79	9.6	21	144
$EDO_{1.2}$	1.2	85	9.6	42	288
$EDO_{2.4}$	2.4	86	9.6	84	576
EDO_{4}	4	47	6.0	88	600
EDO_{8}	8	46	6.0	175	1200

3. Composition

If all the amine functionalities of 1,3-diaminopropane (DAP) form an enamine group in the crosslinked networks, then the decimal amount of nitrogen, N, in the sample is defined by Eq. S1. The 2-methyl hexahydropyrimidine moieties formed in some samples were not included in the formula to simplify the analysis.

$$N = \frac{xM_N}{x(8.5M_C+13M_H+3M_O+1M_N)+y(7M_C+10M_H+4M_C)+z(3M_C+6M_H+2M_O)} \quad \text{Eq. S1}$$

where, M_C, M_H, M_O and M_N are the atomic masses of carbon, hydrogen oxygen and nitrogen, respectively. According to the degree of functionalization of PG with βkest functions found by ^{1}H NMR: z = 0.17 and $x + y = 0.83$. "z" is the fraction of non-functionalized hydroxyl groups of polyglycidol, "x" is the fraction of enamine groups and "y" is the fraction of non-reacted βkest groups.

Then, reformulating Eq. S1, "x" can be calculated by using Eq. S2, where N is the decimal amount of nitrogen determined experimentally and reported in Table S4 [Nitrogen (wt%)/100].

$$x = \frac{144N}{14-19N} \quad \text{Eq. S2}$$

Similarly, the amount of nitrogen, N in the crosslinked networks formed by PG-βkest and 2,2′-(ethylenedioxy)bis(ethylamine) (EDO) is defined by Eq. S3 and "x" by Eq. S4 and that formed by PG-βkest and Jeffamine D230 (Jeff) is defined by Eq. S5 and "x" by Eq. S6.

$$N = \frac{xM_N}{x(10M_C+16M_H+4M_O+1M_N)+y(7M_C+10M_H+4M_C)+z(3M_C+6M_H+2M_O)} \quad \text{Eq. S3}$$

$$x = \frac{144N}{14-56N} \quad \text{Eq. S4}$$

$$N = \frac{xM_N}{x(12.25M_C+20.5M_H+4.25M_O+1M_N)+y(7M_C+10M_H+4M_C)+z(3M_C+6M_H+2M_O)} \quad \text{Eq. S5}$$

$$x = \frac{144N}{14-91.5N} \quad \text{Eq. S6}$$

Finally, to determine the mole equivalents of amine per mol of βkest in the sample, Eq. S7 was employed.

$$\frac{\text{amine}}{\beta\text{kest(mol)}} = \frac{x}{x+y} \quad \text{Eq. S7}$$

Table S4. Amount of nitrogen in the polymer networks determined by elemental analysis.

amine / βkest (mol/mol)	**Nitrogen (wt%) Sample**	**Nitrogen (wt%) Sample**	**Nitrogen (wt%) Sample**
Feed	DAP	EDO	Jeff
0.6	3.81	5.43	3.80
1.2	5.87	6.46	5.06
2.4	6.82	6.45	5.08
3.0	6.57	-	5.10
4.0	6.78	6.53	5.44
8.0	6.6	6.51	5.15

4. Structural characterization

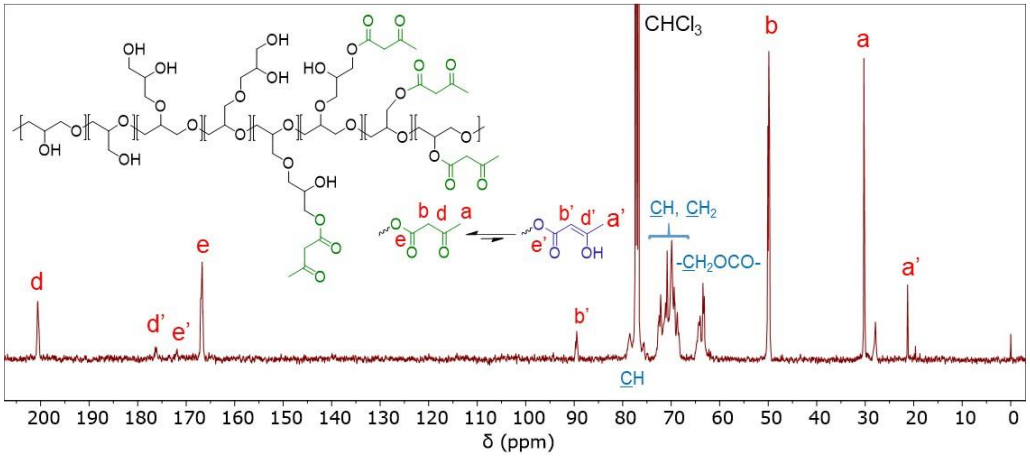

Figure S2. ^{13}C NMR spectrum (in $CDCl_3$) of PG-βkest.

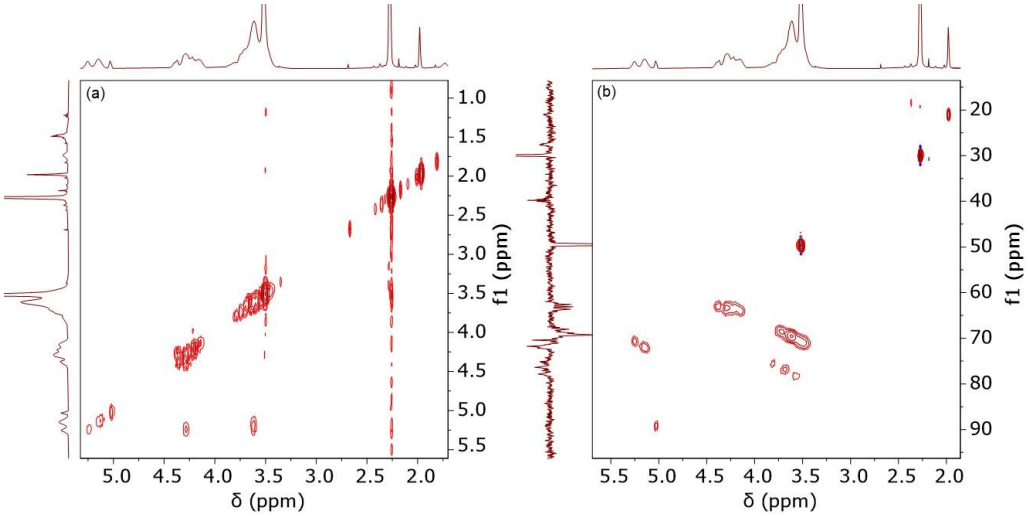

Figure S3. (a) COSY and (b) HSQC-DEPT 135° spectra (in $CDCl_3$) of PG-βkest.

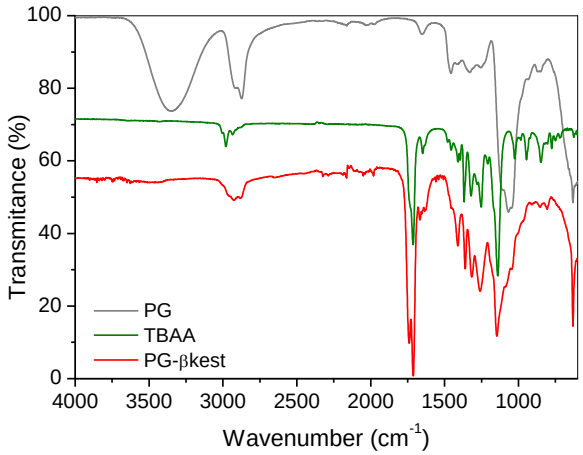

Figure S4. FTIR-ATR spectra vertically shifted for illustrative purposes.

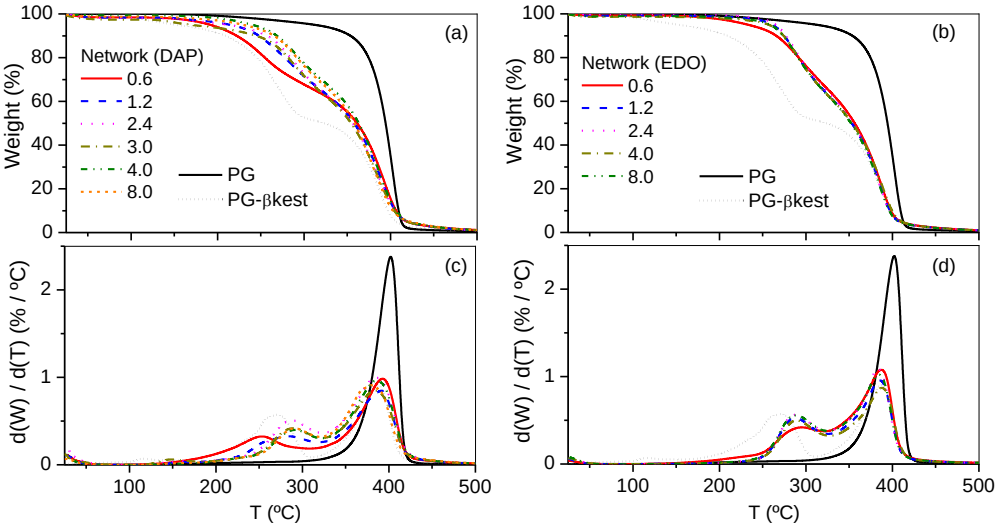

Figure S5. TGA data recorded at 10 ºC/min under nitrogen atmosphere of PG, PG-βkest and crosslinked networks obtained by reaction of (a, c) PG-βkest with DAP and (b, d) PG-βkest with EDO using different amine / βkest molar ratios in the feed (from 0.6 to 8.0). Top: Weight loss. Bottom: First derivative of weight with respect to temperature.

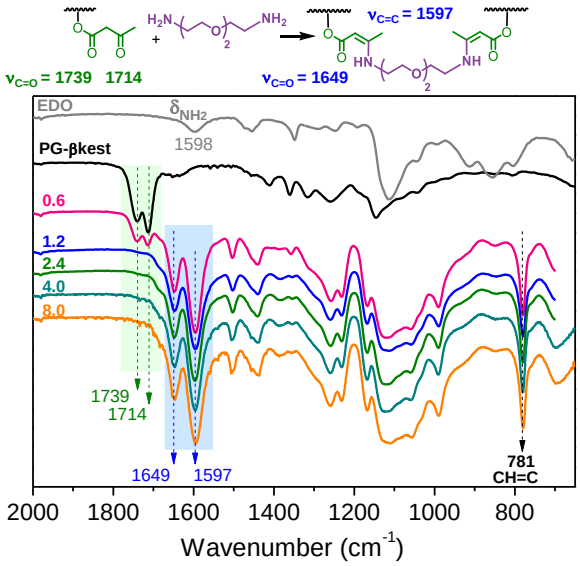

Figure S6. FTIR spectra of the crosslinked networks formed by PG-βkest and EDO obtained with different amine / βkest molar ratios in the feed (from 0.6 to 8.0).

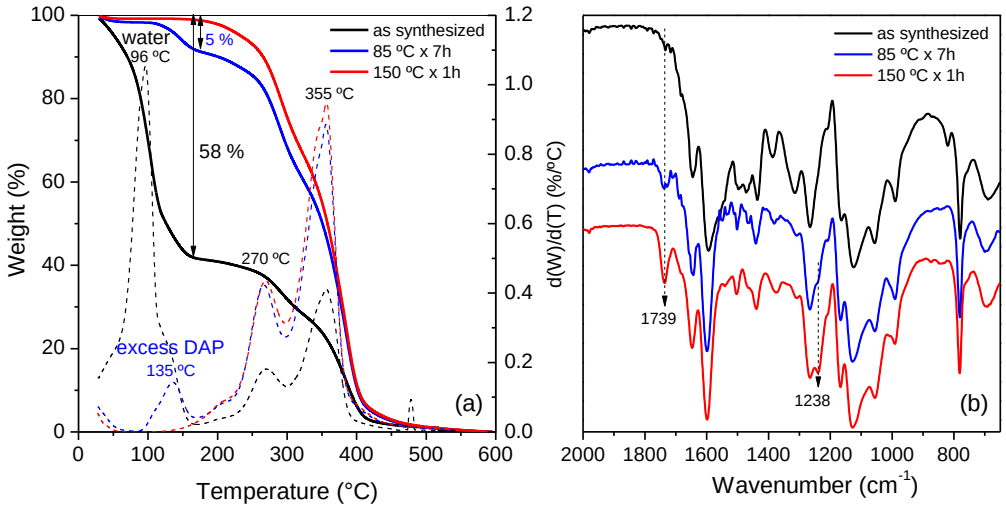

Figure S7. (a) TGA and (b) FTIR spectra of the crosslinked networks formed by PG-βkest and DAP obtained with amine / βkest = 4. Sample "as synthesized" was not heated nor purified. A piece of this sample was heated at 85 ºC for 7 h in vacuum showing unsuccessful removal of DAP while successful removal of water. Another piece of sample was heated at 150 ºC for 1 h in vacuum proving the successful removal of DAP and water. Absorption bands appeared at 1739 and 1238 cm^{-1} upon both thermal treatments, indicating the formation of 2-methyl hexahydropyrimidine moieties.

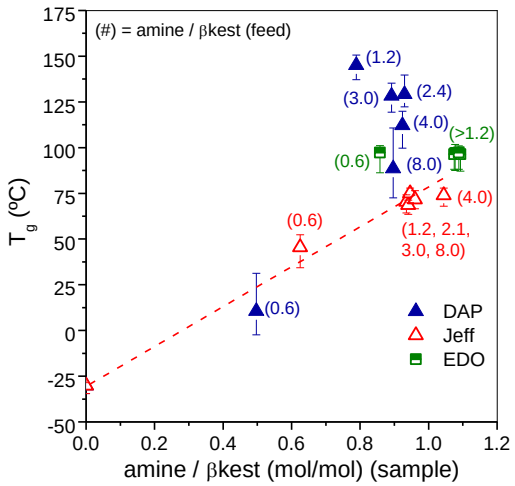

Figure S8. T_g of crosslinked networks as a function of amine / βkest molar ratios in the sample, determined by DSC.

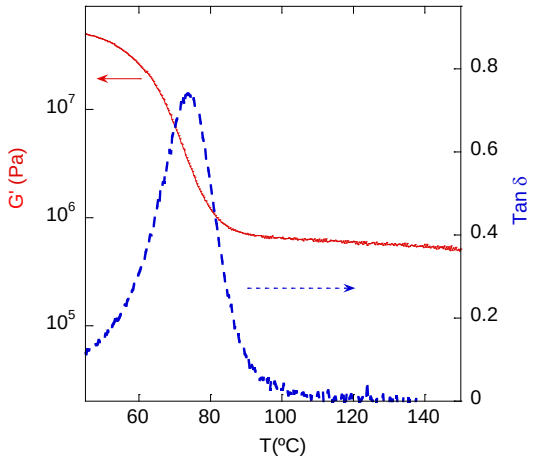

Figure S9. Representative DMA data for $Jeff_{2.4}$ obtained at 0.1% strain at 1 rad/s frequency.

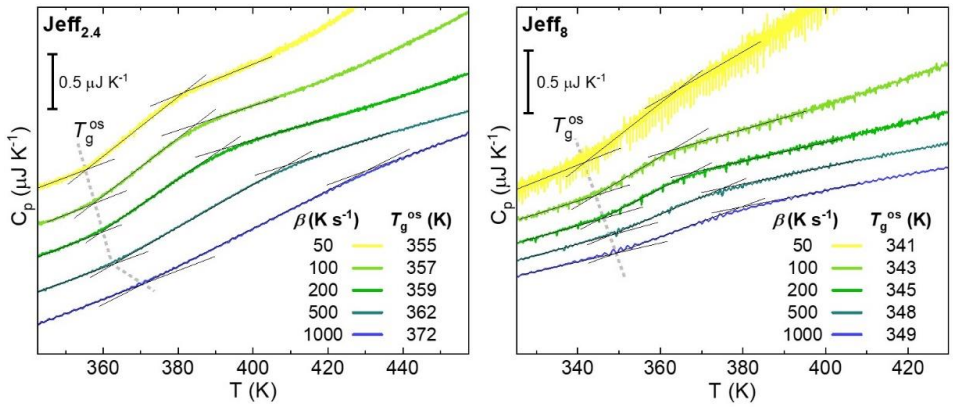

Figure S10. Heating scans for $Jeff_{2.4}$ (left) and $Jeff_8$ (right) at different rates showing the significant thermal lag in the former at 1000 Ks^{-1}.

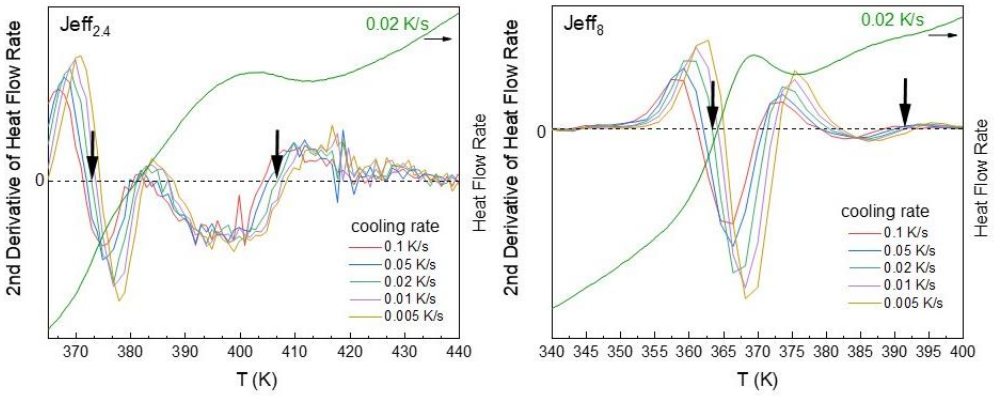

Figure S11. Examples of second derivatives of specific heat scans for $Jeff_{2.4}$ (left) and $Jeff_8$ (right) at 200 K/s.

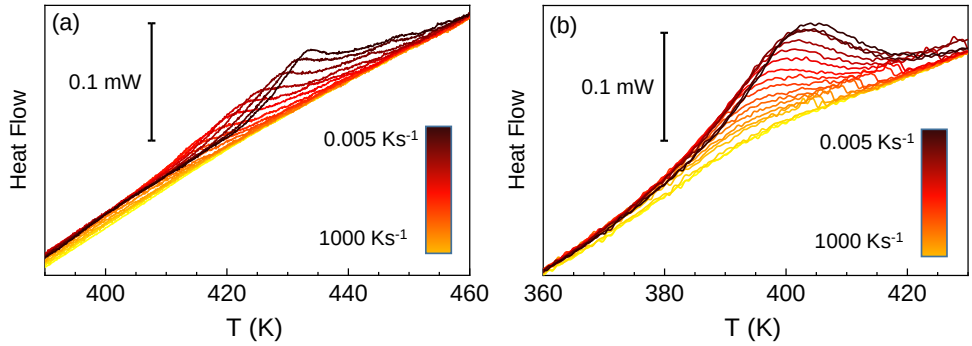

Figure S12. Heat flow rate temperature scans upon heating at 500 Ks^{-1} after cooling at the indicated rates for samples obtained with DAP at an amine / βkest (feed) molar ratio of (a) 2.4 and (b) 8.

5. DFT calculations

The enthalpies of aminal and enamine model compounds formed by DAP, EDO and Jeff were calculated by performing DFT-D3 geometry optimizations using the Gaussian 16 program.[1] The DEF2TZVP basis set[2-3] and the TPSS exchange-correlation functional[4] were used. To simulate the environmental effect, a dielectric constant of 4.7 was used, as in our previous work.[5] Zero-point vibrational energy (ZPVE) and thermal (T = 298 K) vibrational corrections to the enthalpy were implemented. The values of the enthalpy difference between the aminal and enamine model compounds ($\Delta H = H_{aminal} - H_{enamine}$) were calculated as shown in Figure S12. The results show that enamine model compounds are more stable than the aminal ones for the three amines. From this series, the enthalpy of aminal model compound formed by DAP is only 6.69 kcal/mol higher from its enamine analogue, supporting that both compounds can be obtained experimentally. However, in the case of EDO and Jeff, the ΔH between the aminal and enamine model compounds are much higher, 12.51 and 13.12 kcal/mol, respectively. These larger ΔH values and the steric hindrance associated with the formation of larger cyclic compounds support the lack of aminal formation for EDO and Jeff.

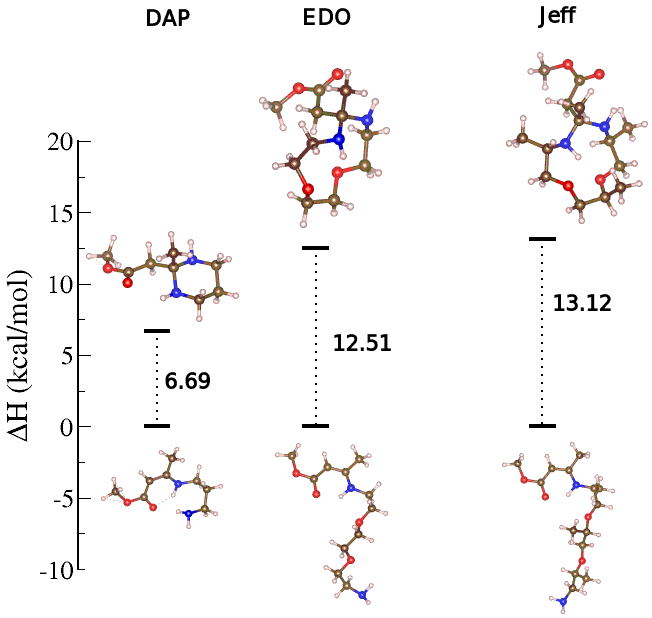

Figure S13. Enthalpy difference (ΔH, kcal/mol) between aminal and enamine model compounds formed by DAP, EDO and Jeff. Atoms are represented by the following color scheme: oxygen (red), nitrogen (blue), carbon (brown), and hydrogen (white).

References

(1) Frisch, M. J.; Trucks, G. W.; Schlegel, H. B.; Scuseria, G. E.; Robb, M. A.; Cheeseman, J. R.; Scalmani, G.; Barone, V.; Petersson, G. A.; Nakatsuji, H.; Li, X.; Caricato, M.; Marenich, A. V.; Bloino, J.; Janesko, B. G.; Gomperts, R.; Mennucci, B.; Hratchian, H. P.; Ortiz, J. V.; Izmaylov, A. F.; Sonnenberg, J. L.; Williams; Ding, F.; Lipparini, F.; Egidi, F.; Goings, J.; Peng, B.; Petrone, A.; Henderson, T.; Ranasinghe, D.; Zakrzewski, V. G.; Gao, J.; Rega, N.; Zheng, G.; Liang, W.; Hada, M.; Ehara, M.; Toyota, K.; Fukuda, R.; Hasegawa, J.; Ishida, M.; Nakajima, T.; Honda, Y.; Kitao, O.; Nakai, H.; Vreven, T.; Throssell, K.; Montgomery Jr., J. A.; Peralta, J. E.; Ogliaro, F.; Bearpark, M. J.; Heyd, J. J.; Brothers, E. N.; Kudin, K. N.; Staroverov, V. N.; Keith, T. A.; Kobayashi, R.; Normand, J.; Raghavachari, K.; Rendell, A. P.; Burant, J. C.; Iyengar, S. S.; Tomasi, J.; Cossi, M.; Millam, J. M.; Klene, M.; Adamo, C.; Cammi, R.; Ochterski, J. W.; Martin, R. L.; Morokuma, K.; Farkas, O.; Foresman, J. B.; Fox, D. J. *Gaussian 16 Rev. C.01*, Wallingford, CT, 2016.

(2) Weigend, F.; Ahlrichs, R., Balanced basis sets of split valence, triple zeta valence and quadruple zeta valence quality for H to Rn: Design and assessment of accuracy. *Phys. Chem. Chem. Phys.* **2005,** *7* (18), 3297-3305.

(3) Weigend, F., Accurate Coulomb-fitting basis sets for H to Rn. *Phys. Chem. Chem. Phys.* **2006,** *8* (9), 1057-1065.

(4) Tao, J.; Perdew, J. P.; Staroverov, V. N.; Scuseria, G. E., Climbing the Density Functional Ladder: Nonempirical Meta--Generalized Gradient Approximation Designed for Molecules and Solids. *Phys. Rev. Lett.* **2003,** *91* (14), 146401.

(5) Gómez Urreizti, E.; Gastearena, X.; Lam, A.; González de San Román, E.; Miranda, J. I.; Matxain, J. M.; Barroso-Bujans, F., Kinetics of heterogeneous polymerization of glycidol with B(C6F5)3 in toluene in the absence and presence of water. *Mater. Today Chem.* **2024,** *37*, 101993.

THE JOURNAL OF PHYSICAL CHEMISTRY B
A JOURNAL OF THE AMERICAN CHEMICAL SOCIETY

pubs.acs.org/JPCB
Article

Identifying the Thermal Barriers of Glass Aging via Isoconversional Analysis

Vasiliki Maria Stavropoulou, Federico Caporaletti,* Florian Pabst, Valerio Di Lisio, Simone Napolitano, and Daniele Cangialosi*

Cite This: J. Phys. Chem. B 2026, 130, 1716−1723

ABSTRACT: We employ isoconversional analysis to gain insights on aging time-dependent thermal barriers in glasses evolving toward equilibrium. This is applied to glasses of different natures, including small molecules and polymers. Our analysis indicates that as relaxation proceeds, equilibration kinetics involves increasingly larger activation barriers. The latter equals that of the α-relaxation at the final stage of aging. In contrast, the relatively low thermal barriers at the initial and intermediate stages of aging indicate that mechanisms different from the α-relaxation mediate aging in these conditions. We discuss the nature of these mechanisms in the light of the complexity of glass aging.

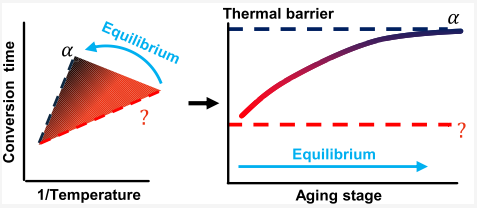

INTRODUCTION

The transformation of a liquid into a glass is known as vitrification or glass transition.[1,2] Over time, as a consequence of its nonequilibrium nature, the glass tends to reduce its free energy via a transformation commonly referred to as physical aging or structural recovery.[3−5] Both vitrification and physical aging represent different aspects of the same underlying problem: the inability of the system to maintain equilibrium when molecular mobility becomes too slow on experimental time scales.

Within the common description, the microscopic mechanism ultimately responsible for both vitrification and physical aging is the main α-relaxation, a molecular process with a characteristic super-Arrhenius temperature dependence. The α-relaxation sets the structural time scale that increases steeply as the glass transition is approached and thus naturally accounts for the dramatic slowdown of dynamics observed in supercooled liquids. This idea has deep historical roots: though conceptually different,[6] vitrification and glassy dynamics are assumed to be equivalent, with the glass transition identified as the point where the α-relaxation time reaches the experimental time scale. Accordingly, vitrification was understood as the arrest of this molecular process and physical aging as its continuation below T_g.

This view holds true for specific cases of vitrification, for instance, in some polymeric systems[7−9] and in low molecular weight glass formers,[10−12] where cooling rate-dependent glass transition temperature, T_g, and temperature-dependent α-relaxation time exhibit the same super-Arrhenius behavior. However, universality of this behavior across all materials remains debated,[13,14] above all when confined glasses are considered.[15−19] In the case of physical aging, the dominant role of the α-relaxation has been demonstrated in thermal protocols involving small temperature steps applied close to T_g.[20−23] These studies have shown that aging follows the same time scale as the α-relaxation, thereby reinforcing the idea that structural recovery is essentially governed by the same molecular process as vitrification. The primary implication of this finding is that because of the high activation energy associated with the α-relaxation, physical aging is expected to rapidly slow down with decreasing temperature. If aging were governed solely by the α-relaxation, one would therefore expect it to vanish not too far below T_g.

However, experimental observations consistently show that physical aging occurs at detectable rate deep into the glassy state.[4] This apparent contradiction indicates that while the α-relaxation dominates the dynamics close to T_g, additional mechanisms must contribute to structural recovery at lower temperatures. Identifying the nature of these mechanisms remains one of the central open challenges in the physics of glasses.

In line with this observation, the traditional α-relaxation-based framework for physical aging has been questioned by experiments examining vitrification kinetics[13,14,16,24] and aging behavior[23,25−28] across broad ranges of cooling rates, aging times, and temperatures. It has been shown that the α-relaxation alone is inadequate to describe the kinetics of such

Received: October 16, 2025
Revised: December 29, 2025
Accepted: January 12, 2026
Published: January 26, 2026

https://doi.org/10.1021/acs.jpcb.5c07109
J. Phys. Chem. B 2026, 130, 1716−1723

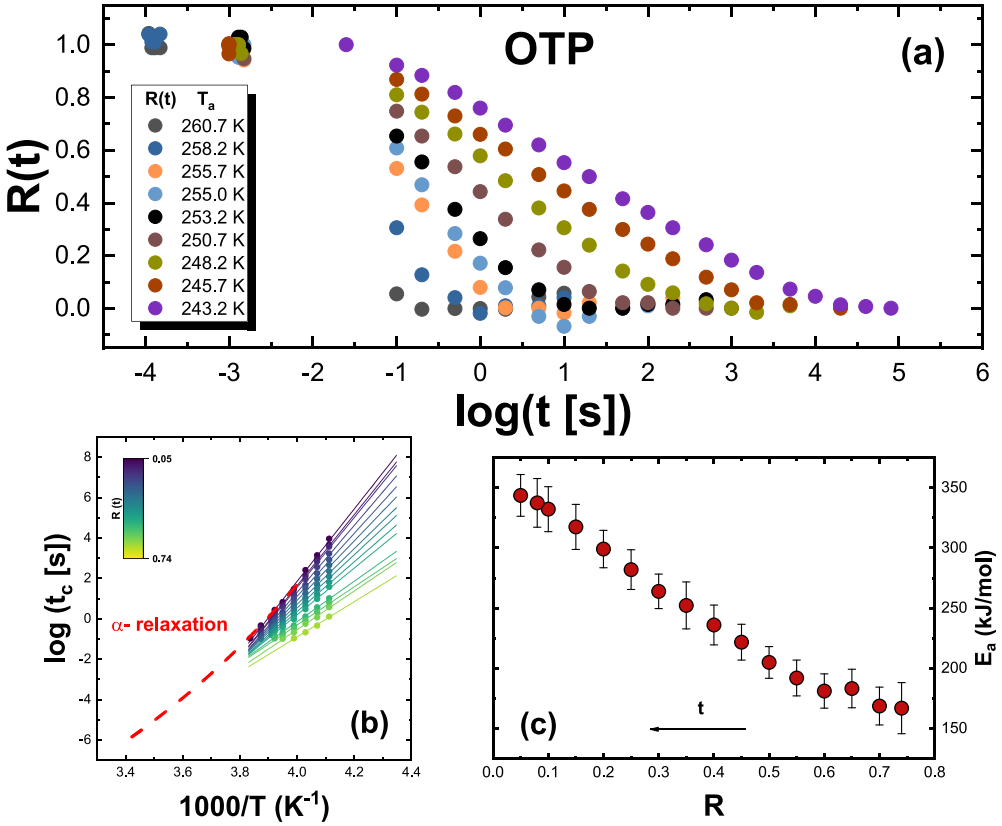

Figure 1. (a) Experimental data of the normalized relaxation function $R(t)$ for all investigated aging temperatures for OTP (T_g = 263 at 1000 K s^{-1}). (b) Logarithm of t_c, the time to reach the degree of relaxation $R(t)$, indicated in the color map as a function of the inverse temperature. The dashed line is the temperature dependence of the α-relaxation time taken from broadband dielectric spectroscopy (BDS) data,[45] and it has been shifted by log t = +2 to match the experimental data. (c) Dependence of the activation energy obtained from the isoconversional method on the extent of aging.

phenomena, especially when it comes to physical aging substantially below T_g and over long aging time scales.[6,25] Specifically, a wealth of experimental effort showed that long-term aging deep in the glassy state for different systems, including polymers,[25,29,30] chalcogenide,[30,31] and metallic glasses,[32,33] exhibits multiple decays toward equilibrium. While the separation of multiple relaxation steps in van der Waals glasses has so far remained elusive, model-dependent analyses of aging data—based on the implementation of density scaling within the so-called single parameter aging (SPA) framework[20,34]—have revealed the inadequacy of the α-relaxation to account for the full recovery of equilibrium deep in the glassy state.[23] These analyses support the conclusion that more than one mechanism contributes to physical aging, although the exact number and nature of such mechanisms remain open questions.

Given these premises, a kinetic approach capable of unraveling the activation energies associated with different stages of glass equilibration is required in order to extract information on the molecular mechanisms that mediate physical aging as a function of the thermodynamic state of the glass as well as of aging time and temperature. A particularly powerful tool in this direction is the so-called isoconversional kinetics,[26,35] which has been extensively employed in the study of a wide range of chemical reactions, including polymerization, cross-linking, thermal and thermo-oxidative degradation, and crystallization/melting processes.[36] The extension of isoconversional methods to the study of glass transition phenomena, and in particular to physical aging,[26,27] was pioneered by Vyazovkin et al.[37−39]

Within this framework, the kinetics of a relaxation or transformation process is analyzed by applying individual Arrhenius equations to different degrees of conversion, thereby evaluating an effective activation energy as a function of the progress of the nonequilibrium process. Instead of assuming a single constant activation barrier, the isoconversional approach maps out how the effective activation energy evolves with conversion, providing a sensitive probe of the underlying molecular mechanisms. In this way, complex temperature dependencies, which may involve a change in dominant relaxation modes or the emergence of additional mechanisms at long times or low temperatures, can be revealed through systematic variations of the effective activation energy with conversion.

An important advantage of isoconversional analysis is that it is not restricted to processes that obey simple Arrhenius kinetics. On the contrary, it is particularly suited to deal with non-Arrhenius processes, such as those typically involved in the glass transition and physical aging, where the apparent activation energy is known to evolve with temperature and

https://doi.org/10.1021/acs.jpcb.5c07109
J. Phys. Chem. B 2026, 130, 1716−1723

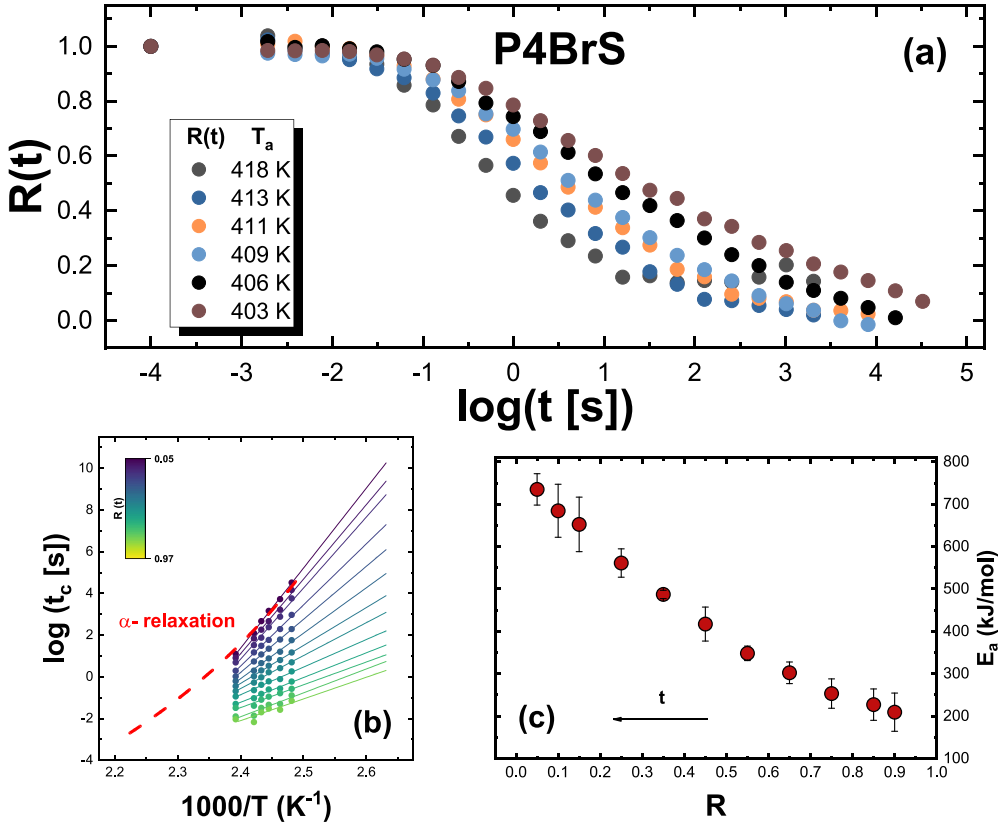

Figure 2. (a) Experimental data of the normalized relaxation function $R(t)$ for all investigated aging temperatures for P4BrS (T_g = 435 at 1000 K s^{-1}). (b) Logarithm of t_c, the time to reach the degree of relaxation $R(t)$, indicated in the color map as a function of the inverse temperature. The dashed line is the temperature dependence of the α-relaxation time taken from BDS data,[46] and it has been shifted by log t = +0.65 to match the experimental data. (c) Dependence of the activation energy obtained from the isoconversional method on the extent of aging.

observation time. Thus, isoconversional kinetics offers a rigorous and versatile framework to disentangle the different molecular mechanisms that contribute to physical aging and to quantify how their relative importance depends on thermal history and depth in the glassy state.

■ ISOCONVERSIONAL KINETIC ANALYSIS

Isoconversional kinetics analysis has been widely applied during the last decades for the study of various thermally stimulated processes in polymers and other molecules.[35] It consists of a system of methods that facilitate the calculation of the kinetic triplet, i.e., the activation energy (E_α), the pre-exponential factor, and transformation model, allowing at the same time making kinetic predictions and obtaining mechanistic insights. This method is particularly useful when the transformation mechanism is unknown or when complex reactions involving several steps take place. The main advantage of this methodology resides in the assessment of the activation energy at any level of conversion during the transformation. The latter can be measured with thermoanalytical techniques, the most common of which are thermogravimetric analysis (TGA), differential scanning calorimetry (DSC), and dielectric relaxation spectroscopy (DRS).[36]

As a general rule, the isoconversional method requires performing a series of experiments, where the transformation under investigation is followed at different temperatures and times. Subsequently, these kinetic data are analyzed to obtain the values of the effective activation energy as a function of conversion, X, which, for aging data, is normally expressed as the extent of relaxation: $R = 1 - X$. The activation energy at a given relaxation, E_R, can be obtained considering the variation with temperature of the time to reach such an extent of relaxation, t_R, in isothermal transformation kinetics data:

$$E_R = k_B \left[\frac{\partial \ln t_R}{\partial T^{-1}}\right]_R \quad (1)$$

where k_B is the Boltzmann constant. Application of eq 1 to different R-values provides the dependence of the activation energy at different stages of the transformation under examination.

In the present work, isoconversional kinetics analysis is applied to a set of physical aging data on different glasses, including small molecules and three glassy polymers, polystyrene (PS), poly(4-chloro styrene) (P4ClS), and poly(4-bromo styrene) (P4BrS). In the case of small molecules and PS and P4ClS, we refer to previously reported physical aging kinetics,[23,40,41] where the enthalpy evolution toward equilibrium was determined by fast scanning calorimetry (FSC)[42] after rapid quenches (1000 K s^{-1}) from the supercooled liquid to various aging temperatures. For P4BrS, we acquired new

https://doi.org/10.1021/acs.jpcb.5c07109
J. Phys. Chem. B 2026, 130, 1716−1723

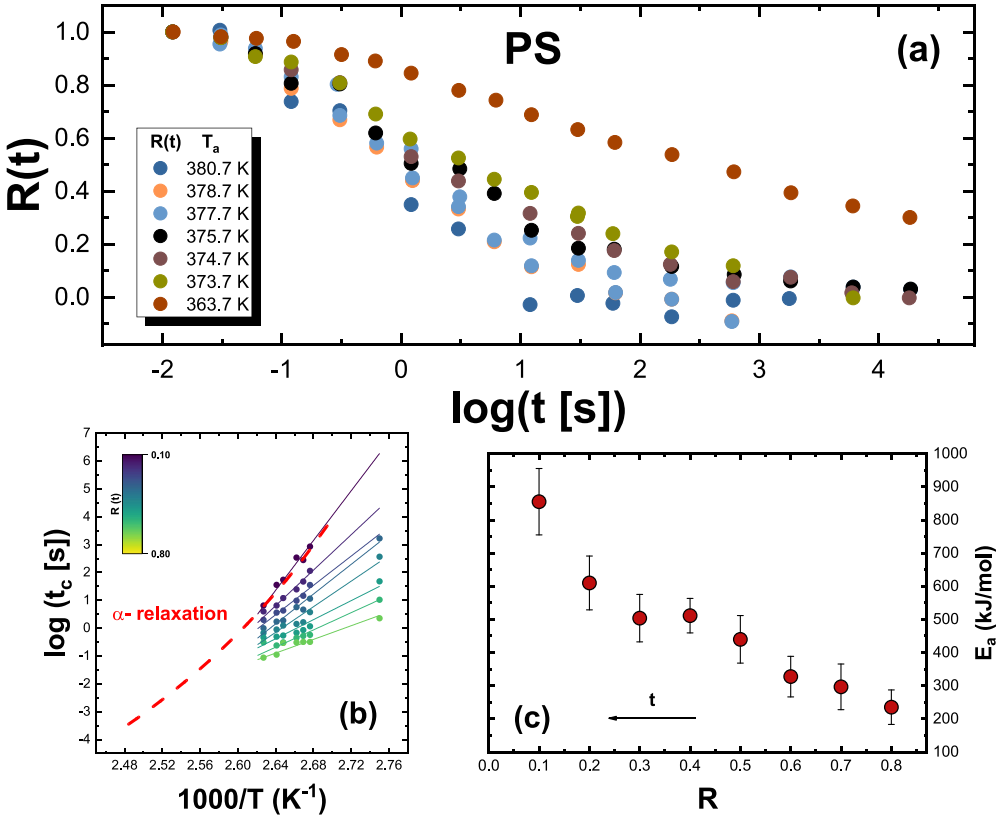

Figure 3. (a) Experimental data of the normalized relaxation function $R(t)$ for all investigated aging temperatures for PS (T_g = 390 at 1000 K s^{-1}). (b) Logarithm of t_c, the time to reach the degree of relaxation $R(t)$, indicated in the color map, as a function of the inverse temperature. The dashed line is the temperature dependence of the α-relaxation time taken from BDS data,[47] and it has been shifted by log t = −0.22 to match the experimental data. (c) Dependence of the activation energy obtained from the isoconversional method on the extent of aging.

data using an analogous protocol (see Supporting Information for details). The extent of enthalpy change is quantified via the concept of fictive temperature, T_f, introduced by Tool,[43] defined as the intersection of the glass line, drawn from the thermodynamic state of a glass with the melt line. Hence, low T_fs correspond to low enthalpy glasses and glasses completely relaxed to equilibrium exhibit $T_f = T_a$, where T_a is the aging temperature. The extent of relaxation can be written as

$$R(t) = \frac{T_f(t) - T_a}{T_f(0) - T_a} \tag{2}$$

where $T_f(t)$ and $T_f(0)$ are the time-dependent fictive temperature and the one at the beginning of the aging process, which in the case of the considered set of aging data is the T_f after cooling at 1000 K s^{-1}.

RESULTS AND DISCUSSION

Figures 1−3, panel (a), show the aging time-dependent evolution of the $R(t)$ function at different aging temperatures for *o*-terphenyl (OTP),[44] P4BrS, and PS.[40] Analogous plots, reported in the Supporting Information, are shown for all other investigated glasses, including o-cresolphthalein dimethyl ether (KDE), phenolphthalein dimethyl ether (PDE), 1,1-bis (4-methoxyphenyl)cyclohexane (BMMPC), 1,1-di(*p*-methoxyphenyl)cyclohexane (BMPC), and P4ClS. As can be observed, the aging time evolution of $R(t)$ exhibits the common patterns typical of glass aging. These are the shifts of $R(t)$ to longer aging times with decreasing temperature and the typical sigmoidal shape. Nevertheless, the aging time evolution of $R(t)$ appears to be more or less stretched, depending on the material. Specifically, PS appears to exhibit a more stretched aging evolution with respect to its bromo-substituted homologue, P4BrS, hinting at the influence of chemical structure on aging behavior. KDE exhibits larger time scale span at two consecutive temperatures than PDE, likely as a result of the larger fragility of the former.

To perform isoconversional analysis, a certain degree of relaxation is needed. Since experimental data are typically taken at specific discrete values of the aging time, our data spectrum needs to be interpolated. This was performed in close proximity to the experimentally collected data. For each data set, we defined a discrete set of relaxation levels spaced at intervals of ≈0.05 and interpolated the time axis to determine the corresponding relaxation time scale, t_R, the time required to reach a given extent of relaxation. Because the interpolation spacing is determined by R, this procedure results in a nearly logarithmic sampling of the time axis. For each temperature, interpolation was carried out within the experimentally accessible range of R values. Consequently, at higher temperatures—where only the later stages of the aging kinetics could be monitored—the data primarily contribute to lower

https://doi.org/10.1021/acs.jpcb.5c07109
J. Phys. Chem. B 2026, 130, 1716−1723

relaxation levels. Other approaches, for example, interpolating R directly on a logarithmically spaced time axis and then determining t_R, yield comparable outcome, confirming the robustness of the numerical implementation here employed in the isoconversional analysis. A graphical description on the way interpolation is performed in reported in Supporting Information (see Figure S2).

For experiments conducted under isothermal conditions, the activation energy, E_R, at a given extent of relaxation R,is given by eq 1. Panels (b) of Figures 1−3 show the outcome of the analysis of relaxation data reported in panels (a) of the same figures for a discrete set of $R(t)$ at different temperatures and times for OTP, P4BrS, and PS. Similar panels are shown in the Supporting Information for the other investigated glasses. Specifically, several isoconversional plots with log t vs $1000/T$ for different extents of $R(t)$ are shown. As can be observed, as $R(t)$ decreases, the slope of the linear fittings increases and, as a consequence, so does the effective activation energy during the aging process. This can be seen in panels (c) of Figures 1−3 for OTP, P4BrS, and PS (and the corresponding ones in the Supporting Information for the other glasses), where the dependence of the activation energy on the extent of relaxation is presented.

A common feature of the dependence of the activation energy on the extent of relaxation, in line with previous reports,[26,27] is that it varies from a lower bound in the order of ∼100 kJ mol^{-1} to values as large as several hundreds kJ mol^{-1} at the end of the aging process. The latter can be compared to that of the main α- relaxation, whose temperature dependence of the typical relaxation time, conveniently shifted to match aging times, is presented in panels (b) of Figures 1−3 (and the corresponding panels in the Supporting Information for the other glasses). As can be observed, in all cases, the activation energy at the end of the aging process matches with that of the α-relaxation, indicating that the latter is the leading mechanism mediating the final stages of approach to equilibrium. Here, it is worth remarking that the shift of the α relaxation times is described within the Frenkel−Kobeko−Reiner (FKR) framework: $\beta_c = C\tau_\alpha^{-1}$, where $C = \Delta\log t$ is the logarithmic shift, meaning the number of time decades, which needs to be added to $\log(\tau_\alpha)$ to match the logarithm of the cooling rate, $\log(\beta_c)$, which sets the vitrification temperature.[7] In essence, the parameter C underlines the efficiency of the α relaxation in keeping the supercooled liquid at equilibrium on cooling.

The relatively low activation energy at small and intermediate extents of relaxation could also be attributed to the role of the α-relaxation in nonequilibrium conditions. A wealth of experiments carried out in the nonequilibrium glass actually show that the measured relaxation time exhibits moderate activation energy,[48−55] in line with the outcome of our analysis. However, this interpretation would entail a discontinuity of the temperature dependence of the α-relaxation time as the system transforms from the supercooled liquid to the nonequilibrium glass. This scenario is at odds with the description of aging kinetics as a single activated event.[56] Specifically, within the thermally activated description of the dynamics of glass forming systems, the freezing of configurational degrees of freedom leading to vitrification results in a temperature independent activation energy equal to that of the equilibrium systems just before vitrification. Seen from the viewpoint of the Adam−Gibbs theory,[57] the aforementioned freezing implies that the configurational entropy remains constant below T_g and equal to that of the supercooled liquid before vitrification takes over.

Given these premises, the discontinuity in the glass activation energy with respect to that of the equilibrium supercooled liquid warrants an interpretation based on the role of other molecular mechanisms mediating physical aging at weak and moderate extents of relaxation. The most immediate candidate would be the β-relaxation detected by standard spectroscopic techniques.[58] This was actually the interpretation in studies where isoconversional analysis conveyed a relaxation-dependent evolution of the activation energy analogous to that of our work.[26,27] Furthermore, this is in line with recent analysis on a metallic glasses where the kinetics of devitrification a previously aged glass was shown to be sequentually mediated by γ, β, and ultimately α relaxation.[28] However, among the investigated glass formers, KDE and BMMPC do not exhibit any trace of a β-relaxation by dielectric relaxation spectroscopy.[59,60] Nevertheless, their behavior in terms of relaxation-dependent activation energy, as detected by isoconversional analysis, is completely analogous to that of their homologous glass formers, PDE and BMPC, where a secondary relaxation is clearly visible in dielectric relaxation spectroscopy experiments.[59,60]

The absence of β-relaxation in KDE and BMMPC may reflect limitations of the technique rather than a genuine lack of secondary dynamics. Thus, β-processes cannot be entirely ruled out. We also stress that recent work[61] proposes that the β relaxation is best regarded as a generic process associated with local equilibration in the heterogeneous glassy structure, and activation energies extracted from calorimetric aging experiments often reflect mixed α−β dynamics rather than a single, species-specific mechanism. At the same time, the systematic observation of low-E_a values across different glass formers suggests the involvement of a more universal mechanism. A strong candidate is the slow Arrhenius process (SAP),[62] a relaxation mode consistently identified in both polymers[63,64] and small molecule glasses,[65,66] and commonly ascribed to collective small displacements (CSD) involving localized, constrained rearrangements of molecular groups.[67] Unlike the β-relaxation, which is often material-specific and sensitive to detection methods, SAP is characterized by a nearly temperature-invariant activation barrier, with values ranging from roughly 30−200 kJ mol^{-1} depending on the system. Importantly, the SAP has also been associated with other equilibration mechanisms in molecular glasses,[68−70] further strengthening its relevance as a generic contributor to structural recovery both above and below T_g.

Within this framework, the low thermal barriers detected as $R \rightarrow 1$ could be attributed to SAP-mediated rearrangements, which remain active even deep below T_g, where the α-process is essentially frozen. Previous studies have already correlated the first regime of physical aging kinetics with the SAP,[68] associating the early stages of equilibration with these localized displacements, before the system gradually crosses over to the higher barriers characteristic of α-controlled recovery. Our isoconversional results reinforce this view: the activation energy initially reflects the SAP scale and then progressively increases, converging to α-relaxation at larger extents of relaxation. This supports a two-step equilibration scenario in which the SAP governs the onset of aging and the α-process dominates the final approach to equilibrium.

We remark that, in some cases, the present analysis depicts an even more complex scenario than that where a monotonic

https://doi.org/10.1021/acs.jpcb.5c07109
J. Phys. Chem. B 2026, 130, 1716−1723

increase in the activation energy is observed. In particular, data obtained for PS[40] and P4ClS,[41] including isothermal aging experiments spanning a large temperature range down to temperatures significantly below T_g, reveal that $E(R)$ is no longer described by a smooth, monotonous function. Instead, distinct features emerge in the evolution of $E(R)$, suggesting the occurrence of multiple consecutive steps in the aging process. Such complexity appears to be a general feature of glass-forming systems, as similar multistep aging dynamics have been reported in small organic molecules,[71] polymers,[25,29,30,72,73] metallic,[32,33] and chalcogenide[31,74] glasses.

In providing the value of the activation energy at given degrees of relaxation, isoconversional analysis can provide insights on the respective roles of β-relaxations, and the slow Arrhenius process (SAP), thereby improving our ability to distinguish between these mechanisms and to quantify their contributions to the early stages of physical aging. However, while isoconversional methods are very powerful because of their model-free character, their applicability is intrinsically limited to regions of the kinetics, where the extent of relaxation evolves measurably with time. As a consequence, they do not allow one to reliably access the limiting activation barriers in the asymptotic regimes $R \to 0$ and $R \to 1$, nor in the presence of intermediate plateaus associated with nearly invariant relaxation rates,[25] owing to their mathematical definition. In such flat regions of the kinetics, the characteristic time associated with a given relaxation becomes poorly defined, and even small experimental noise in the relaxation can translate into large uncertainties in the extracted times and, consequently, in the apparent activation energies. Access to these limiting barriers therefore requires dedicated experiments spanning sufficiently broad time scales to explicitly include regimes where the kinetics becomes effectively time independent, as occurs at very short and very long times. A promising strategy to disentangle their roles lies in combining isoconversional and inflectional analyses. In such cases, the latter strategy, based on determining via model-free approaches the time scales associated with changes in the logarithmic slopes of $R(t)$, as originally proposed by Kovacs,[75] provides a viable route. Extending this approach to systems in which the activation barriers of the SAP and the β process are known and sufficiently distinct would enable quantitative separation of their respective contributions. In parallel, systematic aging studies performed far below T_g will be essential to capture the complex, nonmonotonic evolution of $E(R)$ and to unravel the interplay of relaxation mechanisms governing long-term equilibration in glassy materials, where different processes are expected to become increasingly separated, potentially allowing distinct γ, β/SAP and α activation barriers to emerge also in organic glasses.

CONCLUSIONS

In summary, by applying isoconversional analysis to a broad set of physical aging data on polymers and small molecule glasses, we have mapped the evolution of the effective activation barrier as a function of the extent of relaxation. Our results reveal a systematic increase of the activation energy from relatively small extent of relaxation to values comparable with the α-relaxation at large extents of relaxation. The low barriers detected at the onset of relaxation indicate that, in addition to the α-process, *additional molecular mechanisms must contribute to equilibration*. These early stages could involve secondary relaxations, such as the β-process, but the systematic character of the low activation energies across different systems points to the relevance of the slow Arrhenius process (SAP), associated with localized collective displacements and nearly temperature-invariant barriers. Taken together, our findings support a multiple-step scenario of glass equilibration in which low-barrier processes mediate the initial stages of aging, while the α-relaxation dominates the final approach to equilibrium. Disentangling the relative contributions of β-relaxations and the SAP is warranted in order to build a comprehensive picture of the microscopic dynamics underlying early stage glass aging.

ASSOCIATED CONTENT

Supporting Information

The Supporting Information is available free of charge at https://pubs.acs.org/doi/10.1021/acs.jpcb.5c07109.

Experimental procedures and results for the other glass formers not shown in the main manuscript (PDF)

AUTHOR INFORMATION

Corresponding Authors

Federico Caporaletti − *Laboratory of Polymer and Soft Matter Dynamics, Experimental Soft Matter and Thermal Physics (EST), Université Libre de Bruxelles (ULB), Brussels 1050, Belgium;* orcid.org/0000-0002-1634-0734; Email: federico.caporaletti@ulb.be

Daniele Cangialosi − *Centro de Física de Materiales (CSIC−UPV/EHU), 20018 San Sebastián, Spain; Donostia International Physics Center, 20018 San Sebastián, Spain;* orcid.org/0000-0002-5782-7725; Email: daniele.cangialosi@ehu.eus

Authors

Vasiliki Maria Stavropoulou − *Centro de Física de Materiales (CSIC−UPV/EHU), 20018 San Sebastián, Spain; PMAS, Faculty of Chemistry, University of the Basque Country (UPV/EHU), 20018 Donostia-San Sebastián, Spain;* orcid.org/0009-0009-8223-1438

Florian Pabst − *Laboratory of Polymer and Soft Matter Dynamics, Experimental Soft Matter and Thermal Physics (EST), Université Libre de Bruxelles (ULB), Brussels 1050, Belgium;* Present Address: SISSA-Scuola Internazionale Superiore di Studi Avanzati, 34136 Trieste, Italy; orcid.org/0000-0001-9331-5172

Valerio Di Lisio − *Centro de Física de Materiales (CSIC−UPV/EHU), 20018 San Sebastián, Spain; Donostia International Physics Center, 20018 San Sebastián, Spain;* orcid.org/0000-0001-7729-8069

Simone Napolitano − *Laboratory of Polymer and Soft Matter Dynamics, Experimental Soft Matter and Thermal Physics (EST), Université Libre de Bruxelles (ULB), Brussels 1050, Belgium*

Complete contact information is available at: https://pubs.acs.org/10.1021/acs.jpcb.5c07109

Notes

The authors declare no competing financial interest.

ACKNOWLEDGMENTS

F.C. is a Chargé de Recherches of the Fonds de la recherche scientifique-FNRS. SN acknowledges financial support from Action de Recherche Concertée ULB under grant ARC

"COHESAP". D.C. acknowledges financial support from Eusko Jaurlaritza (Basque Government) through the grant IT-1566-22.

REFERENCES

(1) Schmelzer, J. W. P.; Gutzow, I. S. *Glasses and the Glass Transition*; John Wiley & Sons, Ltd: 2011; *Chapter 1*, pp 1−8.
(2) Napolitano, S.; Glynos, E.; Tito, N. B. Glass transition of polymers in bulk, confined geometries, and near interfaces. *Rep. Prog. Phys.* **2017**, *80*, No. 036602.
(3) Kovacs, A. J. Glass transition in amorphous polymers: a phenomenological study. *Fortsch. Hochpolym.-Forsch.* **1963**, *3*, 394−508.
(4) Struik, L. C. E. *Physical aging in amorphous polymers and other materials*; Technische Hogeschool Delft: 1977.
(5) Cangialosi, D.; Boucher, V. M.; Alegria, A.; Colmenero, J. Physical aging in polymers and polymer nanocomposites: recent results and open questions. *Soft Matt.* **2013**, *9*, 8619−8630.
(6) Cangialosi, D. Physical aging and vitrification in polymers and other glasses: Complex behavior and size effects. *J. Polym. Sci.* **2024**, *62*, 1952−1974.
(7) Schawe, J. E. K. Vitrification in a wide cooling rate range: The relations between cooling rate, relaxation time, transition width, and fragility. *J. Chem. Phys.* **2014**, *141*, 184905.
(8) Dhotel, A.; Rijal, B.; Delbreilh, L.; Dargent, E.; Saiter, A. Combining Flash DSC, DSC and broadband dielectric spectroscopy to determine fragility. *J. Therm. Anal. Calorim.* **2015**, *121*, 453−461.
(9) Lapuk, S.; Ponomareva, M.; Ziganshin, M.; Larionov, R.; Mukhametzyanov, T.; Schick, C.; Lounev, I.; Gerasimov, A. Some aspects of the glass transition of polyvinylpyrrolidone depending on the molecular mass. *Phys. Chem. Chem. Phys.* **2023**, *25*, 10706−10714.
(10) Wang, L.-M.; Velikov, V.; Angell, C. A. Direct determination of kinetic fragility indices of glassforming liquids by differential scanning calorimetry: Kinetic versus thermodynamic fragilities. *J. Chem. Phys.* **2002**, *117*, 10184−10192.
(11) Saini, M. K.; Jin, X.; Wu, T.; Liu, Y.; Wang, L.-M. Interplay of intermolecular interactions and flexibility to mediate glass forming ability and fragility: A study of chemical analogs. *J. Chem. Phys.* **2018**, *148*, 124504.
(12) Jin, X.; Li, Z.; Liu, Y.; Feng, S.; Wang, L.-M. Identifying the structural relaxation dynamics in a strongly asymmetric binary glass former. *J. Chem. Phys.* **2021**, *154*, 144504.
(13) Monnier, X.; Cangialosi, D.; Ruta, B.; Busch, R.; Gallino, I. Vitrification decoupling from α-relaxation in a metallic glass. *Sci. Adv.* **2020**, *6*, No. eaay1454.
(14) Robertson, C. G.; Santangelo, P.; Roland, C. Comparison of glass formation kinetics and segmental relaxation in polymers. *J. Non-Cryst. Sol.* **2000**, *275*, 153−159.
(15) Perez-de Eulate, N. G.; Di Lisio, V.; Cangialosi, D. Glass Transition and Molecular Dynamics in Polystyrene Nanospheres by Fast Scanning Calorimetry. *ACS Macro Lett.* **2017**, *6*, 859−863.
(16) Priestley, R. D.; Cangialosi, D.; Napolitano, S. On the equivalence between the thermodynamic and dynamic measurements of the glass transition in confined polymers. *J. Non-Cryst. Sol.* **2015**, *407*, 288−295.
(17) Boucher, V. M.; Cangialosi, D.; Alegría, A.; Colmenero, J. Enthalpy recovery in nanometer to micrometer thick PS films. *Macromolecules* **2012**, *45*, 5296−5306.
(18) Fukao, K.; Miyamoto, Y. Glass transitions and dynamics in thin polymer films: Dielectric relaxation of thin films of polystyrene. *Phys. Rev. E* **2000**, *61*, 1743.
(19) Lupascu, V.; Picken, S. J.; Wubbenhorst, M. Cooperative and non-cooperative dynamics in ultra-thin films of polystyrene studied by dielectric spectroscopy and capacitive dilatometry. *J. Non-Cryst. Sol.* **2006**, *352*, 5594−5600.
(20) Riechers, B.; Roed, L. A.; Mehri, S.; Ingebrigtsen, T. S.; Hecksher, T.; Dyre, J. C.; Niss, K. Predicting nonlinear physical aging of glasses from equilibrium relaxation via the material time. *Sci. Adv.* **2022**, *8*, No. eabl9809.
(21) Niss, K. A density scaling conjecture for aging glasses. *J. Chem. Phys.* **2022**, *157*, No. 054503.
(22) Mansuri, A.; Münzner, P.; Feuerbach, T.; Vermeer, A.; Hoheisel, W.; Böhmer, R.; Thommes, M.; Gainaru, C. The relaxation behavior of supercooled and glassy imidacloprid. *J. Chem. Phys.* **2021**, *155*, 174502.
(23) Di Lisio, V.; Stavropoulou, V.-M.; Cangialosi, D. Physical aging in molecular glasses beyond the α relaxation. *J. Chem. Phys.* **2023**, *159*, No. 064505.
(24) Kisliuk, A.; Ding, Y.; Hwang, J.; Lee, J.; Annis, B.; Foster, M.; Sokolov, A. Influence of molecular architecture on fast and segmental dynamics and the glass transition in polybutadiene. *J. Polym. Sci. B: Polym. Phys.* **2002**, *40*, 2431−2439.
(25) Cangialosi, D.; Boucher, V. M.; Alegría, A.; Colmenero, J. Direct Evidence of Two Equilibration Mechanisms in Glassy Polymers. *Phys. Rev. Lett.* **2013**, *111*, No. 095701.
(26) Chen, K.; Vyazovkin, S. Isoconversional Kinetics of Glass Aging. *J. Phys. Chem. B* **2009**, *113*, 4631−4635.
(27) Vyazovkin, S.; Chen, K. Increase in effective activation energy during physical aging of a glass. *Chem. Phys. Lett.* **2007**, *448*, 203−207.
(28) Song, L.; Gao, Y.; Zou, P.; Xu, W.; Gao, M.; Zhang, Y.; Huo, J.; Li, F.; Qiao, J.; Wang, L.-M.; et al. Detecting the exponential relaxation spectrum in glasses by high-precision nanocalorimetry. *Proc. Natl. Acad. Sci. U. S. A.* **2023**, *120*, No. e2302776120.
(29) Monnier, X.; Marina, S.; Lopez de Pariza, X.; Sardón, H.; Martin, J.; Cangialosi, D. Physical aging behavior of a glassy polyether. *Polymers* **2021**, *13*, 954.
(30) Morvan, A.; Delpouve, N.; Vella, A.; Saiter-Fourcin, A. Physical aging of selenium glass: Assessing the double mechanism of equilibration and the crystallization process. *J. Non-Cryst. Sol.* **2021**, *570*, No. 121013.
(31) Golovchak, R.; Kozdras, A.; Balitska, V.; Shpotyuk, O. Stepwise kinetics of natural physical ageing in arsenic selenide glasses. *J. Phys: Cond. Matt.* **2012**, *24*, 505106.
(32) Gallino, I.; Cangialosi, D.; Evenson, Z.; Schmitt, L.; Hechler, S.; Stolpe, M.; Ruta, B. Hierarchical aging pathways and reversible fragile-to-strong transition upon annealing of a metallic glass former. *Acta Mater.* **2018**, *144*, 400−410.
(33) Song, L.; Xu, W.; Huo, J.; Wang, J.-Q.; Wang, X.; Li, R. Two-step relaxations in metallic glasses during isothermal annealing. *Intermetallics* **2018**, *93*, 101−105.
(34) Hecksher, T.; Olsen, N. B.; Dyre, J. C. Communication: Direct tests of single-parameter aging. *J. Chem. Phys.* **2015**, *142*, 241103.
(35) Vyazovkin, S. *Isoconversional kinetics of thermally stimulated processes*; Springer: 2015.
(36) Sbirrazzuoli, N. Interpretation and Physical Meaning of Kinetic Parameters Obtained from Isoconversional Kinetic Analysis of Polymers. *Polymers* **2020**, *12*, 1280.
(37) Vyazovkin, S.; Sbirrazzuoli, N.; Dranca, I. Variation of the Effective Activation Energy Throughout the Glass Transition. *Mac. Rap. Comm.* **2004**, *25*, 1708−1713.
(38) Vyazovkin, S.; Dranca, I. A DSC Study of α-and β-Relaxations in a PS- Clay System. *J. Phys. Chem. B* **2004**, *108*, 11981−11987.
(39) Vyazovkin, S.; Sbirrazzuoli, N.; Dranca, I. Variation in Activation Energy of the Glass Transition for Polymers of Different Dynamic Fragility. *Mac. Chem. Phys.* **2006**, *207*, 1126−1130.
(40) Grassia, L.; Koh, Y. P.; Rosa, M.; Simon, S. L. Complete set of enthalpy recovery data using Flash DSC: experiment and modeling. *Macromolecules* **2018**, *51*, 1549−1558.
(41) Di Lisio, V.; Rocchi, L. A.; Cangialosi, D. Twofold facet of kinetics of glass aging. *Phys. Rev. Lett.* **2024**, *133*, No. 048201.
(42) Schick, C.; Mathot, V. *Fast scanning calorimetry*; Springer: 2016.
(43) Tool, A. Relation between inelastic deformability and thermal expansion of glass in its annealing range. *J. Am. Ceram. Soc.* **1946**, *29*, 240−253.

https://doi.org/10.1021/acs.jpcb.5c07109
J. Phys. Chem. B 2026, 130, 1716−1723

(44) Di Lisio, V.; Gallino, I.; Riegler, S.; Frey, M.; Neuber, N.; Kumar, G.; Schroers, J.; Busch, R.; Cangialosi, D. Size dependent vitrification in metallic glasses. *Nat. Commun.* **2023**, *14*, 4698.
(45) Richert, R. On the dielectric susceptibility spectra of supercooled o-terphenyl. *J. Chem. Phys.* **2005**, *123*, 154502.
(46) Thoms, E.; Li, C.; Napolitano, S. Tracing the slow Arrhenius process deep in the glassy state−quantitative evaluation of the dielectric relaxation of bulk samples and thin polymer films in the temperature domain. *J. Chem. Phys.* **2024**, *160*, No. 034901.
(47) Richert, R. Scaling vs. Vogel-Fulcher-type structural relaxation in deeply supercooled materials. *Physica A* **2000**, *287*, 26−36.
(48) Dhinojwala, A.; Wong, G. K.; Torkelson, J. M. Rotational reorientation dynamics of nonlinear optical chromophores in rubbery and glassy polymers:. alpha.-relaxation dynamics probed by second harmonic generation and dielectric relaxation. *Macromolecules* **1993**, *26*, 5943−5953.
(49) Dhinojwala, A.; Wong, G. K.; Torkelson, J. M. Rotational reorientation dynamics of disperse red 1 in polystyrene: α-relaxation dynamics probed by second harmonic generation and dielectric relaxation. *J. Chem. Phys.* **1994**, *100*, 6046−6054.
(50) Alegria, A.; Guerrica-Echevarria, E.; Goitiandia, L.; Telleria, I.; Colmenero, J. alpha.-Relaxation in the Glass Transition Range of Amorphous Polymers. 1. Temperature Behavior across the Glass transition. *Macromolecules* **1995**, *28*, 1516−1527.
(51) Goitiandia, L.; Alegria, A. Physical aging of poly (vinyl acetate). A thermally stimulated depolarization current investigation. *J. Non-Cryst. Sol.* **2001**, *287*, 237−241.
(52) Cangialosi, D.; Schut, H.; Van Veen, A.; Picken, S.; et al. Dynamics of polycarbonate far below the glass transition temperature: A positron annihilation lifetime study. *Phys. Rev. B* **2004**, *69*, No. 134206.
(53) Casalini, R.; Roland, C. Aging of a low molecular weight poly (methyl methacrylate). *J. Non-Crys. Sol.* **2011**, *357*, 282−285.
(54) Wojnarowska, Z.; Roland, C.; Kolodziejczyk, K.; Swiety-Pospiech, A.; Grzybowska, K.; Paluch, M. Quantifying the structural dynamics of pharmaceuticals in the glassy state. *J. Phys. Chem. Lett.* **2012**, *3*, 1238−1241.
(55) Ruta, B.; Chushkin, Y.; Monaco, G.; Cipelletti, L.; Pineda, E.; Bruna, P.; Giordano, V. M.; Gonzalez-Silveira, M. Atomic-Scale Relaxation Dynamics and Aging in a Metallic Glass Probed by X-Ray Photon Correlation Spectroscopy. *Phys. Rev. Lett.* **2012**, *109*, No. 165701.
(56) Avramov, I. Non-equilibrium viscosity and activation energy. *J. Non-Cryst. Sol.* **2009**, *355*, 1769−1771.
(57) Adam, G.; Gibbs, J. H. On the Temperature Dependence of Cooperative Relaxation Properties in Glass-Forming Liquids. *J. Chem. Phys.* **1965**, *43*, 139−146.
(58) McCrum, N.; Read, B.; Williams, G. *Anelastic and d ̈i electric effects in polymeric solids*; John Wiley: 1967.
(59) Meier, G.; Gerharz, B.; Boese, D.; Fischer, E. Dynamical processes in organic glassforming van der Waals liquids. *J. Chem. Phys.* **1991**, *94*, 3050−3059.
(60) Kahle, S.; Gapinski, J.; Hinze, G.; Patkowski, A.; Meier, G. A comparison of relaxation processes in structurally related van der Waals glass formers: The role of internal degrees of freedom. *J. Chem. Phys.* **2005**, *122*, No. 074506.
(61) Vyazovkin, S. DSC to explore activation energy landscape of glass relaxation. *Thermochim. Acta* **2025**, *748*, No. 179985.
(62) Song, Z.; Rodríguez-Tinoco, C.; Mathew, A.; Napolitano, S. Fast equilibration mechanisms in disordered materials mediated by slow liquid dynamics. *Sci. Adv.* **2022**, *8*, No. eabm7154.
(63) Thoms, E.; Song, Z.; Wang, K.; Napolitano, S. Simple Model to Predict the Adsorption Rate of Polymer Melts. *Phys. Rev. Lett.* **2024**, *132*, No. 248101.
(64) Thoms, E.; Napolitano, S. Enthalpy-entropy compensation in the Slow Arrhenius Process. *J. Chem. Phys.* **2023**, *159*, 161103.
(65) Caporaletti, F.; Napolitano, S. The slow Arrhenius process in small organic molecules. *Phys. Chem. Chem. Phys.* **2024**, *26*, 745−748.
(66) Caporaletti, F.; Bock, H.; Napolitano, S. Slow liquid dynamics promotes orientational ordering in a columnar liquid crystalline glass-former. *J. Mol. Liq.* **2025**, *433*, No. 127902.
(67) White, R. P.; Napolitano, S.; Lipson, J. E. G. Mechanistic picture for the slow Arrhenius process (SAP) in glass forming systems: The collective small displacements model. *Phys. Rev. Lett.* **2025**, *134*, No. 098203.
(68) Song, Z.; Rodríguez-Tinoco, C.; Mathew, A.; Napolitano, S. Fast equilibration mechanisms in disordered materials mediated by slow liquid dynamics. *Sci. Adv.* **2022**, *8*, No. eabm7154.
(69) Thoms, E.; Wang, K.; Chandran, S.; Napolitano, S. Fast Processing Affects the Relaxation of Polymers: The Slow Arrhenius Process Can Probe Stress at the Molecular Level. *J. Phys. Chem. Lett.* **2024**, *15*, 4838−4843.
(70) Caporaletti, F.; Villanueva, M. E.; Molitor, S.; Zuo, B.; Napolitano, S. Predicting how fast crystals grow at the free surface of molecular glasses. *Mater. Horiz.* **2026**, *13*, 491.
(71) Miller, R. S.; MacPhail, R. A. Ultraslow nonequilibrium dynamics in supercooled glycerol by stimulated Brillouin gain spectroscopy. *J. Chem. Phys.* **1997**, *106*, 3393−3401.
(72) Buquet, C. L.; Hamonic, F.; Saiter, A.; Dargent, E.; Langevin, D.; Nguyen, Q. Physical ageing and molecular mobilities of sulfonated polysulfone for proton exchange membranes. *Thermochim. Acta* **2010**, *509*, 18−23.
(73) Mejres, M.; Hallavant, K.; Guidotti, G.; Soccio, M.; Lotti, N.; Esposito, A.; Saiter-Fourcin, A. Physical aging of a biodegradable alicyclic polymer: poly (pentamethylene trans-1, 4-cyclohexanedicarboxylate). *J. Non-Cryst. Sol.* **2024**, *629*, No. 122874.
(74) Golovchak, R.; Kozdras, A.; Shpotyuk, O.; Balitska, V. Crossover between cooperative and fractal relaxation in complex glass-formers. *J. Phys.: Cond. Matt.* **2016**, *28*, 355101.
(75) Braun, G.; Kovacs, A. Glass transition in powdered polystyrene. *Phys. Chem. Glasses* **1963**, *4*, 1152−1160.

https://doi.org/10.1021/acs.jpcb.5c07109
J. Phys. Chem. B 2026, 130, 1716−1723

Identifying the Thermal Barriers of Glass Aging via Isoconversional Analysis

Vasiliki Maria Stavropoulou,[†,‡] , Federico Caporaletti,[§] Florian Pabst,[§||] Valerio Di Lisio,[†,¶] Simone Napolitano, [§] and Daniele Cangialosi[*,#]

[†]Centro de Física de Materiales (CSIC–UPV/EHU), Paseo Manuel de Lardizábal 5, 20018 San Sebastián, Spain

[‡]PMAS, Faculty of Chemistry, University of the Basque Country (UPV/EHU), Paseo Manuel Lardizábal 3, 20018 Donostia-San Sebastián, Spain

[§]Laboratory of Polymer and Soft Matter Dynamics, Experimental Soft Matter and Thermal Physics (EST), Université libre de Bruxelles (ULB), Brussels, 1050, Belgium

[¶]Donostia International Physics Center, Paseo Manuel de Lardizábal 4, 20018 San Sebastián, Spain

[||]Current address: SISSA-Scuola Internazionale Superiore di Studi Avanzati, 34136 Trieste, Italy

Materials

Poly(4-bromostyrene) (P4BrS) with molecular weight of M_w=6.5 $\times 10^4$ g/mol was purchased from Sigma Aldrich and used as received.

Fast scanning calorimetry measurements

Fast Scanning Calorimetry (FSC) measurements were performed with a Mettler-Toledo Flash Differential Scanning Calorimeter (DSC 2+) equipped with an intracooling stage. The sample chamber was maintained under a dry nitrogen atmosphere (20 ml/min). The investigated materials were directly deposited onto Mettler-Toledo UFS 1 chips.

The thermal protocol for aging experiments is illustrated in Fig. S1. Samples were first heated to ~T_g + 100K, then quenched at a cooling rate of q = 1000 Ks^{-1} to the aging temperature T_a, where they were held isothermally for a variable time t_a. After each isothermal hold, samples were quenched to 183 K at 1000 Ks^{-1}, followed by the heating scan for data collection with a heating rate of 1000 Ks^{-1}.

Physical aging was identified by the development of an endothermic overshoot upon heating, superimposed on the specific-heat step at the glass transition (see Fig. S1). The

overshoot grows with increasing t_a and shifts to higher temperatures as the glass approaches more stable thermodynamic states. The degree of equilibration was quantified via the fictive temperature $T_f(t_a, T_a)$, evaluated using Moynihan's area matching method,[1] following standard practice in the field.

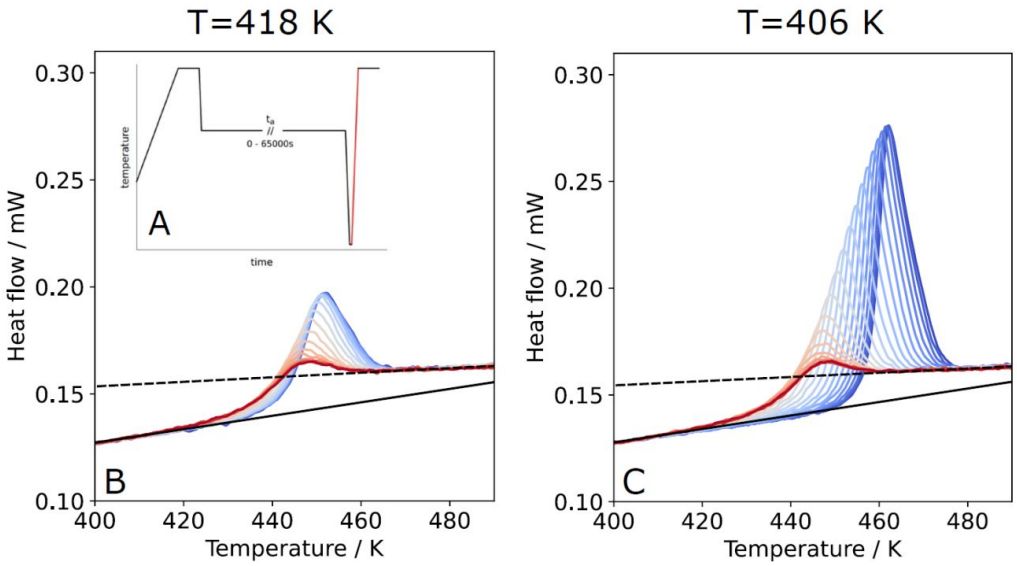

Figure S1: *FSC scans of P4BrS after aging between 0.01 and 32768 s with a sampling power with base 2 at the indicated temperatures. The inset shows the thermal protocol for FSC experiments.*

Interpolating the relaxation function

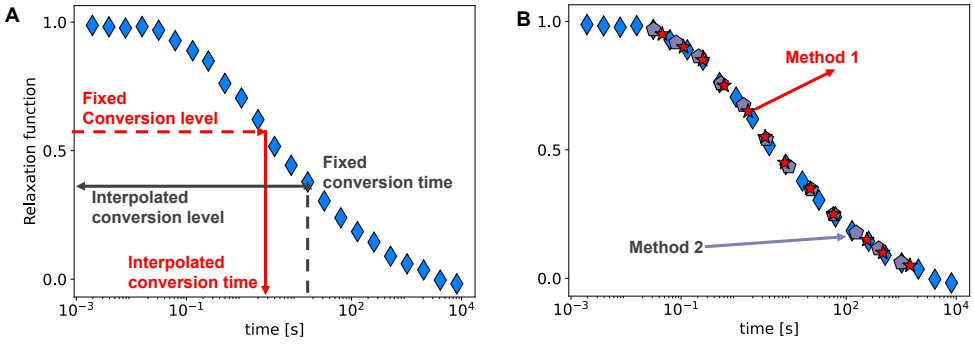

Figure S2. *Example of the interpolation protocols used to process the relaxation functions analyzed in this work. Blue diamonds in panels A and B represent experimental data from a P4BrS sample quenched at 1000 K/s from the liquid state to an aging temperature of 409 K.*

Panel A: Two interpolation procedures are illustrated. Method 1 (red): fixed conversion levels are selected along the relaxation function, and the corresponding times are obtained by interpolating the time axis. Method 2 (gray): the relaxation function is interpolated on a logarithmically spaced time grid.

Panel B: Comparison of the two methods, which provides nearly identical interpolated functions. In this work, Method 1 was adopted, as it facilitates the selection of conversion levels close to the experimental data, thereby minimizing potential bias. Nevertheless, the similarity between the two interpolations confirms the robustness of the isoconversional analysis, independently of the interpolation protocol.

Supplementary figures on isoconversional analysis

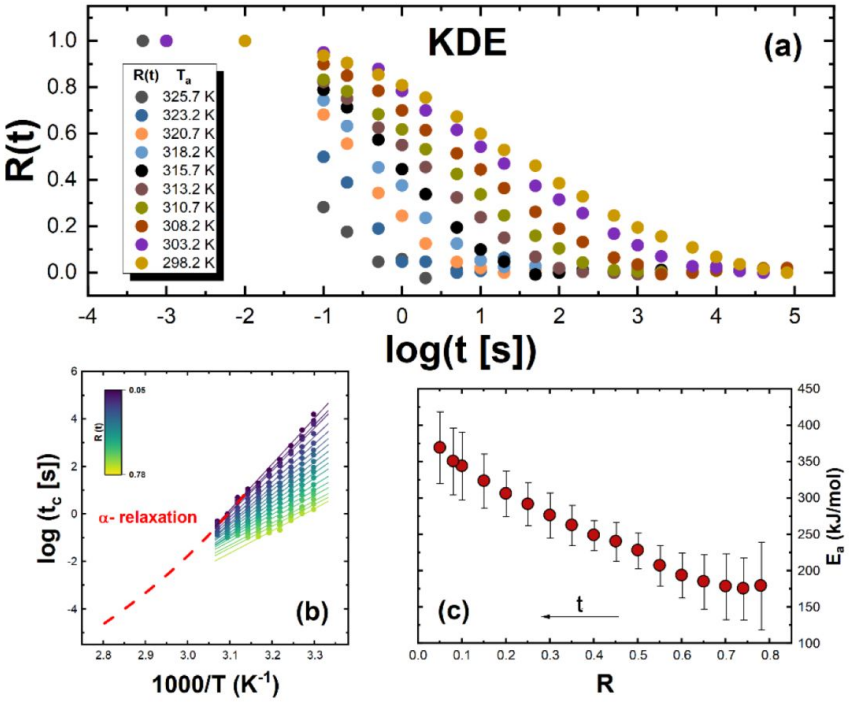

Figure S3: *(a) Experimental data for o-cresolphthalein dimethyl ether (KDE) (T_g = 330.5 K at 1000 Ks^{-1}) of the normalized relaxation function R(t) vs aging time for all investigated aging temperatures. (b) Time to reach the indicated degree of relaxation as a function R(t) of the inverse temperature. The dashed line is the temperature dependence of the α relaxation time taken from ref.* ***[1]*** *for BDS and it has been shifted by $\log t = +0.35$ to match the experimental data. (c) Dependence of the activation energy obtained from the isoconversional method on the extent of aging.*

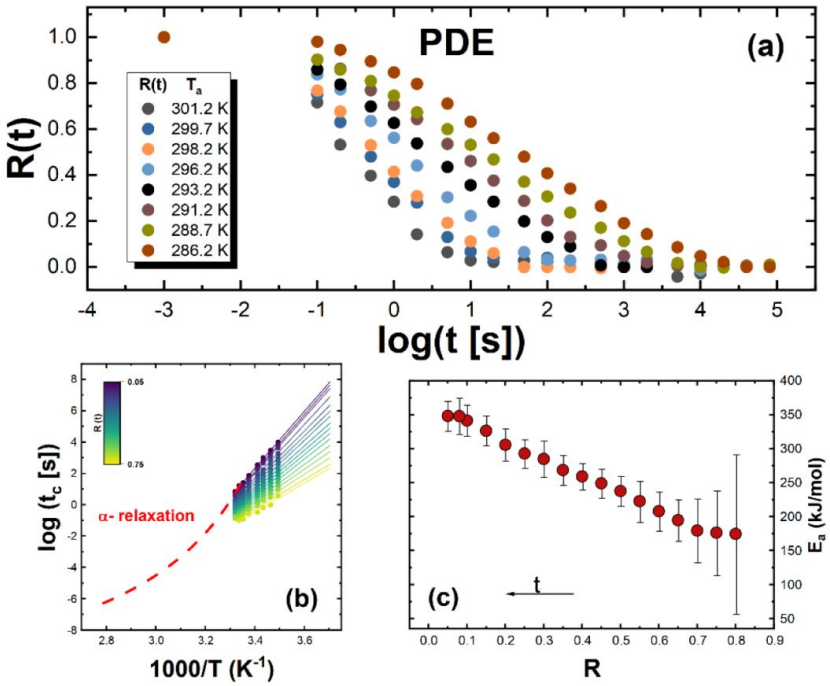

Figure S4: *Same as in Figure S3 for phenolphthalein dimethyl ether (PDE) (T_g = 306.5 K at 1000 Ks^{-1}). The temperature dependence of the α relaxation time is taken from Ref.* ***[2]*** *and it has been shifted by* $\log t = +0.65$ *to match the experimental data.*

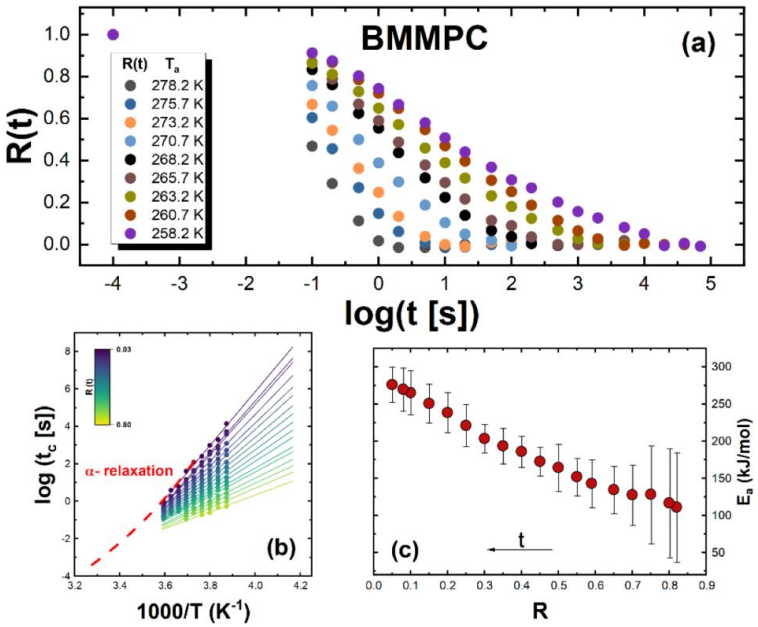

Figure S5: *Same as in Figure S3 for 1,1-bis (4-methoxyphenyl)cyclohexane (BMMPC) (T_g = 277 K at 1000 Ks^{-1}). The temperature dependence of the α relaxation time is taken from Ref.* [2] *and it has been shifted by* $\log t = +1.70$ *to match the experimental data.*

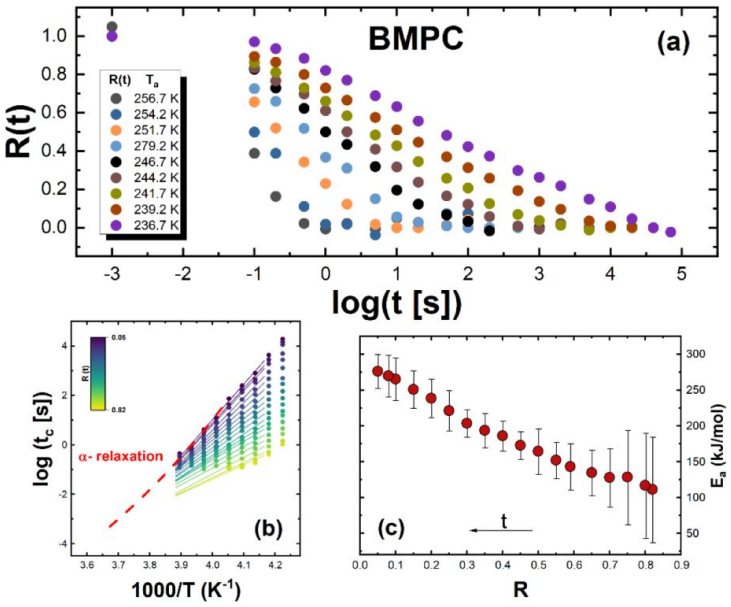

Figure S6: *Same as in Figure S3 for 1,1-di(pmethoxyphenyl)cyclohexane (BMPC) (T_g = 259 K at 1000 Ks^{-1}). The temperature dependence of the α relaxation time taken from Ref.* [2] *and it has been shifted by* $\log t = +1.50$ *to match the experimental data.*

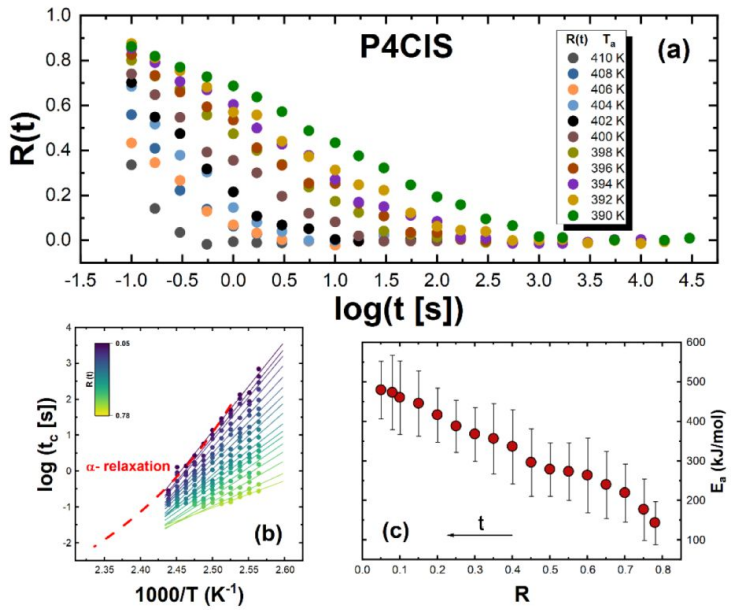

Figure S7: *Same as in Figure S3 for poly(4-chloro styrene) (P4ClS). The temperature dependence of the α relaxation time taken from Ref.* ***[3,4]*** *and it has been shifted by* $\log t = +2.70$ *to match the experimental data.*

References

1. Kahle S, Gapinski ; J, Hinze ; G *et al.* A comparison of relaxation processes in structurally related van der Waals glass formers: The role of internal degrees of freedom. J Chem Phys 2005; 122: 59.

2. Dreyfus C, Le Grand A, Gapinski J, Steffen W, Patkowski A. Scaling the α-relaxation time of supercooled fragile organic liquids. The European Physical Journal B - Condensed Matter and Complex Systems 2004; 42: 309–319.

3. Di Lisio V, Rocchi LA, Cangialosi D. Twofold Facet of Kinetics of Glass Aging. Phys Rev Lett 2024; 133: 048201.

4. Song Z, Rodríguez-Tinoco C, Mathew A, Napolitano S. Fast equilibration mechanisms in disordered materials mediated by slow liquid dynamics. Sci Adv 2022; 8: 7154.

Appendix A

Pre-print manuscript

Below we attach the pre-print publication entitled ”Testing the Validity of Density Scaling in Glass Physical Aging”.

Testing the Validity of Density Scaling in Glass Physical Aging

Vasiliki Maria Stavropoulou,[1,2] Federico Caporaletti,[3] Simone Napolitano,[3] and Daniele Cangialosi[1,4]

[1)] *Centro de Física de Materiales (CSIC–UPV/EHU), San Sebastián 20018, Spain*

[2)] *PMAS, Faculty of Chemistry, University of the Basque Country (UPV/EHU), San Sebastián 20018, Spain*

[3)] *Laboratory of Polymer and Soft Matter Dynamics, Experimental Soft Matter and Thermal Physics (EST), Université libre de Bruxelles (ULB), Brussels 1050, Belgium*

[4)] *Donostia International Physics Center, San Sebastián 20018, Spain*

The density scaling approach, which expresses relaxation times as a function combining temperature T, density ρ, has been established as a powerful framework to rationalize equilibrium dynamics of different glass-forming liquids. Whether this framework also applies in nonequilibrium glasses remains, however, an open question. Here we address this issue by combining time-dependent broadband dielectric spectroscopy measurements with a detailed analysis of aging kinetics in the model Van der Waals molecular glass former, *o*-cresolphthalein dimethyl ether (KDE). During isothermal aging below the glass transition temperature, T_g, we simultaneously tracked the dielectric loss on the high-frequency flank of the α-relaxation and the high-frequency value of the capacitance, reflecting glass densification. We show that the two observables evolve in strict proportionality and that the proportionality factor can be quantitatively obtained from intrinsic glass properties and density scaling parameters at equilibrium. Hence, our findings support that density scaling, initially formulated to account for equilibrium dynamics, also holds in non-equilibrium glasses. This extension significantly broadens the applicability of density scaling and highlights its potential as a unifying principle of glassy dynamics.

I. INTRODUCTION

When a liquid is cooled sufficiently fast to avoid crystallization, it undergoes vitrification and transforms into a glass. The hallmark of this transformation is the drastic reduction of molecular mobility, spanning many orders of magnitude over a narrow temperature interval.[1,2] This slowing-down is commonly rationalized in terms of two concomitant factors: (i) the increase in molecular packing, which reduces the available free volume, and (ii) the decrease of thermal energy, which traps molecules in a rugged potential energy landscape. As a consequence, the glass transition is not a thermodynamic phase transition but a kinetic phenomenon, strongly dependent on timescale and protocol.

To rationalize the dynamics of equilibrium glass-formers, the density scaling approach has emerged as a unifying framework.[3,4] According to this approach, the typical time τ of the main α relaxation of a wide variety of liquids and polymers can be expressed as a function of the temperature, T, and the density, ρ, plus a material specific variable, γ, reflecting the relative importance of density and temperature. The analytical form of this expression has been extensively tested in the following equation:[3,4]

$$\tau = \tau_0 \exp \frac{C}{T\rho^{-\gamma}} \tag{1}$$

As its application over a wide temperature range generally requires refinement, implementation of density scaling has been proposed by Avramov:[5,6]

$$\tau = \tau_0 \exp \left(\frac{C_{\mathrm{Avr}}}{T\rho^{-\gamma_{\mathrm{Avr}}}} \right)^{n_{\mathrm{Avr}}} \tag{2}$$

Where the subscript $_{\mathrm{Avr}}$ is intended to distinguish the scaling parameters within this approach and the standard scaling.

Both the standard empirical and Avramov scaling − the former over relatively narrow temperature/pressure intervals and the latter over a much broader temperature/pressure range − have been remarkably successful in superposing relaxation times measured under diverse thermodynamic conditions, leading to master curves covering several decades in τ. Density scaling has thus been validated for van der Waals liquids,[7–10] hydrogen-bonded systems,[7,8] ionic liquids,[11] and polymers[12,13] of varying fragility, as well as simulated glass formers,[10,14,15] underscoring its broad applicability.

Despite this success, density scaling has been mainly tested under equilibrium conditions, where relaxation times can be directly measured, and, if in non-equilibrium conditions, only above T_g.[16] Glasses, however, are inherently non-equilibrium materials. Below the glass transition temperature T_g, they undergo physical aging, a slow structural relaxation process whereby the system evolves toward the equilibrium supercooled liquid state.[17,18] Aging is accompanied by changes in thermodynamic and dynamic properties, including densification and the evolution of relaxation spectra. Whether the principles of density scaling extend to such out-of-equilibrium processes remains an open question of both fundamental and practical relevance. A positive answer would suggest that the same scaling variable governs relaxation not only at equilibrium but also during the progressive equilibration of glasses.

Whether density scaling applies in non-equilibrium glasses below T_g is challenged by the outcome of aging performed by simulations in isochoric conditions.[19–22] The latter indicate that the relaxation time or any ob-

servable related to it changes even when both temperature and volume are kept constant. Considering that in these simulations pressure changes during the course of aging, this implies that density scaling can only remain valid if equation 2 is extended to include a pressure contribution, or, as recently proposed,[23] an explicit nonequilibrium term written in terms of the glass fictive or effective[24,25]temperature, T_f. The latter, long ago introduced by Tool,[26] defines the glass thermodynamic state.

In this work, we propose an experimental approach to test the validity of density scaling during physical aging. To this end, we analyze broadband dielectric spectroscopy (BDS) measurements on an archetypal small molecule glass interacting via van der Waals forces, *o*-cresolphthalein dimethyl ether (KDE). As our experiments are conducted at constant atmospheric pressure, the aforementioned scenarios, where either a pressure or a non-equilibrium term must be included in the original scaling relation, can be discriminated. By monitoring both the dielectric loss associated with the α-relaxation and the high-frequency capacitance reflecting densification, we investigated whether τ and ρ evolution remain coupled in a way consistent with density scaling predictions (Eq. 2). Our results provide direct evidence that the density scaling framework, well established in equilibrium, is also compatible during nonequilibrium aging dynamics and provides further insight on impact of nonequilibrium on the value of the exponent γ.

II. EXPERIMENTAL

The system investigated was *o*-cresolphthalein dimethyl ether (KDE), provided by Polymer Source ($\geq$ 98 % purity), a low-molecular-weight van der Waals glass former. We employed broadband dielectric spectroscopy (BDS) under isobaric conditions at ambient pressure. For the aging measurements, nanocapacitor geometries were employed, in which the dielectric medium—a thin film of the material under study—was sandwiched between two conductive layers. To fabricate the capacitors, a thin aluminum layer (Sigma-Aldrich, purity $\geq$ 99 %) was first deposited onto circular glass substrates by physical vapor deposition, serving as the bottom electrode. The dielectric film was then prepared by dissolving approximately 50 mg of the sample in chloroform to obtain a 3–5 wt % solution, which was filtered through a 0.4 μm polytetrafluoroethylene membrane and spin-coated at room temperature onto the aluminum surface at a constant rotation speed. Samples were then annealed for 15 minutes at $T_g + 15$ K to evaporate any residual solvent and relax mechanical stresses from the spin-coating procedure. Finally, a second aluminum layer was deposited by the same vapor-deposition procedure to form the top electrode. The resulting capacitor structure used for dielectric aging measurements is schematically illustrated in Figure S1 of Supporting Information.

Dielectric measurements were carried out in the frequency range from 0.05 Hz to 1 MHz using a parallel-plate capacitor geometry. The samples were first equilibrated well above T_g, then cooled at $\sim$ 5 Ks^{-1} to selected temperatures below T_g for aging experiments. At each aging temperature, measurements of both the real and imaginary parts of the complex capacitance, $C^*(\omega) = C'(\omega) - iC''(\omega)$, were collected over logarithmically spaced frequencies.

Aging experiments were performed with durations sufficiently long to allow the system to approach equilibrium. During these runs, the dielectric response was monitored over time. For relatively short aging times, up to $\sim$ 1000 s, the loss $C''(f)$ was monitored at a representative low frequency (25 Hz), probing the high-frequency flank of the α-relaxation, while the storage part of the capacitance C' was measured at 10 kHz. For larger times, the entire dielectric spectrum, in a frequency range 0.1-10^5 Hz, was collected.

III. METHODOLOGY

The chosen observables were selected because they provide complementary information: the low frequency C'' reflects the main α relaxation dynamics,[27,28] whereas C' at high frequencies is directly sensitive to changes in density. Specifically, if C' is measured at frequencies larger than those at which all relaxation processes in the glass take place, the high frequency capacitance, $C_\infty = \epsilon_\infty \epsilon_0 S/h$ is obtained; where ϵ_∞, ϵ_0, S and h are the high frequency dielectric permittivity, the vacuum permittivity, and the area and thickness of the capacitor, respectively. ϵ_∞ provides direct information on the glass density via the Clausius-Mossotti (CM) equation[29–31]:

$$\frac{\epsilon_\infty - 1}{\epsilon_\infty + 2} = \frac{4\pi N\alpha}{3\varepsilon_0 M}\rho \equiv K_{\mathrm{CM}}\rho \tag{3}$$

Where N, α and M are the number of dipoles per unit volume, the polarizability and the molecular weight, respectively. Here, the second term of the CM equation has been grouped into the constant K_{CM}.

The CM equation requires measuring the high frequency capacitance, C_∞. Although C' measured at 10^4 Hz does not coincide with C_∞ due to the presence of residual relaxational contributions to the dielectric spectrum at that frequency, C_∞ can be extracted extrapolating to high frequency the variation of C' during aging (see Supporting Information for details).

To determine how ϵ_∞ (and therefore C_∞) changes with density, we differentiate the left-hand side of eq. 3 with respect to ρ:

$$\frac{d}{d\epsilon_\infty}\left(\frac{\epsilon_\infty - 1}{\epsilon_\infty + 2}\right) = \frac{3}{(\epsilon_\infty + 2)^2} \tag{4}$$

so that:

$$\frac{3}{(\epsilon_\infty+2)^2}\frac{d\epsilon_\infty}{d\rho}=K_{\rm CM} \tag{5}$$

Solving for the derivative gives the microscopic form of the variation of the capacitance with the density:

$$\frac{d\epsilon_\infty}{d\rho}=\frac{4\pi}{9}N_A\frac{\alpha}{M}\,(\epsilon_\infty+2)^2. \tag{6}$$

To obtain a macroscopic expression containing only measurable quantities, we eliminate $K_{\rm CM}$ using the Clausius–Mossotti equation itself:

$$K_{\rm CM}=\frac{\epsilon_\infty-1}{\rho(\epsilon_\infty+2)}, \tag{7}$$

which, combined with Eq. 5, leads to:

$$\frac{d\varepsilon_\infty}{d\rho}=\frac{(\varepsilon_\infty-1)(\varepsilon_\infty+2)}{3\rho} \tag{8}$$

During physical aging the mass per unit area is constant, so that:

$$\rho(t)\,h(t)=\rho(0)\,h(0) \tag{9}$$

and for small variations:

$$\frac{\Delta h}{h}\simeq-\frac{\Delta\rho}{\rho} \tag{10}$$

We now consider the relation between the high frequency capacitance C_∞ and the corresponding permittivity, ϵ_∞ and derive its differential variation with respect to ρ. This results from two contributions: i) the intrinsic variation of ϵ_∞ and ii) that of the sample volume, that is, the thickness variation:[29]

$$\frac{\Delta C_\infty}{C_\infty}=\left(\frac{1}{\varepsilon_\infty}\frac{d\varepsilon_\infty}{d\rho}+\frac{1}{\rho}\right)\Delta\rho \tag{11}$$

We define the macroscopic prefactor:

$$\Lambda=\frac{1}{\varepsilon_\infty}\frac{d\varepsilon_\infty}{d\rho}+\frac{1}{\rho} \tag{12}$$

so that:

$$\frac{\Delta C_\infty}{C_\infty}=\Lambda\,\Delta\rho \tag{13}$$

To provide a quantitative estimation of Λ, we resource to the differential form of the CM equation:

$$\frac{1}{\varepsilon_\infty}\frac{d\varepsilon_\infty}{d\rho}=\frac{(\varepsilon_\infty-1)(\varepsilon_\infty+2)}{3\varepsilon_\infty\rho} \tag{14}$$

Considering a value of $\varepsilon_\infty=n^2\sim 2.25$ (with n the refractive index for a typical transparent glass) and $\rho=1.1$ g cm^{-3} for KDE,[32] we obtain a value of: $\Lambda\sim 1.61$.

We now get back to the density scaling relation, which can be rewritten replacing in terms of the aging temperature T_a:

$$\log\tau(t)=\log\tau_0+\frac{C\rho(t)^\gamma}{\ln 10 T_a} \tag{15}$$

Expanding around $\rho=\rho(0)$, for small density variations, as those observed during physical aging,[33,34]: $\Delta\rho(t)=\rho(t)-\rho(0)\ll\rho(0)$, we can rewrite $\rho(t)^\gamma$ considering the first term of the Taylor expansion:

$$(\rho(0)+\Delta\rho(t))^\gamma\approx\rho(0)^\gamma+\gamma\rho(0)^{\gamma-1}\Delta\rho(t) \tag{16}$$

Hence the variation of τ with the density can be written:

$$\Delta\log\tau(t)=\frac{C\gamma}{\ln 10 T_a}\Delta\rho(t) \tag{17}$$

Finally, replacing $\Delta\rho(t)$ with ΔC_∞ using eq. 13, we obtain:

$$\Delta\log\tau(t)=\frac{C\gamma\rho(0)^{\gamma-1}}{\ln 10 T_a C_\infty\Lambda}\Delta C_\infty(t) \tag{18}$$

In way analogous to the classical scaling, we obtain the relation between the variation of the relaxation time and that of the high frequency capacitance within the Avramov variant of the scaling:[5,6]

$$\Delta\log\tau(t)=\frac{C_{\rm Avr}n_{\rm Avr}\gamma_{\rm Avr}\rho(0)^{\gamma_{\rm Avr}n_{\rm Avr}-1}}{\ln 10 T_a^{n_{Avr}}C_\infty\Lambda}\Delta C_\infty(t) \tag{19}$$

Considering that C_∞ undergoes small variations during aging (see Figs. 1 and 2), a quantitative test of the density scaling relations via Eqs. 18 and 19 implies that the proportionality between the variation of τ and that of C_∞ must be fulfilled; and that the proportionality coefficient, that is, the slope of the line $\Delta\log\tau$ vs ΔC_∞ must have a specified value, derived from the density scaling parameters obtained at equilibrium.

IV. RESULTS

The dielectric response of KDE in terms of the loss part of the permittivity, C'', is shown in the main panel of Fig.

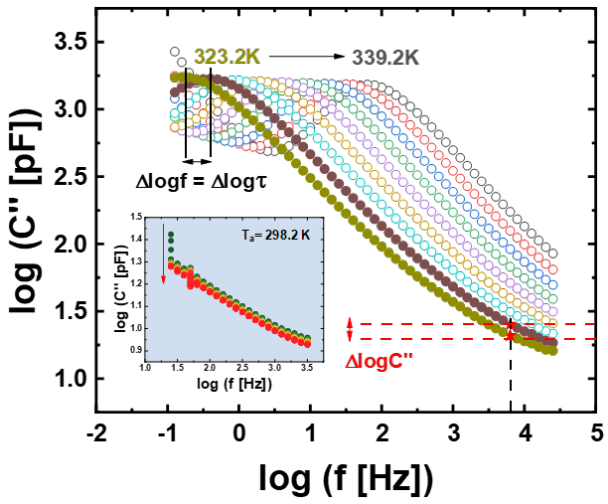

FIG. 1. Loss part of the capacitance at different frequencies and temperatures for KDE. The way a reduction in C'' reflects in shift to lower frequency of the peak in C'' is indicated. (Inset) Time dependent evolution of C'' during physical aging. The arrow marks increasing aging times at 298.2 K.

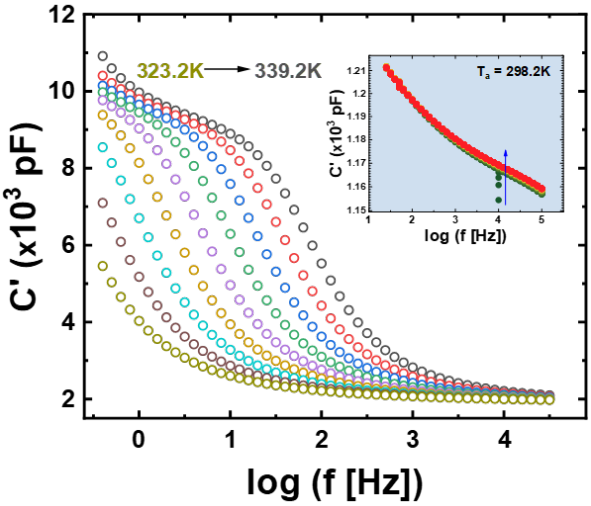

FIG. 2. Real part of the capacitance at different frequencies and temperatures for KDE at 298.2 K. (Inset) Time dependent evolution of C' during physical aging. The arrow marks increasing aging times.

1. As customary, we detect the α relaxation as a peak in C'' shifting to lower frequencies with decreasing temperature. The peak frequency, f_{max}, provides information on the α relaxation time: $\tau = 1/(2\pi f_{max})$. A τ variation, for instance the downward shift of the peak frequency with decreasing temperature, can be tracked by a concomitant decrease in C'' in the high frequency flank of the relaxation: $\Delta \log \tau = -A\Delta \log C''$; where A is a proportionality factor that can be extracted from equilibrium dielectric spectra (see Fig. 1). In the frequency range at which C'' has values comparable to those in aging regime, we obtain a proportionality factor of: $A = 5.10 \pm 0.25$. The inset of Fig. 1 shows the time evolution of C'' when the KDE sample was cooled below T_g and held isothermally at 298.2 K. Similar results, reported in Supporting Information, were obtained at other aging temperatures. The reduction of C'' reflects the progressive slowing-down of the α relaxation as the glass evolves toward equilibrium.

Figure 2 shows the frequency/temperature evolution of C' both above T_g, where the typical step from high to low values when increasing the frequency is observed, and in the aging regime, where only the high frequency flank of the α relaxation is visible, whereas the C' approaches a plateau at higher frequencies. The aging time dependent frequency sweeps, presented in the inset of Fig. 2 at 298.2 K, for KDE exhibit a significant increase with aging time of the C', measured at 10 kHz, consistent with densification of the material. The decrease of C' with frequency observed in the inset of Fig. 2 indicates that some residual relaxation is present in this range and, therefore, the change of C' observed at 10 kHz does not result exclusively from the increase of C_∞. To obtain the change

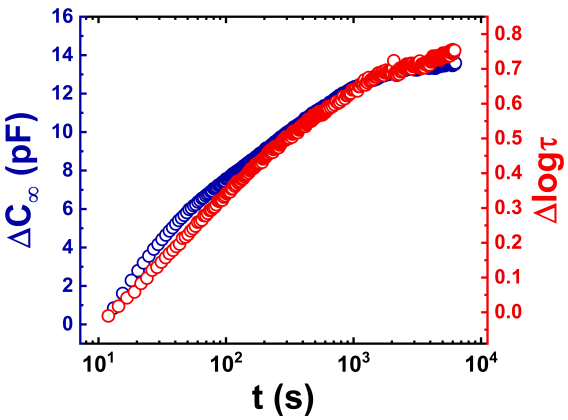

FIG. 3. Aging time evolution of the high frequency capacitance (left axis) and the relaxation time (right part) at 298.2 K.

of the latter with physical aging, we have rescaled the C' variation at 10 kHz to the high frequency limit using aging data obtained over a broad frequency range, that is, above $t_a \sim 1000s$ (see Supporting Information for details).

Figure 3 shows the aging time evolution of both the variation of the relaxation time, $\Delta \log \tau(t)$, and that of the high frequency capacitance $\Delta C_\infty(t)$ for KDE at 298.2 K. Analogous plots are shown in the Supporting Information for the aging temperatures of 300.2 and 303.2 K.

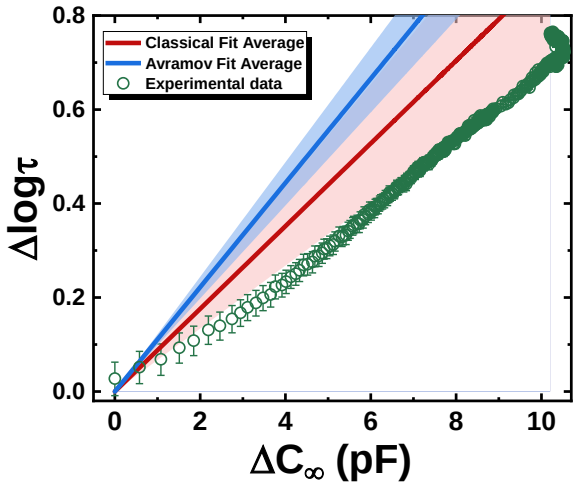

FIG. 4. Time dependent variation of the relaxation time as a function of the corresponding variation of the high frequency capacitance at 298.2 K.

Though the differences are subtle, given the small explored aging temperature range, we observe a general trend toward a reduction of the time to reach equilibrium and the amount of recovery of both observable with increasing aging temperature. Both results are in line with the general phenomenology of physical aging.[35] Importantly, the evolution of the two observable exhibits analogous aging time dependence, both reaching a stable equilibrium value after sufficiently long times at all investigated temperatures. These parallel trends already qualitatively suggest a strong coupling between structural relaxation and volume recovery.

A step forward in the analysis of aging data is reported in Fig. 4, where the time evolution of $\Delta \log \tau(t)$ is reported as a function of $\Delta C_\infty(t)$ at 298.2 K. Analogous plots are reported for 300.2 and 303.2 K in Supporting Information. In all cases, a linear dependence between the two observables is observed. The latter outcome fulfills the predictions of density scaling (Eq. 18). A more stringent test of density scaling can be done predicting the slope of $\Delta \log \tau(t)$ *vs* $\Delta C_\infty(t)$ according to Eqs. 18 and 19 for both classical and Avramov scaling employing parameters for KDE at equilibrium. These are generally obtained by BDS experiments over a wide range of temperature and pressure[4,36] and reported in the Supporting Information. Figure 4 shows the range of prediction based on density scaling considering both mentioned variants of density scaling. Considering that all parameters are taken from relaxation data at equilibrium and, therefore, no fitting parameters are required, the agreement of density scaling with experimental results is remarkable, although the slope predicted by the classical scaling appears to be closer to the experimental one than that predicted within the Avramov variant.

V. DISCUSSION

The central question addressed in this work is whether the density scaling framework, well-established for equilibrium dynamics of glass-forming liquids,[3,4,8] remains valid under nonequilibrium conditions during physical aging. Our experimental approach, conveying simultaneous information on the $\alpha-$relaxation dynamics, via low-frequency dielectric loss, and densification, via high-frequency capacitance, in KDE, provides a direct test of this hypothesis.

The outcome of our analysis aligns with previous work showing that density scaling successfully captures the dynamics of thin polymer layers even under out-of-equilibrium 1D confinement: in freshly spin-coated poly(4-chlorostyrene) films, where the interfacial layer is far from equilibrium, the same scaling exponent γ determined from bulk high-pressure measurements was able to describe the α-dynamics of the bulk melt as well as that of confined films measured above T_g during their equilibration.[16,37]

This behavior is in fact already embedded in the Cooperative Free Volume model,[38] which describes segmental relaxation in terms of an activation free energy that increases with the number of cooperatively rearranging units, itself inversely proportional to the available free volume. Within this framework, the material parameter b—analytically related to the density-scaling exponent γ and thus roughly scaling as $1/\gamma$—[5] controls the α-dynamics, regardless of the equilibrium conditions of the system. Importantly, the same value of b describes both the bulk dynamics and that of non-equilibrium freshly spin-coated films. In the latter case, the non-equilibrium character arises from the interfacial region[39], where the free volume exceeds the bulk value[40], and CFV consider a bulk b value, independent on film thickness[38].

In the specific case of aging, if density scaling is valid in non-equilibrium, the connection between the variation of the α relaxation time and that of the high frequency capacitance must fulfill two main conditions: i) the two magnitudes must be proportional; and ii) the proportionality factor between them must be a specific value derived from intrinsic properties of the glass, including the fitting parameters used to describe relaxation data at equilibrium. Figure 4 demonstrates that both conditions are generally fulfilled, thereby providing the first evidence of the validity of density scaling in nonequilibrium.

The ability of describing aging data with the γ value obtained from equilibrium relaxation data has two important implications. First, it confirms that γ is indeed a material constant that does not depend on the thermodynamic path used to probe the relationship between τ, T, and ρ. Second, it suggests that the molecular interactions governing the relative importance of thermal energy and packing are unchanged as the system falls out of equilibrium. This is perhaps expected given that van der Waals interactions, which dominate in KDE, are not fundamentally altered by the glassy state, but the

experimental confirmation is nonetheless significant.

Our findings bear the deep implication that the α relaxation of a nonequilibrium glass during aging can be described within density scaling framework, an approach widely validated for equilibrium glass forming liquids in a broad range of condition with varying pressure and temperature. In other words, our results imply that applying density scaling in the aging regime does not require the introduction of any additional term accounting for the nonequilibrium nature of glasses. The main consequence of this outcome is that the description via density scaling of aging results obtained in simulations,[19–22] where the relaxation time changes at constant volume, rather than requiring a non-equilibrium additional term, must account for the change of pressure taking place in these conditions.

A further implication of the validity of the density scaling approach to non-equilibrium glasses is that it can be applied to predict the evolution of a given observable with aging time. This has been recently done in combination with the single parameter aging (SPA) approach to describe enthalpy relaxation results in different low molecular weight glass formers, including KDE.[36] It was shown that such approach was able to describe enthalpy relaxation results for relatively small jump and in proximity of the glass T_g. However, it failed for larger jumps. Given the outcome of the present work, the failure of density scaling combined with the SPA approach, rather than being due to inaccuracy of density scaling, must be attributed to the inability of the α relaxation alone to catch the overall phenomenology of physical aging. Hence, the role of secondary mechanisms in the kinetics of physical aging must be considered. These must bear great potential for glass equilibration. This is the case of the recently identified slow Arrhenius process (SAP),[41,42] whose effects in the kinetics of different nonequilibrium processes has been demonstrated.[43–45]

VI. CONCLUSIONS

We have investigated the validity of density scaling in non-equilibrium glasses by analyzing the physical aging of an archetypal molecular glass former (KDE) through broadband dielectric spectroscopy. By monitoring the dielectric loss on the high-frequency flank of the α-relaxation together with the high-frequency capacitance, we established that the time evolution of structural relaxation and densification follows the same trajectory. In both systems and at all studied aging temperatures, the two observables were found to be strictly proportional. Furthermore, the proportionality factor between the variation of the relaxation time and that of the high frequency capacitance can be predicted using density scaling parameters obtained at equilibrium within the classical scaling and Avramov variant. The prediction remarkably catches the connection between the time dependent variation of the relaxation time and that of density.

[1] C. A. Angell, Science **267**, 1924 (1995).
[2] M. D. Ediger, C. A. Angell, and S. R. Nagel, Journal of Physical Chemistry **100**, 13200 (1996).
[3] R. Casalini and C. M. Roland, Physical Review E **69**, 062501 (2004).
[4] C. M. Roland and R. Casalini, Reports on Progress in Physics **68**, 1405 (2005).
[5] R. P. White and J. E. Lipson, Eur. Phys. J. E **42**, 100 (2019).
[6] I. Avramov, J. Non-Cryst. Sol. **262**, 258 (2000).
[7] C. Roland, S. Bair, and R. Casalini, J. Chem. Phys. **125** (2006).
[8] C. Dreyfus, A. Le Grand, J. Gapinski, W. Steffen, and A. Patkowski, Eur. Phys. J. B **42**, 309 (2004).
[9] A. Reiser, G. Kasper, and S. Hunklinger, Phys. Rev. E **72**, 094204 (2005).
[10] L. Bøhling, T. S. Ingebrigtsen, A. Grzybowski, M. Paluch, J. C. Dyre, and T. B. Schrøder, New J. Phys. **14**, 113035 (2012).
[11] H. W. Hansen, F. Lundin, K. Adrjanowicz, B. Frick, A. Matic, and K. Niss, Phys. Chem. Chem. Phys. **22**, 14169 (2020).
[12] C. Roland, Macromolecules **43**, 7875 (2010).
[13] G. A. Schwartz, J. Colmenero, and Á. Alegría, Macromolecules **39**, 3931 (2006).
[14] D. Coslovich and C. Roland, J. Phys. Chem. B **112**, 1329 (2008).
[15] K. Koperwas, A. Grzybowski, and M. Paluch, Phys. Rev. E **101**, 012613 (2020).
[16] K. Adrjanowicz, R. Winkler, A. Dzienia, M. Paluch, and S. Napolitano, ACS macro letters **8**, 304 (2019).
[17] L. C. E. Struik, *Physical aging in amorphous polymers and other materials* (Elsevier, Amsterdam, 1978).
[18] D. Cangialosi, in *Glassy, Amorphous and Nano-Crystalline Materials: Volume 2*, Vol. 1375, edited by I. Pérez-Castellanos and C. Prieto (ACS Symposium Series, 2021) pp. 101–124.
[19] A. Smessaert and J. Rottler, Phys. Rev. E **88**, 022314 (2013).
[20] K. Vollmayr-Lee, J. Chem. Phys. **121**, 4781 (2004).
[21] M. Utz, P. G. Debenedetti, and F. H. Stillinger, Phys. Rev. Lett. **84**, 1471 (2000).
[22] W. Kob and J.-L. Barrat, Phys. Rev. Lett. **78**, 4581 (1997).
[23] K. Niss, The Journal of Chemical Physics **157** (2022).
[24] L. F. Cugliandolo, J. Kurchan, and L. Peliti, Phys. Rev. E **55**, 3898 (1997).
[25] J. Kurchan, Nature **433**, 222 (2005).
[26] A. Tool, J. Am. Ceram. Soc. **29**, 240 (1946).
[27] V. M. Boucher, D. Cangialosi, A. Alegría, and J. Colmenero, Phys. Rev. E **86**, 041501 (2012).
[28] P. Lunkenheimer, R. Wehn, U. Schneider, and A. Loidl, Phys. Rev. Lett. **95**, 055702 (2005).
[29] D. Cangialosi, V. M. Boucher, A. Alegría, and J. Colmenero, J. Pol. Sci. B: Pol. Phys. **51**, 847 (2013).
[30] K. Fukao and H. Koizumi, Phys. Rev. E **77**, 021503 (2008).
[31] C. Bauer, R. Böhmer, S. Moreno-Flores, R. Richert, H. Sillescu, and D. Neher, Phys. Rev. E **61**, 1755 (2000).
[32] R. Casalini and C. Roland, Phys. Rev. B **71**, 014210 (2005).
[33] R. Wimberger-Friedl and J. De Bruin, Macromolecules **29**, 4992 (1996).
[34] J. Hadač, P. Slobodian, P. Říha, P. Saha, R. Rychwalski, I. Emri, and J. Kubát, J. Non-Cryst. Sol. **353**, 2681 (2007).
[35] D. Cangialosi, V. M. Boucher, A. Alegria, and J. Colmenero, Soft Matt. **9**, 8619 (2013).
[36] V. Di Lisio, V.-M. Stavropoulou, and D. Cangialosi, J. Chem. Phys. **159**, 064505 (2023).
[37] A. Panagopoulou and S. Napolitano, Physical review letters **119**, 097801 (2017).
[38] R. P. White and J. E. Lipson, Macromolecules **51**, 7924 (2018).
[39] S. Napolitano, Soft Matter **16**, 5348 (2020).
[40] A. Panagopoulou, C. Rodríguez-Tinoco, R. P. White, J. E. Lipson, and S. Napolitano, Physical review letters **124**, 027802 (2020).
[41] Z. Song, C. Rodríguez-Tinoco, A. Mathew, and S. Napolitano, Sci. Adv. **8**, eabm7154 (2022).
[42] F. Caporaletti and S. Napolitano, Phys. Chem. Chem. Phys. **26**, 745 (2024).

[43]E. Thoms, Z. Song, K. Wang, and S. Napolitano, Physical review letters **132**, 248101 (2024).

[44]F. Caporaletti, M. E. Villanueva, S. Molitor, B. Zuo, and S. Napolitano, Materials Horizons (2026).

[45]K. Wang, M. E. Villanueva, F. Caporaletti, R. P. White, J. E. Lipson, S. Napolitano, and P. Losada-Pérez, Small , e12844 (2026).

Supporting Information for "Testing the Validity of Density Scaling in Glass Physical Aging"

Vasiliki Maria Stavropoulou[1,2], Federico Caporaletti[3], Simone Napolitano[3], and Daniele Cangialosi[1,4]

[1] *Centro de Física de Materiales (CSIC–UPV/EHU), San Sebastián 20018, Spain*
[2] *PMAS, Faculty of Chemistry, University of the Basque Country (UPV/EHU), San Sebastián 20018, Spain*
[3] *Laboratory of Polymer and Soft Matter Dynamics, Experimental Soft Matter and Thermal Physics (EST), Université libre de Bruxelles (ULB), Brussels 1050, Belgium*
[4] *Donostia International Physics Center, San Sebastián 20018, Spain*

1 Nanocapacitor Structure

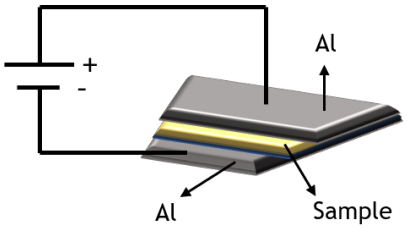

Figure S1: Schematic illustration of the nanocapacitor used for BDS and aging experiments.

In Fig. S1 the structure of the nanocapacitor used for the BDS experiments is presented. At first, a layer of aluminum is deposited on a glass substrate and then the solution of the substance under study is spin-coated onto this layer. After the deposition of the sample, a small quantity is removed with chloroform from the center so as to leave the aluminum exposed (light gray area in the center). Then, a second layer of aluminum is deposited, as shown in the figure, to complete the nanocapacitor formation.

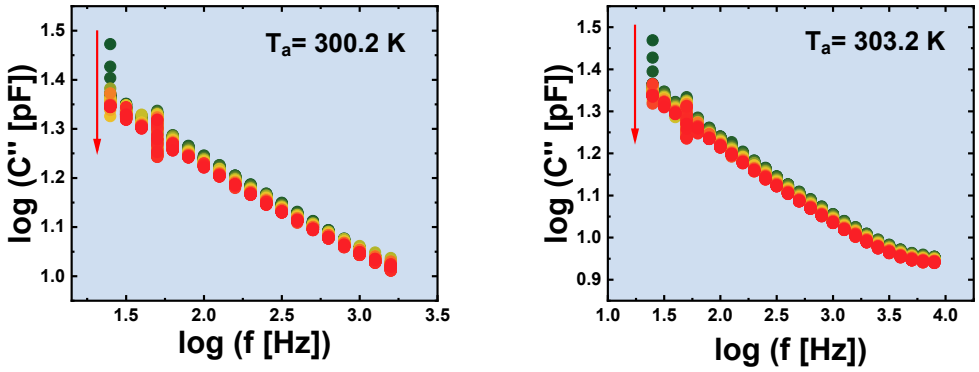

(a) (b)

Figure S2: Time dependent evolution of C'' during physical aging for (a) 300.2 K and (b) 303.2 K. The arrow marks increasing aging times.

2 Time evolutions of C''

The time evolution of C'' (25 Hz) for aging temperatures equal to $T_a = 300.2$ K and $T_a = 303.2$ K is presented in Fig.S2.

3 Calculation of ΔC_∞

For physical aging measurements, during the first ~ 1000 s, only three discrete frequencies were measured (25 Hz, 5 kHz, and 10 kHz). Full frequency spectra were acquired only after this initial period and can be seen in the inset of Figure 2 of the main manuscript for $T_a = 298.2$ K and in Fig. S3 for the other two aging temperatures.

Measurements at $f = 10$ kHz do not yield the relaxed value of C' and therefore, cannot be associated to C_∞. The use of the value of C' corresponding to $f = 10$ kHz in the subsequent analysis would have introduced significant errors in the density scaling analysis described in the main manuscript. Thus, it was essential to develop a method to estimate the value of C' at frequencies of the order of 1 MHz from the available data, which, in contrast provides the value of C_∞. Indeed, at this frequency practically no residual contribution of relaxation to C' are observed.

This was achieved by considering $\Delta C'$, defined as the difference between the value of C' at $t = 1000$ s and its value at infinite time, for all measured frequencies. The resulting behavior is shown in Fig. S4 for all aging temperatures for KDE. As previously discussed, the densification occurring during physical aging, results in an increase in the value of the

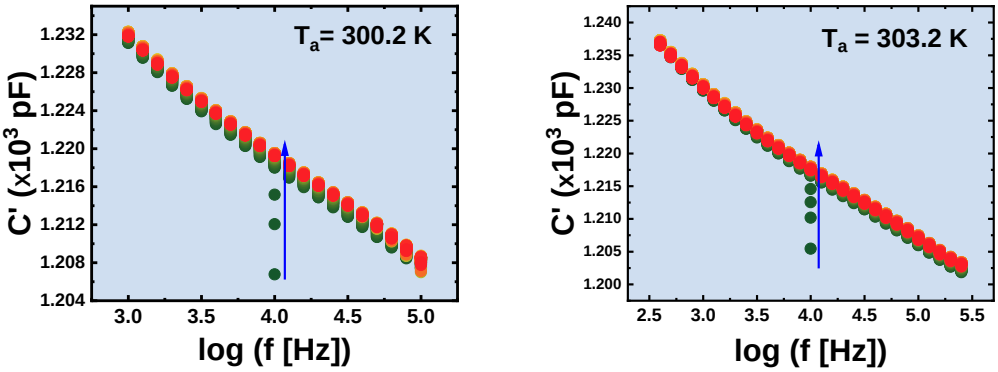

(a) (b)

Figure S3: Time dependent evolution of C' during physical aging for (a) 300.2 K and (b) 303.2 K. The arrow marks increasing aging times.

high-frequency flank of C', which is more pronounced than the corresponding increase at intermediate frequencies. Consequently, the values of $\Delta C'$ are expected to increase with frequency, until they reach a plateau. This behavior is confirmed in Fig. S4, where the plateau values for each aging temperature are indicated by dotted lines. As expected, the $\Delta C'$ at $f = 10$ kHz is smaller compared to the high frequency plateau value.

Hence, we can now find the total change at high frequency, $\Delta C_{\infty,tot}$, starting from $t_a = 0$, by multiplying the total $\Delta C'_{tot}$ at $f = 10$ kHz by a factor equal to the ratio $\Delta C_\infty / \Delta C'_{10kHz}$. The calculation of this factor for all aging temperatures of KDE is briefly presented in Table 1.

T_a (K)	$\Delta C'_{10kHz}$ (pF)	ΔC_∞ (pF)	$\Delta C_\infty / \Delta C'_{10kHz}$
298.2	2.03	2.50	**1.23**
300.2	1.53	1.60	**1.08**
303.2	1.35	1.50	**1.11**

Table 1: Calculation of the factor $\Delta C_\infty / \Delta C'_{10kHz}$ for all aging temperatures for KDE.

4 ΔC_∞ and $\Delta log\tau$ time evolutions

The time evolutions of ΔC_∞ and $\Delta log\tau$ for $T_a = 300.2$ K and $T_a = 303.2$ K are shown in Fig.S5.

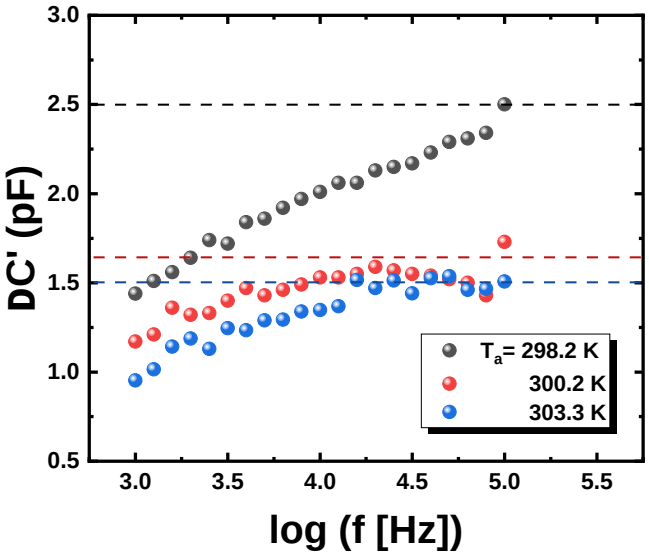

Figure S4: The change of $\Delta C'$, defined as the difference between the value of C' at $t = 1000$ s and its value at infinite time for KDE at aging temperatures 298.2 K, 300.2 K and 303.2K. Dotted lines indicate the plateau value at each aging temperature.

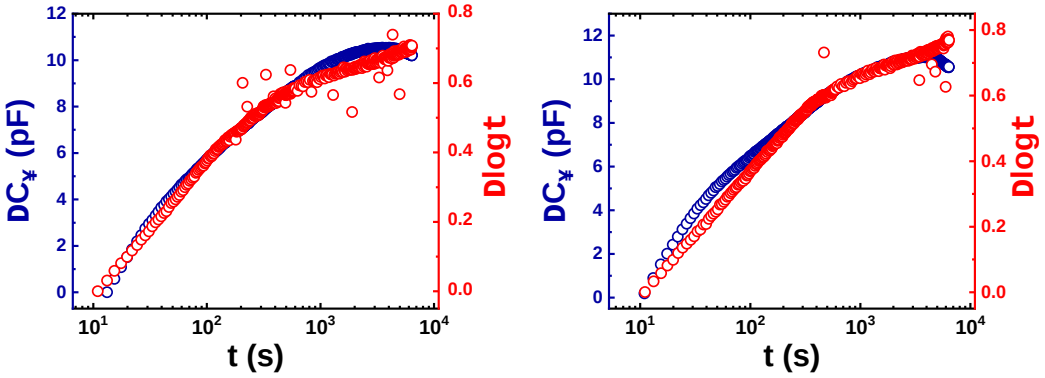

Figure S5: Aging time evolution of the high frequency capacitance (left axis) and the relaxation time (right part) at (a) 300.2 K and (b) 303.2 K.

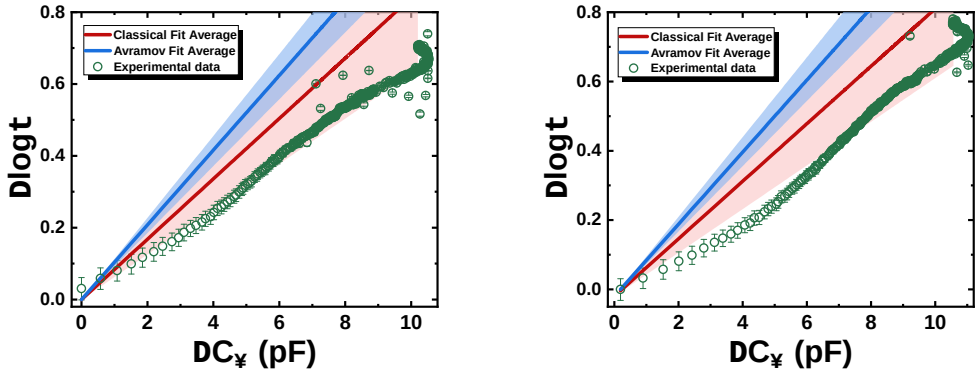

(a) (b)

Figure S6: Time dependent variation of the relaxation time as a function of the corresponding variation of the high frequency capacitance at (a) 300.2 K and (b) 303.2 K. The colored areas are the range of prediction of the classical (red) and Avramov (blue) scaling and the corresponding lines are the average value.

5 $\Delta log\tau$ vs ΔC_∞ plots

In Fig. S6, we present the time-dependent variation of the relaxation time as a function of the corresponding variation of the high frequency capacitance for T_a = 300.2 K and T_a = 303.2 K and the predictions of the classical and the Avramov scalings as the red and blue colored areas, respectively.

The fitting parameters for both models are shown in Table 2.

	C (K $(g/cm^3)^\gamma$)	$C\gamma$ error (K $(g/cm^3)^\gamma$)	C_{Avr} error (K $(g/cm^3)^\gamma$)	γ	n_{Avr}
Classical Scaling	3760	± 18000		5.4	
Avramov Scaling	5.08 10^8		± 0.50 10^8	5.3	3.2

Table 2: Fitting parameters of the Classical and the Avramov scaling.

The parameters in Table 2 are obtained from the fit of equilibrium data. These are shown in Fig. S7. This figure shows the application of the classical and Avramov scaling on KDE equilibrium data obtained under at atmospheric pressure [1] and varying temperature and pressure [2]. The classical scaling is applied only in the low-temperature range, as if all the range is considered, the fit appears to be inadequate. In contrast, the Avramov scaling adequately catches experimental data over the entire temperature/pressure range at which experimental data are available.

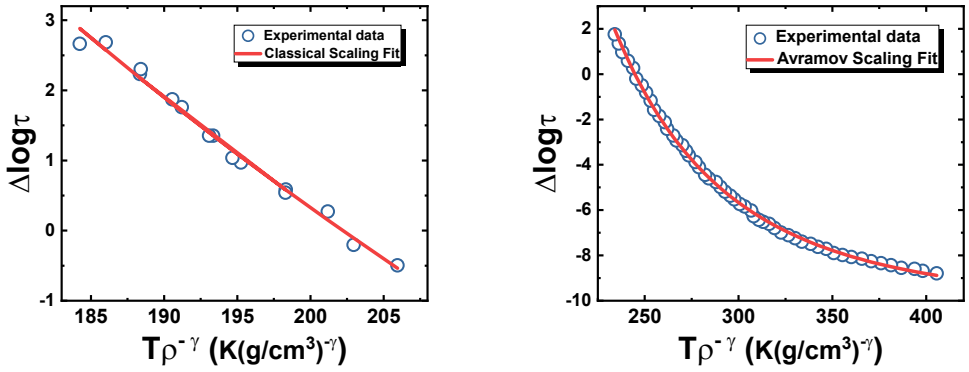

(a) (b)

Figure S7: (a) Classical and (b) Avramov scaling fits of experimental equilibrium data for KDE obtained at atmospheric pressure [1] and over a broad temperature and pressure range [2].

References

(1) Di Lisio, V.; Stavropoulou, V.-M.; Cangialosi, D. *The Journal of Chemical Physics* **2023**, *159*, 064505, DOI: 10.1063/5.0157994.

(2) Roland, C. M.; Hensel-Bielowka, S; Paluch, M; Casalini, R *Reports on Progress in Physics* **2005**, *68*, 1405, DOI: 10.1088/0034-4885/68/6/R03.

Bibliography

(1) Tammann, G.; Mehl, R., *The States of Aggregation: The Changes in the State of Matter in Their Dependence Upon Pressure and Temperature*; Constable: 1925.

(2) Demirel, Y. In *Nonequilibrium Thermodynamics (Second Edition)*; Elsevier Science B.V.: Amsterdam, 2007.

(3) ANGELINI, I.; GRATUZE, B.; ARTIOLI, G. In *The Contribution of Mineralogy to Cultural Heritage*; Mineralogical Society of Great Britain and Ireland: 2019, DOI: 10.1180/EMU-notes.20.3.

(4) Chopinet, M.-H. In *Springer Handbook of Glass*, Musgraves, J. D., Hu, J., Calvez, L., Eds.; Springer International Publishing: Cham, 2019, pp 1–47, DOI: 10.1007/978-3-319-93728-1_1.

(5) Debenedetti, P. G., *Metastable Liquids: Concepts and Principles*; Princeton University Press, Princeton: 1996.

(6) Schmelzer, J. W. P.; Gutzow, I. S., *Glasses and the glass transition*; Wiley-VCH, Weinheim: 2011.

(7) Cangialosi, D. In *Recent Advances, Techniques and Applications*, Vyazovkin, S., Koga, N., Schick, C., Eds.; Handbook of Thermal Analysis and Calorimetry, Vol. 6; Elsevier Science B.V.: 2018, pp 301–337, DOI: https://doi.org/10.1016/B978-0-444-64062-8.00013-9.

(8) Angell, C. *Science* **1995**, *267*, 1924–1935, DOI: 10.1126/science.267.5206.1924.

(9) Debenedetti, P.; Stillinger, F. *Nature* **2001**, *410*, 259–67, DOI: 10.1038/35065704.

(10) Vyazovkin, S., *Isoconversional Kinetics of Thermally Stimulated Processes*, 2015, DOI: 10.1007/978-3-319-14175-6.

(11) Tool, A. *J. Am. Ceram. Soc.* **1946**, *29*, 240–253, DOI: https://doi.org/10.1111/j.1151-2916.1946.tb11592.x.

(12) Prigogine, I.; Defay, R., *Chemical Thermodynamics*; Longman: London, 1954; Chapter 19.

(13) Simon, F. *Zeitschrift für anorganische und allgemeine Chemie* **1931**, *203*, 219–227, DOI: https://doi.org/10.1002/zaac.19312030120.

(14) Tropin, T. V.; Schmelzer, J. W. P.; Gutzow, I.; Schick, C. *The Journal of Chemical Physics* **2012**, *136*, 124502, DOI: 10.1063/1.3694531.

(15) Jaeger, G. *Archive for History of Exact Sciences* **1998**, *53*, 51–81, DOI: 10.1007/s004070050021.

(16) Landau, L. D.; Lifshitz, E. M., *Course in Theoretical Physics, Vol. 5: Statistical Physics*; Course of Theoretical Physics, Vol. 5; Akademie-Verlag: Berlin, 1969.

(17) Ryogo, K., *Thermodynamics*; North Holland: Amsterdam, 1968.

(18) Schmelzer, J. W. P.; Gutzow, I. S. In *Glasses and the Glass Transition*; John Wiley & Sons, Ltd: 2011; Chapter 1, pp 1–8, DOI: https://doi.org/10.1002/9783527636532.ch1.

(19) Schmelzer, J. W. P. *The Journal of Chemical Physics* **2012**, *136*, 074512, DOI: 10.1063/1.3685510.

(20) Schmelzer, J.; Tropin, T.; Schick, C; Röpke, G; Priezzhev, V. *Nucleation Theory and Applications* **2011**, 355–428.

(21) Prigogine, I.; Defay, R. In 1950.

(22) Cangialosi, D. In *Broadband Dielectric Spectroscopy: A Modern Analytical Technique*; Chapter 6, pp 133–156, DOI: 10.1021/bk-2021-1375.ch006.

(23) Rössler, E.; Sokolov, A. *Chemical Geology* **1996**, *128*, 5TH Silicate Melt Workshop, 143–153, DOI: https://doi.org/10.1016/0009-2541(95)00169-7.

(24) Angell, C. *Journal of Non-Crystalline Solids* **1985**, *73*, Glass Science and Technology Problems and Prospects for 2004, 1–17, DOI: https://doi.org/10.1016/0022-3093(85)90334-5.

(25) Vogel, D. H. *Physikalische Zeitschrift* **1921**, *22*, 645–646.

(26) Fulcher, G. S. *J. Am. Ceram. Soc.* **1925**, *8*, 339–355, DOI: https://doi.org/10.1111/j.1151-2916.1925.tb16731.x.

(27) Tammann, G.; Hesse, W. *Zeitschrift für anorganische und allgemeine Chemie* **1926**, *156*, 245–257, DOI: https://doi.org/10.1002/zaac.19261560121.

(28) Vassilikou-Dova, A.; Kalogeras, I. M. In *Thermal Analysis of Polymers*; John Wiley & Sons, Ltd: 2009; Chapter 6, pp 497–613, DOI: https://doi.org/10.1002/9780470423837.ch6.

(29) Angell, C. *J. Non-Cryst. Sol.* **1991**, *131*, 13–31, DOI: https://doi.org/10.1016/0022-3093(91)90266-9.

(30) Böhmer, R.; Ngai, K.; Angell, C.; Plazek, D. *The Journal of Chemical Physics* **1993**, *99*, Cited by: 2369, 4201 –4209, DOI: 10.1063/1.466117.

(31) Nyquist, H *Phys. Rev.* **1928**, *32*, 110–113, DOI: 10.1103/PhysRev.32.110.

(32) Callen, H.; Greene, R. *Phys. Rev.* **1952**, *86*, 702–710, DOI: 10.1103/PhysRev.86.702.

(33) Kovacs, A. J. *Fortsch. Hochpolym. Fo.* **1963**, *3*, 394–508.

(34) McKenna, G. B. In *Long-Term Durability of Polymeric Matrix Composites*, Pochiraju, K. V., Tandon, G. P., Schoeppner, G. A., Eds.; Springer US: Boston, MA, 2012, pp 237–309.

(35) Struik, L. C. E., *Physical aging in amorphous polymers and other materials*; Technische Hogeschool Delft: 1977.

(36) Cangialosi, D.; Boucher, V. M.; Alegria, A.; Colmenero, J. *Soft Matt.* **2013**, *9*, 8619–8630, DOI: 10.1039/C3SM51077H.

(37) Cui, L.; Imre, B.; Tátraaljai, D.; Pukánszky, B. *Polymer* **2020**, *186*, 122014, DOI: https://doi.org/10.1016/j.polymer.2019.122014.

(38) Jensen, M.; Smedskjaer, M. M.; Wang, W.; Chen, G.; Yue, Y. *Journal of Non-Crystalline Solids* **2012**, *358*, 129–132, DOI: https://doi.org/10.1016/j.jnoncrysol.2011.07.041.

(39) MOYNIHAN, C. T.; EASTEAL, A. J.; De BOLT, M. A.; TUCKER, J. *Journal of the American Ceramic Society* **1976**, *59*, 12–16, DOI: https://doi.org/10.1111/j.1151-2916.1976.tb09376.x.

(40) Kovacs, A. J.; Aklonis, J. J.; Hutchinson, J. M.; Ramos, A. R. *J. Pol. Sci., Part B: Pol. Phys.* **1979**, *17*, 1097–1162, DOI: https://doi.org/10.1002/polb.1996.944.

(41) Narayanaswamy, O. *J. Am. Cer. Soc.* **1971**, *54*, 491–498.

(42) Wang, L.; Velikov, V.; Angell, C. *The Journal of Chemical Physics* **2002**, *117*, 10184, DOI: 10.1063/1.1517607.

(43) Saini, M. K.; Jin, X.; Wu, T.; Liu, Y.; Wang, L.-M. *The Journal of Chemical Physics* **2018**, *148*, 124504, DOI: 10.1063/1.5019968.

(44) Donth, E.; Korus, J.; Hempel, E.; Beiner, M. *Thermochimica Acta* **1997**, *304-305*, Temperature Modulated Calorimetry, 239–249, DOI: https://doi.org/10.1016/S0040-6031(97)00027-0.

(45) Schawe, J. E. K. *The Journal of Chemical Physics* **2014**, *141*, 184905.

(46) Lapuk, S.; Ponomareva, M.; Ziganshin, M.; Larionov, R.; Mukhametzyanov, T.; Schick, C.; Lounev, I.; Gerasimov, A. *Phys. Chem. Chem. Phys.* **2023**, *25*, 10706–10714, DOI: 10.1039/D2CP05972J.

(47) Rault, J *J. Phys.: Cond. Matt.* **2003**, *15*, S1193, DOI: 10.1088/0953-8984/15/11/338.

(48) Lunkenheimer, P.; Wehn, R.; Schneider, U.; Loidl, A. *Phys. Rev. Lett.* **2005**, *95*, 055702, DOI: 10.1103/PhysRevLett.95.055702.

(49) Richert, R.; Lunkenheimer, P.; Kastner, S.; Loidl, A. *The Journal of Physical Chemistry B* **2013**, *117*, 12689–12694, DOI: 10.1021/jp311149n.

(50) Mansuri, A; Münzner, P; Feuerbach, T; Vermeer, A.; Hoheisel, W; Böhmer, R; Thommes, M; Gainaru, C *J. Chem. Phys.* **2021**, *155*, 174502, DOI: 10.1063/5.0067404.

(51) Richert, R. *J. Chem. Phys.* **2022**, *157*, 224501, DOI: 10.1063/5.0131342.

(52) Monnier, X.; Cangialosi, D.; Ruta, B.; Busch, R.; Gallino, I. *Science Advances* **2020**, *6*, eaay1454, DOI: 10.1126/sciadv.aay1454.

(53) Di Lisio, V; Gallino, I; Riegler, S.; Frey, M; Neuber, N; Kumar, G; Schroers, J; Busch, R; Cangialosi, D *Nat. Comm.* **2023**, *14*, DOI: 10.1038/s41467-023-40417-4.

(54) Monnier, X.; Cangialosi, D. *Phys. Rev. Lett.* **2018**, *121*, 137801, DOI: 10.1103/PhysRevLett.121.137801.

(55) Cangialosi, D.; Boucher, V. M.; Alegría, A.; Colmenero, J. *Phys. Rev. Lett.* **2013**, *111*, 095701, DOI: 10.1103/PhysRevLett.111.095701.

(56) Morvan, A.; Delpouve, N; Vella, A; Saiter-Fourcin, A *J. Non-Cryst. Sol.* **2021**, *570*, 121013, DOI: https://doi.org/10.1016/j.jnoncrysol.2021.121013.

(57) Pyda, M.; Czerniecka-Kubicka, A. *Adv. Pol. Sci* **2018**, 153–193, DOI: 10.1007/12_2017_19.

(58) Gallino, I.; Cangialosi, D.; Evenson, Z.; Schmitt, L.; Hechler, S.; Stolpe, M.; Ruta, B. *Acta Mat.* **2018**, *144*, 400–410, DOI: https://doi.org/10.1016/j.actamat.2017.10.060.

(59) Song, L.; Xu, W.; Huo, J.; Wang, J.-Q.; Wang, X.; Li, R. *Intermetallics* **2018**, *93*, 101 –105, DOI: https://doi.org/10.1016/j.intermet.2017.11.016.

(60) Golovchak, R; Kozdras, A; Balitska, V; Shpotyuk, O *J Phys: Cond Matt* **2012**, *24*, 505106, DOI: 10.1088/0953-8984/24/50/505106.

(61) Miller, R. S.; MacPhail, R. A. *J. Chem. Phys.* **1997**, *106*, 3393–3401, DOI: 10.1063/1.473068.

(62) Wojnarowska, Z.; Paluch, M. *J. Phys. Chem. Lett.* **2021**, *12*, 11779–11783, DOI: 10.1021/acs.jpclett.1c03572.

(63) Chandler, D.; Weeks, J. D.; Andersen, H. C. *Science* **1983**, *220*, 787–794, DOI: 10.1126/science.220.4599.787.

(64) Casalini, R.; Roland, C. *Physical review. E, Statistical, nonlinear, and soft matter physics* **2004**, *69*, 062501, DOI: 10.1103/PhysRevE.69.062501.

(65) Casalini, R.; Roland, C. M. *Phys. Rev. B* **2005**, *71*, 014210, DOI: 10.1103/PhysRevB.71.014210.

(66) Tölle, A. *Reports on Progress in Physics* **2001**, *64*, 1473–1532, DOI: 10.1088/0034-4885/64/11/203.

(67) Dreyfus, C.; Aouadi, A.; Gapinski, J.; Matos-Lopes, M.; Steffen, W.; Patkowski, A.; Pick, R. M. *Phys. Rev. E* **2003**, *68*, 011204, DOI: 10.1103/PhysRevE.68.011204.

(68) Paluch, M.; Casalini, R.; Roland, C. M. *Phys. Rev. B* **2002**, *66*, 092202, DOI: 10.1103/PhysRevB.66.092202.

(69) Hensel-Bielowka, S.; Paluch, M.; Ziolo, J.; Roland, C. M. *The Journal of Physical Chemistry B* **2002**, *106*, 12459–12463, DOI: 10.1021/jp0264228.

(70) Hoover, W. G.; Rossj, M. *Contemporary Physics* **1971**, *12*, 339–356, DOI: 10.1080/00107517108205268.

(71) March, N. H.; Tosi, M. P., *Introduction to liquid state physics*; World Scientific: 2002.

(72) Kob, W.; Barrat, J.-L. *Phys. Rev. Lett.* **1997**, *78*, 4581–4584, DOI: 10.1103/PhysRevLett.78.4581.

(73) Utz, M.; Debenedetti, P. G.; Stillinger, F. H. *Phys. Rev. Lett.* **2000**, *84*, 1471–1474, DOI: 10.1103/PhysRevLett.84.1471.

(74) Vollmayr-Lee, K. *The Journal of Chemical Physics* **2004**, *121*, 4781–4794, DOI: 10.1063/1.1778155.

(75) Smessaert, A.; Rottler, J. *Phys. Rev. E* **2013**, *88*, 022314, DOI: 10.1103/PhysRevE.88.022314.

(76) Niss, K. *Phys. Rev. Lett.* **2017**, *119*, 115703, DOI: 10.1103/PhysRevLett.119.115703.

(77) Niss, K. *J. Chem. Phys.* **2022**, *157*, 054503, DOI: 10.1063/5.0090869.

(78) Bailey, N. P.; Pedersen, U. R.; Gnan, N.; Schrøder, T. B.; Dyre, J. C. *The Journal of Chemical Physics* **2008**, *129*, 184507, DOI: 10.1063/1.2982247.

(79) Dyre, J. C. *The Journal of Physical Chemistry B* **2014**, *118*, PMID: 25011702, 10007–10024, DOI: 10.1021/jp501852b.

(80) Cugliandolo, L. F.; Kurchan, J *Journal of Physics A: Mathematical and General* **1994**, *27*, 5749, DOI: 10.1088/0305-4470/27/17/011.

(81) Riechers, B.; Roed, L. A.; Mehri, S.; Ingebrigtsen, T. S.; Hecksher, T.; Dyre, J. C.; Niss, K. *Sci. Adv.* **2022**, *8*, eabl9809, DOI: 10.1126/sciadv.abl9809.

(82) Scherer, G., *Relaxation in Glass and Composites*; Wiley: 1986.

(83) Sbirrazzuoli, N. *Polymers* **2020**, *12*, DOI: 10.3390/polym12061280.

(84) Chen, K.; Vyazovkin, S. *The journal of physical chemistry. B* **2009**, *113*, 4631–5, DOI: 10.1021/jp811412q.

(85) Vyazovkin, S.; Chen, K. *Chemical Physics Letters* **2007**, *448*, 203–207, DOI: https://doi.org/10.1016/j.cplett.2007.10.007.

(86) Denissen, W.; Winne, J. M.; Du Prez, F. E. *Chem. Sci.* **2016**, *7*, 30–38, DOI: 10.1039/C5SC02223A.

(87) Samanta, S.; Kim, S.; Saito, T.; Sokolov, A. P. *The Journal of Physical Chemistry B* **2021**, *125*, 9389–9401, DOI: 10.1021/acs.jpcb.1c03511.

(88) Zheng, N.; Xu, Y.; Zhao, Q.; Xie, T. *Chemical Reviews* **2021**, *121*, 1716–1745, DOI: 10.1021/acs.chemrev.0c00938.

(89) Maes, S.; Badi, N.; Winne, J. M.; Du Prez, F. *Nature Reviews Chemistry* **2025**, *9*, 144–158, DOI: 10.1038/s41570-025-00686-7.

(90) Zhang, V.; Kang, B.; Accardo, J. V.; Kalow, J. A. *Journal of the American Chemical Society* **2022**, *144*, 22358–22377, DOI: 10.1021/jacs.2c08104.

(91) Kloxin, C. J.; Scott, T. F.; Adzima, B. J.; Bowman, C. N. *Macromolecules* **2010**, *43*, 2643–2653, DOI: 10.1021/ma902596s.

(92) Bowman, C. N.; Kloxin, C. J. *Angewandte Chemie International Edition* **2012**, *51*, 4272–4274, DOI: https://doi.org/10.1002/anie.201200708.

(93) Kloxin, C. J.; Bowman, C. N. *Chem. Soc. Rev.* **2013**, *42*, 7161–7173, DOI: 10.1039/C3CS60046G.

(94) Lei, Z.; Chen, H.; Huang, S.; Wayment, L. J.; Xu, Q.; Zhang, W. *Chemical Reviews* **2024**, *124*, 7829–7906, DOI: 10.1021/acs.chemrev.3c00926.

(95) Elling, B. R.; Dichtel, W. R. *ACS Central Science* **2020**, *6*, 1488–1496, DOI: 10.1021/acscentsci.0c00567.

(96) Montarnal, D.; Capelot, M.; Tournilhac, F.; Leibler, L. *Science* **2011**, *334*, 965–968, DOI: 10.1126/science.1212648.

(97) Van Zee, N. J.; Nicolaÿ, R. *Progress in Polymer Science* **2020**, *104*, 101233, DOI: https://doi.org/10.1016/j.progpolymsci.2020.101233.

(98) Capelot, M.; Unterlass, M. M.; Tournilhac, F.; Leibler, L. *ACS Macro Letters* **2012**, *1*, 789–792, DOI: 10.1021/mz300239f.

(99) Capelot, M.; Montarnal, D.; Tournilhac, F.; Leibler, L. *Journal of the American Chemical Society* **2012**, *134*, 7664–7667, DOI: 10.1021/ja302894k.

(100) Dyre, J. C. *Rev. Mod. Phys.* **2006**, *78*, 953–972, DOI: 10.1103/RevModPhys.78.953.

(101) Porath, L.; Soman, B.; Jing, B. B.; Evans, C. M. *ACS Macro Letters* **2022**, *11*, 475–483, DOI: 10.1021/acsmacrolett.2c00038.

(102) Soman, B.; Schweizer, K. S.; Evans, C. M. *Macromolecules* **2023**, *56*, 166–176, DOI: 10.1021/acs.macromol.2c01657.

(103) Menczel, J. D.; Prime, R. B.; Gallagher, P. K. In *Thermal Analysis of Polymers*; John Wiley & Sons, Ltd: 2009; Chapter 1, pp 1–6, DOI: https://doi.org/10.1002/9780470423837.ch1.

(104) Gabbott, P. In *Principles and Applications of Thermal Analysis*; John Wiley & Sons, Ltd: 2008; Chapter 1, pp 1–50, DOI: https://doi.org/10.1002/9780470697702.ch1.

(105) Craig, D.; Reading, M., *Thermal Analysis of Pharmaceuticals*; CRC Press: 2006.

(106) Silvester, L.; Touloumet, Q.; Auroux, A. In *Springer Handbook of Advanced Catalyst Characterization*, Wachs, I. E., Bañares, M. A., Eds.; Springer International Publishing: Cham, 2023, pp 1031–1059, DOI: 10.1007/978-3-031-07125-6_46.

(107) Menczel, J. D.; Judovits, L.; Prime, R. B.; Bair, H. E.; Reading, M.; Swier, S. In *Thermal Analysis of Polymers*; John Wiley & Sons, Ltd: 2009; Chapter 2, pp 7–239, DOI: https://doi.org/10.1002/9780470423837.ch2.

(108) Danley, R. L. *Thermochimica Acta* **2002**, *395*, 201–208, DOI: https://doi.org/10.1016/S0040-6031(02)00212-5.

(109) Mathot, V.; Pyda, M.; Pijpers, T.; Vanden Poel, G.; van de Kerkhof, E.; van Herwaarden, S.; van Herwaarden, F.; Leenaers, A. *Thermochimica Acta* **2011**, *522*, Special Issue: Interplay between Nucleation, Crystallization, and the Glass Transition, 36–45, DOI: https://doi.org/10.1016/j.tca.2011.02.031.

(110) F, T.; Goderis, B.; Scherrenberg, R.; Vegte, E. *Macromolecules* **2002**, *35*, DOI: 10.1021/ma011122u.

(111) Aubuchon, S.; Danley, R.; Caulfield, P. *American Laboratory* **2008**, *41*, 9.

(112) Allen, L. H.; Ramanath, G.; Lai, S. L.; Ma, Z.; Lee, S.; Allman, D. D. J.; Fuchs, K. P. *Applied Physics Letters* **1994**, *64*, 417–419, DOI: 10.1063/1.111116.

(113) Adamovsky, S.; Minakov, A.; Schick, C *Thermochimica Acta* **2003**, *403*, Thermodynamics and Calorimetry of Small Systems Papers Presented at the 7th Laehnwitzseminar on Calorimetry, 55–63, DOI: https://doi.org/10.1016/S0040-6031(03)00182-5.

(114) Schick, C.; Zhuravlev, E.; Androsch, R.; Wurm, A.; Schmelzer, J. *Glass: Selected Properties and Crystallization* **2014**, 1–93, DOI: 10.1515/9783110298581.1.

(115) Schawe, J. E. K.; Pogatscher, S. In *Fast Scanning Calorimetry*, Schick, C., Mathot, V., Eds.; Springer International Publishing: Cham, 2016, pp 3–80, DOI: 10.1007/978-3-319-31329-0_1.

(116) van Herwaarden, S.; Iervolino, E.; van Herwaarden, F.; Wijffels, T.; Leenaers, A.; Mathot, V. *Thermochimica Acta* **2011**, *522*, Special Issue: Interplay between Nucleation, Crystallization, and the Glass Transition, 46–52, DOI: https://doi.org/10.1016/j.tca.2011.05.025.

(117) Tool, A. Q. *Journal of the American Ceramic Society* **1946**, *29*, 240–253, DOI: https://doi.org/10.1111/j.1151-2916.1946.tb11592.x.

(118) Abate, A. A.; Cangialosi, D.; Napolitano, S. *Thermochimica Acta* **2022**, *707*, 179084, DOI: https://doi.org/10.1016/j.tca.2021.179084.

(119) Merzlyakov, M.; Schick, C. *Thermochimica Acta* **2001**, *380*, 5–12, DOI: https://doi.org/10.1016/S0040-6031(01)00631-1.

(120) Shoifet, E.; Schulz, G.; Schick, C. *Thermochimica Acta* **2015**, *603*, Chip Calorimetry, 227–236, DOI: https://doi.org/10.1016/j.tca.2014.10.010.

(121) Weyer, S.; Merzlyakov, M.; Schick, C. *Thermochimica Acta* **2001**, *377*, Frequency and Time-Dependent Heat Capacity. A collection of Papers from the 6th Lahnwitzseminar on Calorimetry Kuhlungsborn, Germany, 12-18 June 2000, 85–96, DOI: https://doi.org/10.1016/S0040-6031(01)00543-3.

(122) Kremer, F.; Schönhals, A., *Broadband Dielectric Spectroscopy*, 2003, DOI: 10.1007/978-3-642-56120-7.

(123) Boucher, V. M.; Cangialosi, D.; Alegría, A.; Colmenero, J. *Phys. Rev. E* **2012**, *86*, 041501, DOI: 10.1103/PhysRevE.86.041501.

(124) Cangialosi, D.; Boucher, V. M.; Alegría, A.; Colmenero, J. *J. Pol. Sci. Part B: Pol. Phys.* **2013**, *51*, 847–853, DOI: 10.1002/polb.23282.

(125) Fukao, K.; Koizumi, H. *Phys. Rev. E* **2008**, *77*, 021503, DOI: 10.1103/PhysRevE.77.021503.

(126) Song, Z.; Rodríguez-Tinoco, C.; Mathew, A.; Napolitano, S. *Science Advances* **2022**, *8*, eabm7154, DOI: 10.1126/sciadv.abm7154.

(127) Caporaletti, F.; Bock, H.; Napolitano, S. *Journal of Molecular Liquids* **2025**, *433*, 127902, DOI: https://doi.org/10.1016/j.molliq.2025.127902.

(128) Hecksher, T.; Olsen, N. B.; Dyre, J. C. *J. Chem. Phys.* **2015**, *142*, 241103, DOI: 10.1063/1.4923000.

(129) Roed, L. A.; Hecksher, T.; Dyre, J. C.; Niss, K. *J. Chem. Phys.* **2019**, *150*, 044501, DOI: 10.1063/1.5066387.

(130) Roland, C.; Hensel-Bielowka, S; Paluch, M; Casalini, R *Rep. Progr. Phys.* **2005**, *68*, 1405, DOI: 10.1088/0034-4885/68/6/R03.

(131) Hecksher, T.; Nielsen, A. I.; Olsen, N. B.; Dyre, J. C. *Nat. Phys.* **2008**, *4*, 737–741, DOI: 10.1038/nphys1033.

(132) Hodge, I. M. *Macromolecules* **1983**, *16*, 898–902, DOI: 10.1021/ma00240a013.

(133) O'Reilly, J. M. *Crit. Rev. Sol. St. Mat. Sci.* **1987**, *13*, 259–277, DOI: 10.1080/10408438708242179.

(134) McKenna, G.; Angell, C. *J. Non-Cryst. Sol.* **1991**, *131*, 528–536, DOI: https://doi.org/10.1016/0022-3093(91)90353-8.

(135) Righetti, M.; Johari, G. *Thermochim. Acta* **2015**, *607*, 19–29, DOI: https://doi.org/10.1016/j.tca.2015.03.012.

(136) Toda, A. *Thermochim. Acta* **2023**, *721*, 179433, DOI: https://doi.org/10.1016/j.tca.2023.179433.

(137) Moynihan, C. T.; Macedo, P. B.; Montrose, C. J.; Gupta, P. K.; De Bolt, M. A.; Dill, J. F.; Dom, B. E.; Drake, P. W.; Eastel, A. J.; Elterman, P. B.; Moeller, R. P.; Sasabe, H; Wilder, J. A. *Ann. NY Acad. Sci.* **1976**, *279*, 15–35, DOI: https://doi.org/10.1111/j.1749-6632.1976.tb39688.x.

(138) Donth, E. J., *The Glass Transition*; Springer-Verlag, Berlin Heidelberg: 2001.

(139) Cangialosi, D.; Alegria, A.; Colmenero, J. *Prog. Pol. Sci.* **2016**, *54-55*, 128 –147, DOI: https://doi.org/10.1016/j.progpolymsci.2015.10.005.

(140) Cangialosi, D.; Alegría, A.; Colmenero, J. *Phys. Rev. B* **2008**, *78*, 176301, DOI: 10.1103/PhysRevB.78.176301.

(141) Ngai, K. *Phys. Chem. Chem. Phys.* **2021**, *23*, 13468–13472, DOI: 10.1039/D1CP01445E.

(142) Kahle, S.; Gapinski, J.; Hinze, G.; Patkowski, A.; Meier, G. *The Journal of Chemical Physics* **2005**, *122*, 074506, DOI: 10.1063/1.1846653.

(143) Johari, G. P.; Goldstein, M. *The Journal of Chemical Physics* **1970**, *53*, 2372–2388, DOI: 10.1063/1.1674335.

(144) Meier, G; Gerharz, B; Boese, D; Fischer, E. *J. Chem. Phys.* **1991**, *94*, 3050–3059, DOI: https://doi.org/10.1016/0022-3093(91)90290-M.

(145) Chen, K.; Vyazovkin, S. *J. Phys. Chem. B* **2009**, *113*, 4631–4635.

(146) Vyazovkin, S.; Sbirrazzuoli, N.; Dranca, I. *Macromolecular Rapid Communications* **2004**, *25*, 1708–1713, DOI: https://doi.org/10.1002/marc.200400268.

(147) Vyazovkin, S.; Dranca, I. *The Journal of Physical Chemistry B* **2004**, *108*, 11981–11987, DOI: 10.1021/jp048702o.

(148) Vyazovkin, S.; Sbirrazzuoli, N.; Dranca, I. *Macromolecular Chemistry and Physics* **2006**, *207*, 1126–1130, DOI: https://doi.org/10.1002/macp.200600095.

(149) Grassia, L.; Koh, Y. P.; Rosa, M.; Simon, S. L. *Macromolecules* **2018**, *51*, 1549–1558, DOI: 10.1021/acs.macromol.7b02277.

(150) Di Lisio, V.; Rocchi, L. A.; Cangialosi, D. *Phys. Rev. Lett.* **2024**, *133*, 048201, DOI: 10.1103/PhysRevLett.133.048201.

(151) Dhinojwala, A.; Wong, G. K.; Torkelson, J. M. *Macromolecules* **1993**, *26*, 5943–5953, DOI: 10.1021/ma00074a016.

(152) Dhinojwala, A.; Wong, G. K.; Torkelson, J. M. *The Journal of chemical physics* **1994**, *100*, 6046–6054, DOI: 10.1063/1.467115.

(153) Alegria, A; Guerrica-Echevarria, E; Goitiandia, L; Telleria, I; Colmenero, J *Macromolecules* **1995**, *28*, 1516–1527, DOI: 10.1021/ma00109a025.

(154) Cangialosi, D.; Wübbenhorst, M.; Schut, H.; van Veen, A.; Picken, S. J. *Phys. Rev. B* **2004**, *69*, 134206, DOI: 10.1103/PhysRevB.69.134206.

(155) Casalini, R; Roland, C. *J. Non-Crys. Sol.* **2011**, *357*, 282–285, DOI: https://doi.org/10.1016/j.jnoncrysol.2010.07.048.

(156) Wojnarowska, Z.; Roland, C. M.; Kolodziejczyk, K.; Swiety-Pospiech, A.; Grzybowska, K.; Paluch, M. *The Journal of Physical Chemistry Letters* **2012**, *3*, 1238–1241, DOI: 10.1021/jz300349a.

(157) Ruta, B.; Chushkin, Y.; Monaco, G.; Cipelletti, L.; Pineda, E.; Bruna, P.; Giordano, V. M.; Gonzalez-Silveira, M. *Phys. Rev. Lett.* **2012**, *109*, 165701, DOI: 10.1103/PhysRevLett.109.165701.

(158) Avramov, I. *J. Non-Cryst. Sol.* **2009**, *355*, 1769–1771, DOI: https://doi.org/10.1016/j.jnoncrysol.2009.07.006.

(159) Adam, G.; Gibbs, J. H. *J. Chem. Phys.* **1965**, *43*, 139–146, DOI: 10.1063/1.1696442.

(160) McCrum, N.; Read, B.; Williams, G., *Anelastic and dïelectric effects in polymeric solids*; John Wiley: 1967.

(161) Song, L.; Gao, Y.; Zou, P.; Xu, W.; Gao, M.; Zhang, Y.; Huo, J.; Li, F.; Qiao, J.; Wang, L.-M.; Wang, J.-Q. *Proceedings of the National Academy of Sciences* **2023**, *120*, e2302776120, DOI: 10.1073/pnas.2302776120.

(162) Thoms, E.; Song, Z.; Wang, K.; Napolitano, S. *Phys. Rev. Lett.* **2024**, *132*, 248101, DOI: 10.1103/PhysRevLett.132.248101.

(163) Thoms, E.; Napolitano, S. *The Journal of Chemical Physics* **2023**, *159*, 161103, DOI: 10.1063/5.0174213.

(164) Caporaletti, F.; Napolitano, S. *Phys. Chem. Chem. Phys.* **2024**, *26*, 745–748, DOI: 10.1039/D3CP05044K.

(165) White, R. P.; Napolitano, S.; Lipson, J. E. G. *Phys. Rev. Lett.* **2025**, *134*, 098203, DOI: 10.1103/PhysRevLett.134.098203.

(166) Thoms, E.; Wang, K.; Chandran, S.; Napolitano, S. *The Journal of Physical Chemistry Letters* **2024**, *15*, 4838–4843, DOI: 10.1021/acs.jpclett.4c00902.

(167) Caporaletti, F.; Villanueva, M. E.; Molitor, S.; Zuo, B.; Napolitano, S. *Mater. Horiz.* **2026**, *13*, 491–498, DOI: 10.1039/D5MH01335F.

(168) White, R. P.; Lipson, J. E. *Eur. Phys. J. E* **2019**, *42*, 100.

(169) Avramov, I. *Journal of Non-Crystalline Solids* **2000**, *262*, 258–263, DOI: https://doi.org/10.1016/S0022-3093(99)00712-7.

(170) Roland, C. M.; Bair, S.; Casalini, R. *The Journal of Chemical Physics* **2006**, *125*, 124508, DOI: 10.1063/1.2346679.

(171) Dreyfus, C; Le Grand, A; Gapinski, J; Steffen, W; Patkowski, A *Eur. Phys. J. B* **2004**, *42*, 309–319.

(172) Reiser, A.; Kasper, G.; Hunklinger, S. *Phys. Rev. B* **2005**, *72*, 094204, DOI: 10.1103/PhysRevB.72.094204.

(173) Bøhling, L; Ingebrigtsen, T. S.; Grzybowski, A; Paluch, M; Dyre, J. C.; Schrøder, T. B. *New Journal of Physics* **2012**, *14*, 113035, DOI: 10.1088/1367-2630/14/11/113035.

(174) Hansen, H. W.; Lundin, F.; Adrjanowicz, K.; Frick, B.; Matic, A.; Niss, K. *Phys. Chem. Chem. Phys.* **2020**, *22*, 14169–14176, DOI: 10.1039/D0CP01258K.

(175) Roland, C. M. *Macromolecules* **2010**, *43*, 7875–7890, DOI: 10.1021/ma101649u.

(176) Schwartz, G. A.; Colmenero, J.; Alegría, A. *Macromolecules* **2006**, *39*, 3931–3938, DOI: 10.1021/ma052464t.

(177) Bauer, C.; Böhmer, R.; Moreno-Flores, S.; Richert, R.; Sillescu, H.; Neher, D. *Phys. Rev. E* **2000**, *61*, 1755–1764, DOI: 10.1103/PhysRevE.61.1755.

(178) Di Lisio, V.; Stavropoulou, V.-M.; Cangialosi, D. *The Journal of Chemical Physics* **2023**, *159*, 064505, DOI: 10.1063/5.0157994.

(179) Guerre, M.; Taplan, C.; Winne, J. M.; Du Prez, F. E. *Chem. Sci.* **2020**, *11*, 4855–4870, DOI: 10.1039/D0SC01069C.

(180) Martins, M. L.; Zhao, X.; Demchuk, Z.; Luo, J.; Carden, G. P.; Toleutay, G.; Sokolov, A. P. *Macromolecules* **2023**, *56*, 8688–8696, DOI: 10.1021/acs.macromol.3c01545.

(181) Hubbard, A. M.; Ren, Y.; Konkolewicz, D.; Sarvestani, A.; Picu, C. R.; Kedziora, G. S.; Roy, A.; Varshney, V.; Nepal, D. *ACS Applied Polymer Materials* **2021**, *3*, 1756–1766, DOI: 10.1021/acsapm.0c01290.

(182) Liu, T.; Zhao, B.; Zhang, J. *Polymer* **2020**, *194*, 122392, DOI: https://doi.org/10.1016/j.polymer.2020.122392.

(183) Yang, Y.; Zhang, S.; Zhang, X.; Gao, L.; Wei, Y.; Ji, Y. *Nature Communications* **2019**, *10*, 3165, DOI: 10.1038/s41467-019-11144-6.

(184) Arbe, A.; Alegría, A.; Colmenero, J.; Bhaumik, S.; Ntetsikas, K.; Hadjichristidis, N. *ACS Macro Letters* **2023**, *12*, 1595–1601, DOI: 10.1021/acsmacrolett.3c00586.

(185) Schick, C.; Mathot, V., *Fast scanning calorimetry*; Springer: 2016.

(186) Lessard, J. J.; Garcia, L. F.; Easterling, C. P.; Sims, M. B.; Bentz, K. C.; Arencibia, S.; Savin, D. A.; Sumerlin, B. S. *Macromolecules* **2019**, *52*, 2105–2111, DOI: 10.1021/acs.macromol.8b02477.

(187) Tellers, J.; Pinalli, R.; Soliman, M.; Vachon, J.; Dalcanale, E. *Polym. Chem.* **2019**, *10*, 5534–5542, DOI: 10.1039/C9PY01194C.

(188) Zhu, Y.; Gao, F.; Zhong, J.; Shen, L.; Lin, Y. *European Polymer Journal* **2020**, *135*, 109865, DOI: https://doi.org/10.1016/j.eurpolymj.2020.109865.

(189) Hajiali, F.; Tajbakhsh, S.; Marić, M. *Polymer* **2021**, *212*, 123126, DOI: https://doi.org/10.1016/j.polymer.2020.123126.

(190) Pagnacco, C.; Kravicz, M.; Sica, F.; Fontanini, V.; González de San Román Martín, E.; Lund, R.; Re, F.; Barroso-Bujans, F. *Biomacromolecules* **2024**, *25*, DOI: 10.1021/acs.biomac.4c00210.

(191) Kissinger, H. E. *Analytical Chemistry* **1957**, *29*, 1702–1706, DOI: 10.1021/ac60131a045.

(192) Blaine, R. L.; Kissinger, H. E. *Thermochimica Acta* **2012**, *540*, 1–6, DOI: https://doi.org/10.1016/j.tca.2012.04.008.

(193) Tropin, T. V.; Schulz, G.; Schmelzer, J. W.; Schick, C. *J. Non-Cryst. Sol.* **2015**, *409*, 63–75, DOI: https://doi.org/10.1016/j.jnoncrysol.2014.11.001.

(194) Melillo, J. H.; Cangialosi, D.; Lisio, V. D.; Steinrücken, E.; Vogel, M.; Cerveny, S. *Proceedings of the National Academy of Sciences* **2024**, *121*, e2407030121, DOI: 10.1073/pnas.2407030121.

(195) Martín, J.; Stingelin, N.; Cangialosi, D. *J. Phys. Chem. Lett.* **2018**, *9*, 990–995, DOI: 10.1021/acs.jpclett.7b03110.

(196) Mittemeijer, E. J. *Journal of Materials Science* **1992**, *27*, 3977–3987, DOI: 10.1007/BF01105093.

(197) Vyazovkin, S. *Molecules* **2020**, *25*, 2813, DOI: 10.3390/molecules25122813.

(198) Cangialosi, D. *Journal of Polymer Science*, *62*, 1952–1974, DOI: https://doi.org/10.1002/pol.20230850.

(199) Perez-de Eulate, N. G.; Di Lisio, V.; Cangialosi, D. *ACS Macro Lett.* **2017**, *6*, 859–863, DOI: 10.1021/acsmacrolett.7b00484.

(200) *Thermochimica Acta* **1995**, *266*, Transition Phenomena in Condensed Matter, 97–111, DOI: https://doi.org/10.1016/0040-6031(95)02552-9.

(201) Reading, M.; Hourston, D. J., *Modulated Temperature Differential Scanning Calorimetry: Theoretical and Practical Applications in Polymer Characterisation*, 1st ed.; Springer: 2006, DOI: 10.1007/1-84628-060-5.

(202) Lin, T.-W.; Mei, B.; Dutta, S.; Schweizer, K. S.; Sing, C. E. *Macromolecules* **2025**, *58*, 1481–1497, DOI: 10.1021/acs.macromol.4c02659.

(203) Boehm, L; Angell, C. *J. Non-Cryst. Solids* **1980**, *40*, 83–92, DOI: https://doi.org/10.1016/0022-3093(80)90095-2.

(204) Greiner, R.; Schwarzl, F. R. *Rheol. Acta* **1984**, *23*, 378–395, DOI: 10.1007/BF01329190.

(205) Perez-De Eulate, N. G.; Cangialosi, D. *Phys. Chem. Chem. Phys.* **2018**, *20*, 12356–12361, DOI: 10.1039/C8CP01940A.

(206) Welch, R. C.; Smith, J. R.; Potuzak, M.; Guo, X.; Bowden, B. F.; Kiczenski, T.; Allan, D. C.; King, E. A.; Ellison, A. J.; Mauro, J. C. *Phys. Rev. Lett.* **2013**, *110*, 265901, DOI: 10.1103/PhysRevLett.110.265901.

(207) Grigoriadi, K.; Putzeys, T.; Wübbenhorst, M.; van Breemen, L. C.; Anderson, P. D.; Hütter, M. *J. Pol. Sci. B: Pol. Phys.* **2019**, *57*, 1394–1401, DOI: https://doi.org/10.1002/polb.24883.

(208) Yin, H.; Chapala, P.; Bermeshev, M.; Schönhals, A.; Böhning, M. *ACS Macro Lett.* **2017**, *6*, 813–818, DOI: 10.1021/acsmacrolett.7b00456.

(209) Vogiatzis, G. G.; van Breemen, L. C.; Hütter, M.; Theodorou, D. N. *Mol. Sys. Des. Eng.* **2023**, DOI: 10.1039/D2ME00256F.

(210) Gibbs, J. H.; DiMarzio, E. A. *J. Chem. Phys.* **1958**, *28*, 373–383, DOI: 10.1063/1.1744141.

(211) Kauzmann, W *Chem. Rev.* **1948**, *43*, 219–256, DOI: 10.1021/cr60135a002.

(212) Welch, R. S.; Zanotto, E. D.; Wilkinson, C. J.; Cassar, D. R.; Montazerian, M.; Mauro, J. C. *Acta Mater.* **2023**, *254*, 118994, DOI: https://doi.org/10.1016/j.actamat.2023.118994.

(213) Braun, G; Kovacs, A. *Phys. Chem. Glasses* **1963**, *4*, 1152–160.

(214) Xing, K.; Tress, M.; Cao, P.; Cheng, S.; Saito, T.; Novikov, V. N.; Sokolov, A. P. *Soft Matter* **2018**, *14*, 1235–1246, DOI: 10.1039/C7SM01805C.

(215) Robles-Hernández, B.; González-Burgos, M.; Malo de Molina, P.; Asenjo-Sanz, I.; Radulescu, A.; Pomposo, J. A.; Arbe, A.; Colmenero, J. *Macromolecules* **2023**, *56*, 8971–8979, DOI: 10.1021/acs.macromol.3c01333.